AD NUMBER

ADB013900

LIMITATION CHANGES

TO:

Approved for public release; distribution is unlimited.

FROM:

Distribution authorized to U.S. Gov't. agencies only; Test and Evaluation; JUN 1976. Other requests shall be referred to Army Night Vision Laboratory, Attn: DRSEl-NV-FIR, Fort Belvoir, VA 22060.

AUTHORITY

anveol, d/a ltr, 21 aug 1978

L

AD

AD B013900

DDC FILE COPY

AD No. ____

(6) DEVELOPMENT OF HIGH-SPEED IV-VI PHOTODIODES.
FINAL REPORT

(11) Jun~~e~~ 1976 (12) 168 p.

prepared by

FORD MOTOR COMPANY S/C 401367.
RESEARCH STAFF

(9) Final rept. Jan 75-Mar 76,

for

NIGHT VISION LABORATORY
U. S. ARMY ELECTRONICS COMMAND
FORT BELVOIR, VIRGINIA 22060

(10) H. J. Holloway,
M. D. Hurley,
E. B. Schermer K. F. Yeung

under contract

(15) DAAK02-75-C-0106

Distribution Statement

Distribution limited to U. S. Government Agencies only; covers the test and evaluation of military hardware, June 1976. Other requests for this document must be referred to the Director, Night Vision Laboratory, Attention DRSEL-NV-FIR, Fort Belvoir, Virginia 22060.

DDC
RECEIVED
OCT 7 1976
D

401367 DN

Ford RESEARCH

CONTENTS

		Page
1	INTRODUCTION	1
2	EXPERIMENTAL	2
3	JUNCTION CAPACITANCE	3
4	THE PINCHED-OFF PHOTODIODE	8
	4.1 General Considerations	8
	4.2 Quarter-Wave Structures in PbTe	12
	4.2.1 Fabrication	13
	4.2.2 Quantum Efficiencies and Thermal Degradation	14
	4.2.3 Noise	15
	4.2.4 Capacitance	16
	4.2.5 Detectivity	16
	4.2.6 Measurements of Quarter-Wave Devices	17
	4.3 Three-Quarter-Wave Structures in PbTe	22
	4.3.1 Fabrication	22
	4.3.2 Thermal Stability	22
	4.3.3 Reversed-Bias Noise	23
	4.3.4 Capacitance	24
	4.3.5 Quantum Efficiency	26
	4.3.6 Detectivity	26
	4.3.7 Measurements of Three-Quarter-Wave Devices	27
	4.4 Pinched-off $PbSe_{0.8}Te_{0.2}$ Devices	33
	4.5 Summary of Results for Pinched-off Photodiodes	37

		Page
5	LATERAL-COLLECTION PHOTODIODES	39
	5.1 General Considerations	39
	5.1.1 Collection Efficiency of an Array of Stripes	40
	5.1.2 Collection Efficiency of an Array of Dots	42
	5.1.3 The Trade-Off Between Quantum Efficiency and Capacitance Reduction	43
	5.1.4 Increased Detectivity, a Simplified Model	44
	5.1.5 The Scaling of Resistance with Junction Area	46
	5.1.6 The Projected Detectivity of 3-5 μm Lateral Collection Devices	51
	5.2 Experimental Results	54
	5.2.1 The Diffusion Length in $PbSe_{0.8}Te_{0.2}$	54
	5.2.2 Fabrication of Lateral Collection Devices	55
	5.2.3 Measurements of Devices with Stripe Collectors	57
	5.3 Summary of Results for Lateral-Collection Devices	62
6	CONCLUSIONS	63
	APPENDIX I - Calculation of the Reflection-Loss-Limited Quantum Efficiency for PbTe Devices	65
	APPENDIX II - Attempts to Grow $PbSe_{0.8}Te_{0.2}$ with Reduced Acceptor Concentration	68
	REFERENCES	69

1. INTRODUCTION

The work described here was performed by Ford Motor Company, Research Staff in the period January 1975 to March 1976. The principal investigator was H. Holloway and other contributors were M. D. Hurley, E. B. Schermer and K. F. Yeung. The contract was monitored by R. E. Callender of NVL.

The studies that are described were aimed at reduction of the capacitance of IV-VI semiconductor photodiodes, with particular emphasis upon 3-5 μm (micrometer) devices that are suitable for lightweight thermal imaging systems. The starting point was the thin-film Pb barrier IV-VI photodiodes that were discovered and developed by Ford Research Staff. The essential references to this previous work and to new experimental details are given in Section 2 of the report. Section 3 goes on to a brief analysis of the influence of capacitance on the bandwidth of IV-VI photodiode/preamplifier combinations and describes an approach that has led to two novel photodiode concepts. The new devices, which we have named the pinched-off photodiode and the lateral-collection photodiode, are described in detail in Sections 4 and 5, respectively. Section 6 summarizes the results and draws conclusions about the preferred course for further work.

2. EXPERIMENTAL

The techniques for thin-film growth and for diode fabrication generally followed those that are described in our previous reports.[1-4] P-type layers of PbTe and $PbSe_{0.8}Te_{0.2}$ were grown epitaxially at 1-2 μm/hr on cleaved BaF_2 substrates at 300-425°C in vacuum. The binary components, PbTe and PbSe, were evaporated at 700-725°C from graphite effusion cells, with use of an isothermal double cell[5] for the alloy $PbSe_{0.8}Te_{0.2}$. Secondary sources of Pb and of Se were used in an unsuccessful attempt to grow $PbSe_{0.8}Te_{0.2}$ layers with $p < 10^{17} cm^{-3}$. The rationale for these experiments is given in Section 4 and the experiments are described in Appendix II.

Photodiodes were made as previously[2,3] using vacuum-deposited Pb films to form barriers and sputtered Pt films for ohmic contacts. The diode areas were delineated by opening windows in a vacuum-deposited insulating film of BaF_2 following the technique of Asch *et al.*[4] This method required some modifications for the lateral-collection devices and these details are described in Section 5.

Measurement techniques followed our previous work with the exception of capacitance, resistance, and responsivity mapping. The C-V and R-V characteristics were obtained simultaneously using the lockin technique that is shown schematically in Fig. 1. Responsivity mapping was performed with a flying-spot scanner* (Fig. 2). The resolution obtained was 15 μm, which is within a factor of two of the estimated diffraction limit for our system.

---

* We are much indebted to R. E. Callender and D. Kaplan of NVL, both for their advice on the design of scanners and for providing us with numerous scans from their system before ours was built. Figures 11, 74, and 78 of this report were provided by NVL.

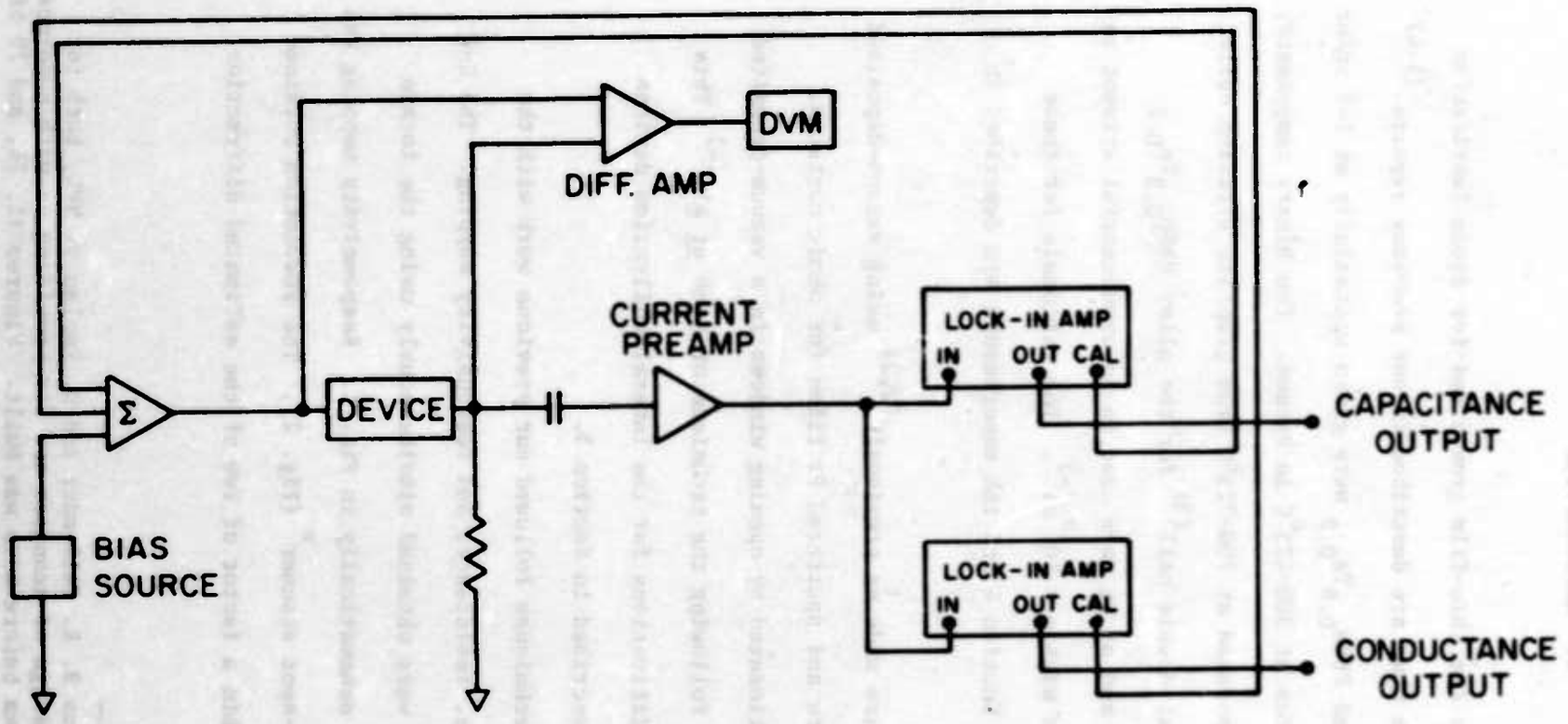

Fig. 1 Schematic of the apparatus for C-V and R-V measurement. The calibration standards were a precision capacitor (GR type 722-N, 1000.0 ± 0.5 pF) and a metal film resistor (Dale, 10^6 ohm ± 1%).

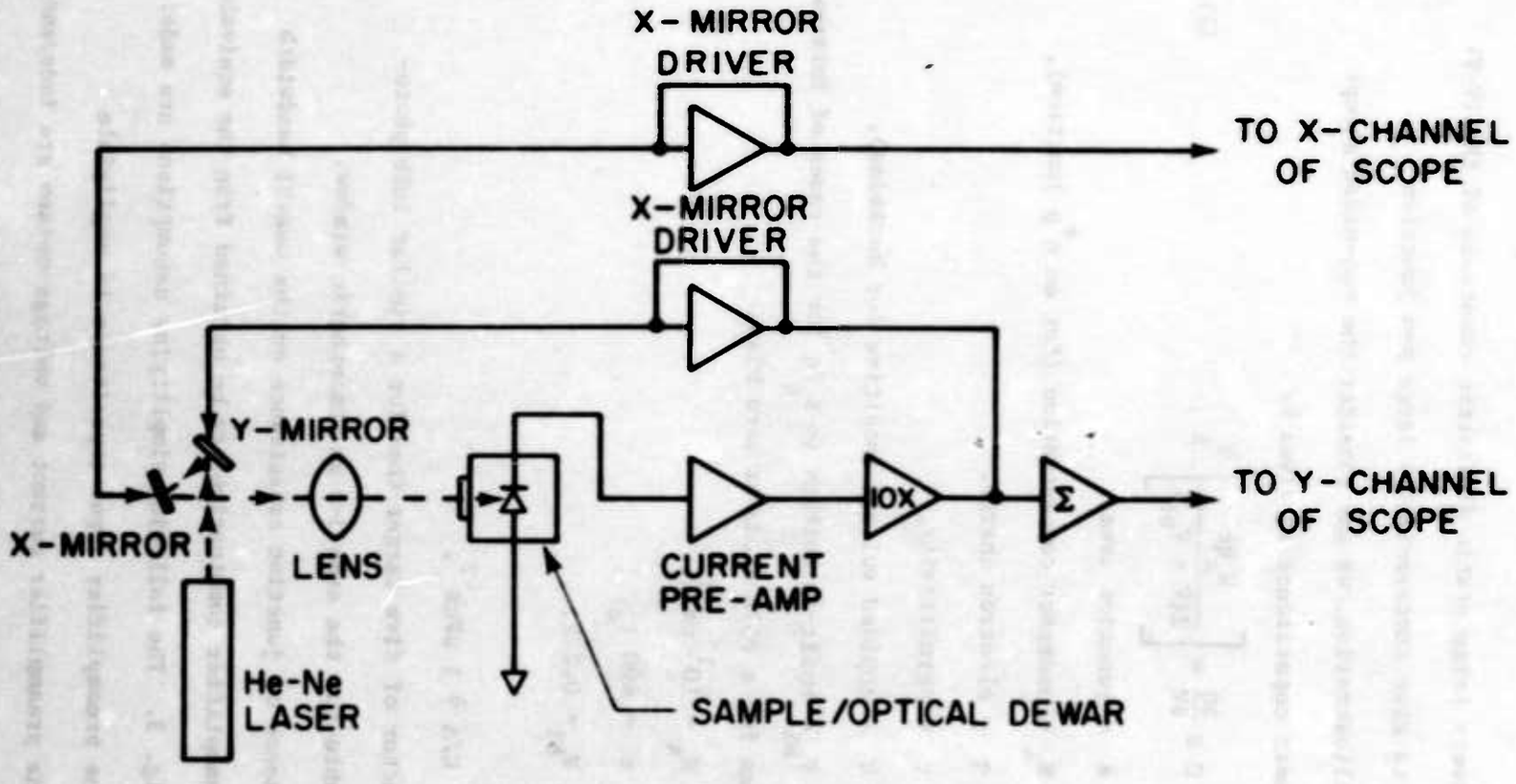

Fig. 2 Schematic of the flying-spot scanner.

3. JUNCTION CAPACITANCE

The relatively large static dielectric constants of the IV-VI semiconductors tend to give inconveniently large p-n junction capacitances. For illustration, we may consider the one-sided abrupt junction, whose dynamic capacitance is given by

$$C \equiv \frac{\partial Q}{\partial V} = \left[\frac{N_A q \varepsilon}{2(V + V_{bi})}\right]^{\frac{1}{2}} A \,, \qquad (1)$$

where A = junction area,

N_A = acceptor concentration (for an n^+p junction),

q = electron charge,

ε = permittivity,

V = applied voltage (positive for backbias),

V_{bi} = built-in voltage ($\approx E_g/q$ for the cases of interest).

Taking typical values for a PbTe diode at zero bias,

$N_A = 10^{17}\,cm^{-3}$,

$\varepsilon = 400\,\varepsilon_o$,

$V_{bi} = 0.22V$,

we obtain

$C/A \approx 1\ \mu F cm^{-2}$,

which is about a factor of five larger than for a similar InSb photodiode that is suitable for the same 3-5 μm atmospheric window.

The influence of junction capacitance on the useful bandwidth of a photodiode/preamplifier combination may be obtained from the equivalent circuit shown in Fig. 3. The following simplifying assumptions are made:

(i) the preamplifier input capacitance is negligible

(ii) the preamplifier current and voltage noises are independent of frequency and they have negligible effect at low frequencies

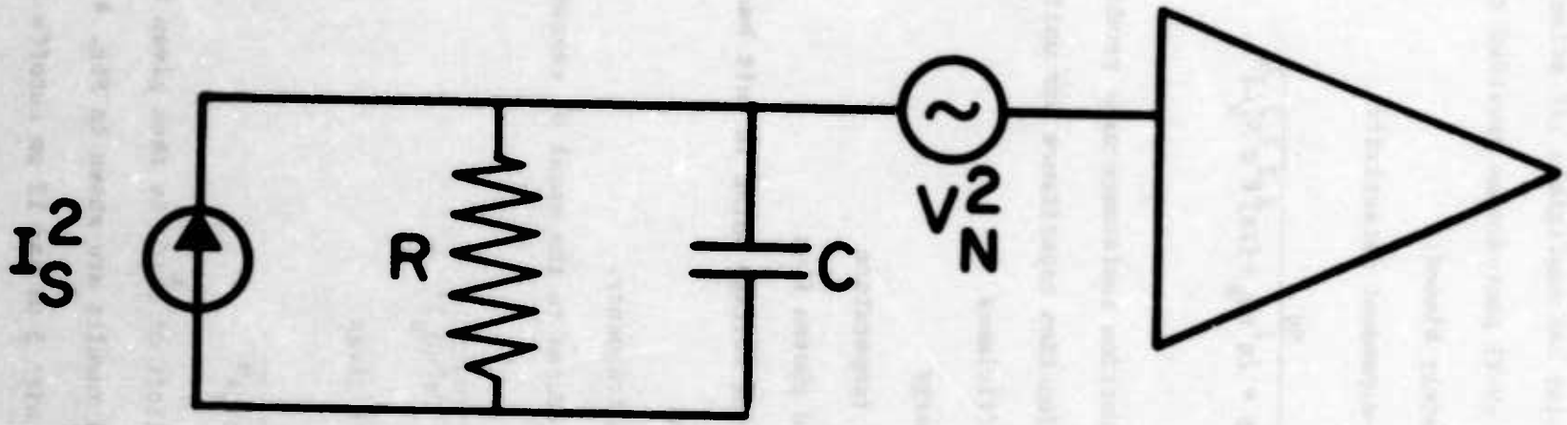

Fig. 3 Equivalent circuit of a detector/preamplifier combination.

(iii) the detector has negligible 1/f noise (this is usually true for IV-VI photodiodes provided that they are appropriately biased).

This leads to a frequency-dependent detectivity

$$D^*(f) = \frac{\eta q}{E_\lambda [4kT/\rho + 2q^2\eta Q_B + (2\pi)^2 f^2 \sigma^2 V_N^2 A]^{1/2}}, \qquad (2)$$

where

ρ = RA, the junction resistance-area product

σ = C/A, the junction capacitance per unit area

η = quantum efficiency

E_λ = photon energy

T = operating temperature

Q_B = background photon flux

V_N = preamplifier voltage noise in unit bandwidth

A = diode area

f = operating frequency.

At low frequencies this reduces to the usual D^* expression

$$D_o^* = \frac{\eta q}{E_\lambda [4kT/\rho + 2q^2\eta Q_B]^{1/2}}$$

and at high frequencies it gives

$$D_\infty^*(f) = \frac{\eta q}{E_\lambda \cdot 2\pi f \sigma V_N A^{1/2}}$$

The 3dB point for the rolloff of $D^*(f)$ is then given by the frequency at which $D_\infty^*(f) = D_o^*$. Some typical results are shown in Fig. 4. Here we consider 2 mil-square photodiodes with 5 μm and 12 μm cutoffs and with low-frequency

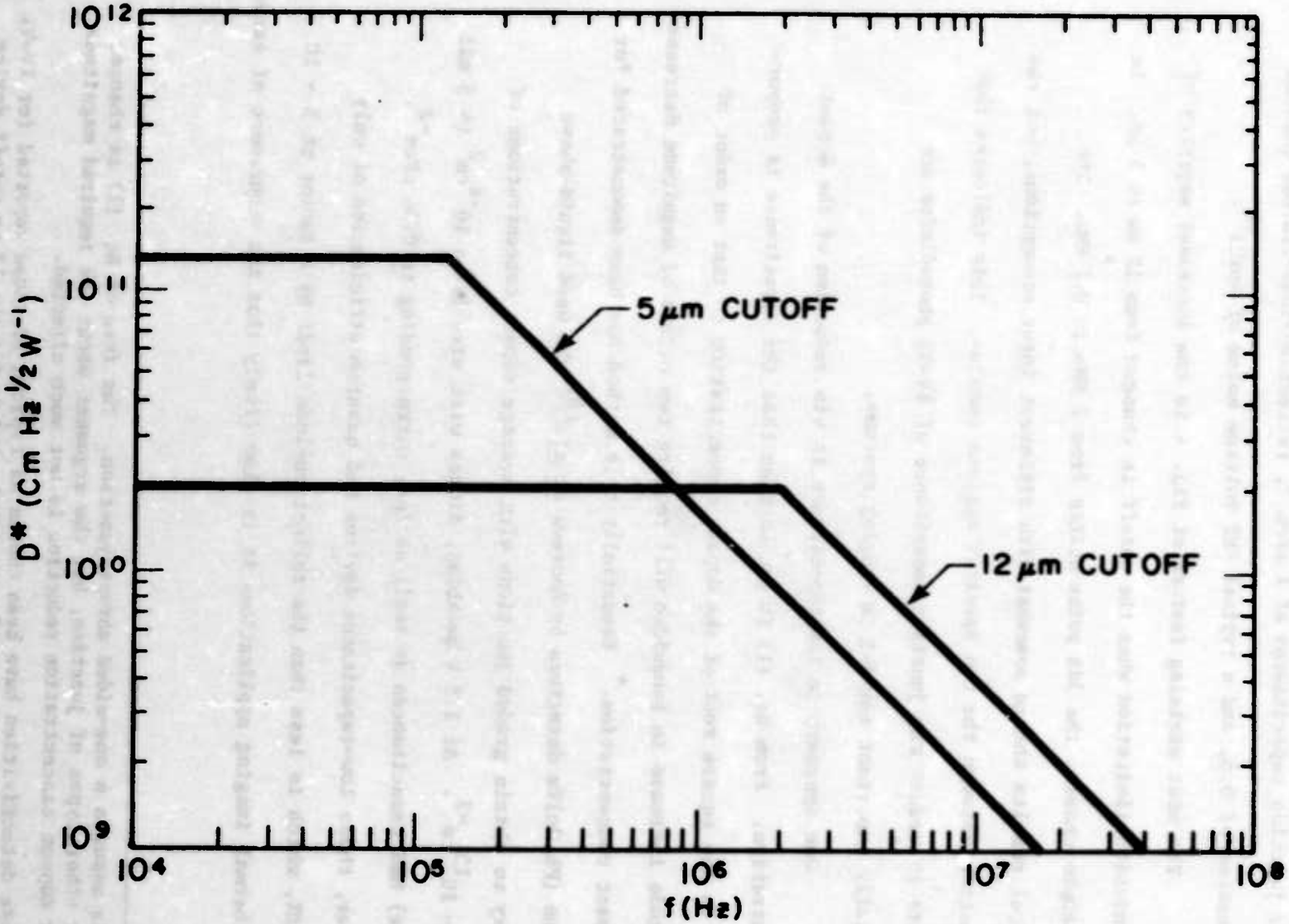

Fig. 4. Frequency dependences of the detectivities of detector/preamplifier combinations. The low-frequency detectivities (D^*_0) were chosen as representative of typical IV-VI detector arrays. The 3db point for other values of D^*_0 may be obtained by extrapolating the frequency-dependent detectivities ($D^*_\infty(f)$) to the new value of D^*_0.

detectivities of 1.3×10^{11} and 2.0×10^{10} $cmHz^{\frac{1}{2}}W^{-1}$, respectively.** We have assumed junction capacitances of 1 μFcm^{-2}, reflection-loss-limited quantum efficiencies of 0.5, and a typical FET voltage noise of $4nVHz^{-\frac{1}{2}}$.

The most striking feature of Fig. 4 is the increased severity of the bandwidth limitation when the cutoff is changed from 12 μm to 5 μm. In the example chosen, the 3dB point shifts from 2 MHz to 0.1 MHz. The numerical results change somewhat with different input assumptions, but the distinction between the two spectral regions remains. This indicates that attempts to reduce the junction capacitance of IV-VI photodiodes are especially important for 3-5 μm imaging systems.

One approach to low capacitance is via reduction of the dopant concentration. From Eq. (1) it can be seen that the capacitance is proportional to the square root of the dopant concentration so that an order of magnitude increase in bandwidth will require two orders of magnitude decrease in dopant concentration.* Essentially this method has been demonstrated for 10.6 μm (Pb,Sn)Te detectors by Andrews et al.[6] who used liquid-phase epitaxy to obtain graded junctions with average dopant concentrations of 10^{14} - $10^{15}cm^{-3}$. At 1.5 V backbias, diodes with area $1.7 \times 10^{-4}cm^2$ (∿ 5 mil square) had capacitances as small as 7pF, corresponding to 0.04 μFcm^{-2}. However, these low-capacitance devices had quantum efficiencies of only 5 - 10%, which is less than the reflection-loss limit by a factor of 5 - 10. For thermal imaging applications it is also likely that the occurrence of excess

---

* This assumes a one-sided abrupt junction. The form of Eq. (1) is changed for other types of junction, but the argument about the required magnitude for dopant concentration reduction is not much affected.

**These detectivities have been chosen as typical of those reported for IV-VI photodiodes at 80K and 180° FOV and the value for the 12 μm cutoff device assumes a significant Johnson noise contribution. The 3dB points for other values of D* may be obtained by extrapolating $D^*_\square(f)$ to the new values of D^*_o.

(1/f) noise will limit the usable backbias to some value less than 1.5 V, so that the appropriate capacitance of these devices may be closer to their zero-bias value of about 0.16 μFcm^{-2}.

In selecting approaches to low-capacitance IV-VI photodiodes for 3-5 μm thermal imaging applications we sought an alternative to the low-dopant concentration method, which appears to have two disadvantages:

(i) The necessary substantial reduction in the dopant concentration requires the development of growth techniques that would be expected to be different for each IV-VI semiconductor. Thus, results obtained with one material such as PbTe, would require significant further materials effort to permit their transfer to another semiconductor, such as Pb(Se,Te) or (Pb,Sn)Se.

(ii) As so far demonstrated with (Pb,Sn)Te, the attainment of small capacitance has required an unacceptable sacrifice of quantum efficiency and hence of detectivity (by a factor of 2-3 in the background limit and of 5-10 for Johnson-noise-limited devices). Thus, it would be necessary to greatly improve upon the quantum efficiency that has been previously obtained with such 10.6 μm devices.

The alternative approaches to low capacitance that we have chosen are based upon the concept that the capacitance of a photodiode may be reduced by reducing the p-n junction area to some fraction of the detector active area. In broad terms, this somewhat resembles the idea of concentrating

the incident photons by use of an immersion lens.* The difference is that here we are concerned with concentration of the photogenerated minority carriers after the photons have been absorbed. This concept gives two branches, both of which lead to radical departures from conventional photodiode geometry.

The first branch leads to a device that we have named the pinched-off photodiode. The idea is shown in Fig. 5a. A thin-film photodiode is configured to have its depletion region extend from an n^+ region right through the semiconductor to an insulating substrate. Thus, the boundary between the depletion and p regions is confined to the periphery of the detector and the dynamic capacitance is reduced to that associated with the peripheral junction area. Photogeneration occurs within the depletion region and the holes are collected at the periphery of the junction.

The second branch leads to another new device that we have named the lateral-collection photodiode. This is illustrated in Fig. 5b. Here the n region of a conventional photodiode is replaced by a matrix of small n regions that give a smaller total junction capacitance. With appropriate choice of dimensions, photogenerated minority carriers diffuse laterally to the small p-n junction collectors with only a minor decrease in the overall quantum efficiency.

The pinched-off and lateral-collection photodiodes are sufficiently different that they are treated separately in Sections 4 and 5, respectively, of this report. A comparison of the two approaches is given in Section 6 together with some recommendations for further development.

---

* In an elegant variation of the immersion lens technique, Andrews et al.[7] have obtained light concentration of an order of magnitude by using total internal reflection from the sides of a tapered PbTe mesa that was terminated by a PbTe/(Pb,Sn)Te heterojunction.

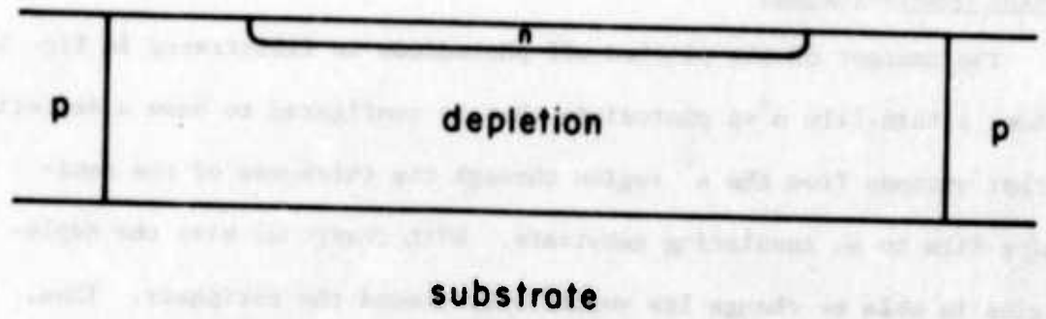

substrate

-a-

p

substrate

-b-

Fig. 5 Schematic diagrams of low-capacitance photodiodes. (a) The pinched-off photodiode. (b) The lateral-collection photodiode.

4. THE PINCHED-OFF PHOTODIODE

4.1 General Considerations

The concept of the pinched-off photodiode is illustrated in Fig. 5a, which shows a thin-film n^+-p photodiode that is configured to have a depletion region that extends from the n^+ region through the thickness of the semiconducting film to an insulating substrate. With change of bias the depletion region is able to change its volume only around the periphery. Thus, the change in the volume of the depletion region and, hence, in the stored charge is greatly reduced from that for a conventional photodiode. Since operationally we are concerned with a dynamic capacitance

$$C \equiv \frac{\partial Q}{\partial V} ,$$

it follows that the arrangement shown will yield a reduction of the junction capacitance.

For further discussion we consider PbTe photodiodes at 80K and use the one-sided abrupt junction approximation, which gives a depletion layer width

$$W_{depl.} = \left[\frac{2\varepsilon(V + V_{bi})}{N_A q} \right]^{\frac{1}{2}} .$$

For pinchoff we require that

$$W_{depl.} \geq d ,$$

where d is the film thickness. Under reasonable biases the depletion layer width will be comparable to the optical absorption length so that the quantum efficiency of the pinched-off photodiode will be modulated by interference.

Selecting the position of the longest-wavelength quantum efficiency maximum to be 5.0 μm, we require that the layer should be approximately* an odd number of quarter waves thick for 5.0 μm radiation. Figure 6 shows the calculated reflection-loss-limited (RLL) quantum efficiencies for such devices with thicknesses from one quarter to seven quarter waves.** The corresponding voltages for pinchoff are given in Table 1. Here we have assumed a typical acceptor concentration of $10^{17} cm^{-3}$. The calculations have been made using both the 300K static dielectric constant with a value of 400 and also a value of 800 to give an idea of the possible influence of the reported paraelectric behavior of PbTe.[8,9]

* For all practical purposes the PbTe/Pb interface behaves as a perfect reflector. However, the phase shift of the reflected wave is not quite π and this gives a slight displacement of the quantum efficiency maxima.

** Details of these calculations are given in Appendix I.

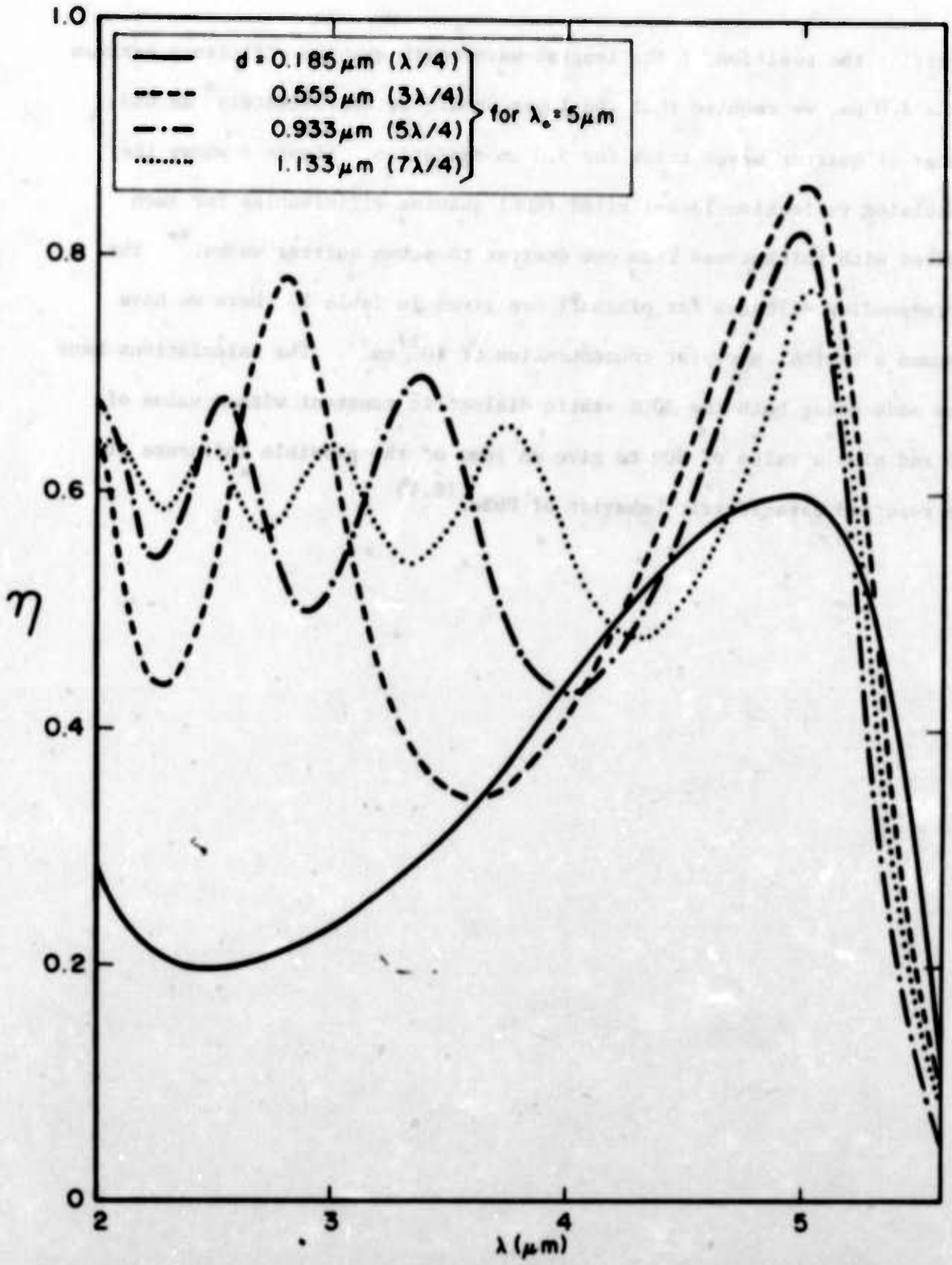

Fig. 6 Calculated RLL quantum efficiencies for PbTe with $p = 10^{17} cm^{-3}$ at 80K.

Table 1. PINCHOFF VOLTAGES FOR PbTe THIN-FILM DIODES

Calculated for $N_A = 10^{17} cm^{-3}$ and $d = \frac{m\lambda}{4}$, (m odd) for 5 μm radiation.

Positive voltages correspond to backbias.

m	d(μm)	V pinchoff (V)	
		$\epsilon = 400\ \epsilon_o$	$\epsilon = 800\ \epsilon_o$
1	0.185	-0.14	-0.18
3	0.555	0.48	0.13
5	0.933	1.75	0.76
7	1.33	3.78	1.78

Inspection of Table 1 shows that the quarter-wave structure should be pinched off at zero bias and that thicker devices should require backbias operation. Generally, zero bias operation is to be preferred because other conditions usually give unacceptable 1/f noise.[2,3,10] However, the lack of experience with very thin (< 0.2 μm) PbTe devices gave uncertainties both about the perfection of quarter-wave layers and about the quality of p-n junctions within them. This led to two approaches.

(i) Use of a quarter-wave structure. Provided that the diode quality and stability were adequate, this would require only about a 25% reduction in the peak RLL quantum efficiencies from those of thicker devices (Fig. 6).

(ii) Use of a three-quarter wave structure. Previous work[2] had demonstrated the RLL quantum efficiency, stability, and zero-bias performance of such devices in PbTe and $PbSe_{0.8}Te_{0.2}$. Success in this approach would depend critically upon reduction of the usual bias-dependent 1/f noise to avoid a sacrifice in detectivity. Devices that are thicker than three-quarter wave were rejected because they would accentuate the 1/f noise problem without giving any obvious advantages.

Having evaluated the RLL quantum efficiency there remains to be considered the collection efficiency for carriers that are generated within the depletion region of the structure in Fig. 5a. Here there is not yet an adequate theoretical analysis. However, early experimental results indicated that collection efficiencies near unity are attainable. Figure 7a shows the C-V characteristic of a typical three-quarter wave PbTe device at 80K. In backbias there is a marked decrease of the capacitance as the diode pinches off. Figure 7b shows a pair of I-V characteristics from the same specimen;

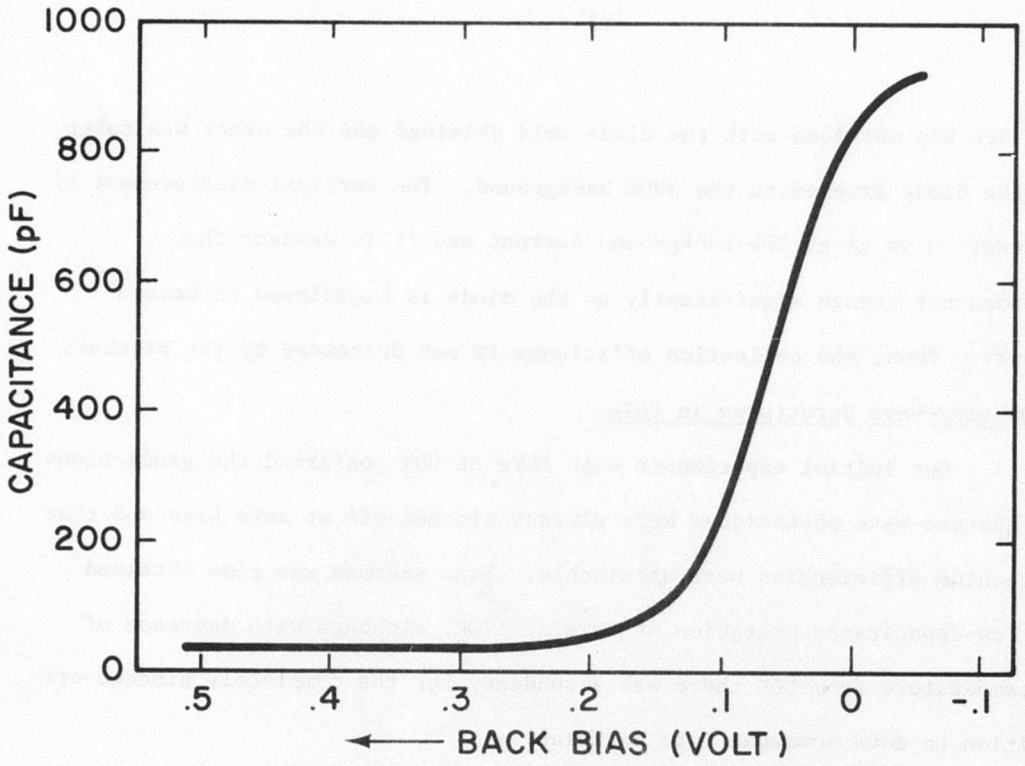

a

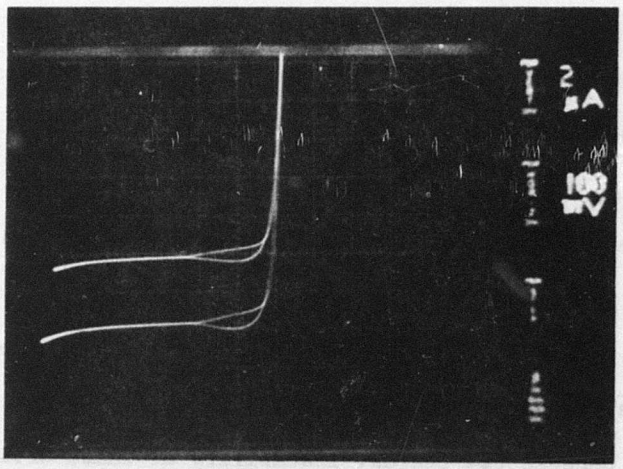

b

Fig. 7 C-V and I-V characteristics of an 18 mil PbTe device at 80K (EW507-5i). In (b) the lower curve shows the response to the 300K background.

one trace was obtained with the diode cold shielded and the other was taken with the diode exposed to the 300K background. The vertical displacement of the lower curve gives the background current and it is evident that this does not change significantly as the diode is backbiased to beyond pinchoff. Thus, the collection efficiency is not decreased by the pinchoff.

4.2 Quarter-Wave Structures in PbTe

Our initial experiments with PbTe at 80K confirmed the predictions that quarter-wave photodiodes were already pinched-off at zero bias and that RLL quantum efficiencies were attainable. Some success was also obtained with low-capacitance operation of PbTe at 170K, although with increase of the temperature from 80K there was a tendency for the completely pinched-off condition to move somewhat into backbias.

In the course of these studies we found that the quarter-wave devices had poor thermal stability, with loss of current response after moderate baking at 150°C. This effect was troublesome experimentally because, as in our previous work[2,3], the PbTe devices required some baking before they would exhibit RLL photocurrents and normal I-V characteristics. The degradation also appears to be practically significant, because stability at temperatures in the range 100-150°C is desirable for reduction of the outgassing in vacuum-packaged devices.

The remainder of this section is devoted to the experimental results with quarter-wave structures. In some cases the conclusions drawn are tentative because the thermal instability of these devices prompted us to move on to the three-quarter-wave structures (described in Section 4.3) rather than attempt a more detailed study of the quarter-wave structures.

4.2.1 Fabrication

Generally, five element arrays of 9 mil-square photodiodes (Fig. 8) were made with techniques that followed those described in previous reports.[1-4] The process steps were:

(i) Growth of PbTe on BaF_2 in vacuum.

(ii) Photoresist delineation and etching of the PbTe using 5% by volume of Br_2 in HBr.

(iii) Photoresist delineation and deposition of Pt ohmic contacts by rf sputtering followed by acetone stripping of the resist to delineate the Pt.

(iv) Vacuum deposition of an insulating layer of BaF_2 with delineation as in Step (iii).

(v) Deposition of Pb through a close-spaced metal mask.

The resist used was Shipley AZ-1350J and Steps (iii) and (iv) were basically those developed by Aeronutronic-Ford for Pb(Se,Te) arrays.[4] One significant difference was that extra precautions were taken in washing the specimens after photoresist development. This modification is particularly relevant to the three-quarter-wave structures and its description and discussion are deferred to Section 4.3.

The deposition of the Pb barrier layer was made using a close-spaced metal mask, rather than with photolithographic delineation, in order to reduce the number of process steps during which the PbTe surface might become contaminated. For the present devices the large diode to diode spacing (30 mil) permits such a simple approach. However, this technique did lead to a relatively large pad area ($2\text{-}4 \times 10^{-3} cm^2$), which with

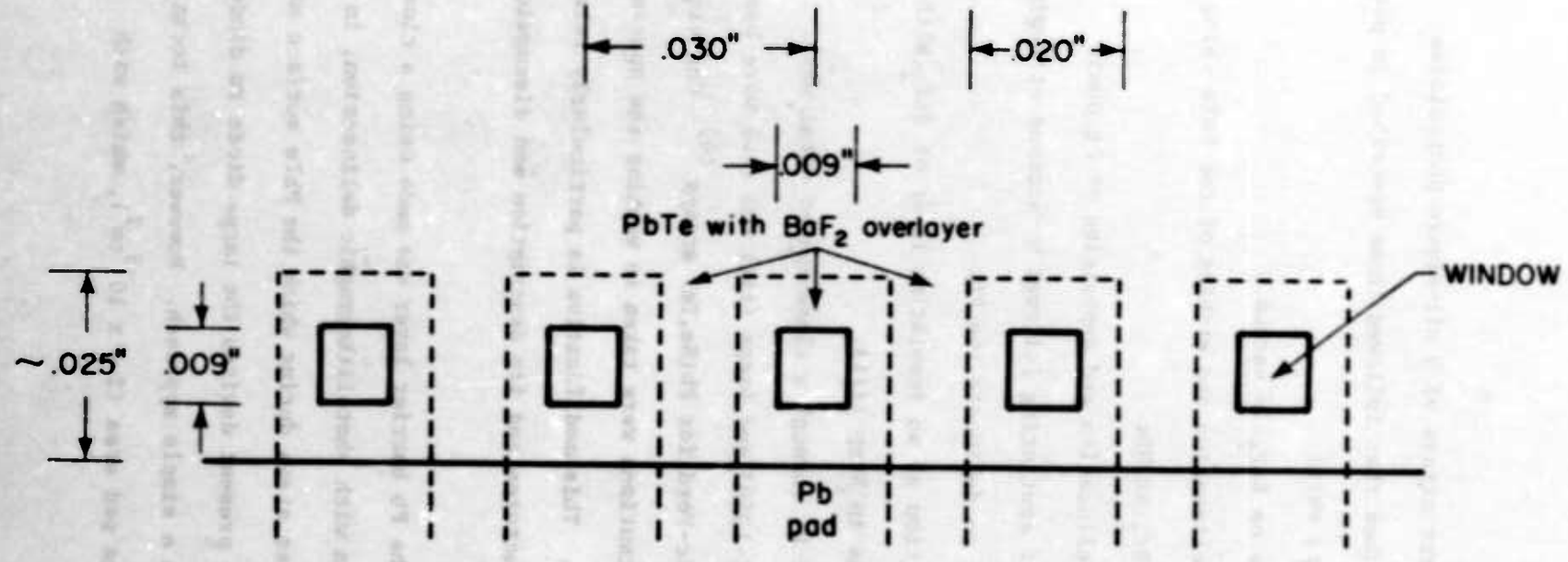

Fig. 8 Layout for 9 mil-square diodes.

typical BaF_2 thicknesses (0.3 - 0.6 μm) gave pad capacitances of 20-80 pF. These pad capacitances are small by comparison with the 500-1000 pF junction capacitance of a conventional 9-mil square photodiode, but they become dominant in the pinched-off mode.

As will be seen, full exploitation of the pinched-off photodiode requires reduction of the pad capacitance and this implies the use of photolithographic techniques for Pb delineation. This extension was not undertaken in the present study. However, for studies of the junction capacitance some improvement in the ratio of pad to junction capacitance was obtained by using large diodes. This approach is described in Section 4.3.

4.2.2 Quantum Efficiencies and Thermal Degradation

Our initial experiments were with PbTe layers whose thicknesses (0.25 ± 0.03 μm) were somewhat larger than the optimum. Consequently, the quantum efficiency near λ = 5 μm was about half of the optimum that was calculated for a quarter-wave structure. However, the spectral quantum efficiency was in fair agreement with the calculated RLL (Fig. 14) implying near unity collection efficiency for the 9 mil pinched-off photodiodes. Reduction of the PbTe layer thickness to about 0.15 μm gave the anticipated improvement in the quantum efficiency near λ = 5 μm, again in agreement with the calculated RLL (Fig. 16).

At this stage we observed that the quarter-wave structures were thermally unstable. As in our previous studies, the diodes as-made had small photocurrents and tunnel-like I-V characteristics. The cause of these anomalies has not been established, but we suspect that they arise from contamination of the PbTe surface, possibly by a thin layer of oxide.

We had previously found that moderate baking (typically 150°C for 10-20 min) led to normal I-V characteristics and RLL photocurrents. This removal of the anomalies could arise from gettering of a surface oxide by the Pb barrier metal. In the case of the quarter-wave photodiodes the increase of photocurrent with baking was followed by a rapid decrease of photocurrent that made difficult the establishment of an optimum heat treatment. Some typical examples of the changes in the response to the 300K background with baking are shown in Fig. 9.*

The observed thermal degradation of the photocurrent led to the suspicion that we might be diffusing the n-region of the diode through to the BaF_2 substrate. This appears to be confirmed by spot scanning of an array of quarter-wave devices which showed that after degradation the response was confined to the peripheries of the 9-mil square diodes (Fig. 11). It is worth noting that the interface regions of epitaxial structures are frequently less perfect than most of the epitaxial layer thickness. Thus, the very thin PbTe layers might give abnormally rapid diffusion of Pb. The variability in the rate of degradation that is shown in Fig. 9 could then be a consequence of variable perfection at the $PbTe/BaF_2$ interface.

4.2.3 Noise

Many of the quarter-wave devices showed significant 1/f noise at zero bias and frequencies up to 5kHz. Such excess noise is occasionally found in conventional IV-VI thin-film Pb barrier devices and there it appears to be associated with the quality of the Pt ohmic contact. The relatively small number of quarter-wave devices that were studied does not permit us to

* The peak values of the background current vary widely from specimen to specimen. However, this variation mostly arises from the very rapid variation of RLL background current with specimen thickness. For the quarter-wave devices, even the uncertainty of ±0.03 μm in the measured thickness corresponds to a large change in the background current. The calculated dependence of the 300K background current upon layer thickness is given in Fig. 10.

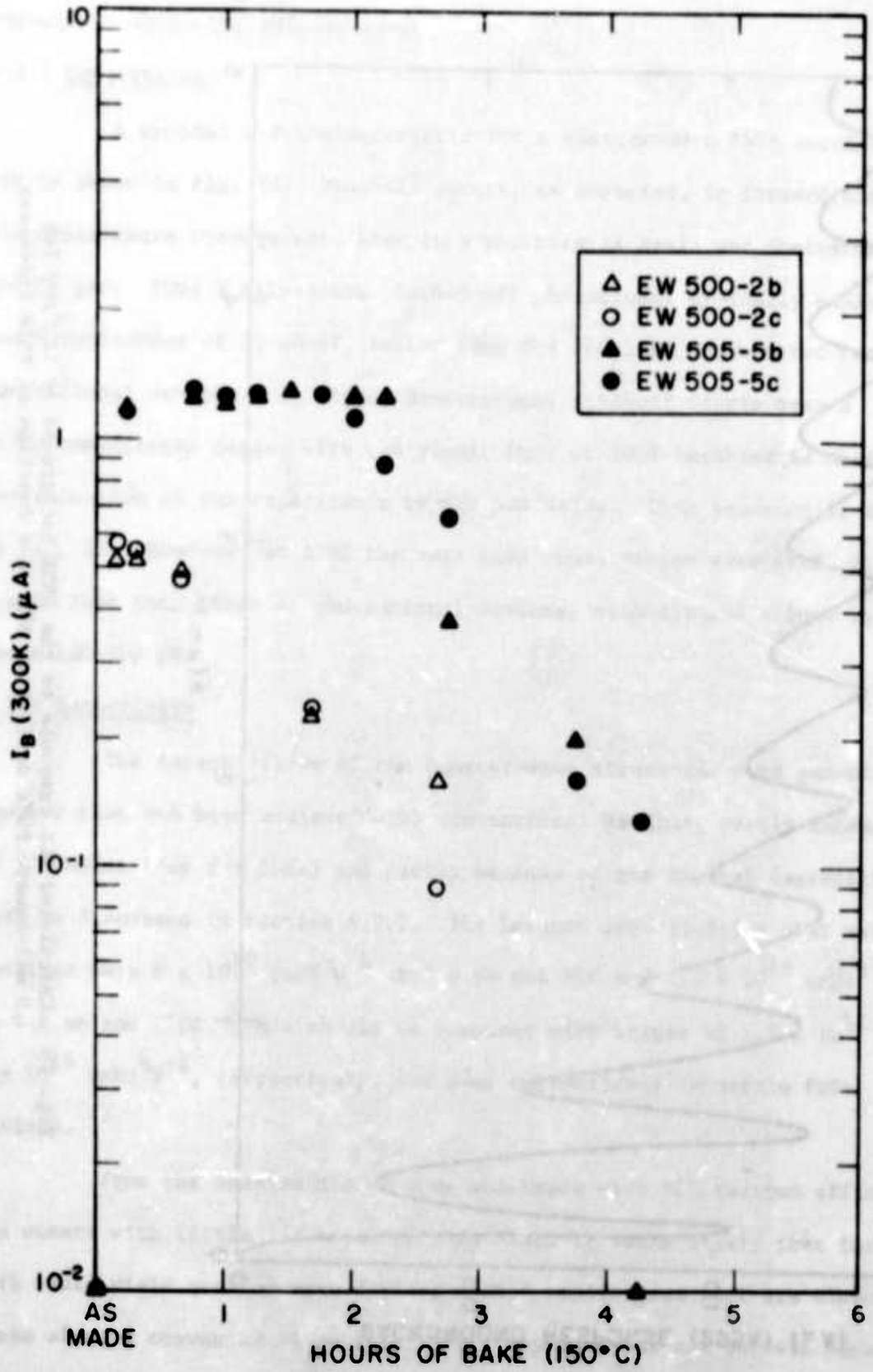

Fig. 9 Degradation of the background response at 80K of λ/4 PbTe devices with baking at 150°C.

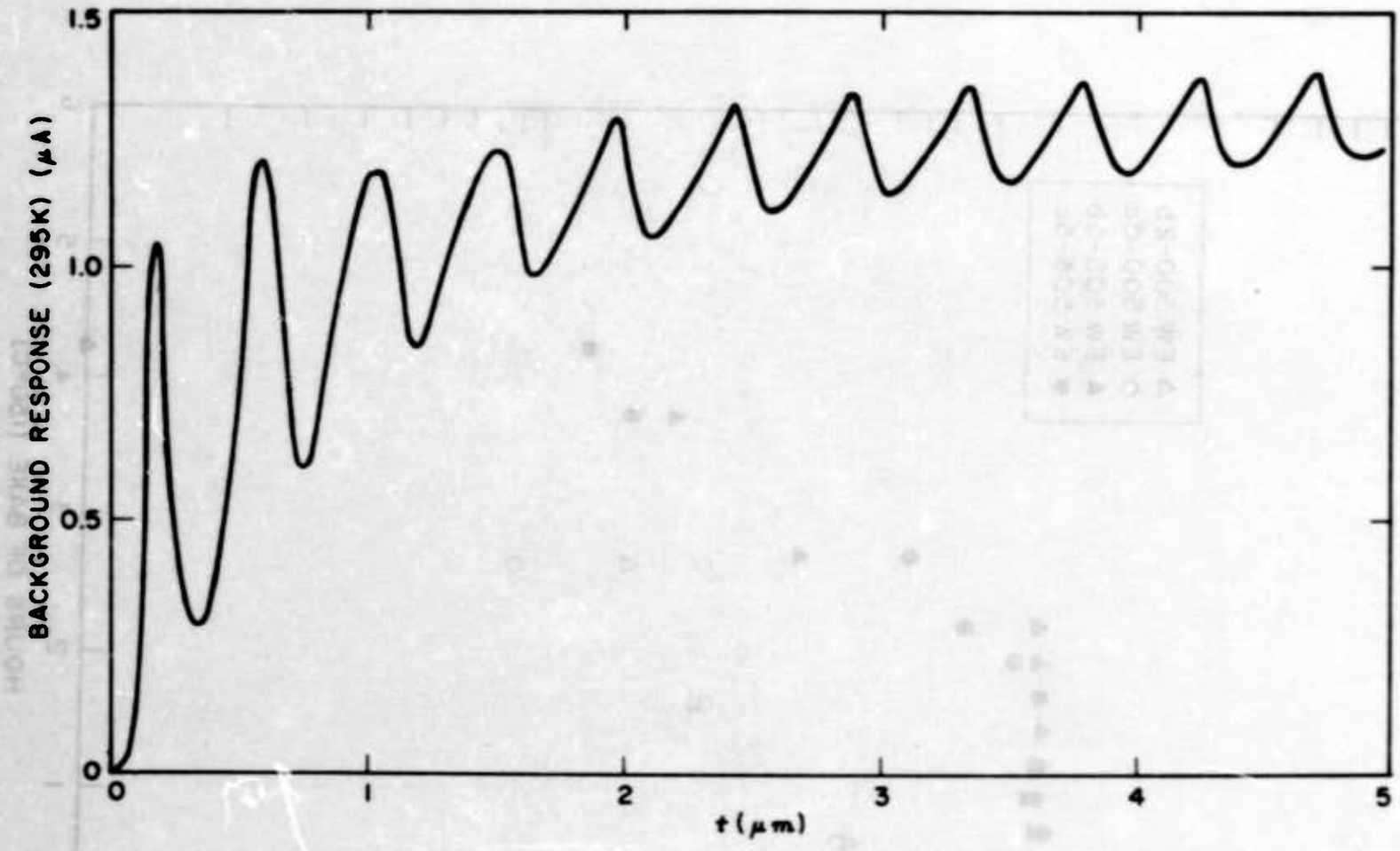

Fig. 10 Calculated RLL response to the 295K background at 180°FOV for 9 mil-square PbTe devices at 80K as a function of PbTe thickness.

decide whether or not 1/f noise is more of a problem with the quarter-wave structures than with thicker devices.

4.2.4 Capacitance

A typical C-V characteristic for a quarter-wave PbTe device at 80K is shown in Fig. 12. Pinchoff occurs, as expected, in forward bias and the capacitance through zero bias into backbias is small and dominated by the Pb pad. Thus 9 mil-square pinched-off photodiodes typically exhibited pad capacitances of 20-80 pF, rather than the 500-1000 pF expected for conventional devices. At higher temperatures pinchoff occurs over a wider temperature range, with the result that at 200K backbias is needed for reduction of the capacitance to the pad value. This behavior is shown in Fig. 13. However, at 170K the zero bias capacitances were still significantly less than those of conventional devices, with typical values in the range 100-200 pF.

4.2.5 Detectivity

The detectivities of the quarter-wave structures were generally smaller than had been achieved with conventional devices, partly because of 1/f noise (for f < 5kHz) and partly because of the thermal degradation that is discussed in Section 4.2.2. The largest detectivities that were obtained were 8×10^{10} $cmHz^{\frac{1}{2}}W^{-1}$ at 5.0 μm and 80K and 1.2×10^{10} $cmHz^{\frac{1}{2}}$ at 4.1 μm and 170K. This should be compared with values of 1.5×10^{11} and 6×10^{10} $cmHz^{\frac{1}{2}}W^{-1}$, respectively, for good conventional thin-film PbTe devices.[2]

From the observation of some specimens with RLL quantum efficiencies and others with little 1/f noise at zero bias, it seems likely that further work would yield quarter-wave devices with detectivities that are closer to those of good conventional devices. This approach was not pursued because of the thermal instability that is discussed in Section 4.2.2.

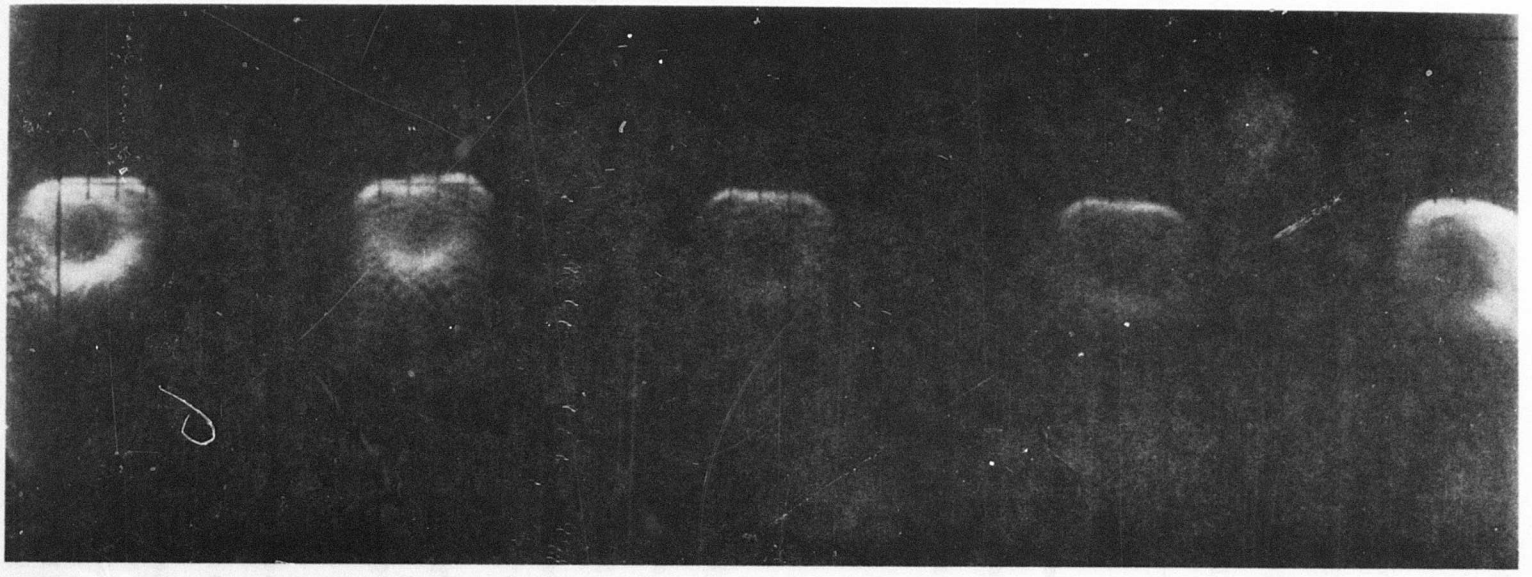

Fig. 11 Spot scan of a thermally-degraded array of λ/4 PbTe devices (EW493B-9). (This scan was supplied by NVL.)

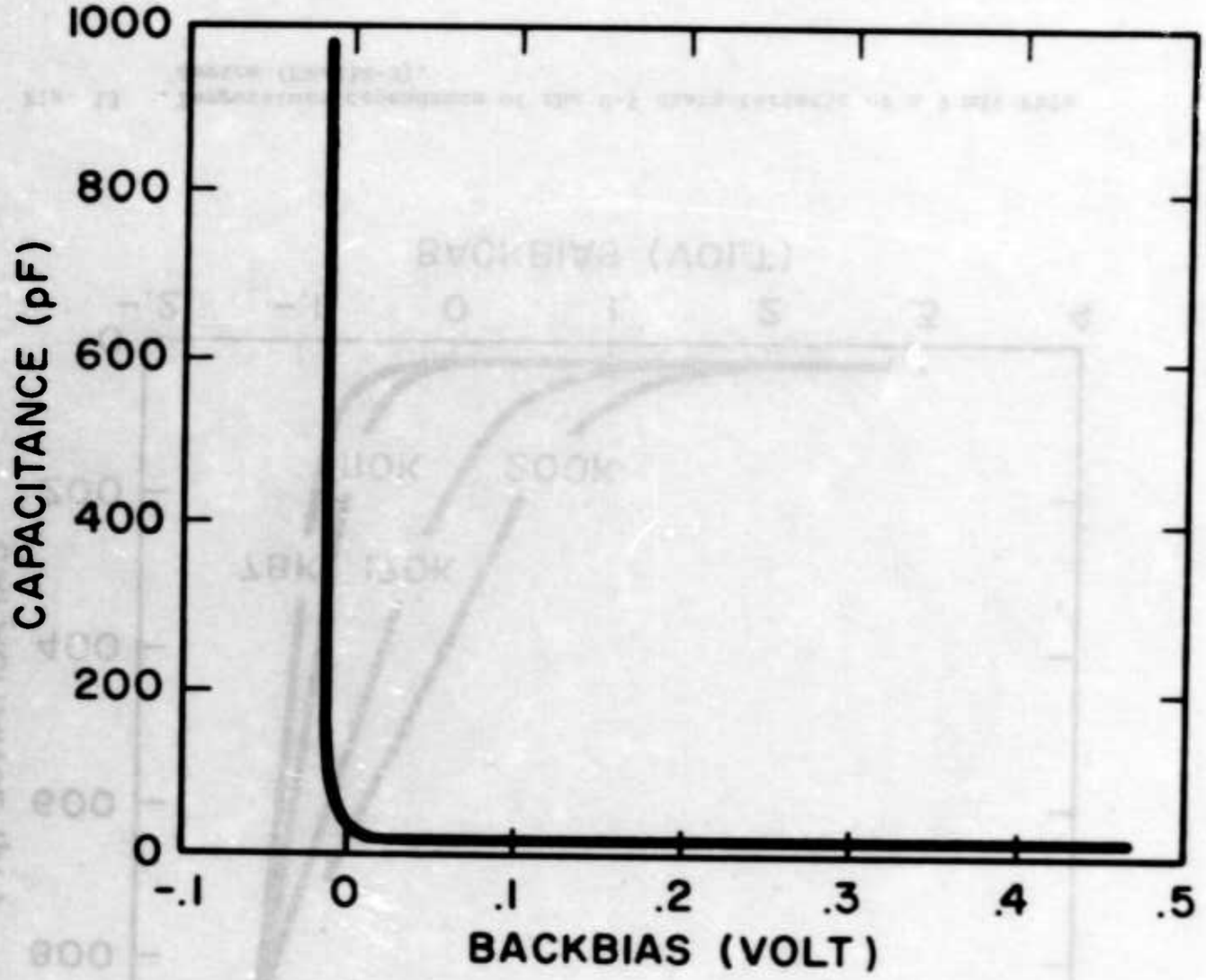

Fig. 12 C-V characteristic of a 9 mil λ/4 PbTe device at 80K (EW494B-7).

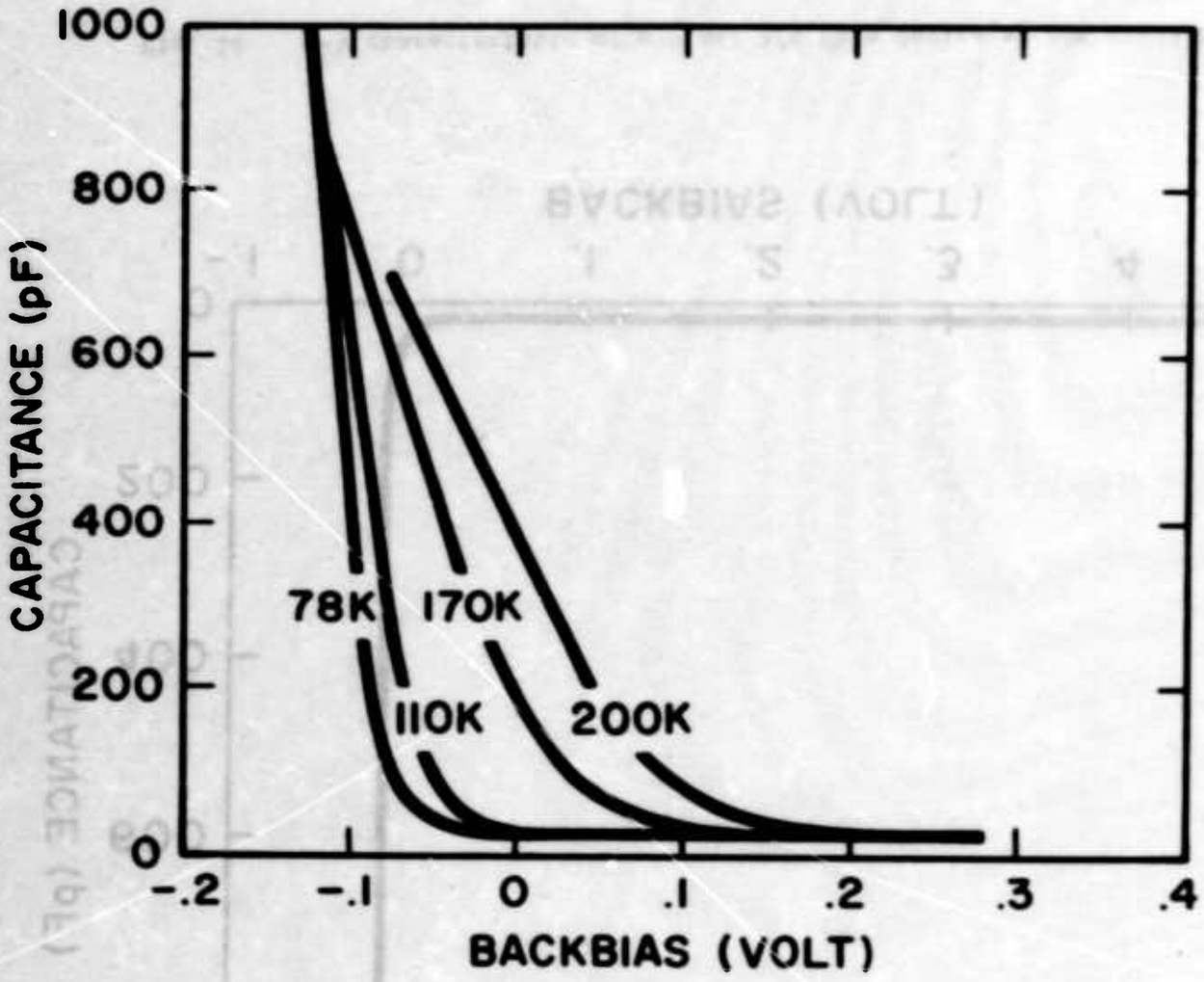

Fig. 13 Temperature dependence of the C-V characteristic of a 9 mil PbTe device (EW493A-3).

4.2.6 Measurements of Quarter-Wave Devices

The specimens that are described here illustrate the features that have been discussed in the preceding Sections.

Table 2 - EW485-3

This array was made from PbTe with thickness 0.25 ± 0.03 μm. This gave a spectral response with nonoptimum shape, but, as shown in Fig. 14, the quantum efficiency was close to the RLL. Two out of the five diodes gave noise that agreed well with that calculated from the background current. Measurements were made at 80K and 990 Hz with 10 Hz bandwidth at zero bias. The diode areas were $5.24 \times 10^{-4} cm^2$. Figure 15 shows the spectral detectivity.

Diode	a	b	c	d	e
Zero-bias Capacitance [pF]	37	37	35	32	24
300K Background Current [μA]	0.51	0.54	0.54	0.53	0.54
Calc. Background Noise [pA]	1.3	1.3	1.3	1.3	1.3
$\mathcal{R}_I$(500K) [AW^{-1}]	0.25	0.275	0.25	0.25	0.24
η(4.7 μm)	0.35	0.38	0.35	0.35	0.33
Noise [pA]	1.2	1.25	6.2	1.7	14*
D*(500K) [$cmHz^{\frac{1}{2}}W^{-1}$]	1.5×10^{10}	1.5×10^{10}	2.9×10^{9}	1.1×10^{10}	1.2×10^{9}
D*(5.0 μm) [$cmHz^{\frac{1}{2}}W^{-1}$]	8.2×10^{10}	8.2×10^{10}	1.6×10^{10}	5.8×10^{10}	6.3×10^{9}

* This specimen initially showed a much smaller noise of 1.8 pA.

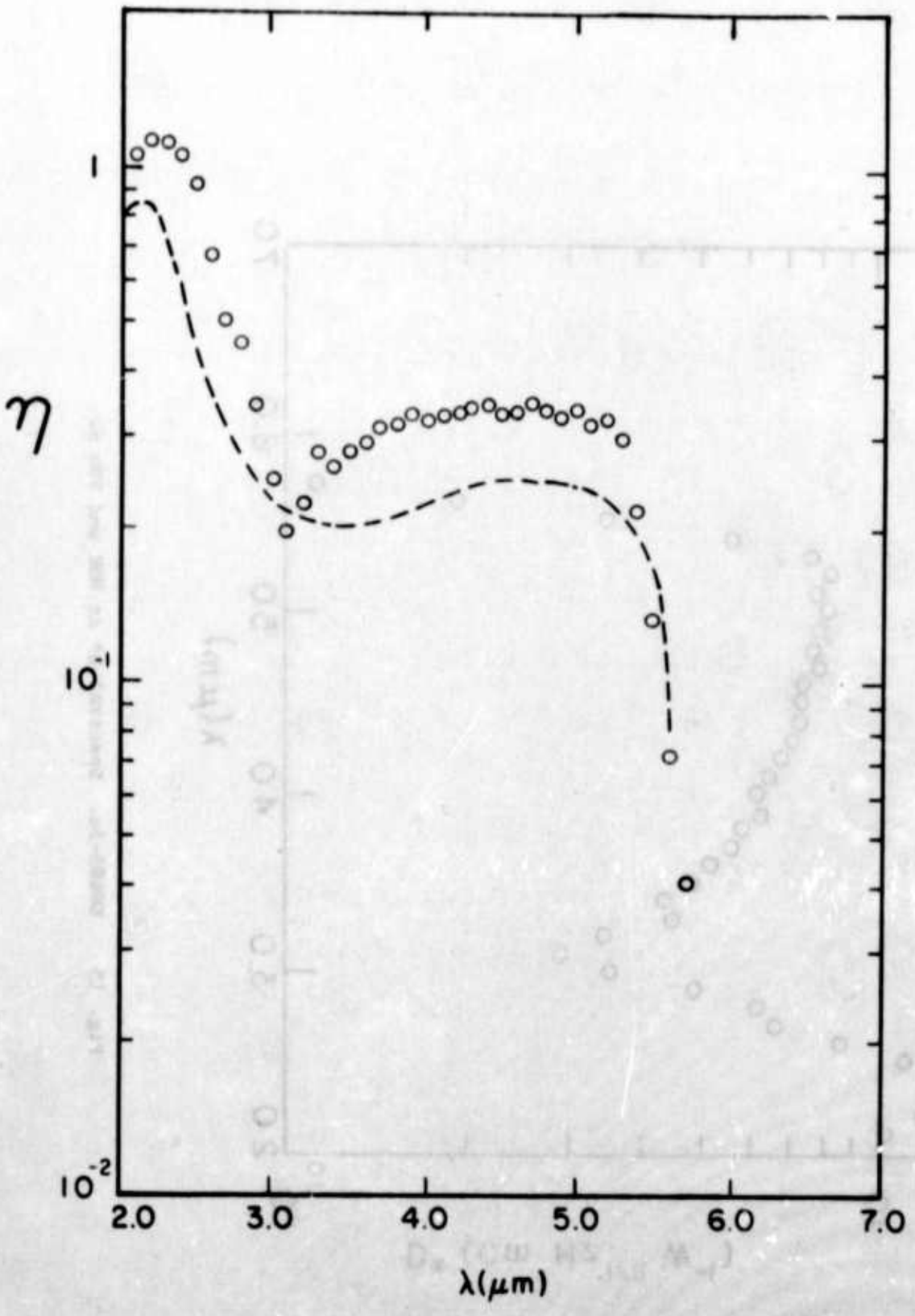

Fig. 14 EW485-3a. Spectral quantum efficiency at 80K. The curve is the calculated RLL.

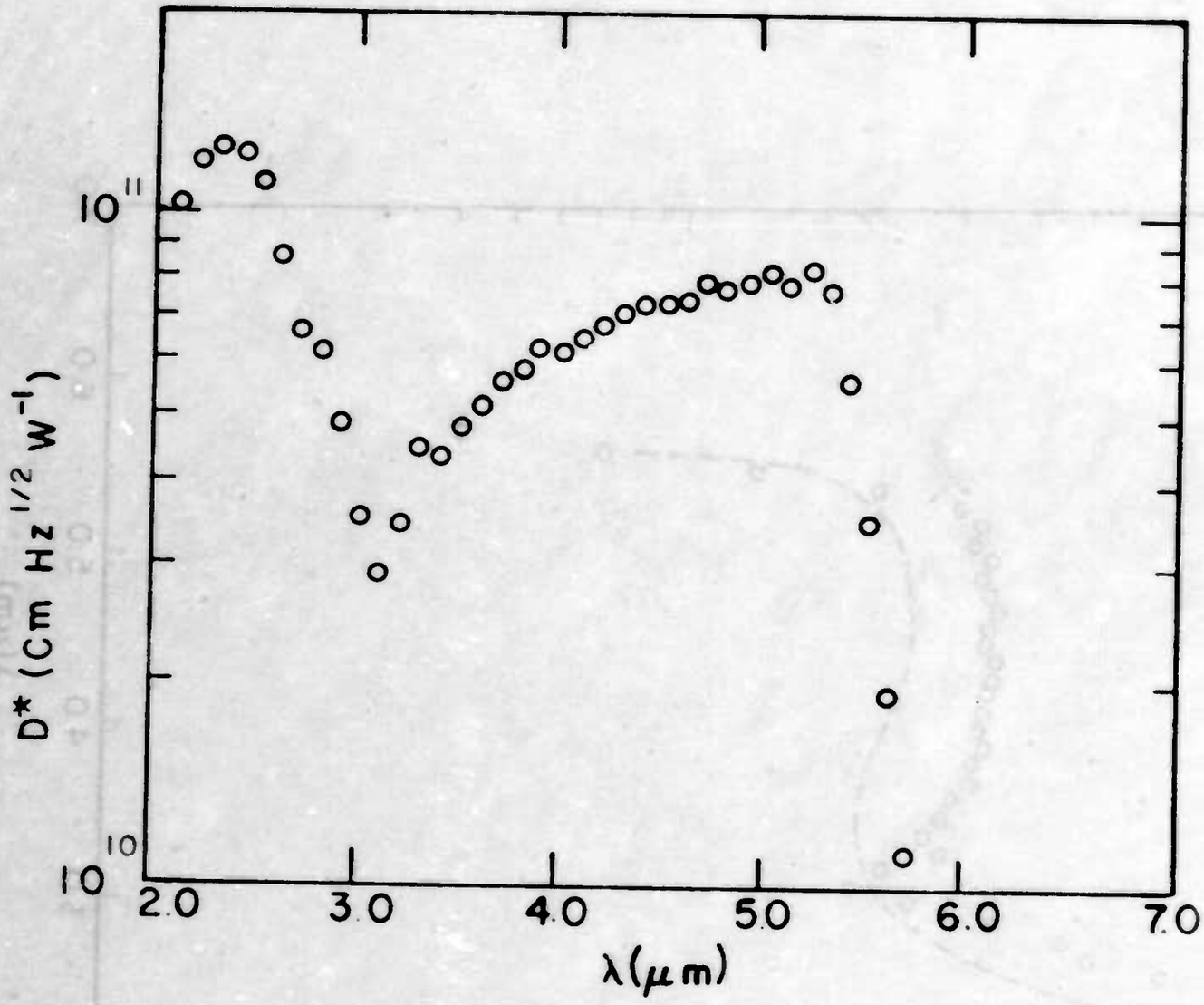

Fig. 15 EW485-3a. Spectral D* at 80K and 990 Hz.

Table 3 - EW494B-7

This array was made from PbTe with thickness 0.16 ± 0.03 μm to give a more usefully shaped spectral response than the preceding example. The spectral quantum efficiency is near the RLL and is shown in Fig. 16. The diode areas were 6.00×10^{-4} cm^2 and measurements were made at 80K with 10 Hz bandwidth. Detailed measurements were made with four diodes, the fifth exhibited a smaller current response. This specimen showed significant 1/f noise for f < 5 kHz. At 170K the pinchoff moved into backbias with consequent increase of the zero bias capacitance from 37 pF and 24 pF to 620 pF and 660 pF for diodes a and c, respectively. The frequency dependences of the current noise and the detectivity are shown in Figs. 17,18.

Diode	a	b	c	d
Zero bias Capacitance [pF]	37	42	24	29
Background Current [μA]	1.03	1.01	1.01	0.76
Calc. Background Noise [pA]	1.82	1.80	1.80	1.56
$\mathcal{R}_I$(500K) [AW^{-1}]				
at 90 Hz	0.44	0.44	0.46	
330 Hz	0.45	0.45	0.44	0.35
990 Hz	0.45	0.46	0.47	
D^*(4.6 μm) [cmHz$^{\frac{1}{2}}$W^{-1}]				
at 90 Hz	1.6×10^{10}	1.9×10^{10}	1.6×10^{10}	
330 Hz	3.5×10^{10}	3.5×10^{10}	3.0×10^{10}	
990 Hz	6.3×10^{10}	6.5×10^{10}	4.7×10^{10}	
5000 Hz	1.1×10^{11}	1.0×10^{11}	8.6×10^{10}	

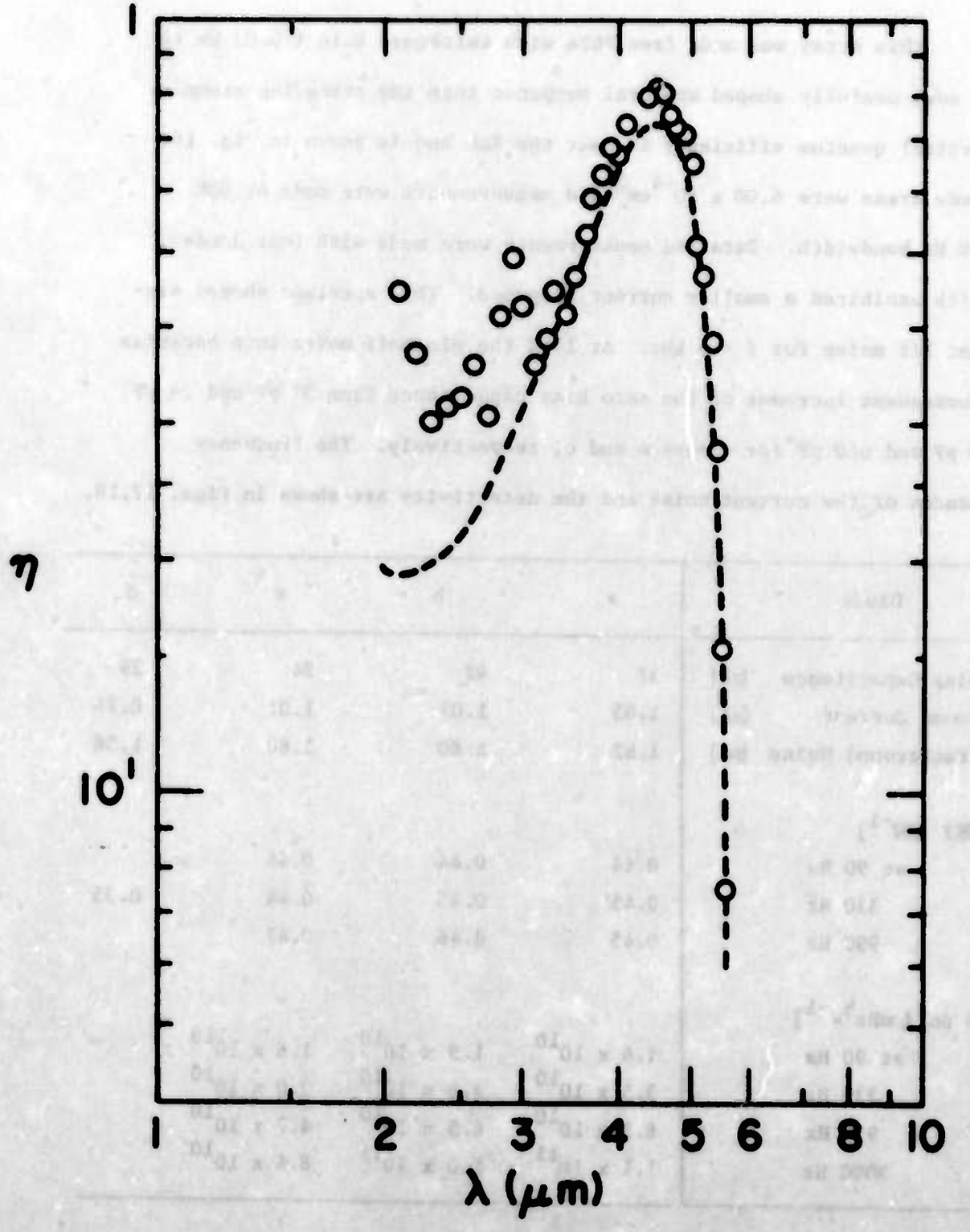

Fig. 16 EW494B-7. Spectral quantum efficiency at 80K. The curve is the calculated RLL.

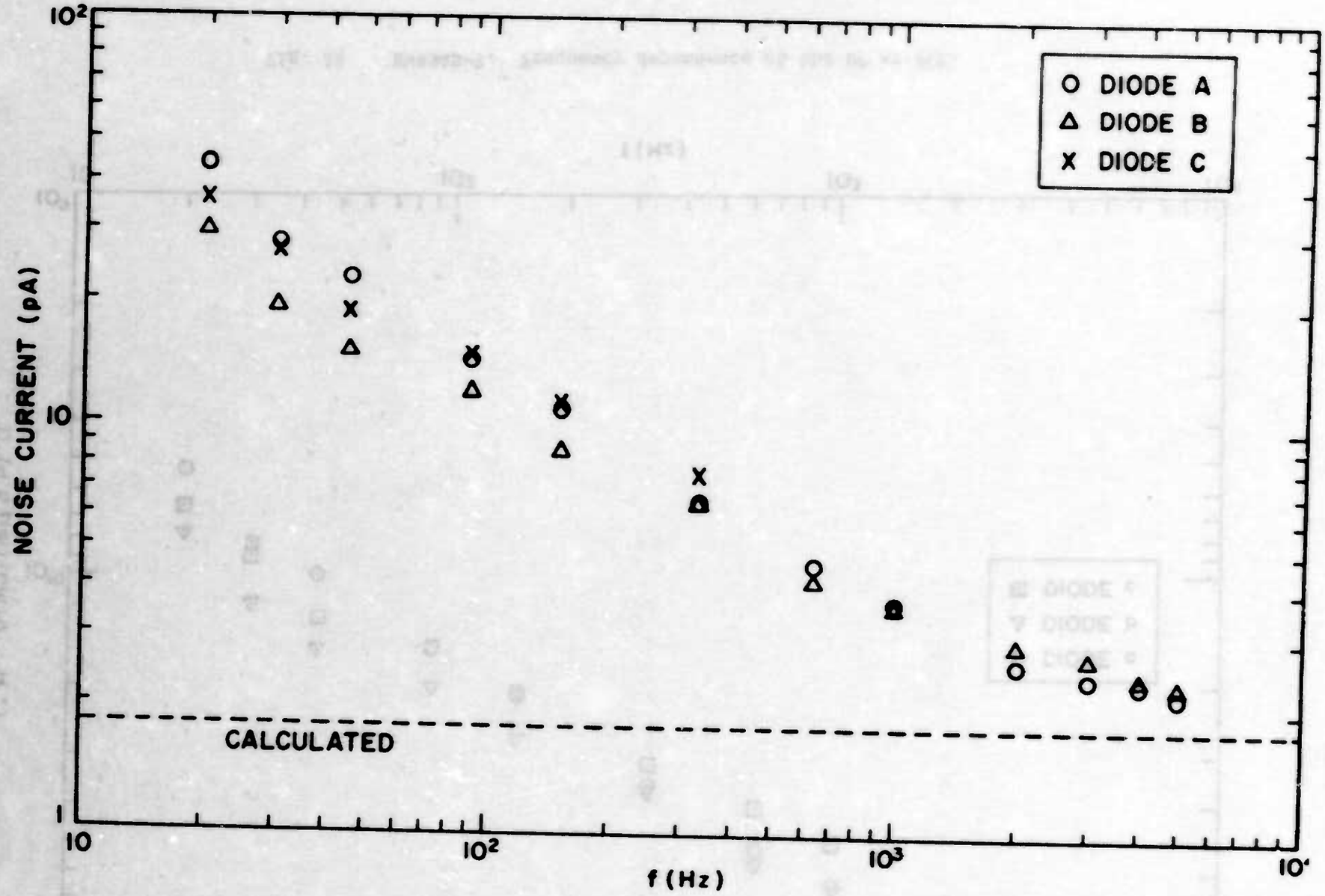

Fig. 17 EW494B-7. Frequency dependence of the noise at 80K (Δf = 10 Hz). The curve is the calculated background noise.

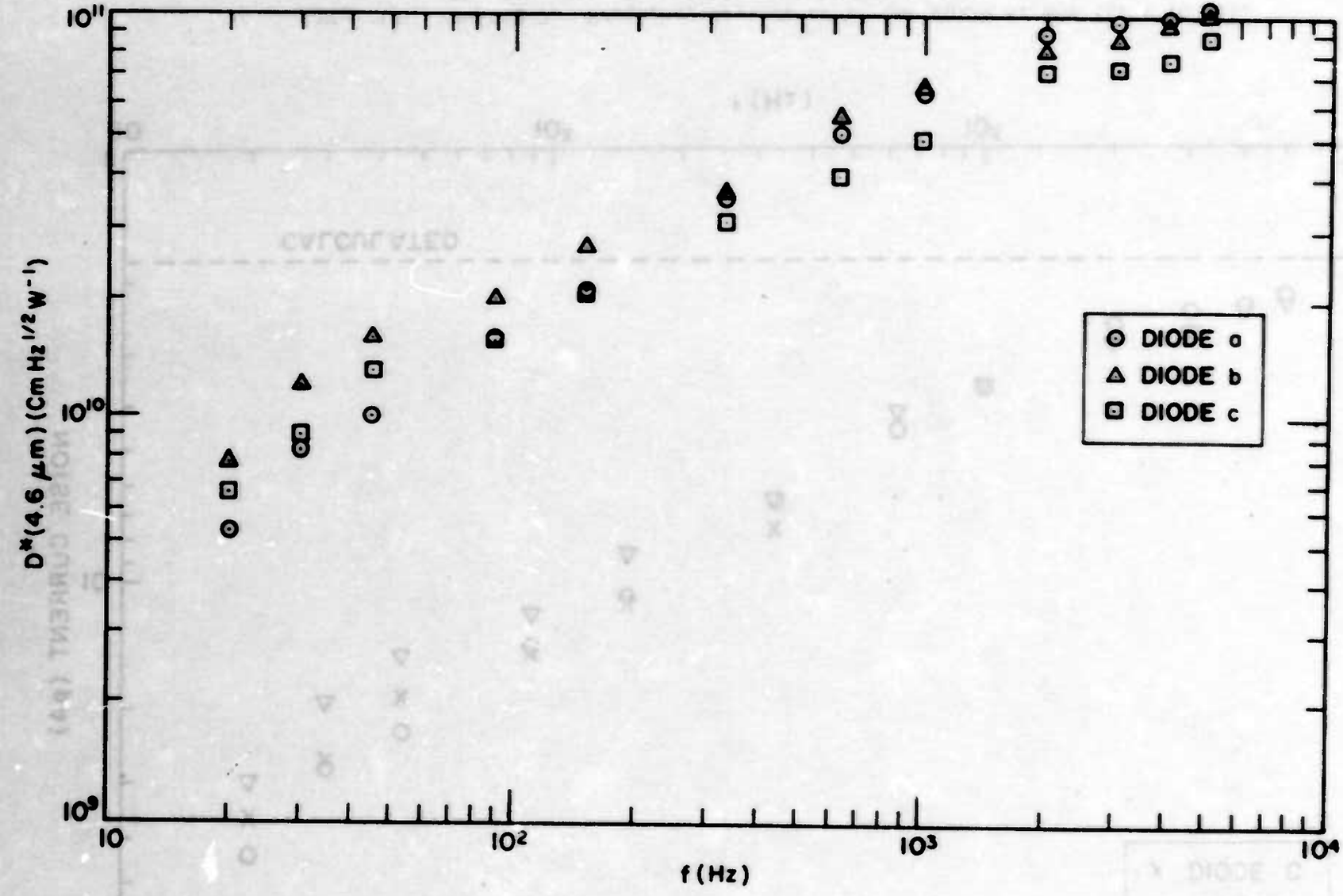

Fig. 18 EW494B-7. Frequency dependence of the D* at 80K.

Table 4 - EW493B-9

This specimen exhibited the thermal degradation of current response that is discussed in Section 4.2.2. There was also significant 1/f noise at 1 kHz. The layer thickness was 9.15 ± 0.03 μm giving a spectral response like that of the preceding example. However, the combination of 1/f noise with small quantum efficiency gave small detectivities. The diode areas were 4.39×10^{-4} cm^2 (180 μm x 244 μm) and the measurements were made at zero bias with 10 Hz bandwidth. The spectral detectivity is shown in Fig. 19.

Diode	a	b	c	d	e
T = 80K, f = 5 kHz					
Zero bias Resistance [ohm]	3.0×10^7	7.7×10^6	1.1×10^7	2.3×10^7	2.0×10^7
R_oA [ohm cm^2]	1.3×10^4	3.4×10^3	4.8×10^3	1.0×10^4	8.8×10^3
Zero bias Capacitance [pF]	35	44	46	46	43
Background Current [μA]	0.083	0.092	0.087	0.116	0.157
Calc. Background Noise [pA]	0.53	0.54	0.53	0.61	0.71
$\mathcal{R}_I$(500K) [AW^{-1}]	0.070	0.083	0.076	0.114	0.150
η(4.1 μm)	0.140	0.166	0.152	0.227	0.299
Noise [pA]	0.85	0.82	0.76	0.81	0.87
D*(4.1 μm) [cmHz$^{\frac{1}{2}}$W^{-1}]	3.6×10^{10}	4.4×10^{10}	4.4×10^{10}	6.2×10^{10}	7.5×10^{10}
T = 170K, f = 990 Hz					
Zero bias Resistance [ohm]	6100	6060	6060	4880	5260
R_oA [ohm cm^2]	2.7	2.7	2.7	2.1	2.3
Zero bias Capacitance [pF]	67	91	91	73	86
Background Current [μA]	0.035	0.038	0.041	0.068	0.079
Calc. Total Noise [pA]	3.9	4.0	4.0	4.4	4.3
$\mathcal{R}_I$(500K) [AW^{-1}]	0.060	0.060	0.064	0.105	0.112
η(3.9 μm)	0.208	0.209	0.223	0.363	0.388
Noise [pA]	5.9	5.8	6.2	6.5	6.7
D*(4.1 μm) [cmHz$^{\frac{1}{2}}$W^{-1}]	7.5×10^9	7.6×10^9	7.6×10^9	1.2×10^{10}	1.2×10^{10}

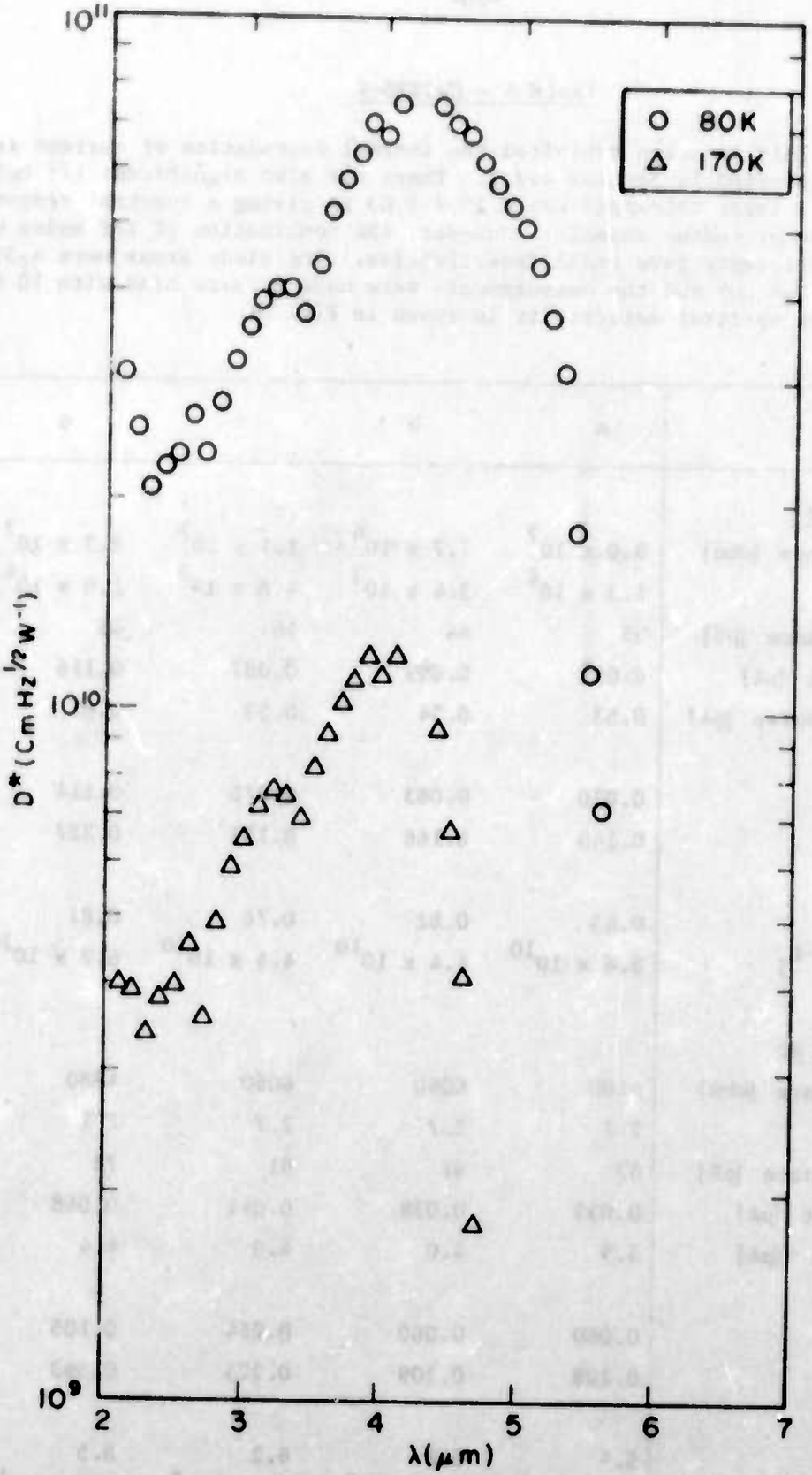

Fig. 19 EW493B-9e. Spectral D* at 80K (5 kHz) and at 170K (990 Hz).

Table 5 - EW500-2

This specimen had close to RLL quantum efficiency. There was some 1/f noise at zero bias for f < 5 kHz. The diode areas were 5.90×10^{-4} cm^2 and the bandwidth was 10 Hz. Measurements were made at 80K. Fig. 20 shows the spectral detectivity, Figs. 21,22 show the bias and frequency dependence of the noise, and Fig. 23 shows the bias dependence of the capacitance.

Diode	a	b	c	d	e
Zero bias Resistance [ohm]	7.46×10^6	7.52×10^6	7.04×10^6	6.90×10^6	
R_oA [ohm cm^2]	4.4×10^3	4.4×10^3	4.2×10^6	4.1×10^6	
Zero bias Capacitance [pF]	96	96	96	96	
Background Current [μA]	0.357	0.357	0.393	0.393	0.200
Calc. Background Noise [pA]	1.07	1.07	1.12	1.12	0.80
$\mathcal{R}_I$(500K) [AW^{-1}]*	0.295	0.290	0.316	0.312	
η(4.8 μm)	0.48	0.48	0.52	0.51	
D*(4.9 μm) at Zero bias [cmHz$^{\frac{1}{2}}$W^{-1} x 10^{10}]					
f = 20 Hz	2.6	2.7	2.3	2.5	
30 Hz	2.9	3.1	3.0	2.8	
45 Hz	3.5	3.4	3.5	3.3	
90 Hz	4.5	5.0	4.4	4.2	
330 Hz	7.7	7.0	7.7	7.7	
990 Hz	10	10	10	10	
2000 Hz	11	11	11	11	
5000 Hz	13	13	14	13	
D*(4.9 μm) at 990 Hz [cmHz$^{\frac{1}{2}}$W^{-1} x 10^{10}]					
backbias = 0 V	10.0	9.4	9.7	9.1	
0.1 V	9.4	9.4	9.1	9.4	
0.2 V	9.1	9.7	4.5	4.9	
0.3 V	8.6	9.1			
0.4 V	7.3	6.9			

*This was independent of backbias in the range 0-300 mV.

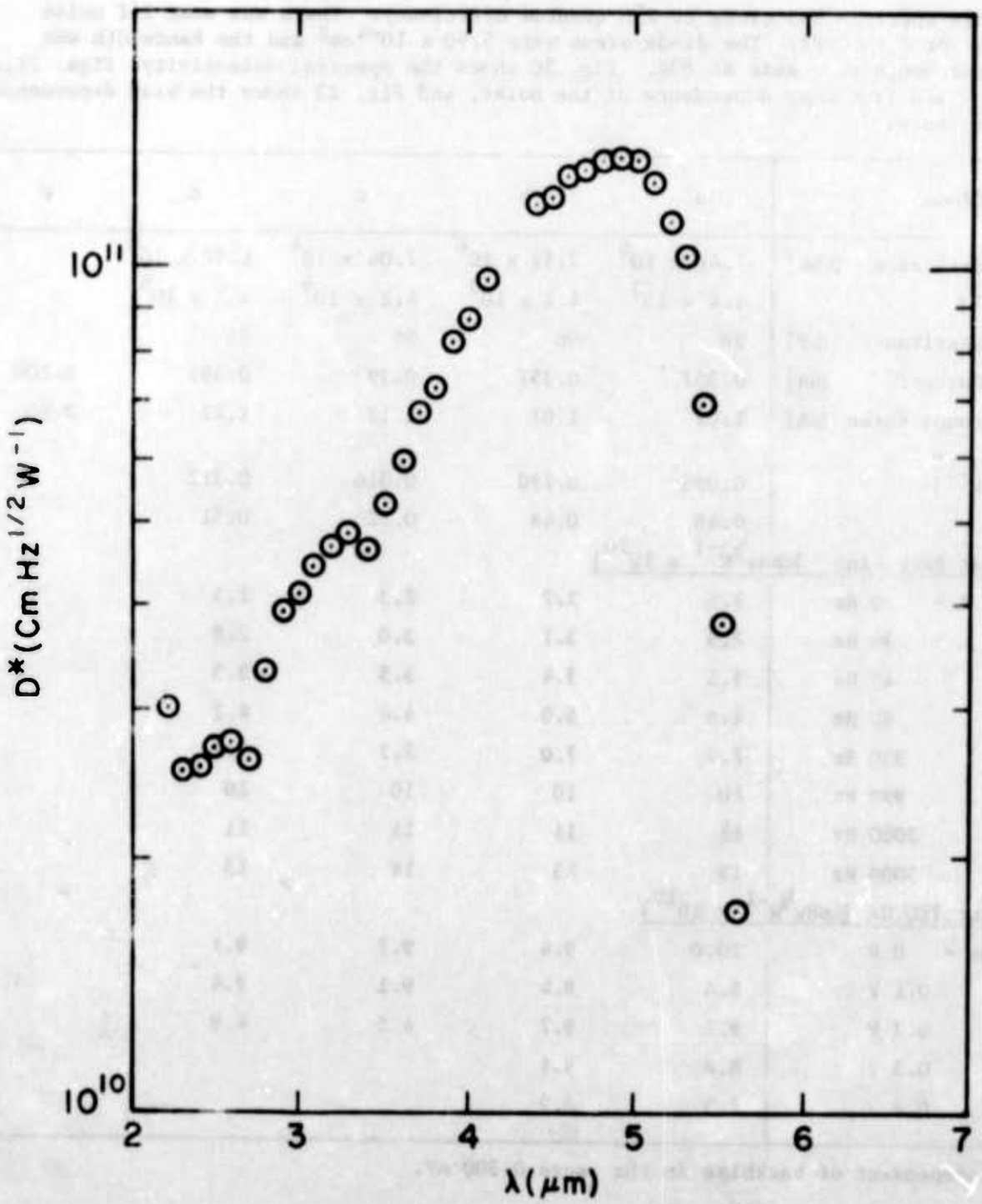

Fig. 20 EW500-2c. Spectral D* at 80K and 5 kHz.

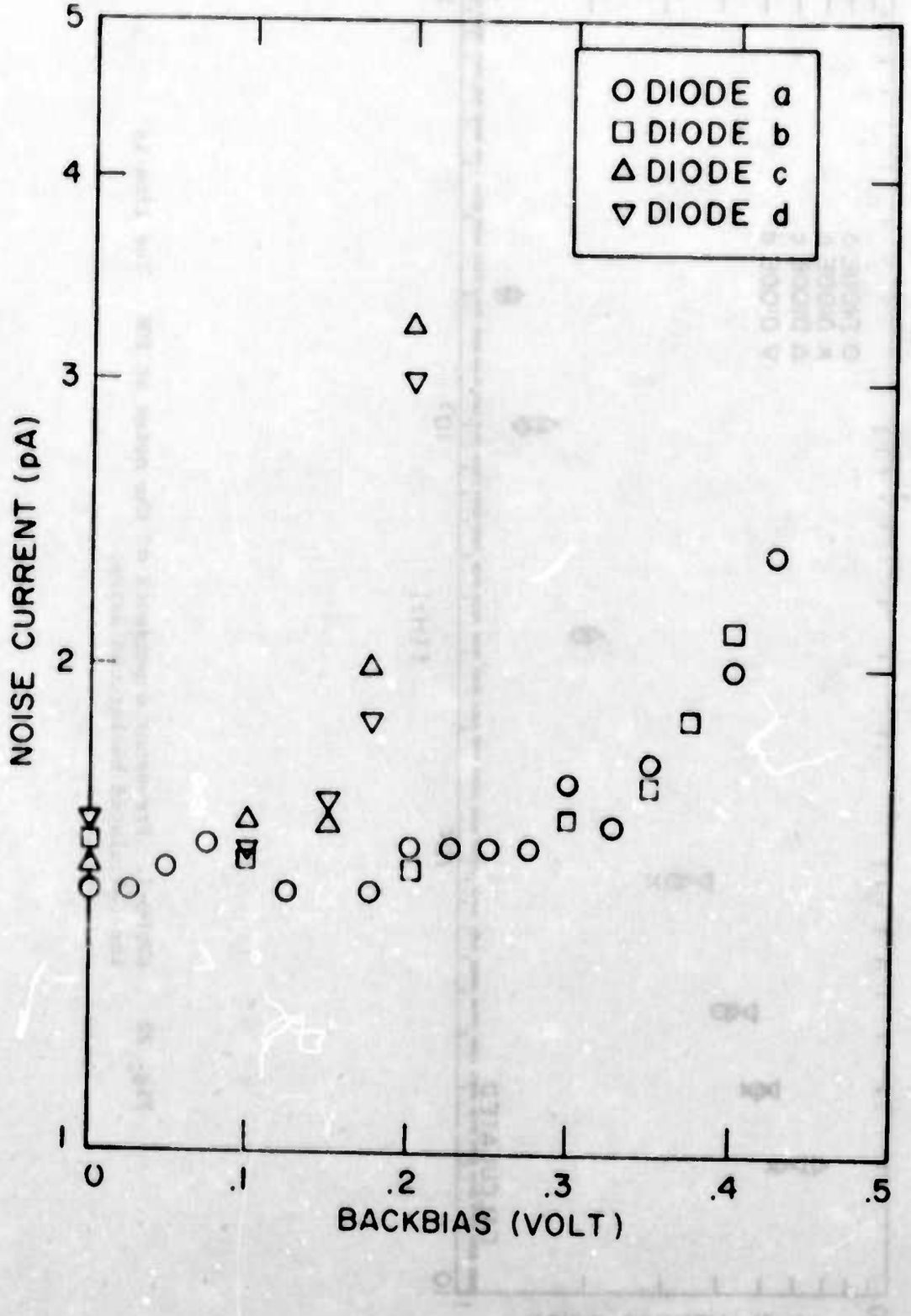

Fig. 21 EW500-2. Bias dependence of the noise at 80K (Δf = 10 Hz).

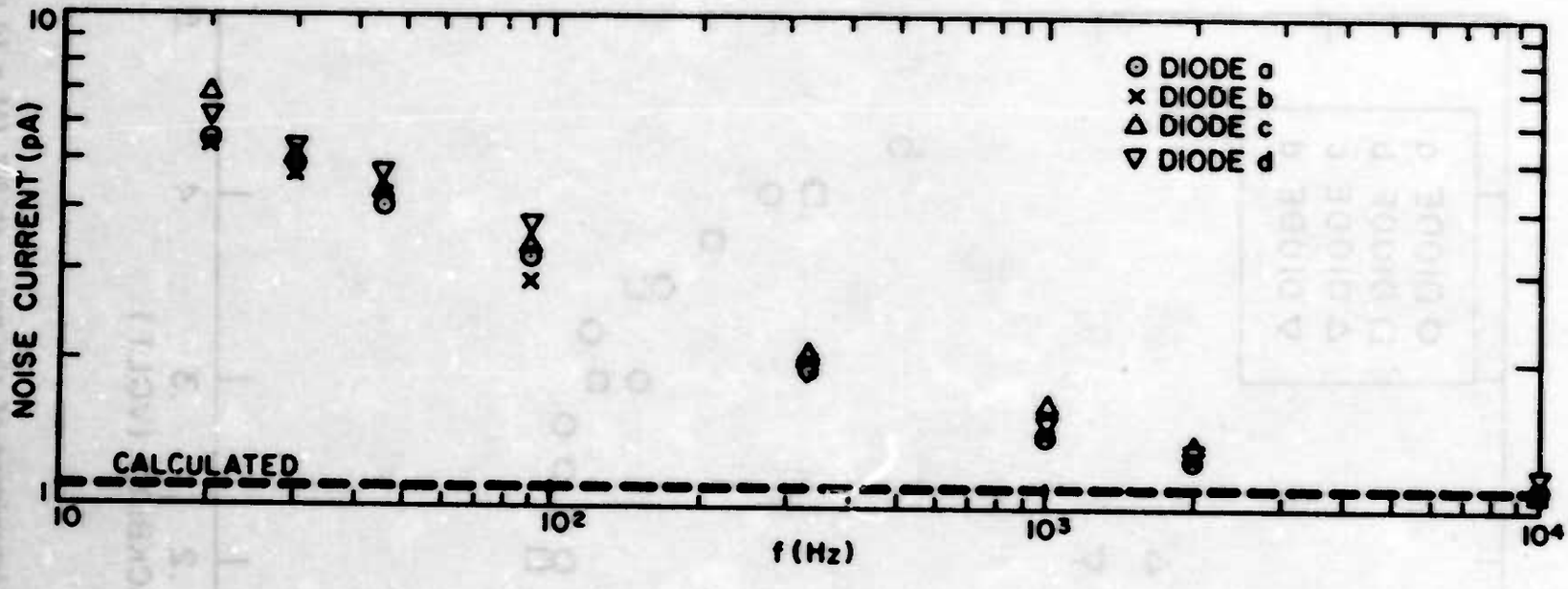

Fig. 22 EW500-2. Frequency dependence of the noise at 80K. The line is the calculated background noise.

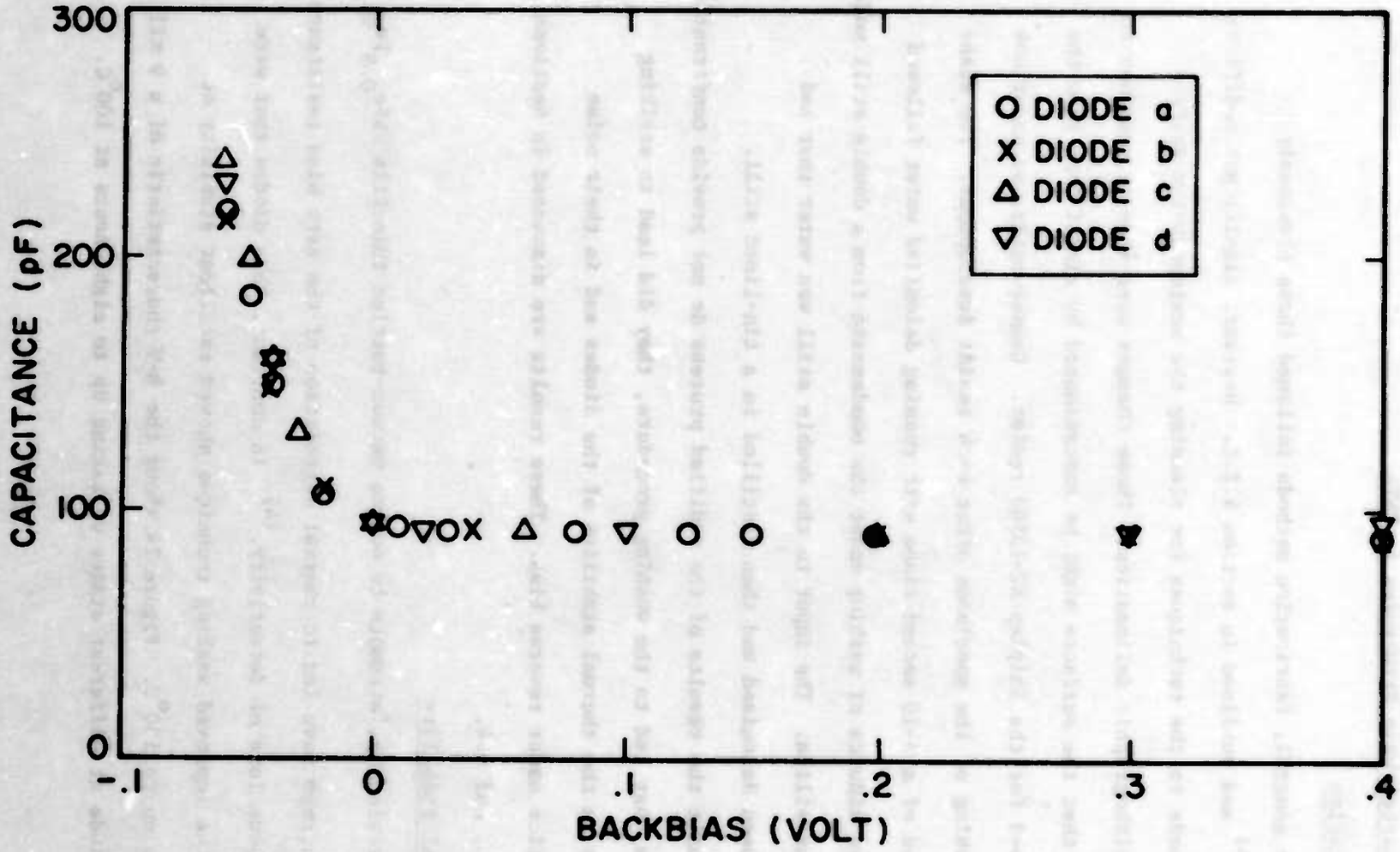

Fig. 23 EW500-2. Bias dependence of the capacitance.

4.3 Three-Quarter-Wave Structures in PbTe

4.3.1 Fabrication

In general, fabrication methods followed those previously reported[2-4] and outlined in Section 4.2.1. However, significant modifications were made to the techniques for cleaning the semiconductor surface after photolithographic delineation. These changes were made in response to the thought that the surfaces might be contaminated by alkali ions from the developer used for the Shipley AZ-1350J resist. Consequently, we undertook thorough washing of the specimens after each resist development. The washing consisted of a 5-10 second rinse with running deionized water followed by about five minutes of washing under the condensate from a double still made from vitreous silica. The input to the double still was water that had previously been deionized and then distilled in a tin-lined still.

While the results of the modified process do not provide confirmation of the guess that led to the washing procedure, they did lead to striking improvements in the thermal stability of the diodes and in their noise characteristics under reverse bias. These results are discussed in Sections 4.3.2, 4.3.3, and 4.4.

4.3.2 Thermal Stability

Previously, attempts to outgas vacuum-bottled thin-film $PbSe_{0.8}Te_{0.2}$ photodiode arrays have led to thermal degradation of the zero bias resistances, with consequent loss of detectivity.[4] In contrast, PbTe diodes that were made using the improved washing technique showed excellent stability at temperatures up to 150°C. Figure 24 shows the R-V characteristic of a 9 mil PbTe photodiode at different stages of baking up to eight hours at 100°C.

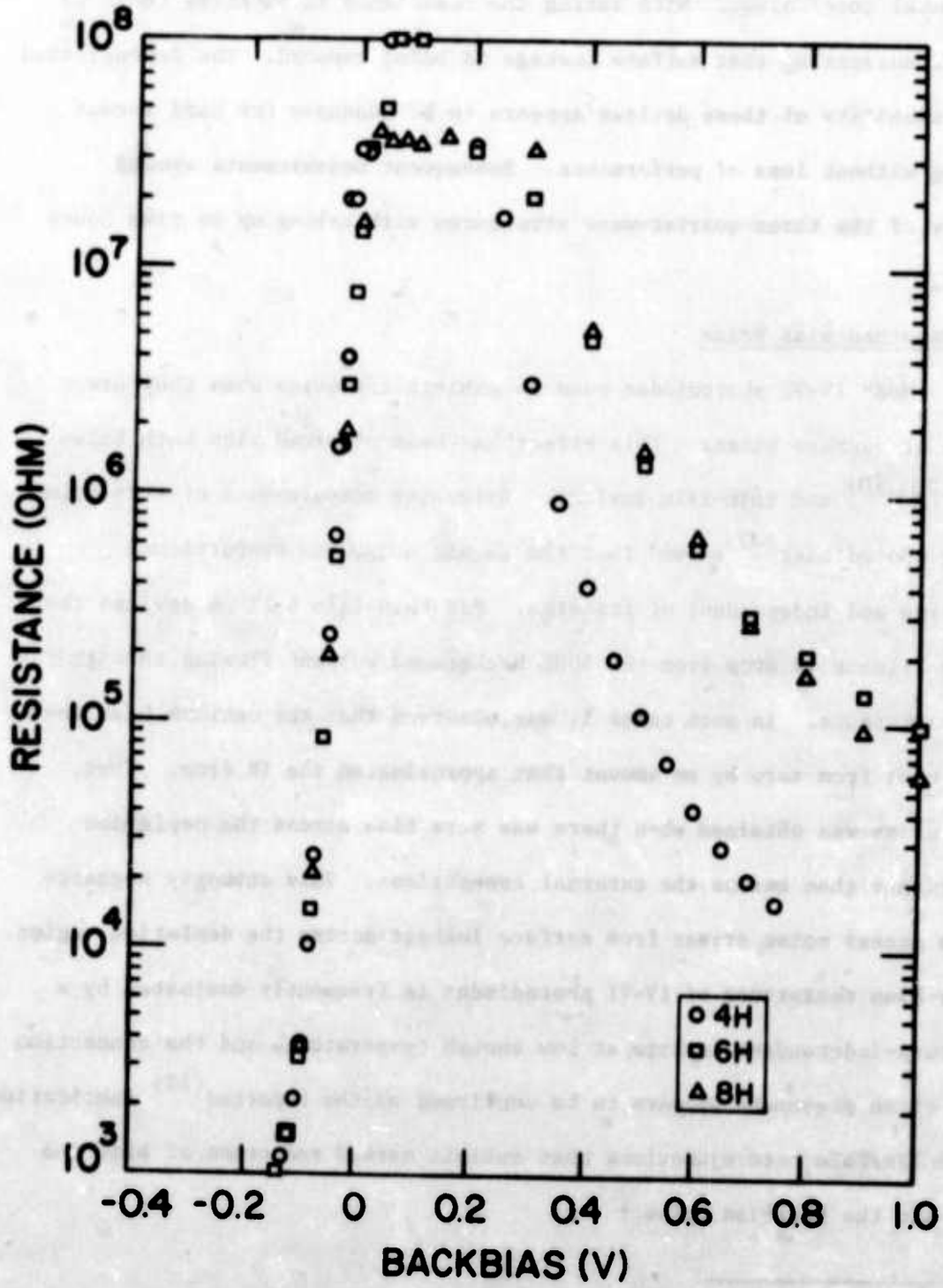

Fig. 24 R-V characteristic of a 9 mil PbTe device (EW473-5e) at 80K after successive heat treatments at 150°C.

It will be noted that the forward characteristic remains constant within our experimental uncertainty. With baking the resistance in backbias tends to increase, suggesting that surface leakage is being reduced. The demonstrated thermal stability of these devices appears to be adequate for hard vacuum packaging without loss of performance. Subsequent measurements showed stability of the three-quarter-wave structures with baking up to five hours at 150°C.

4.3.3. Reversed-Bias Noise

Most IV-VI photodiodes seem to exhibit 1/f noise when they are operated at nonzero biases. This effect has been observed with both bulk-crystal[2,3,10] and thin-film devices. Extensive measurements of thin-film (PbSn)Se photodiodes[3] showed that the excess noise was proportional to the bias and independent of its sign. For thin-film 8-12 μm devices there is a significant IR drop from the 300K background current flowing through the series resistance. In such cases it was observed that the optimum bias was shifted back from zero by an amount that approximated the IR drop. Thus, minimum noise was obtained when there was zero bias across the depletion region rather than across the external connections. This strongly suggests that the excess noise arises from surface leakage across the depletion region. The zero-bias resistance of IV-VI photodiodes is frequently dominated by a temperature-independent leakage at low enough temperatures and the connection between these phenomena appears to be confirmed by the reported[11] fabrication of (Pb,Sn)Te/PbTe heterojunctions that exhibit marked reduction of both the leakage and the backbias noise.*

---

* The process used to effect this improvement was not disclosed.

PbTe photodiodes that were cleaned after photoresist development showed marked reductions in the 1/f noise that accompanies backbias operation. At 80K, the reduction was usually sufficient to permit pinched-off operation of three-quarter-wave photodiodes without loss of detectivity at frequencies as low as 1 kHz. The amount of 1/f noise remained somewhat variable, even with diodes within a single array and an example of this variability is shown in Fig. 25. Figure 26 shows the extreme case of a PbTe device whose 1/f noise at 80K and 990 Hz remained smaller than the 300K background noise at backbias up to 0.5V.

With increase of the operating temperature, the range of usable backbias decreased and at 170K and 1 kHz the excess noise became significant at backbiases of 50 mV or less. Figure 27 shows an example of this behavior.

4.3.4 Capacitance

As predicted the three-quarter-wave PbTe photodiodes gave pinchoff in backbias at 80K. A typical C-V characteristic of such a device is shown in Fig. 28. Pinchoff was associated with a rapid decrease of capacitance with increased backbias and the transition to the low-capacitance regime occurred over a bias range of about 0.1 V. The transition region may arise from the IR drop associated with the 300K background current that flows through the thin p-layer under the depletion region at backbiases slightly less than that required for pinchoff. Under these conditions the periphery of the diode will have a larger backbias than the center and pinchoff will occur first around the edges of the diode. Further backbias would then increase the fraction of the diode that is pinched off. Qualitatively, this resembles the behavior of a JFET, but we do not have a quantitative model for this transitional

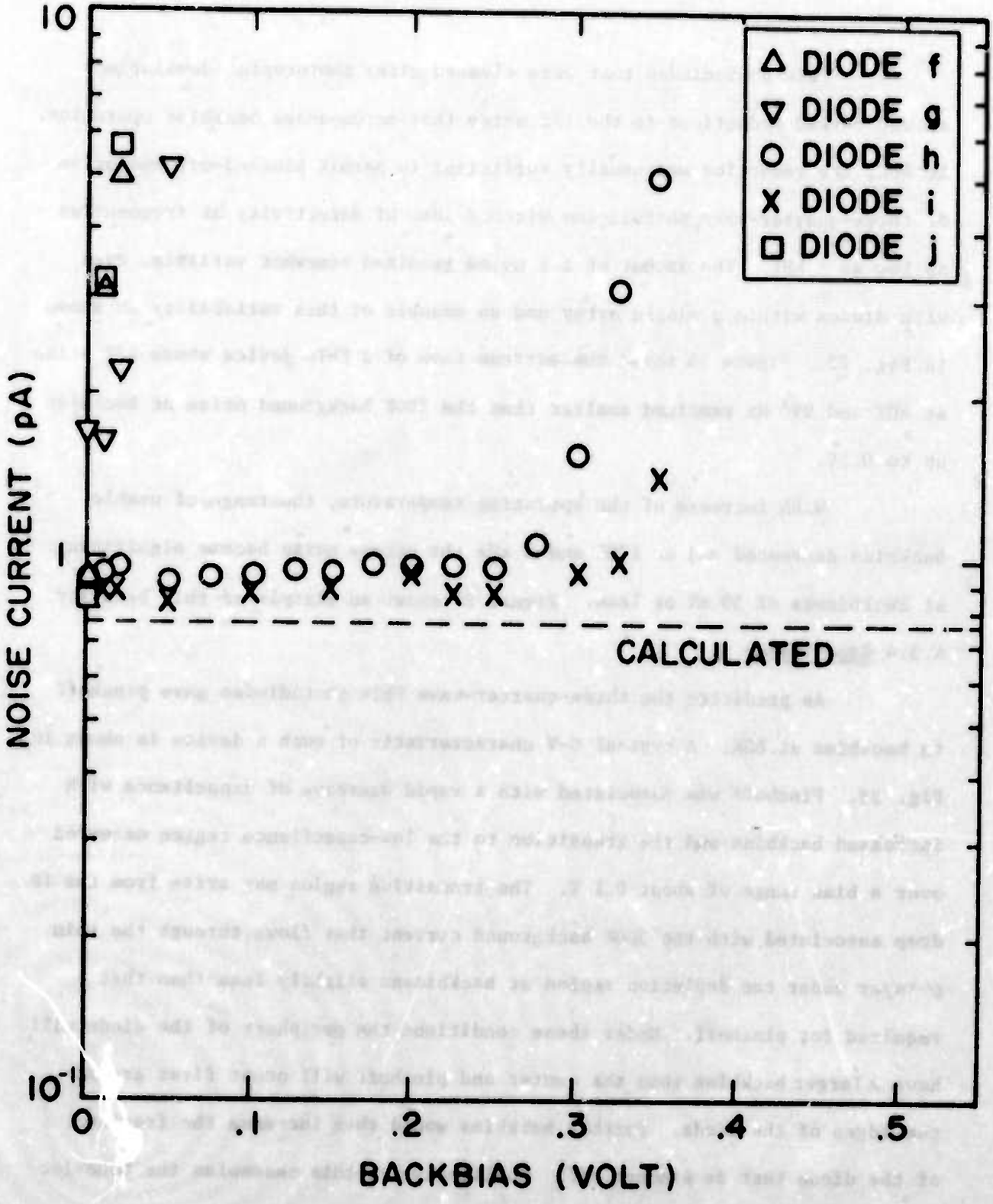

Fig. 25 Bias dependent noise of an array of 3 mil, 3λ/4 PbTe devices at 80K (EW473-5f-j). The bandwidth is 10 Hz and the line shows the calculated background noise.

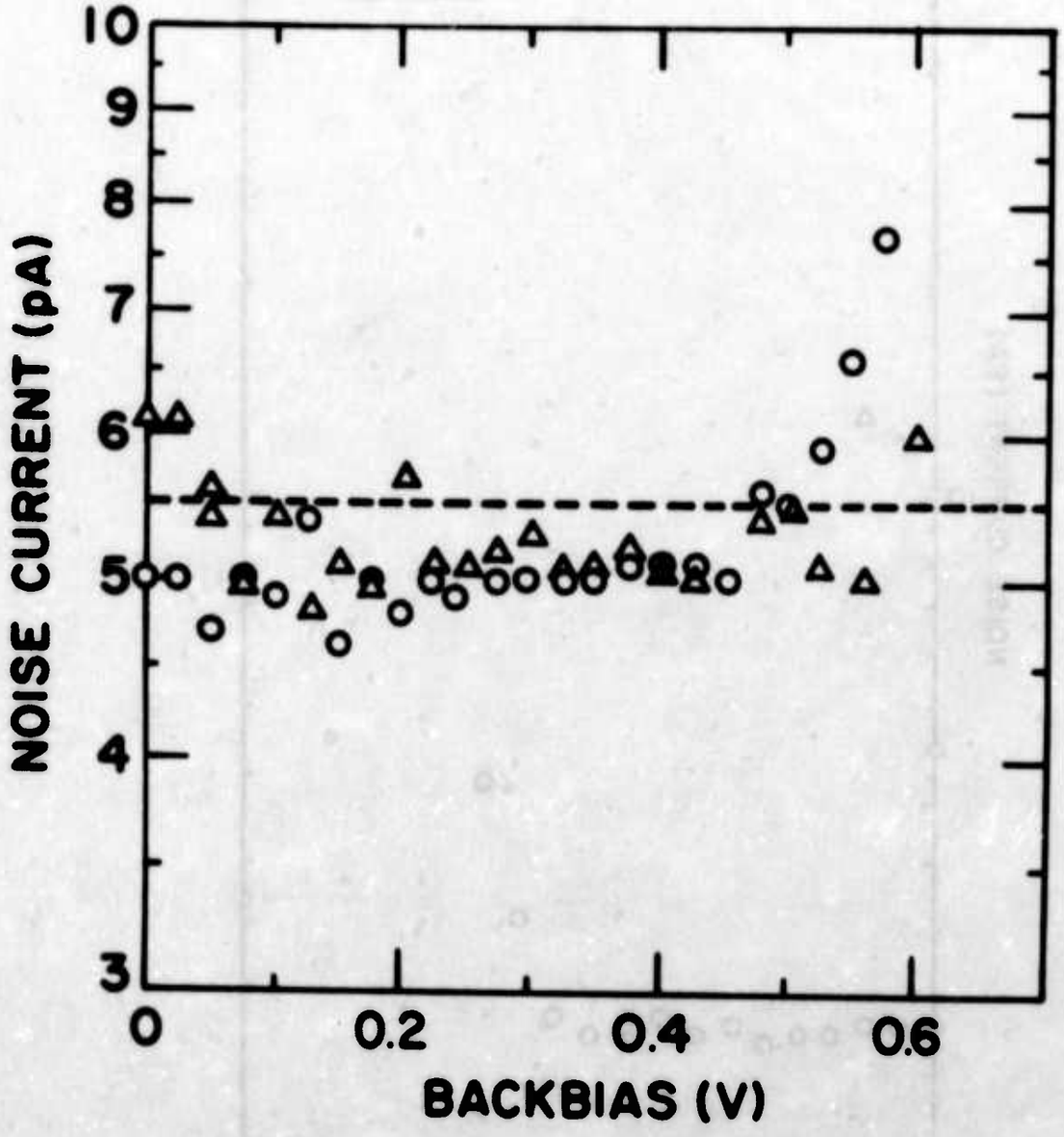

Fig. 26 Bias dependent noise (Δf = 10 Hz) of a 28 mil $3\lambda/4$ PbTe device (EW508-4c) at 80K. The circles and triangles show measurements at 990 Hz and 5 kHz, respectively. The line shows the calculated background noise.

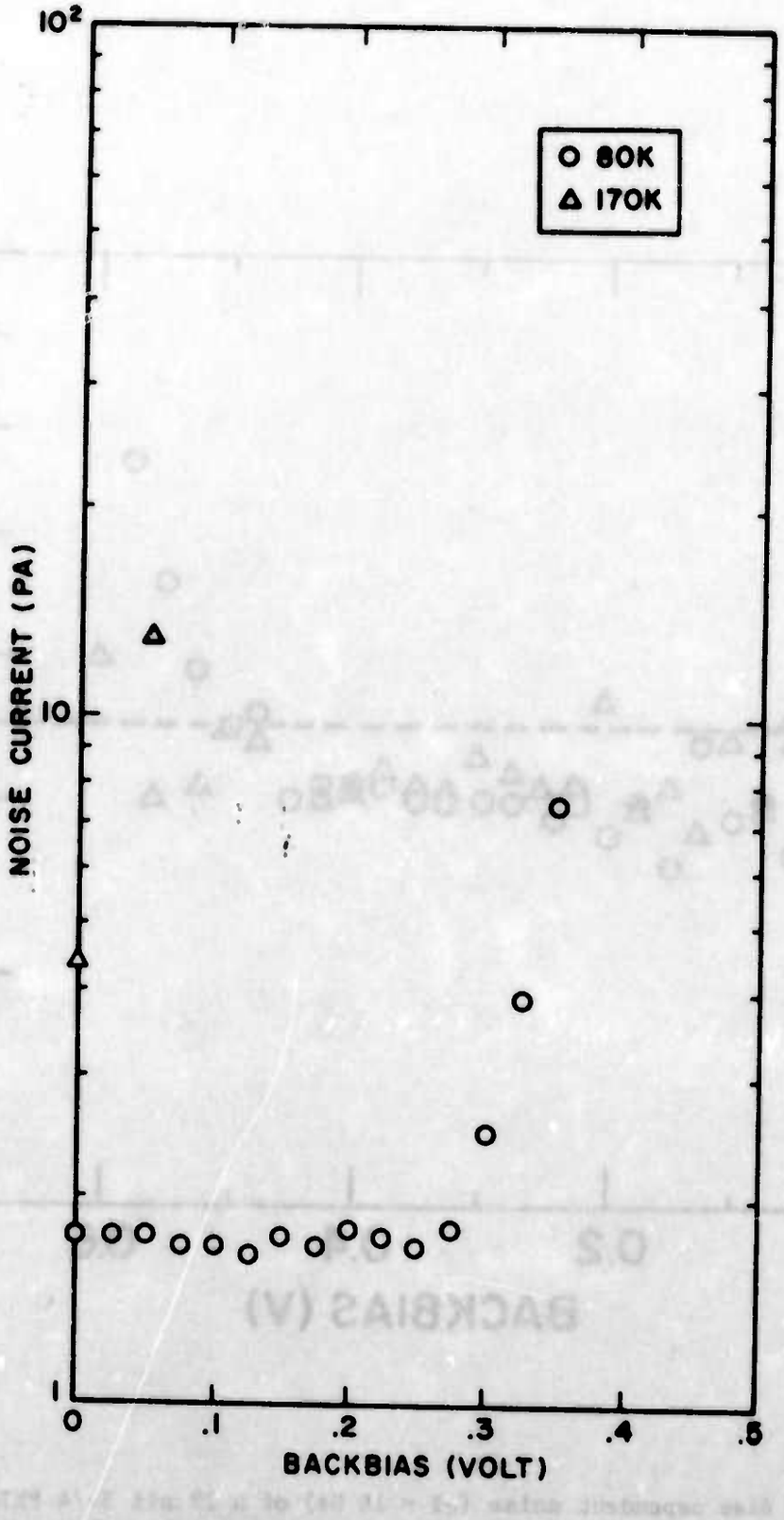

Fig. 27 Bias dependent noise (Δf = 10 Hz) of a 9 mil PbTe diode (EW473-5e) at 80K and 170K.

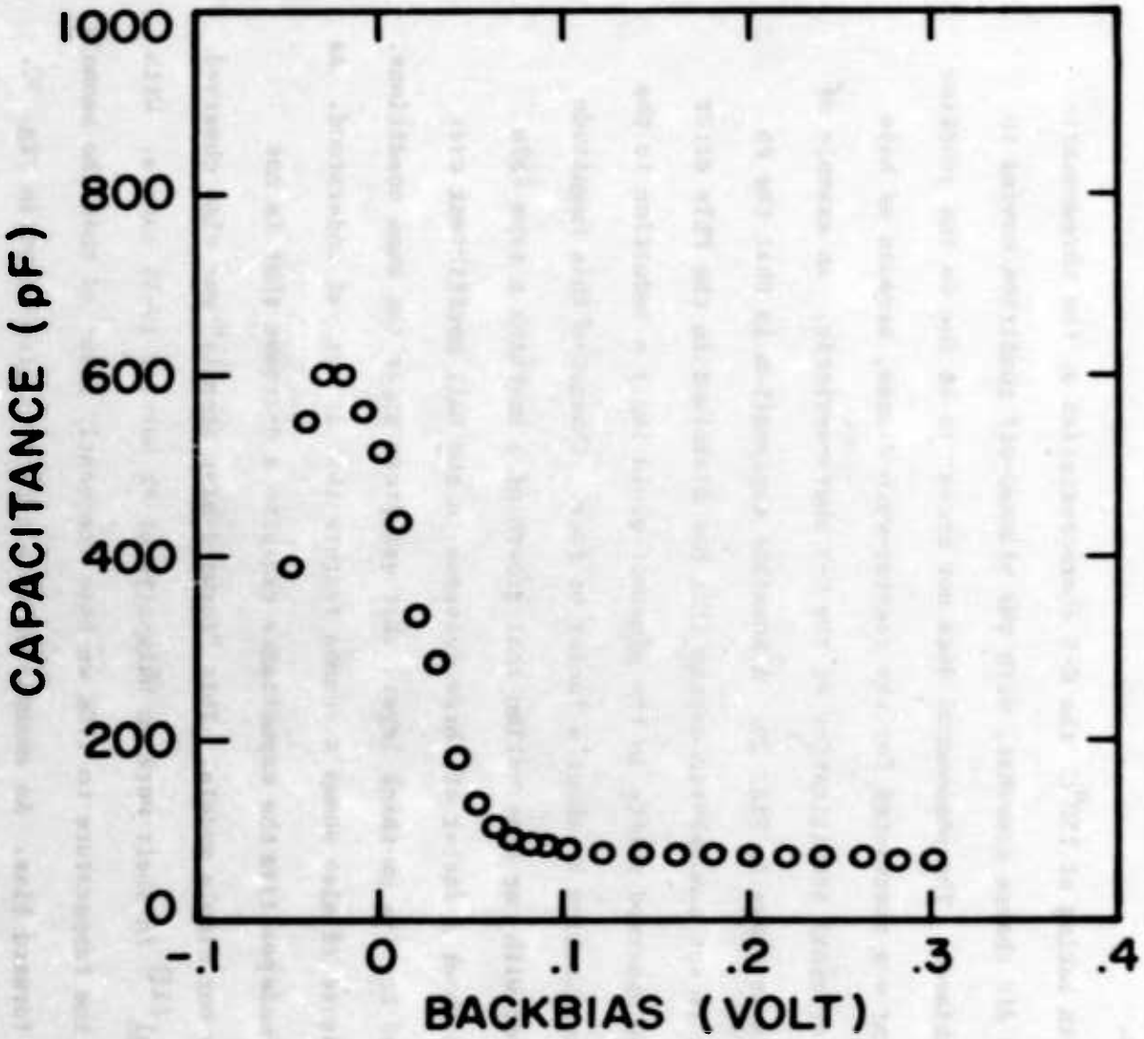

Fig. 28 C-V characteristic of a 9 mil, 3λ/4 PbTe device (EW473-5) at 80K.

behavior in the pinched-off photodiode. Moreover, detailed comparison with the predicted pinchoff voltage is not yet possible because of the uncertainties in the influence of atmospheric oxygen upon the measured acceptor concentration and in the static dielectric constant of PbTe at low temperatures.

With baking at 150°C the C-V characteristics of the three-quarter-wave devices did change somewhat, with the pinched-off condition moving to smaller backbiases. The phenomenon does not appear to be due to the junction diffusion that was postulated for the quarter-wave diodes, because we have observed an eventual stabilization of the C-V characteristic. An example of these effects is shown in Fig. 29. A possible explanation is that the Pb barrier getters out atmospheric oxygen that has dissolved in the PbTe after growth.* The observed shifts in the pinchoff would imply a reduction in the acceptor concentration by about a factor of four. Changes of this magnitude are consistent with our observation that growth of 1 μm-thick p-type PbTe layers gives about a factor of three decrease in the Hall coefficient over that obtained for 3-4 μm-thick layers that are grown under the same conditions.

Figure 28 also shows a common feature that is not yet understood. As the bias is made positive the capacitance exhibits a decrease that is not predicted by our simple models. This "forward-bias anomaly" was also observed by Nill *et al*[12] in their work on bulk-crystal Pb barrier IV-VI lasers. With increase of the temperature to 170K we have frequently observed that the anomaly shifts into forward bias. An example of this effect is also shown in Fig. 30.

---

* Oxygen-induced changes in the carrier concentrations of IV-VI thin films been widely observed[13]. The changes are consistent with an increase in the acceptor concentration.

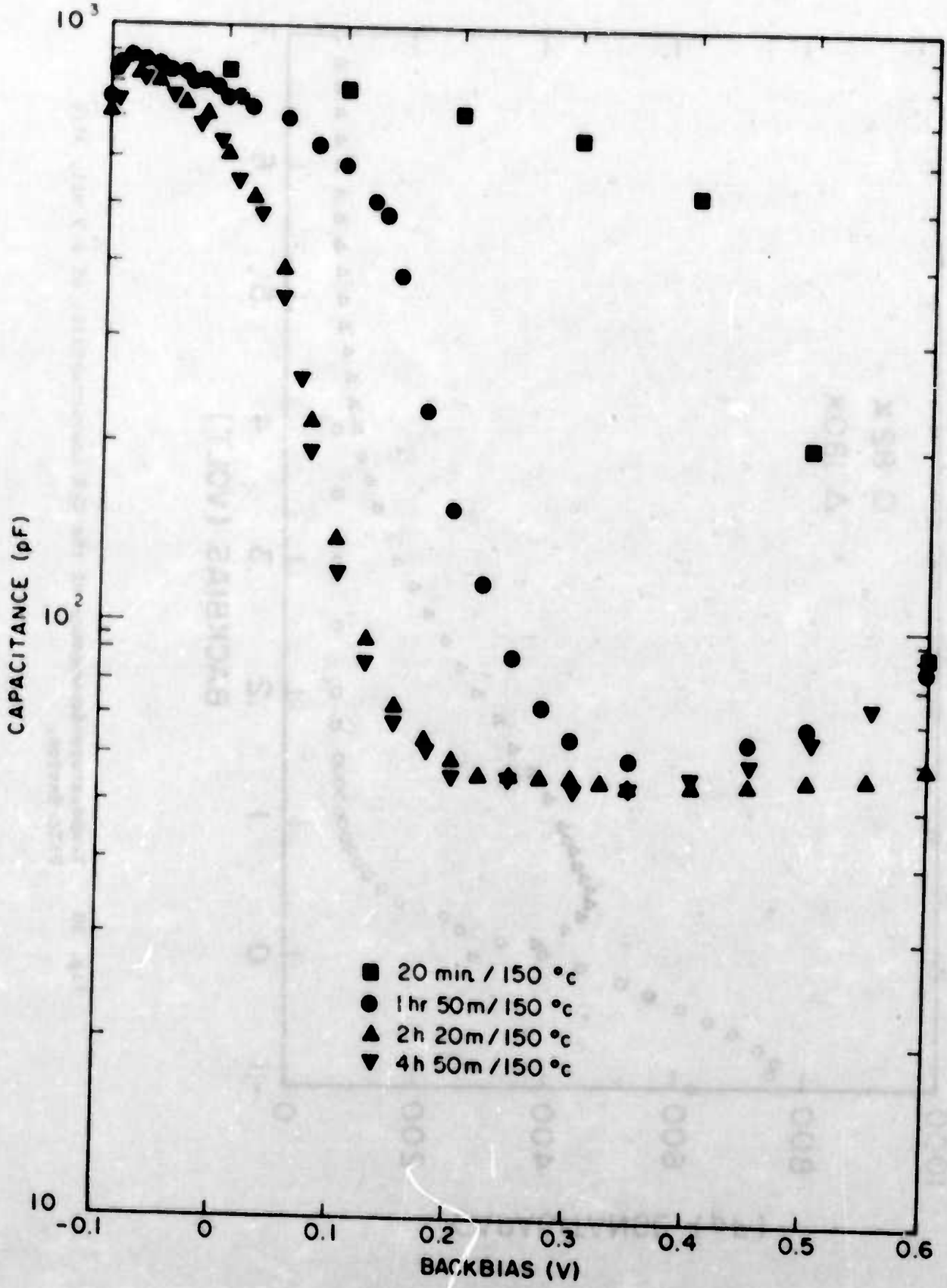

Fig. 29 The effect of baking on the C-V characteristic at 80K of a 9 mil, 3λ/4 PbTe device (EW496B-7b).

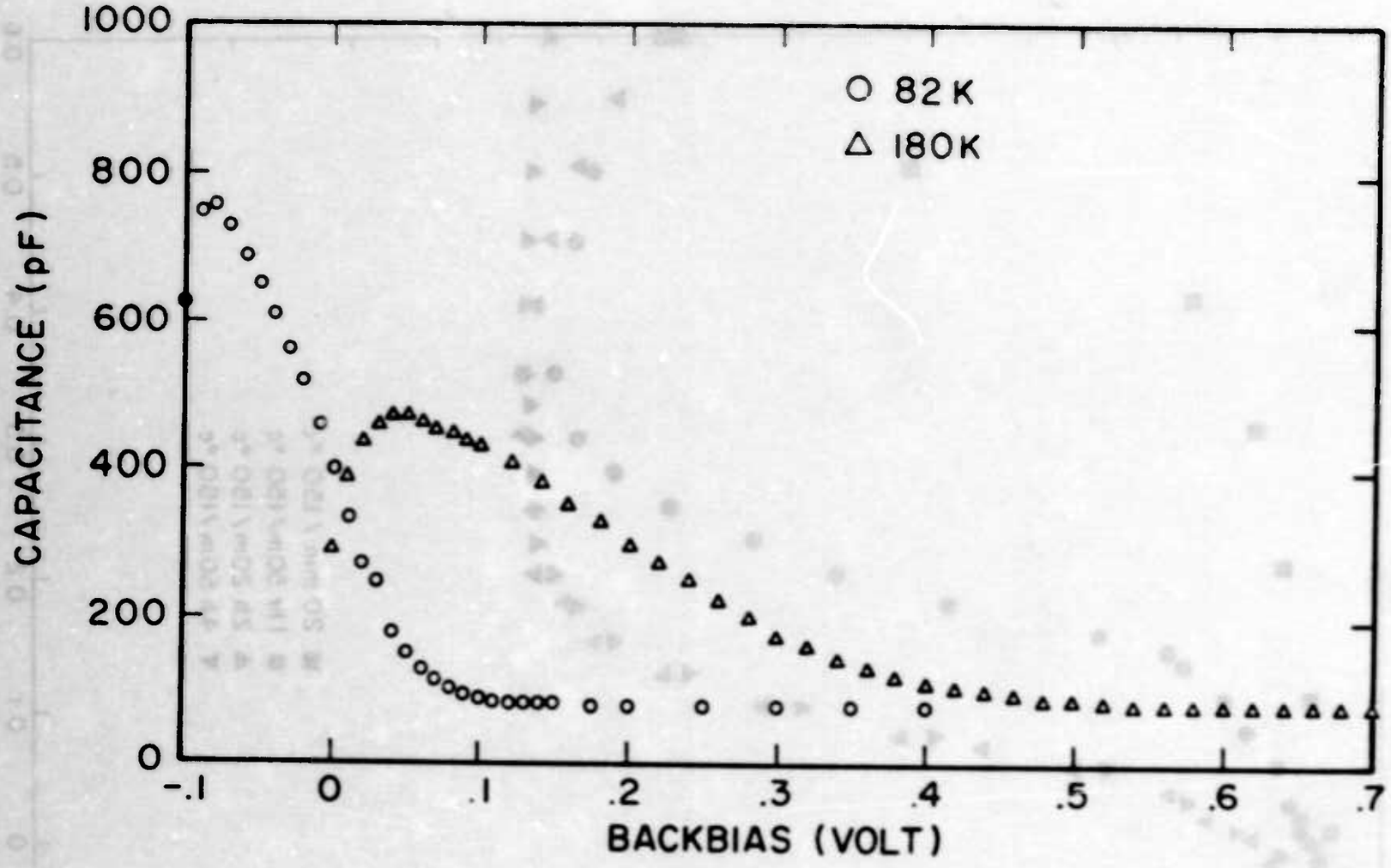

Fig. 30 Temperature-dependence of the C-V characteristic of a 9 mil, 3λ/4 PbTe device.

As discussed in Section 4.2.4, the capacitance of the pinched-off 9 mil-square PbTe devices was dominated by the pad capacitance of 20-80 pF. Further reduction of the capacitance would require development of structures with smaller pad areas. Such a development would appear to be essential for exploitation of pinchoff with PbTe devices with smaller dimensions that are more suited to modern systems applications. Such a development was not made in the present study. However, in order to reduce the influence of the pad capacitance, diodes were made with the dimensions shown in Fig. 31. The bias-dependent capacitance of such a 28 mil-square three-quarter-wave diode is shown in Fig. 32. In backbias the capacitance was reduced by approximately two orders of magnitude to 35 pF, of which 19 pF was estimated to be contributed by the pad.

4.3.5 Quantum Efficiency

The quantum efficiencies of the three-quarter-wave PbTe devices were close to the RLL at all biases and no decrease of the 500K current responsivity was observed when the devices were backbiased past pinchoff. These RLL quantum efficiencies were observed with photodiodes as large as 28 mil-square. Examples of this behavior are given in Section 4.3.8.

4.3.6 Detectivity

The detectivities of three-quarter-wave PbTe devices at 80K were typical of those obtained previously[2] with conventional thin-film devices At 180° field of view we obtained D^* ($\sim$ 5 μm) $\gtrsim 1.5 \times 10^{11}$ cmHz$^{\frac{1}{2}}$W^{-1} over the range of biases for which the 1/f noise was negligible. For most such devices the backbias limit for 1 kHz operation was at least 0.1 V and sometimes as large as 0.5 V so that the zero-bias detectivity was maintained into the pinched-off region. Examples of this behavior are given in Section 4.3.8.

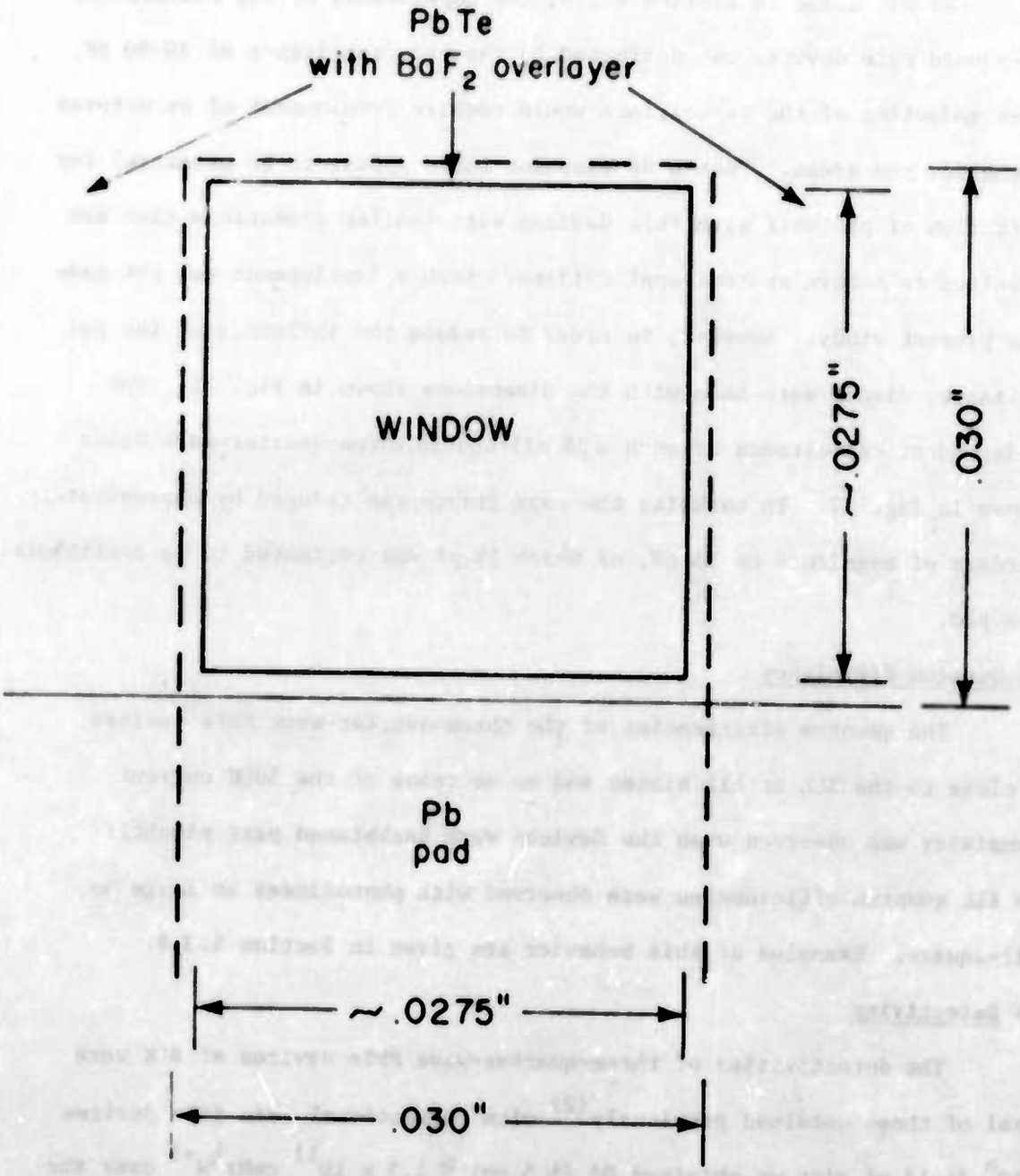

Fig. 31 Schematic of a 28 mil photodiode.

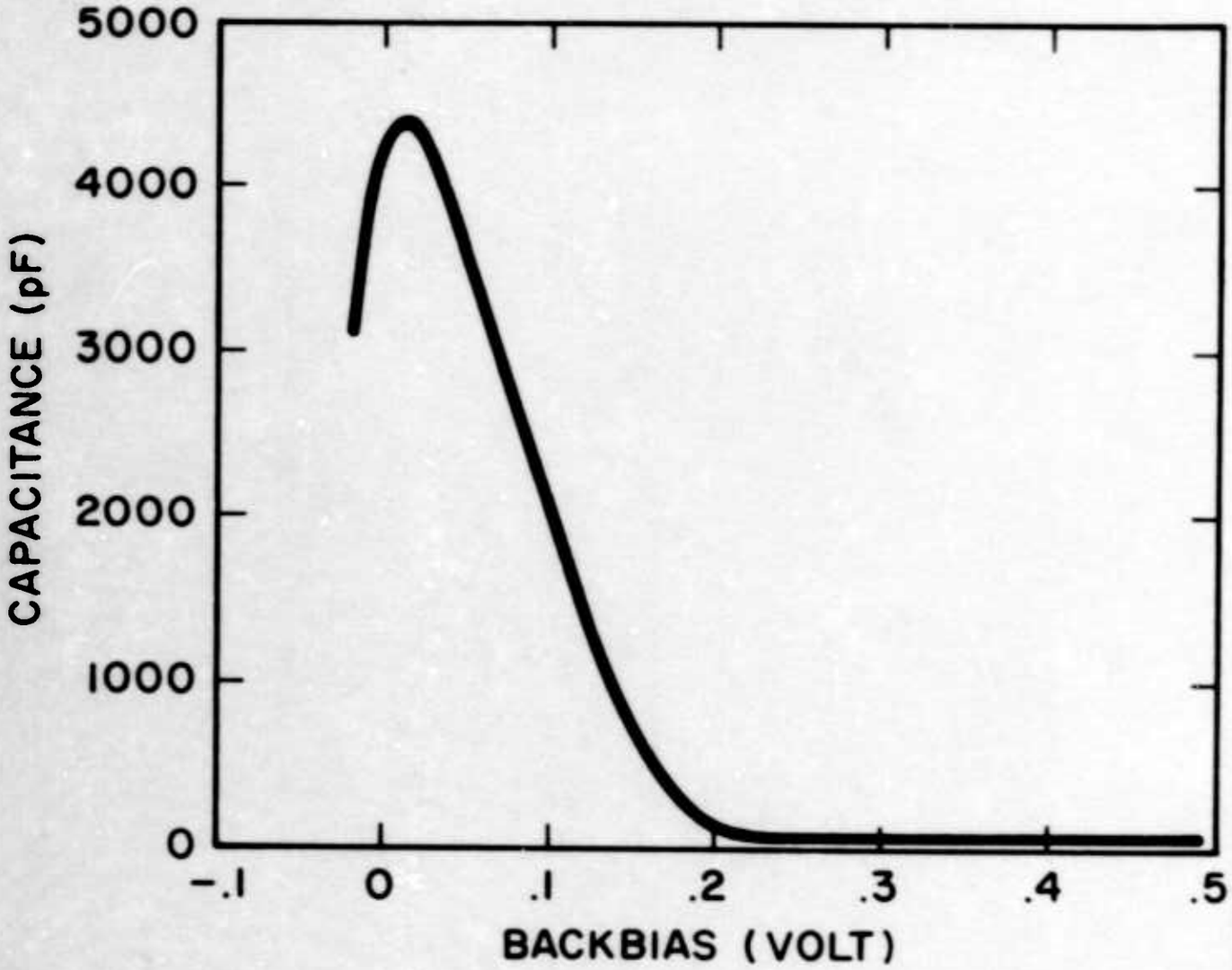

Fig. 32 C-V characteristic of a 28 mil, 3λ/4 diode at 80K (EW507-4c).

4.3.7 Measurements of Three-Quarter-Wave PbTe Photodiodes

The results that are described here illustrate the points that are made in Sections 4.3.3 - 6.

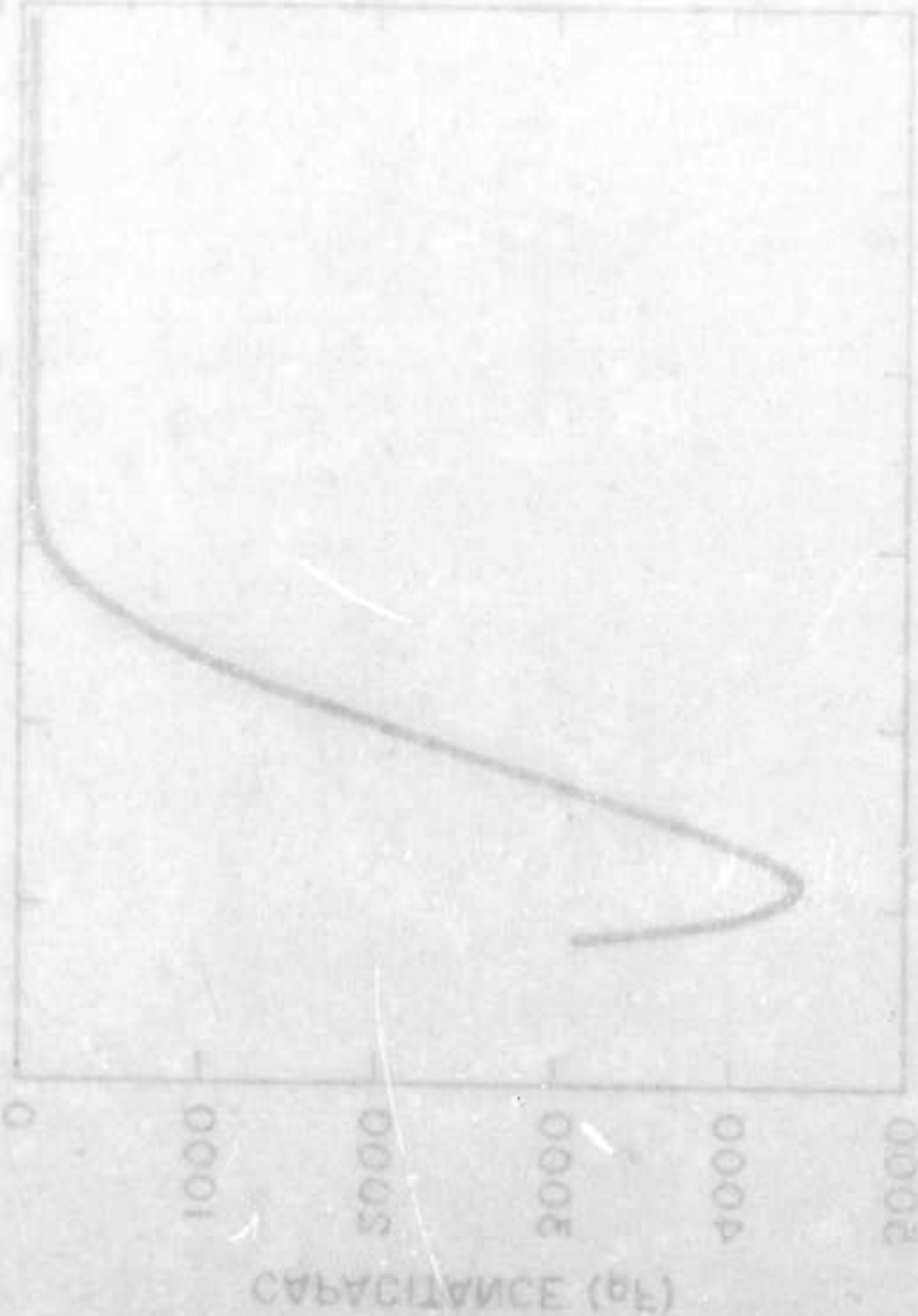

Table 6 - EW473-5e

This specimen was measured at 80K after baking at 100°C for eight hours. The chip had three diodes with area = $6.00 \times 10^{-4} cm^2$ and similar pinchoff behavior (Fig. 33). Only one of the devices had low noise in backbias (Fig. 34) and for this detailed measurements were made (Figs. 35,36). At 170K all three diodes gave excess noise in backbias (Fig. 37).

layer thickness	=	0.62 ± 0.03 μm
frequency	=	990 Hz
bandwidth	=	10 Hz
zero bias resistance	=	2.8×10^6 ohm
background current	=	1.06 μA
calculated noise	=	1.8 pA

Backbias [mV]	Noise [pA]	D*(5.4 μm) [$cmHz^{\frac{1}{2}}W^{-1} \times 10^{11}$]	Capacitance [pF]
0	1.75	1.7	692
25	1.75	1.7	
50	1.75	1.7	321
75	1.7	1.7	
100	1.7	1.7	83
125	1.65	1.8	
150	1.75	1.7	73
175	1.7	1.7	
200	1.8	1.6	73
225	1.75	1.7	
250	1.7	1.7	72
275	1.8	1.6	
300	2.5	1.2	72
325	3.9	0.74	
350	7.5	0.39	72

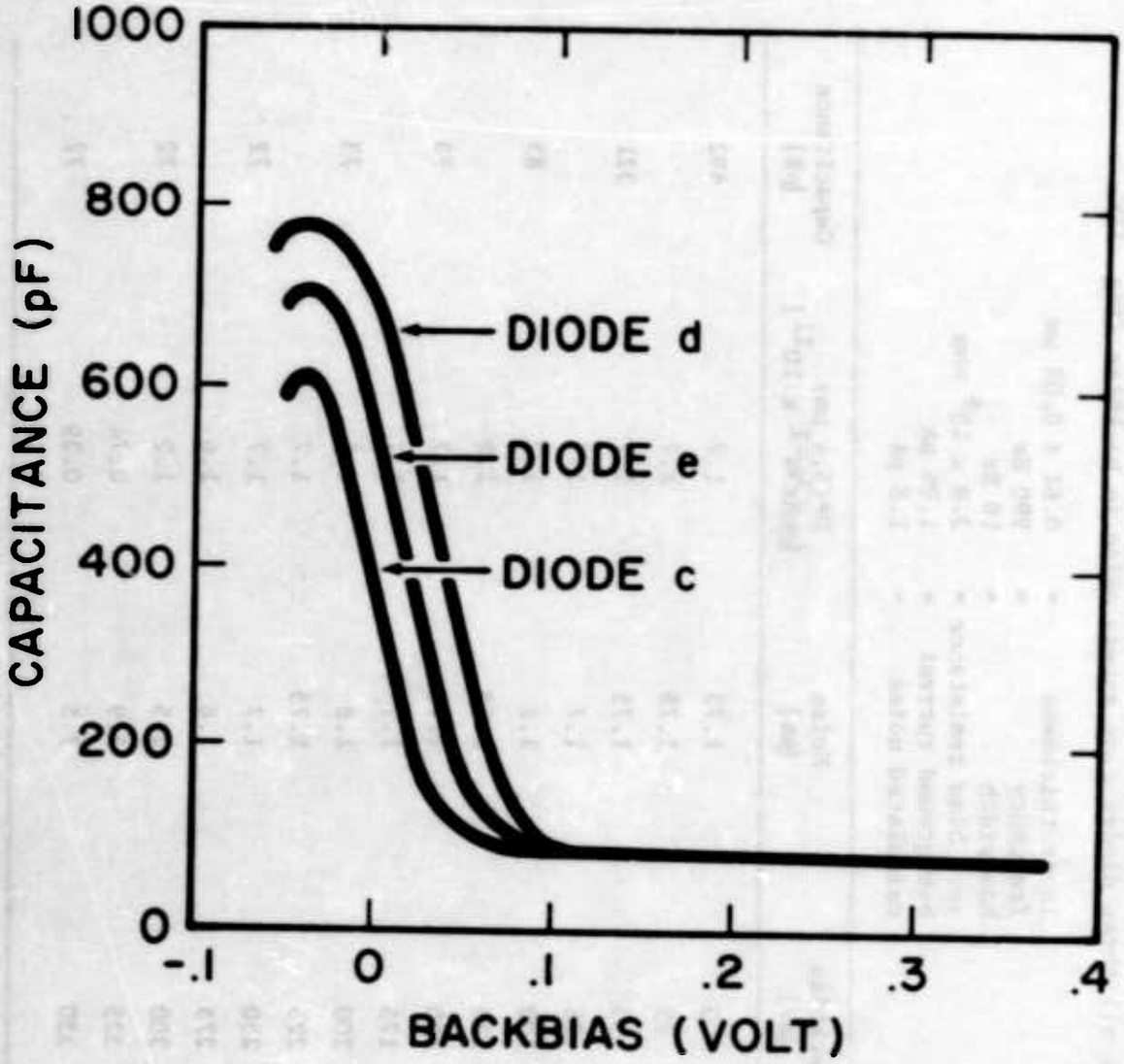

Fig. 33 EW473-5. C-V at 80K.

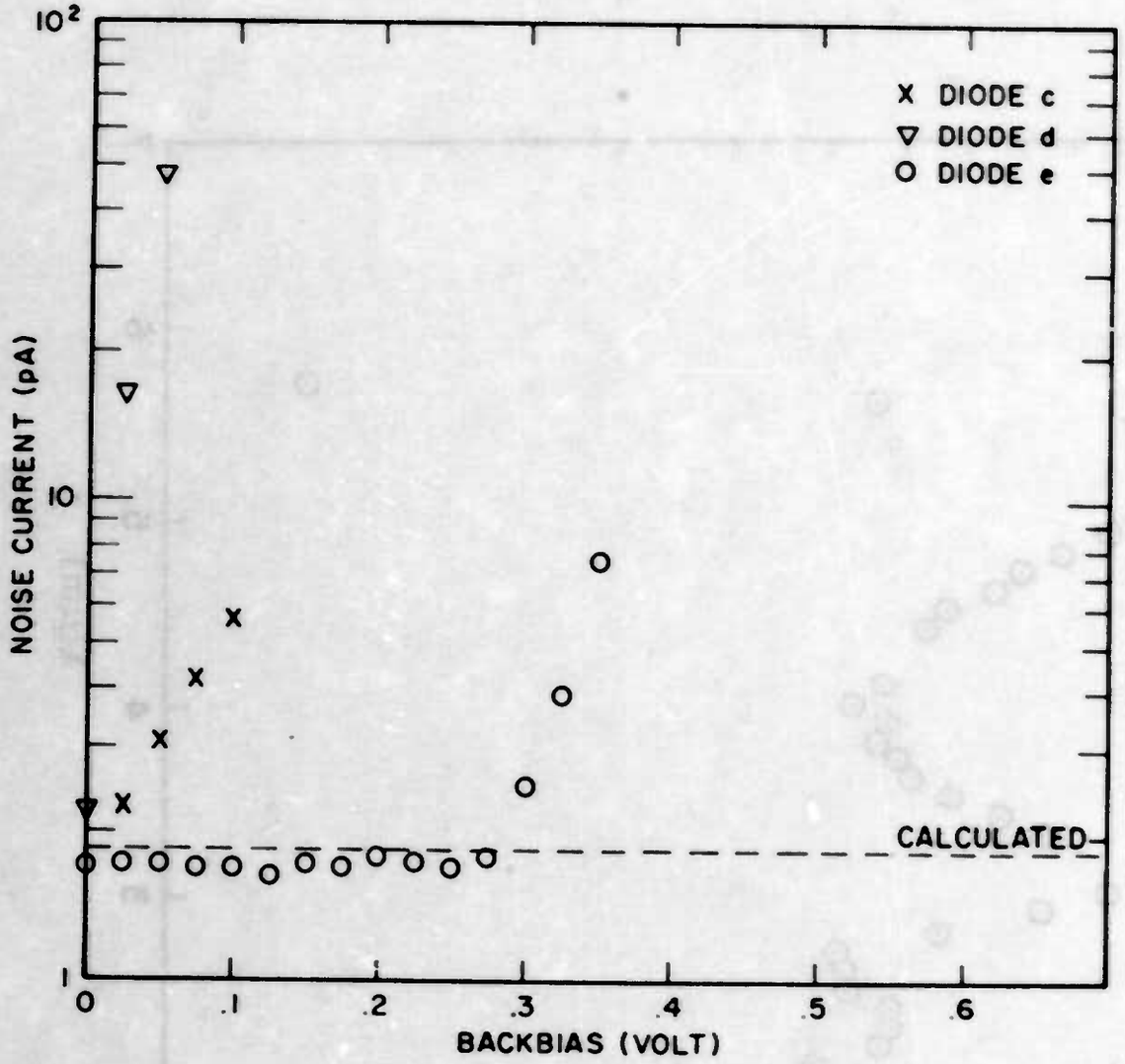

Fig. 34 EW473-5. Bias dependent noise (Δf = 10 Hz) at 80K. The curve shows the calculated background noise.

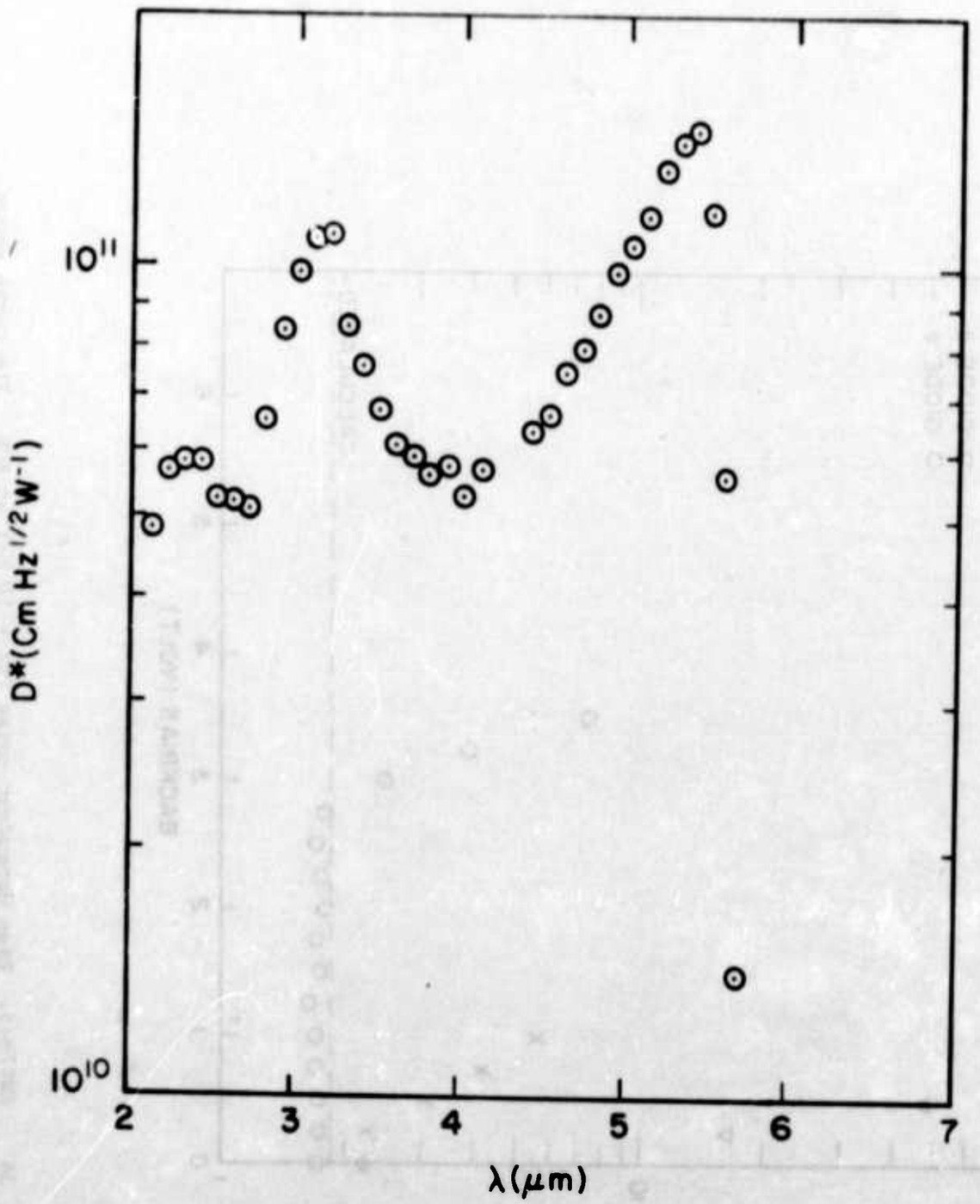

Fig. 35 EW473-5. Spectral D* at 80K and 990 Hz.

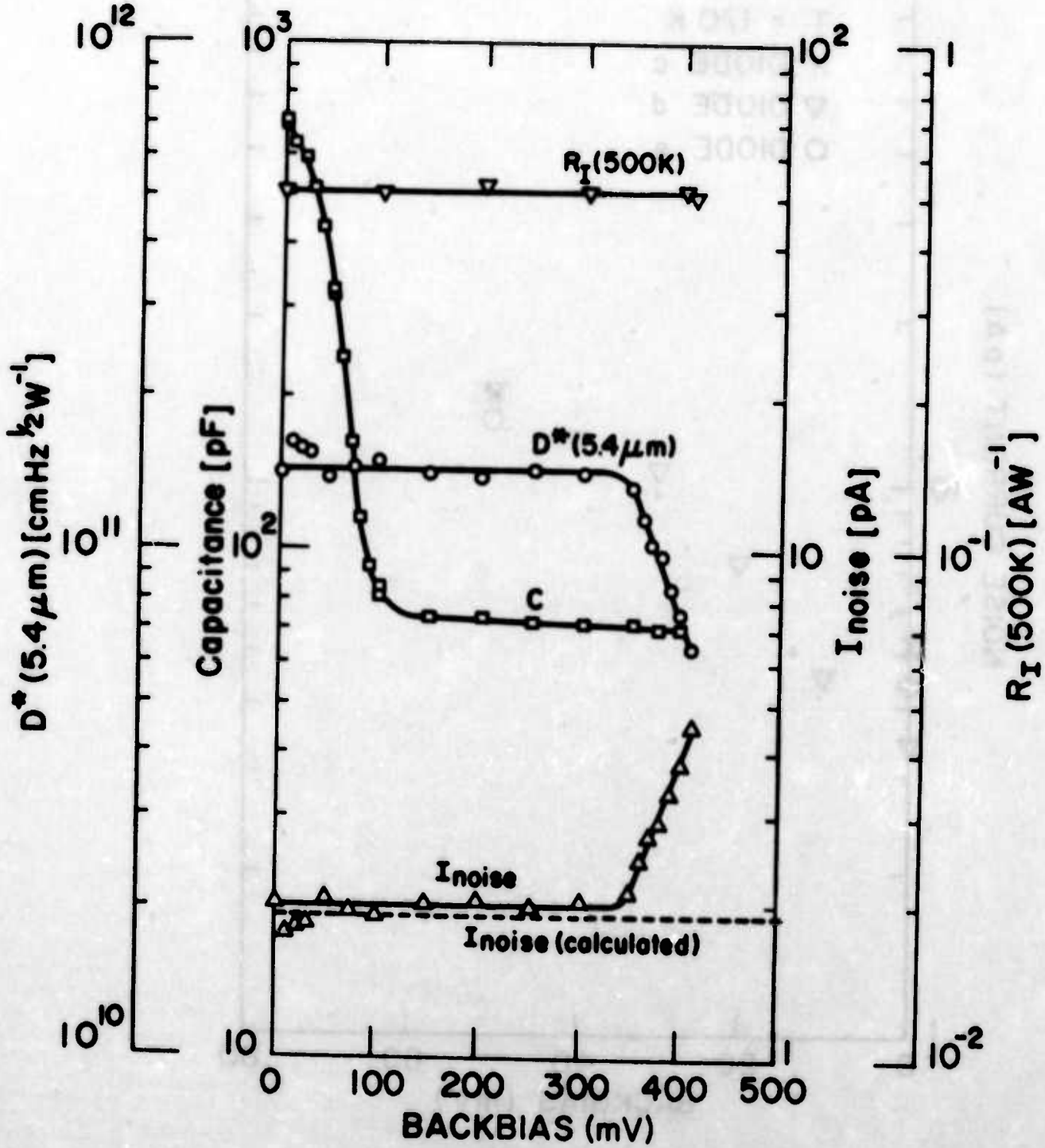

Fig. 36 EW473-5. Bias dependent properties at 80K.

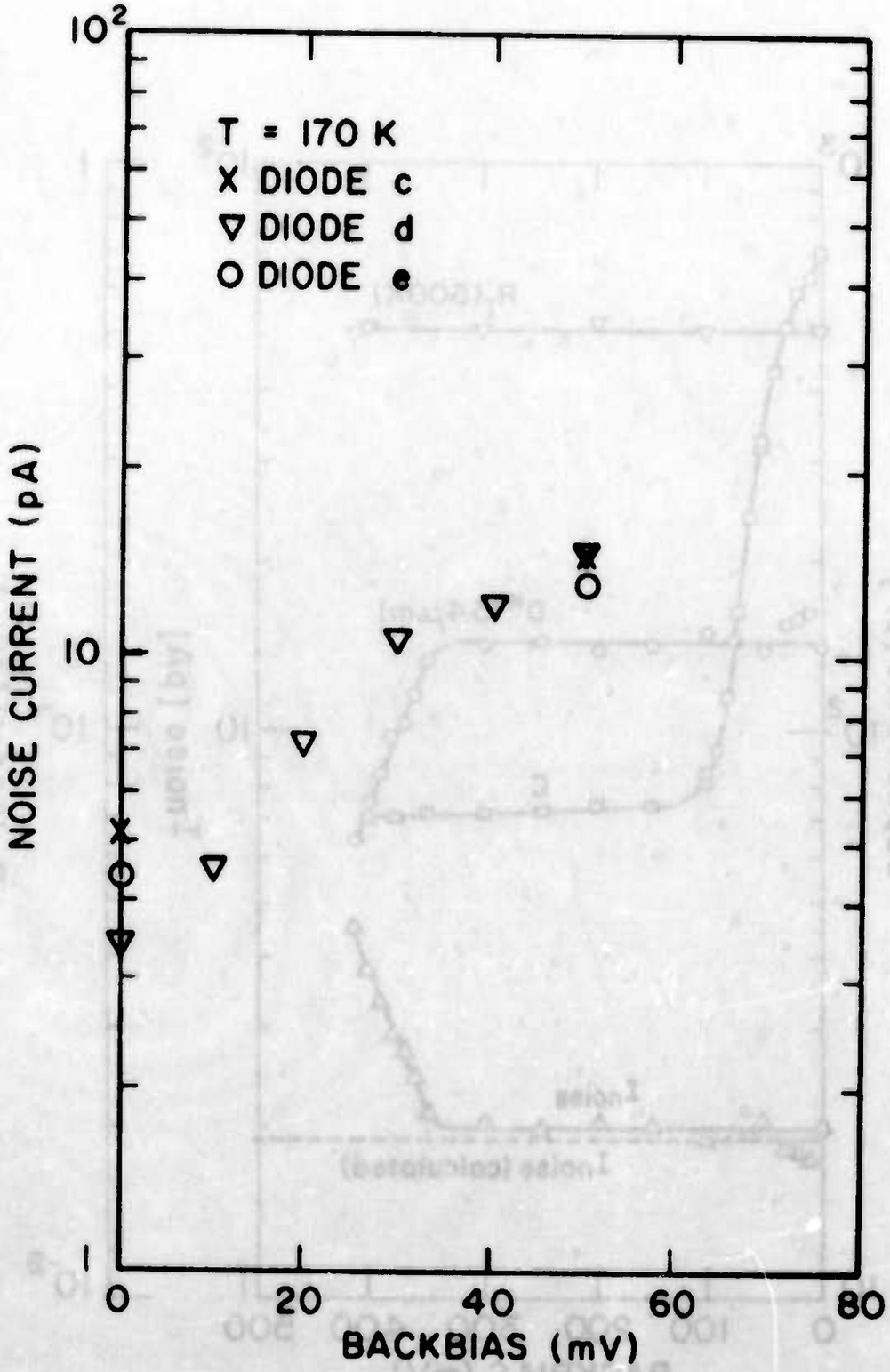

Fig. 37 EW473-5. Bias dependent noise (Δf = 10 Hz) at 1/0K.

Table 7 - EW496B-7

This specimen was measured after baking for 4 hr. 50 min. at 150°C. The changes in the C-V characteristic with baking are discussed in Section 4.3.4. The chip had four diodes with A = 5.37×10^{-4} cm^2 and d = 0.56 ± 0.03 μm. At 80K, capacitances of approximately 80 pF were achieved with backbiases ≥ 150 mV (Fig. 38). Two of the four diodes attained the low capacitance condition without significant excess noise (Fig. 39). With increase of the temperature the backbias required for pinchoff increased (Fig. 40). At 160K there was considerable 1/f noise when the diodes were backbiased (Fig. 41). The spectral D* and the bias-dependent properties at 80K are shown in Figs. 42,43.

Measurements at 80K, f = 990 Hz, Δf = 10 Hz.

Diode	b	c	d	e
Zero-bias resistance [ohm]		5.5×10^6	1.1×10^7	
Background current [μA]	1.054	1.022	0.991	0.971
Calc. background noise [pA]	1.84	1.81	1.78	1.76
Current responsivity [AW^{-1}]				
backbias = 0 mV	0.62	0.62	0.60	0.62
100 mV		0.62	0.58	
200 mV		0.62	0.60	
300 mV		0.61	0.58	
400 mV		0.61	0.59	
D*(5.0 μm) [$cmHz^{1/2}W^{-1} \times 10^{11}$]				
backbias = 0 mV	1.8	1.8	1.7	1.3
25 mV	1.8	1.7	1.8	0.61
50 mV	1.8	1.8	1.8	0.37
75 mV	1.4	1.8	1.7	
100 mV	1.1	1.7	1.9	
125 mV	0.63	1.8	1.9	
150 mV		1.6	1.9	
175 mV		1.7	1.8	
200 mV		1.5	1.8	
225 mV		1.2	1.9	
250 mV		1.1	1.7	
275 mV		0.62	1.6	
300 mV		0.41	1.1	
325 mV		0.24	0.67	
350 mV			0.38	
Capacitance [pF]				
backbias = 0 mV		595	397	
50 mV		302	151	
100 mV		119	90	
150 mV		90	83	
200 mV		86	80	
250 mV		84	79	
300 mV		84	79	
350 mV		83	79	
400 mV		83	79	

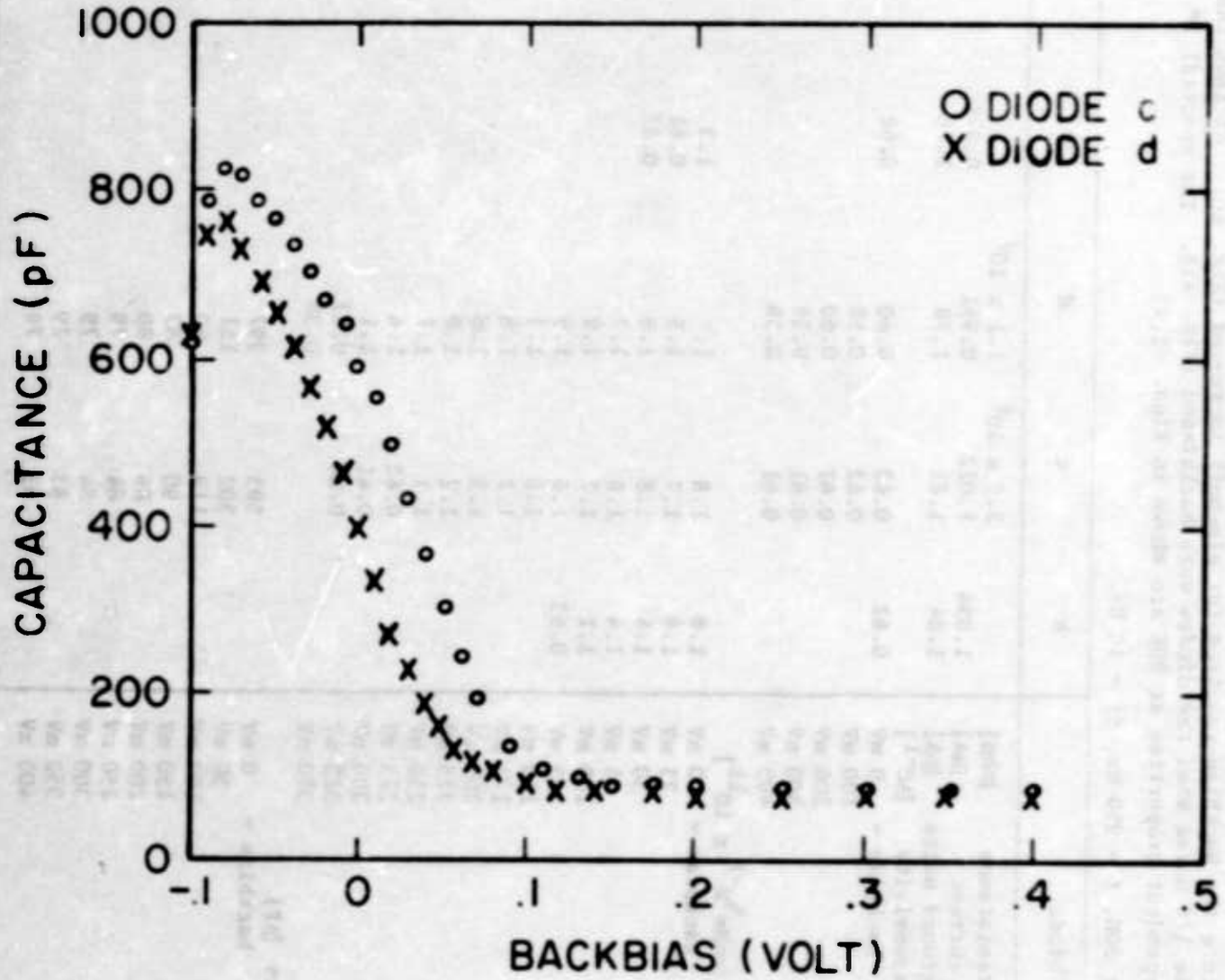

Fig. 38 EW496B-7. C-V at 80K.

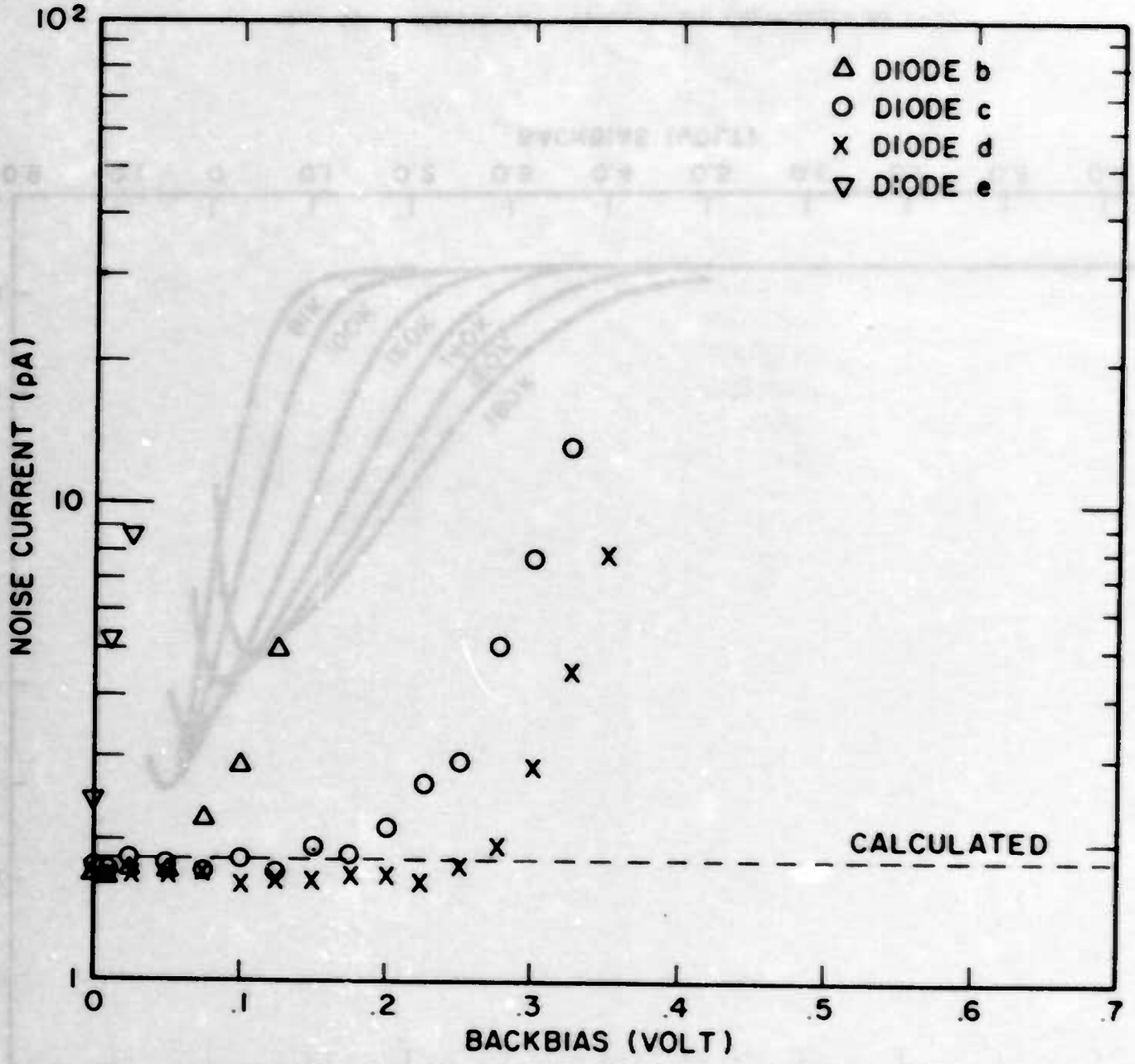

Fig. 39 EW496B-7. Bias dependent noise at 80K and 990 Hz. The line shows the calculated background noise.

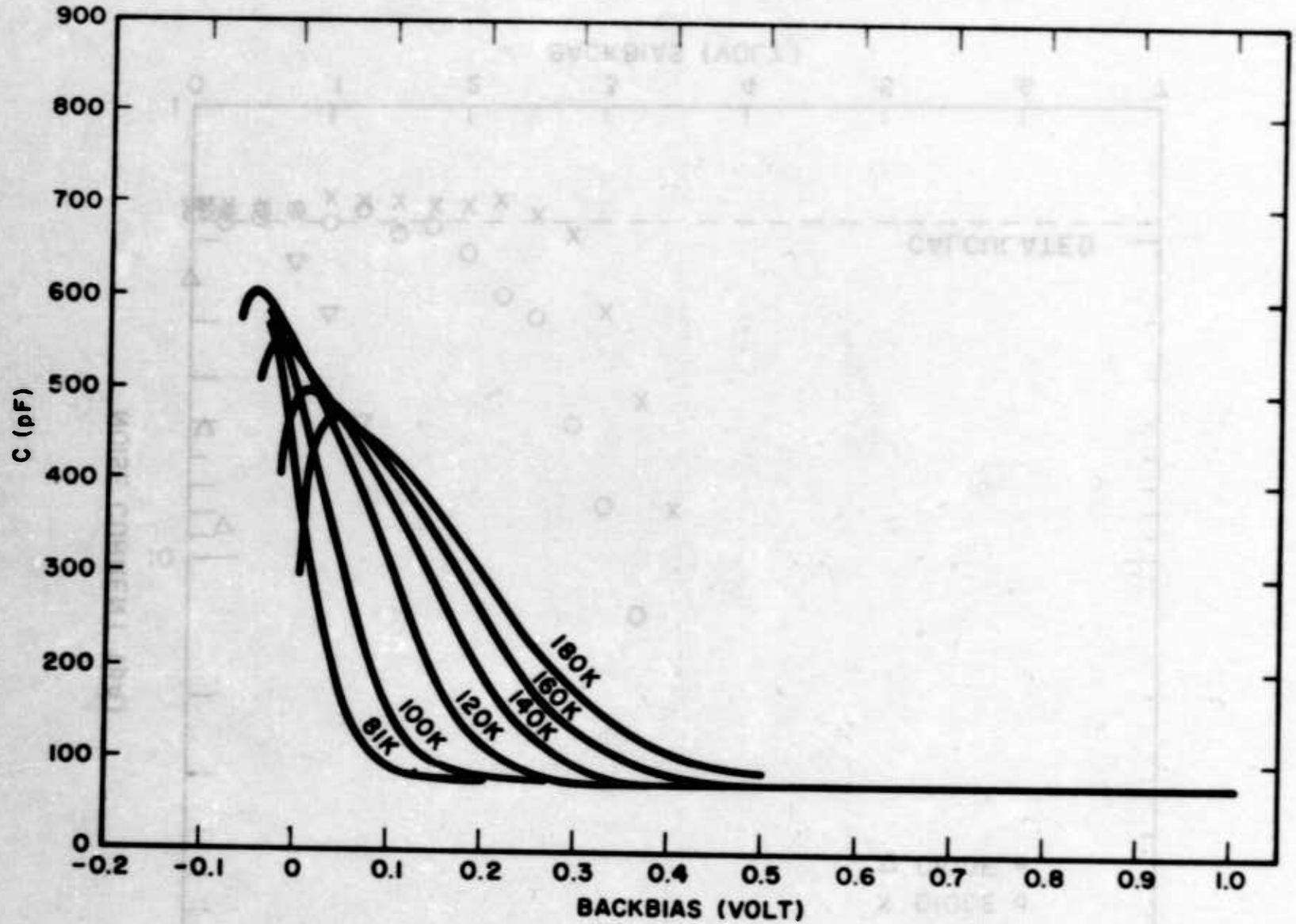

Fig. 40 EW496B-7d. Temperature dependence of C-V.

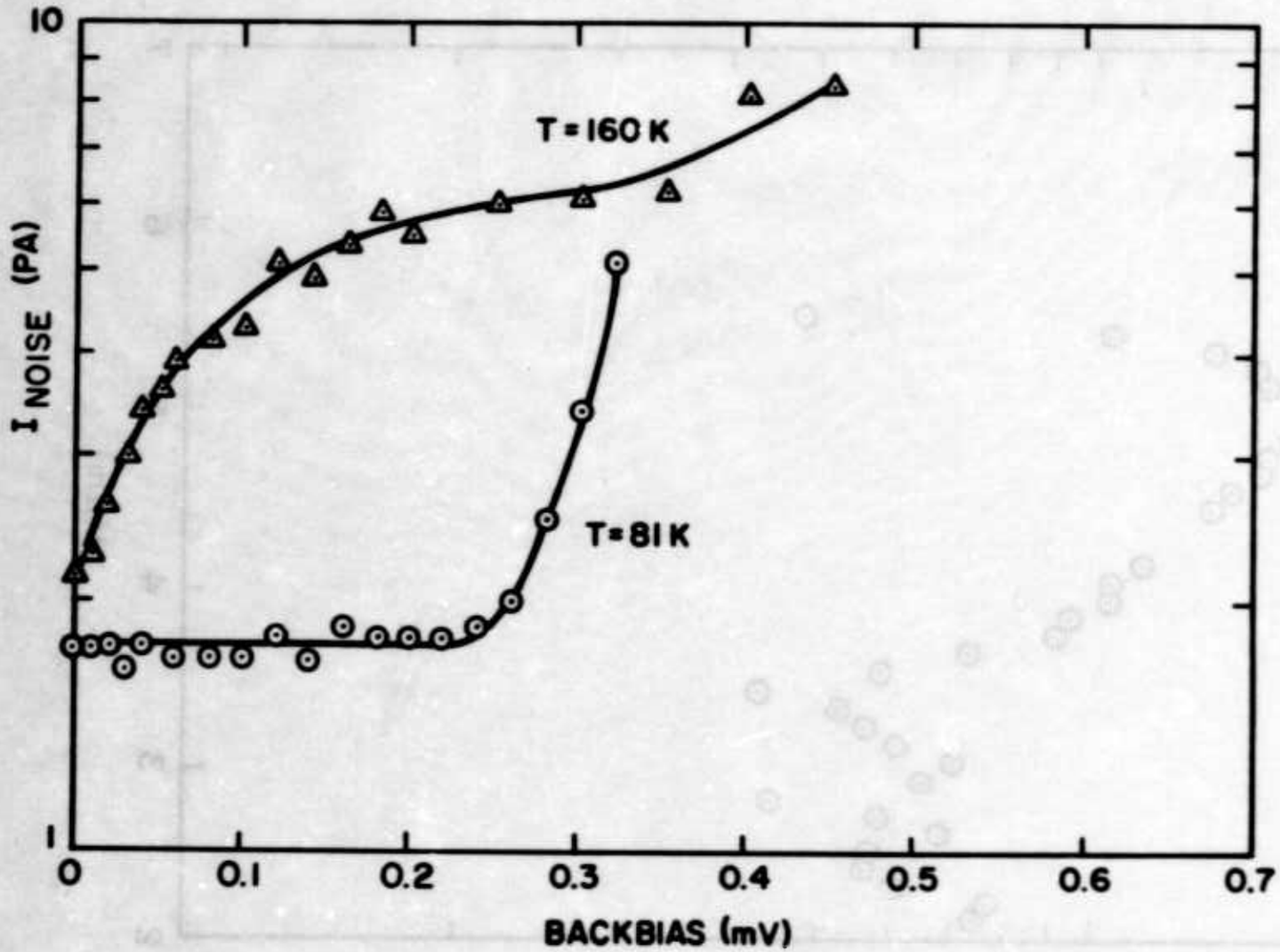

Fig. 41 EW496B-7d. Bias dependent noise (f = 3 kHz, Δf = 10 Hz) at 80K and 160K.

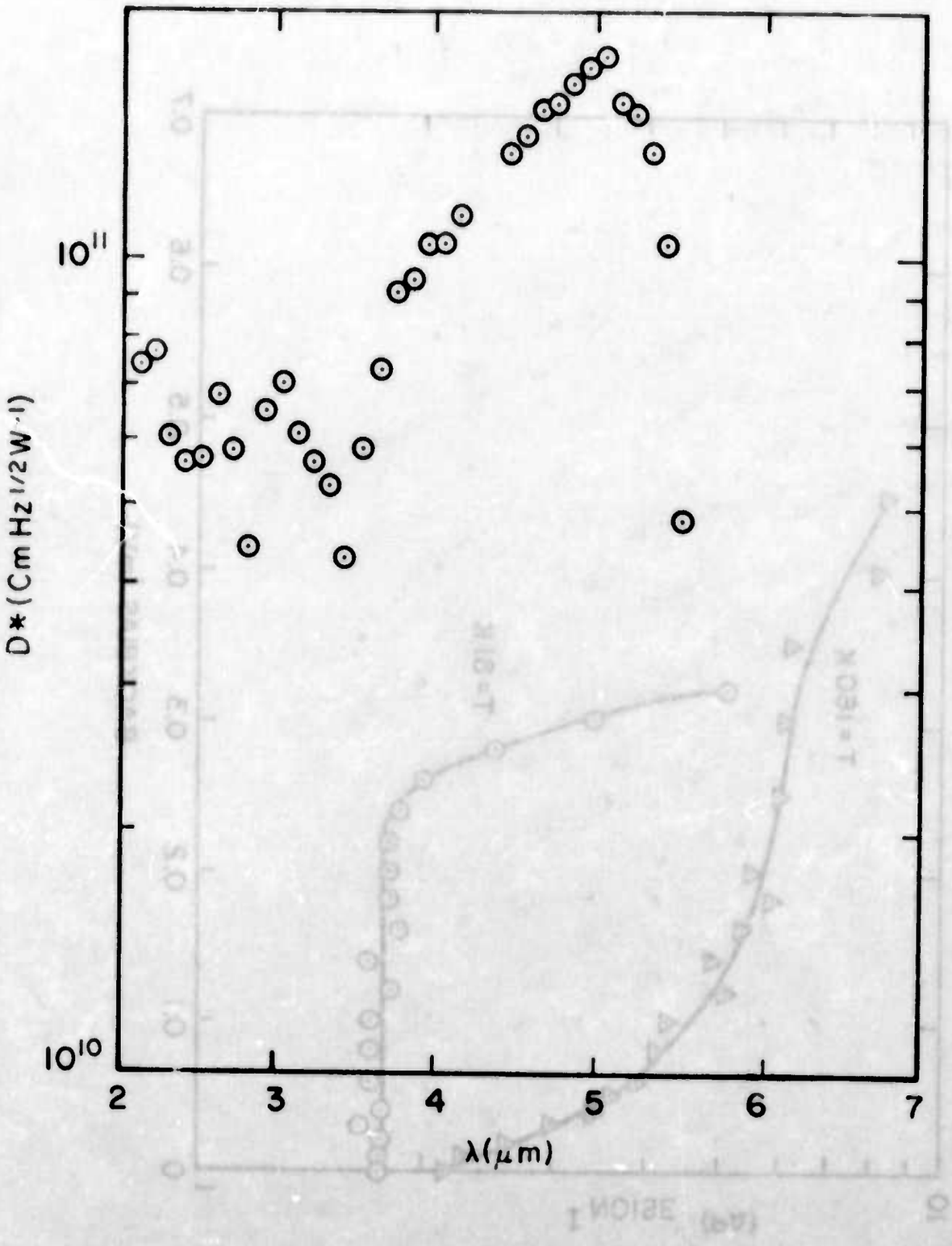

Fig. 42 EW496B-7d. Spectral D* at 80K and 990 Hz.

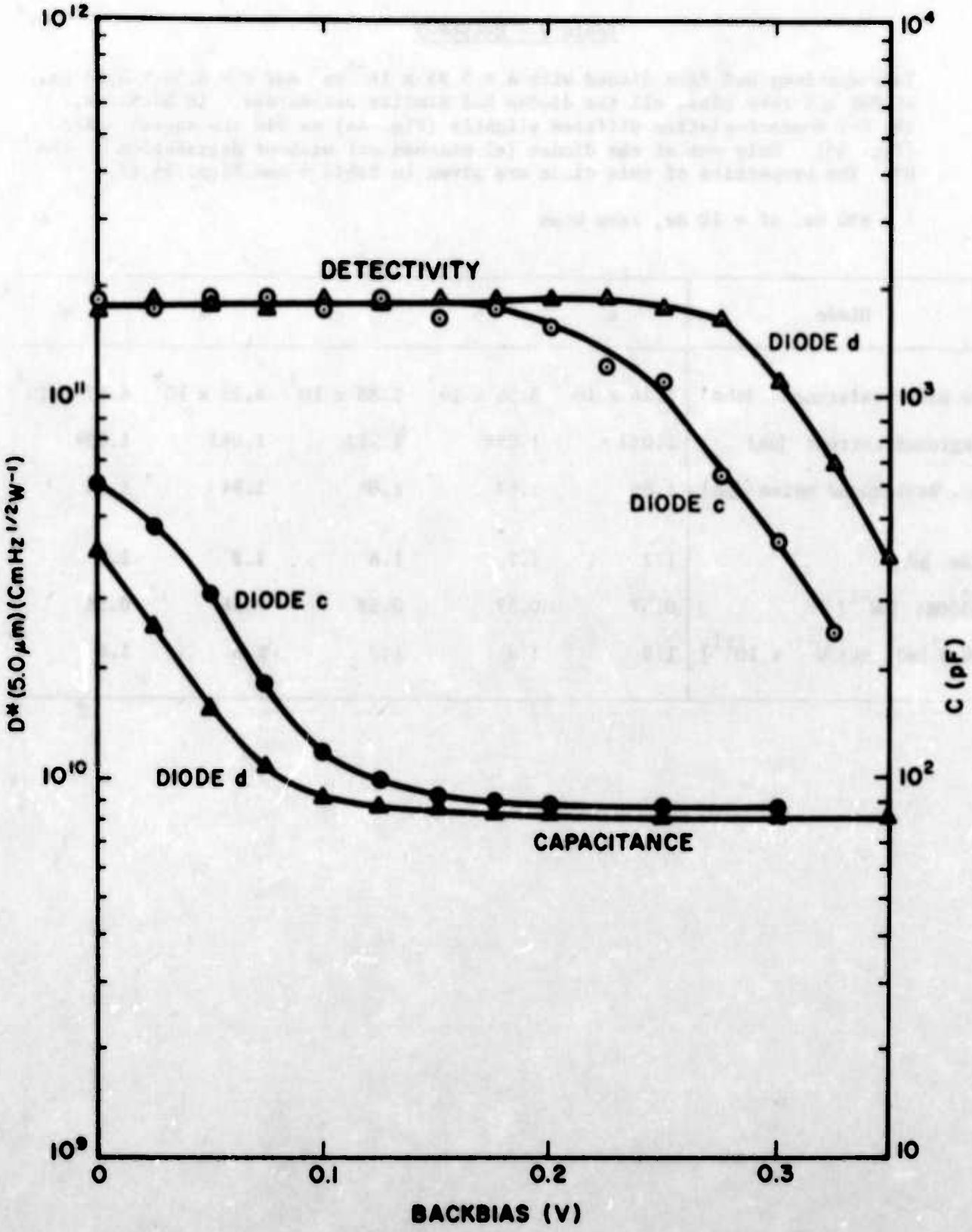

Fig. 43 EW496B-7c. Bias dependent properties at 80K and 990 Hz.

Table 8 - EW496A-3

This specimen had five diodes with A = $5.95 \times 10^{-4} cm^2$ and d = 0.54 ± 0.03 μm. At 80K and zero bias, all the diodes had similar parameters. In backbias, the C-V characteristics differed slightly (Fig. 44) as did the excess noise (Fig. 45). Only one of the diodes (e) pinched off wichout degradation of the D*. The properties of this diode are given in Table 9 and Figs. 46,47.

f = 990 Hz, Δf = 10 Hz, zero bias

Diode	a	b	c	d	e
Zero bias resistance [ohm]	5.26×10^7	5.56×10^7	5.88×10^7	4.35×10^7	4.17×10^7
Background current [μA]	1.083	1.098	1.117	1.063	1.059
Calc. Background noise [pA]	1.86	1.87	1.89	1.84	1.84
Noise [pA]	1.7	1.7	1.8	1.8	1.8
$\mathcal{R}_I$ (500K) [AW^{-1}]	0.57	0.57	0.58	0.56	0.56
D*(4.8 μm) [$cmHz^{\frac{1}{2}}W^{-1} \times 10^{11}$]	1.8	1.8	1.7	1.6	1.6

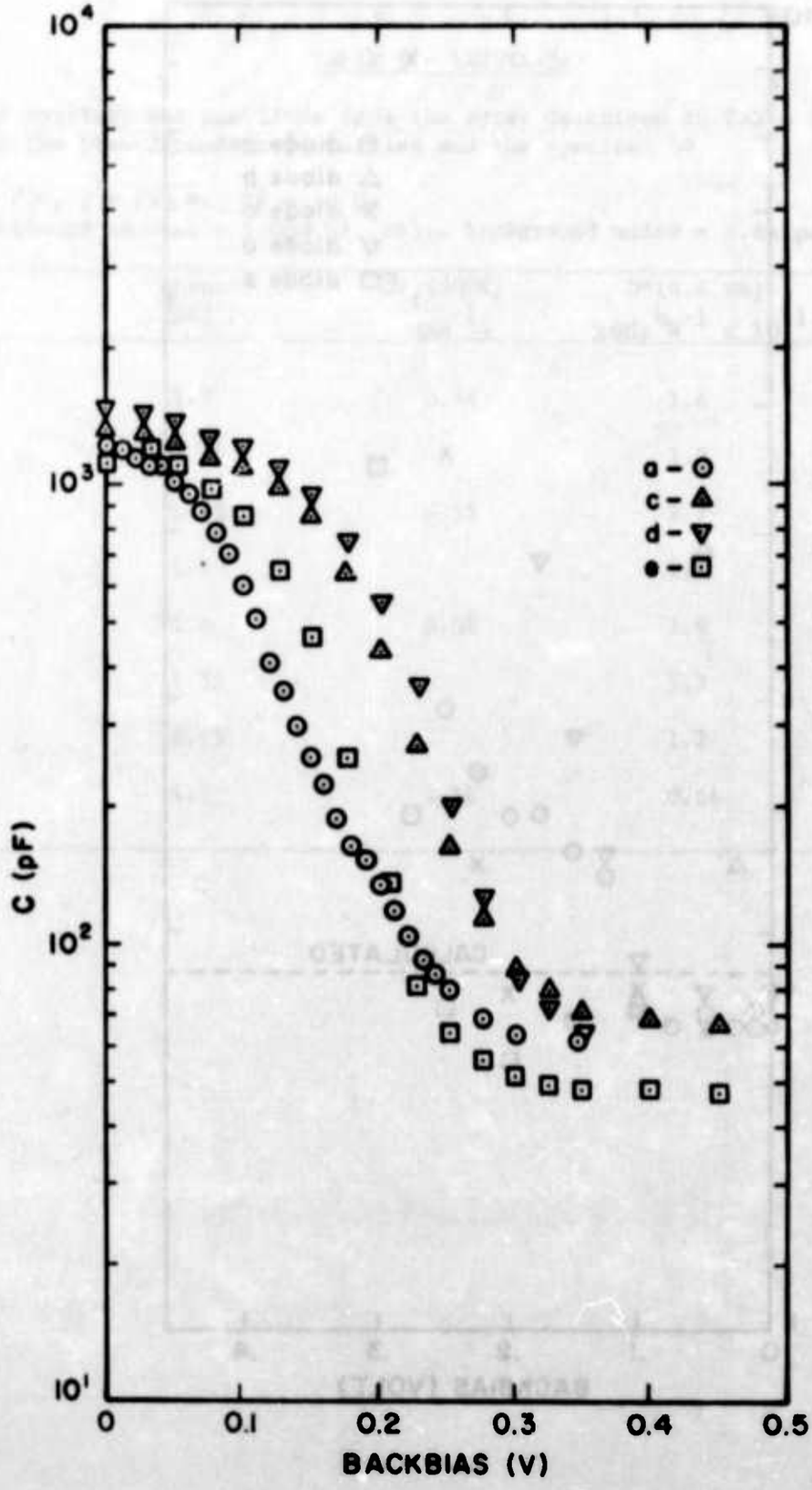

Fig. 44 EW496A-3. C-V at 80K.

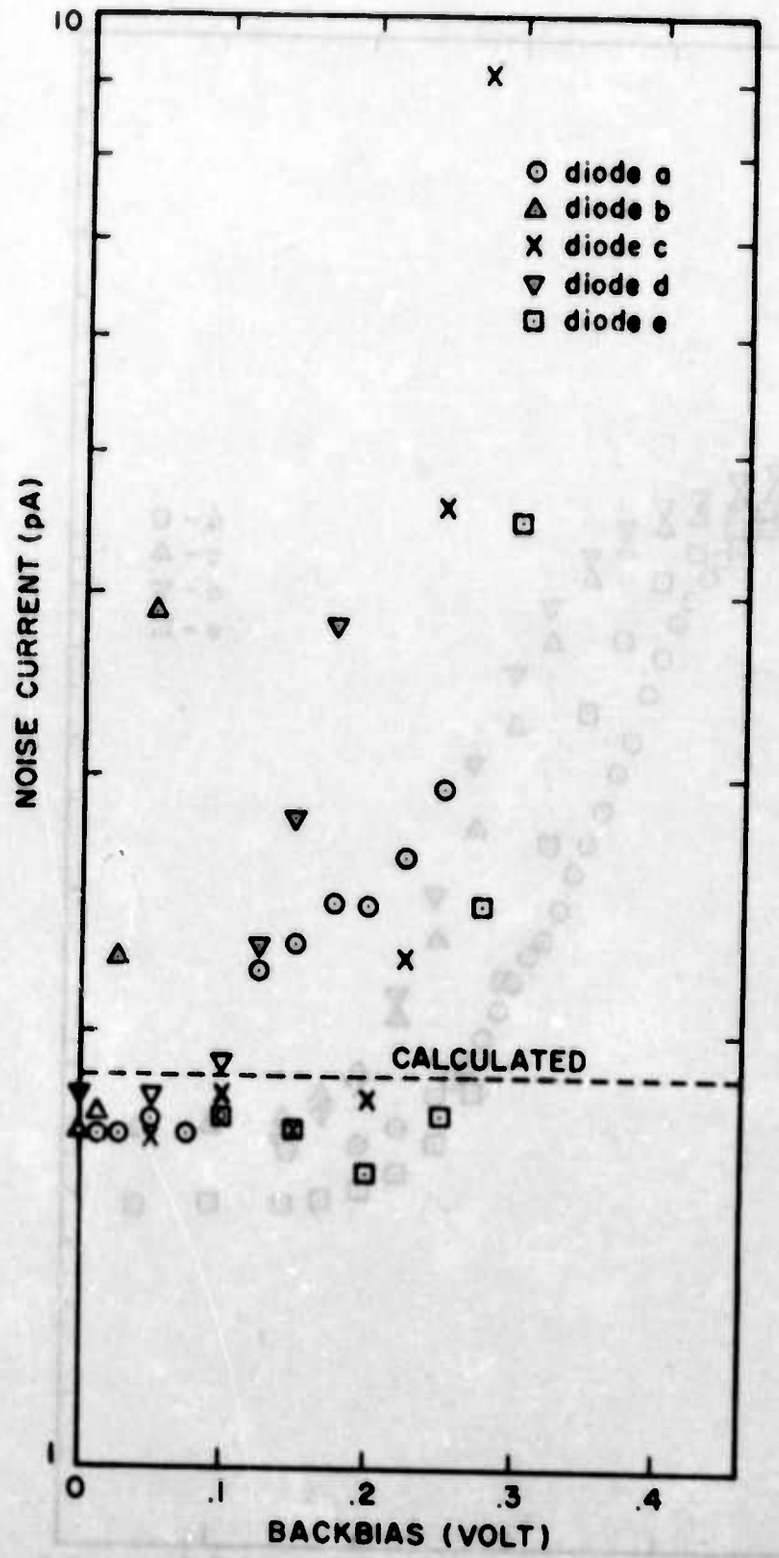

Fig. 45 EW496A-3. Bias dependent noise (Δf = 10 Hz) at 80K and 990 Hz. The line shows the calculated background noise.

Table 9 - EW496A-3e

This specimen was one diode from the array described in Table 8. Figures 46,47 show the bias-dependent properties and the spectral D*.

T = 80K, f = 990 Hz, Δf = 10 Hz
Background current = 1.059 μA, calc. background noise = 1.84 pA

Backbias [mV]	Noise [pA]	$\mathcal{R}_I$(500K) [AW^{-1}]	D*(4.8 μm) [$cmHz^{\frac{1}{2}}W^{-1} \times 10^{11}$]	Capacitance [pF]
0	1.8	0.54	1.6	1220
50	1.75		1.7	1110
100	1.75	0.55	1.7	859
150	1.7		1.7	461
200	1.6	0.58	1.9	134
250	1.75		1.7	64
275	2.45		1.2	56
300	4.5	0.56	0.66	51

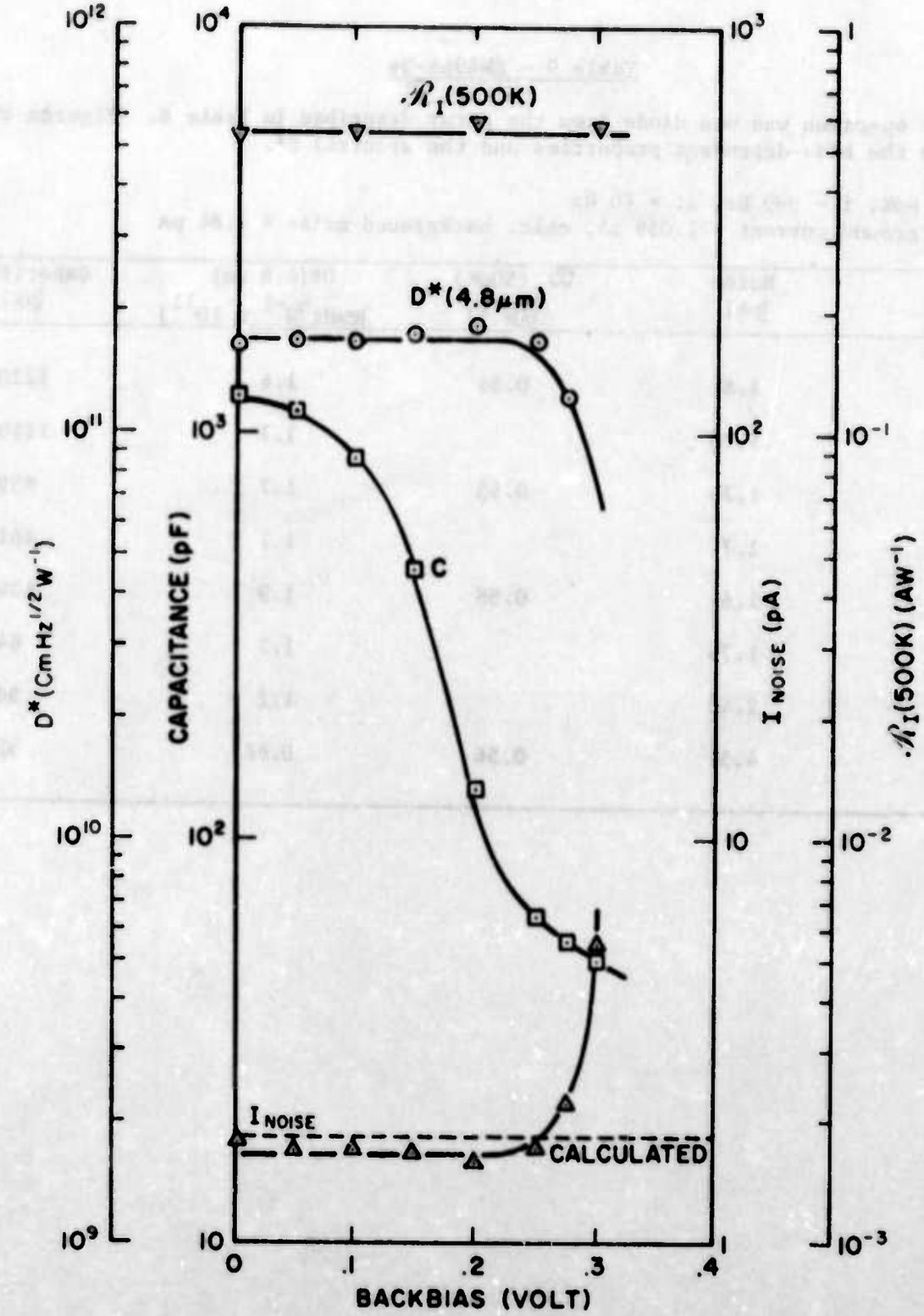

Fig. 46 EW496A-3. Bias dependent properties at 80K and 990 Hz.

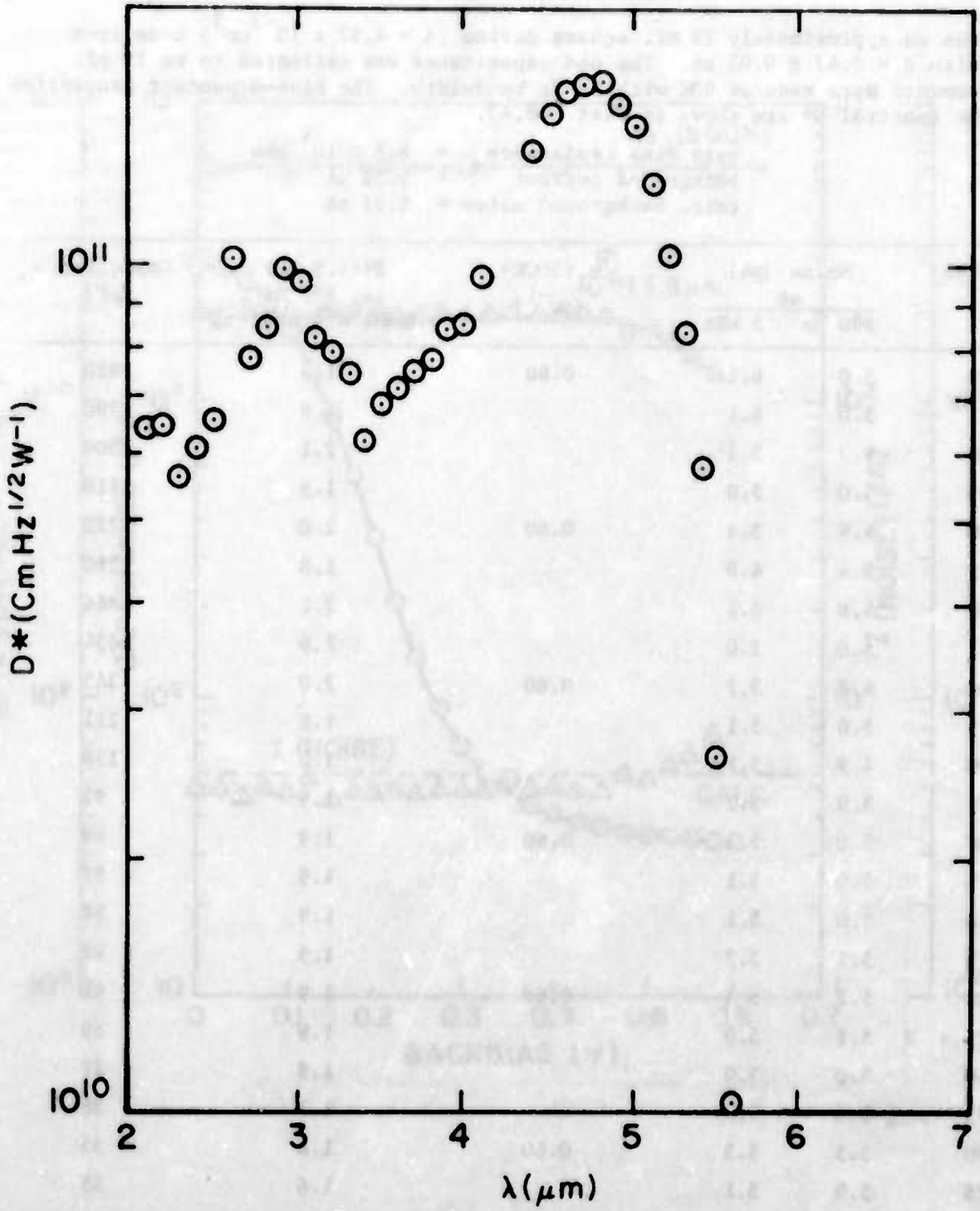

Fig. 47 EW496A-3e. Spectral D* at 80K and 990 Hz.

Table 10 - EW508-4c

This was an approximately 28 mil-square device (A = 4.97×10^{-3} cm^2) made from PbTe with d = 0.47 ± 0.03 μm. The pad capacitance was estimated to be 19 pF. Measurements were made at 80K with 10 Hz bandwidth. The bias-dependent properties and the spectral D* are shown in Figs. 48,49.

zero bias resistance = 6.5×10^5 ohm
background current = 9.52 μA
calc. background noise = 5.52 pA

Backbias [mV]	Noise [pA] at 990 Hz	Noise [pA] at 5 kHz	$\mathcal{R}_I$(500K) [AW^{-1}]	D*(4.9 μm) at 990 Hz [$cmHz^{\frac{1}{2}}W^{-1} \times 10^{11}$]	Capacitance [pF]
0	5.0	6.1	0.60	1.9	2810
25	5.0	6.1		1.9	2790
50	4.7	5.5		2.1	2500
75	5.0	5.0		1.9	2110
100	4.9	5.4	0.60	2.0	1720
125	5.4	4.8		1.8	1260
150	4.6	5.1		2.1	864
175	5.0	5.0		1.9	554
200	4.8	5.7	0.60	2.0	345
225	5.0	5.1		1.9	211
250	4.9	5.1		2.0	139
275	5.0	5.2		1.9	92
300	5.0	5.3	0.60	1.9	69
325	5.0	5.1		1.9	57
350	5.0	5.1		1.9	54
375	5.1	5.2		1.9	44
400	5.1	5.1	0.60	1.9	41
425	5.1	5.0		1.9	39
450	5.0	5.0		1.9	37
475	5.6	5.4		1.7	36
500	5.5	5.5	0.60	1.8	35
525	5.9	5.1		1.6	35
550	6.6	5.0		1.5	34
575	7.7	6.0	0.60	1.3	34
600					33

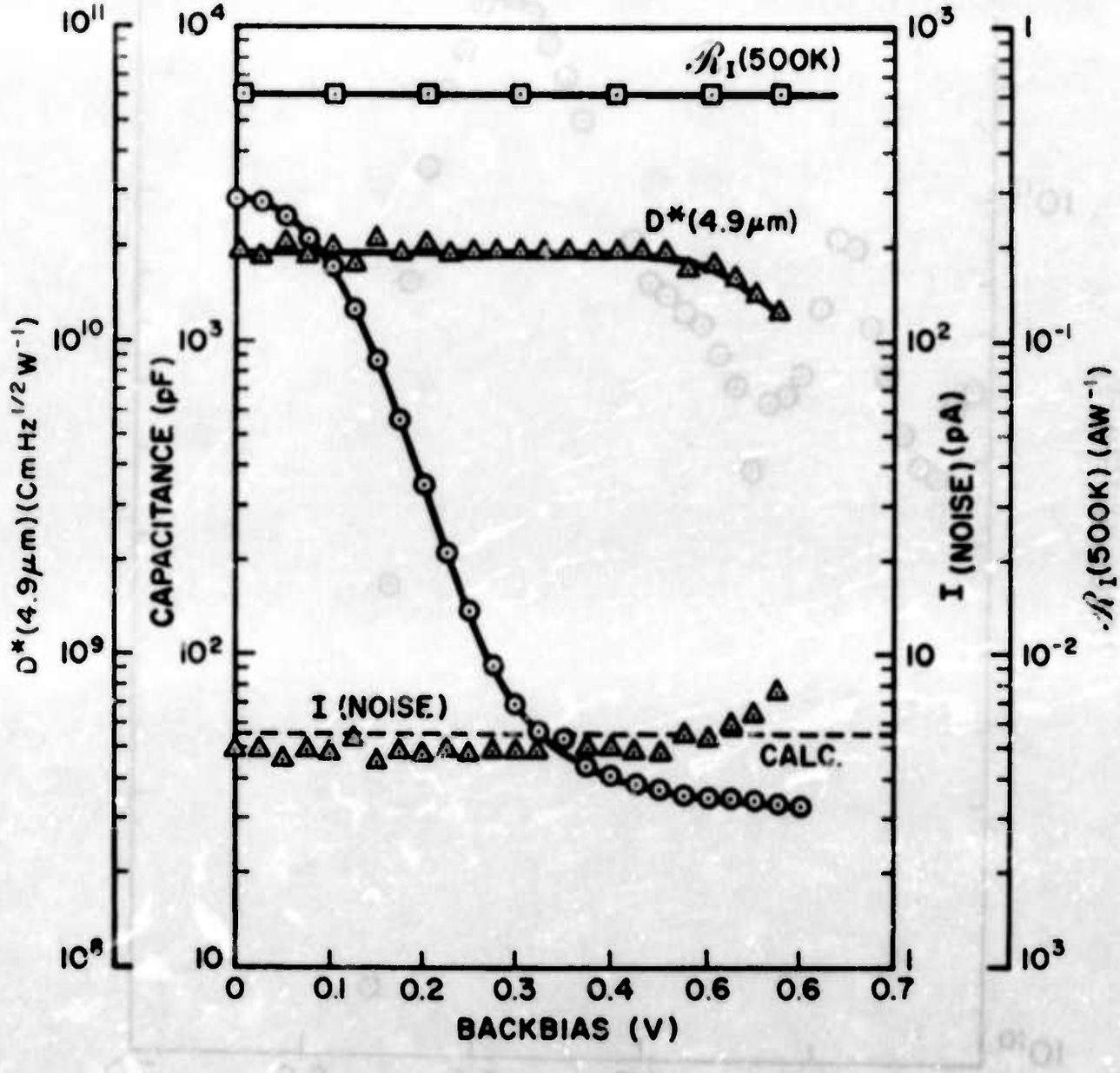

Fig. 48 EW508-4c. Bias dependent properties at 80K and 990 Hz.

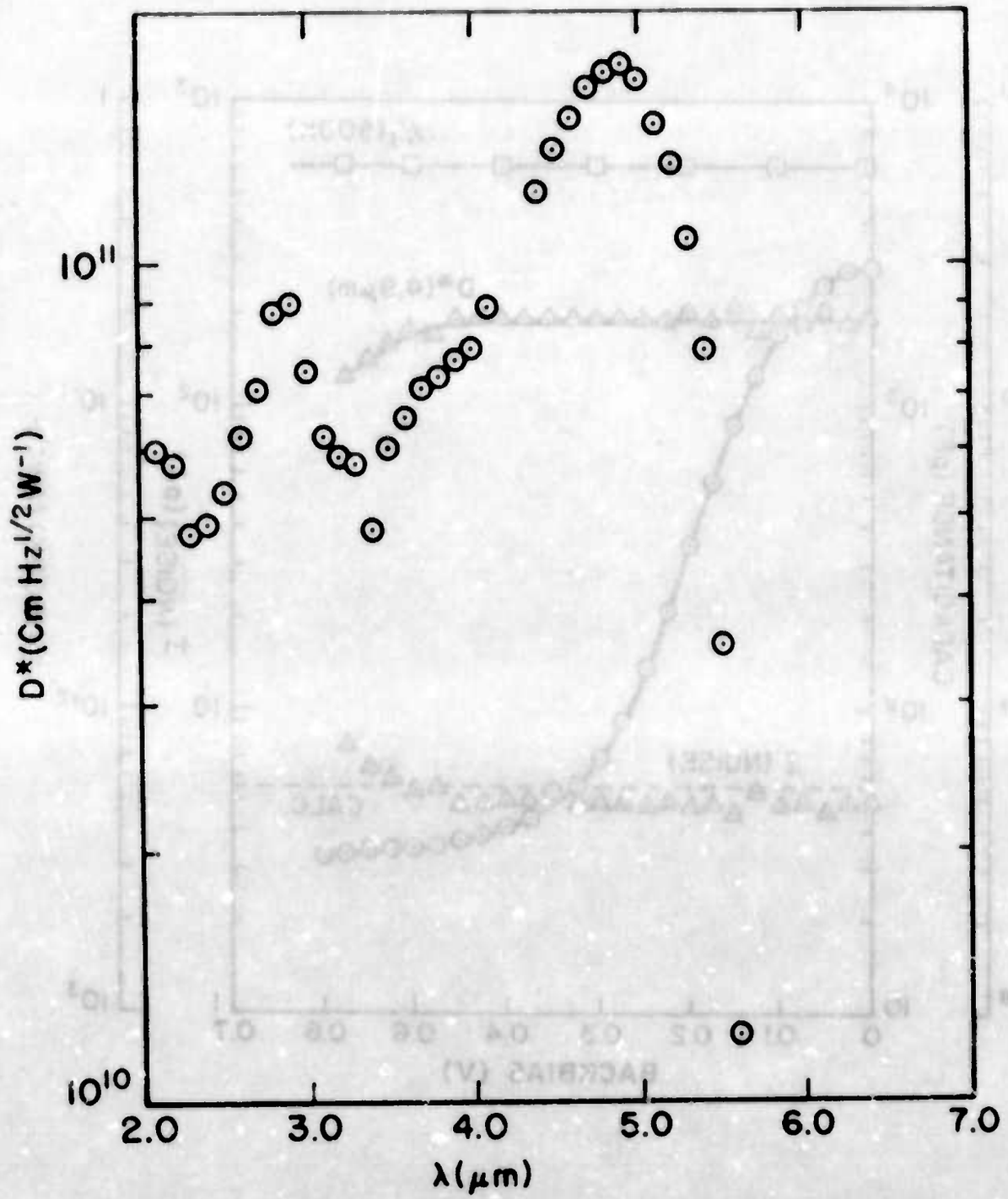

Fig. 49 EW508-4c. Spectral D* at 80K and 990 Hz.

4. Pinched-off $PbSe_{0.8}Te_{0.2}$ Devices

An attempt was made to extend the pinched-off mode from PbTe to $PbSe_{0.8}Te_{0.2}$ to permit full use of the 3-5 μm atmospheric window with photodiodes that operate at 170K. Such band-tailoring has previously been shown to be effective with conventional thin-film devices.(2)

Pinchoff was observed with $PbSe_{0.8}Te_{0.2}$ devices at 80K, but the capacitance decrease occurred at backbiases that were large enough to give significant 1/f noise. This difference from the behavior of PbTe devices appears to arise from a combination of an increase in the acceptor concentration and a decrease in the dielectric constant when $PbSe_{0.8}Te_{0.2}$ is substituted for PbTe. The $PbSe_{0.8}Te_{0.2}$ that was used had acceptor concentrations of about $2 \times 10^{17} cm^{-3}$, which was a factor of 2-3 larger than that of the PbTe layers.* The 300K values of the static dielectric constants of PbTe and PbSe are 430 and 230, respectively.(14) The static dielectric constant of $PbSe_{0.8}Te_{0.2}$ is unknown, but a linear interpolation between the 300K values of PbTe and PbSe suggests a value of around 270. There is the further complication that PbTe appears to be paraelectric(8,9) and its low-field static dielectric constant may be as large as 800 at 80K.** Applying the one-sided abrupt junction model to the just pinched-off diode, with thickness d and pinchoff voltage V_p, we obtain

---

* Here we compare the results of Hall measurements on layers that were 3-4 μm thick. Exposure to oxygen appears to give extra acceptors that cause about a factor of two decrease in the Hall coefficient of layers with thicknesses around 1 μm.

** Using the one-sided abrupt junction approximation, we estimate that most of the depletion region in our junctions has a field less than $10^6 Vm^{-1}$. From the observations of Bate et al(8) this suggests that the critical polarization is only exceeded near the n-region so that the depletion-layer width is dominated by the low-field (temperature-dependent) static dielectric constant.

$$V_p + V_{bi} = \frac{N_A q d^2}{2\epsilon} ,$$

where V_{bi} is approximately 0.22V and 0.25V for PbTe and $PbSe_{0.8}Te_{0.2}$, respectively. We find that the changes in N_A and ϵ on going from PbTe to $PbSe_{0.8}Te_{0.2}$ may increase $(V_p + V_{bi})$ for a given d by a factor between three and nine. Figure 50 shows the corresponding changes in V_p that could arise on going from PbTe to $PbSe_{0.8}Te_{0.2}$ as a result of such changes in N_A and ϵ.

An example of the pinchoff in a 9 mil-square $PbSe_{0.8}Te_{0.2}$ diode is shown in Fig. 51. Here the devices with thickness 0.18 ± 0.03 μm are pinched off at 80K with backbiases greater than about 0.6V. The required backbias is striking when compared with the forward bias pinchoff of similar quarter-wave PbTe diodes. With increase in the temperature, pinchoff moves further into backbias (Fig. 52) as with PbTe devices.

The improved processing that was described in Section 4.3.1 gave significant improvements in both the thermal stability and the backbias noise of $PbSe_{0.8}Te_{0.2}$ devices. Thus, the R_oA product at 80K was maintained after baking at 150°C for periods of up to four hours (Fig. 53). Also at 80K, low-noise operation has been demonstrated with backbiases of up to 0.4 V (Fig. 54). However, as with the PbTe devices, the backbias noise remains significant at 170K (Fig. 55).

In the course of our investigation we did not obtain a $PbSe_{0.8}Te_{0.2}$ pinched-off photodiode that permitted low-noise operation at 80K. The closest approach was a quarter-wave specimen that showed pinchoff beyond the backbias at which the 1/f noise became significant.* The properties of this device

* It is of interest that this specimen did not show significant degradation of the current response after baking at 150°C for four hours. Thus, the thermal instability that was observed with quarter-wave PbTe devices may not be as severe with $PbSe_{0.8}Te_{0.2}$.

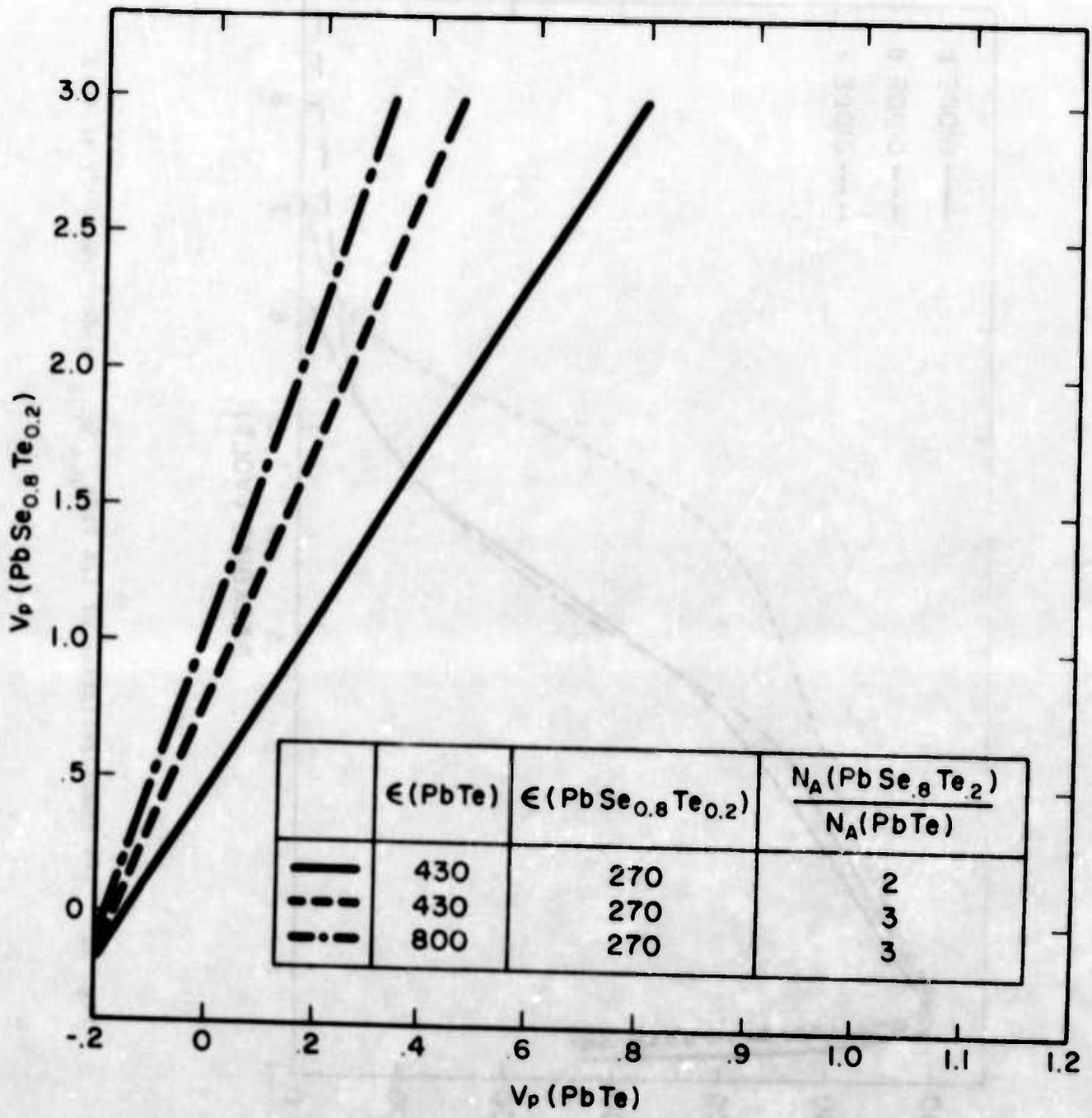

Fig. 50 Calculated relationships between pinchoff voltages of PbTe and $PbSe_{0.8}Te_{0.2}$.

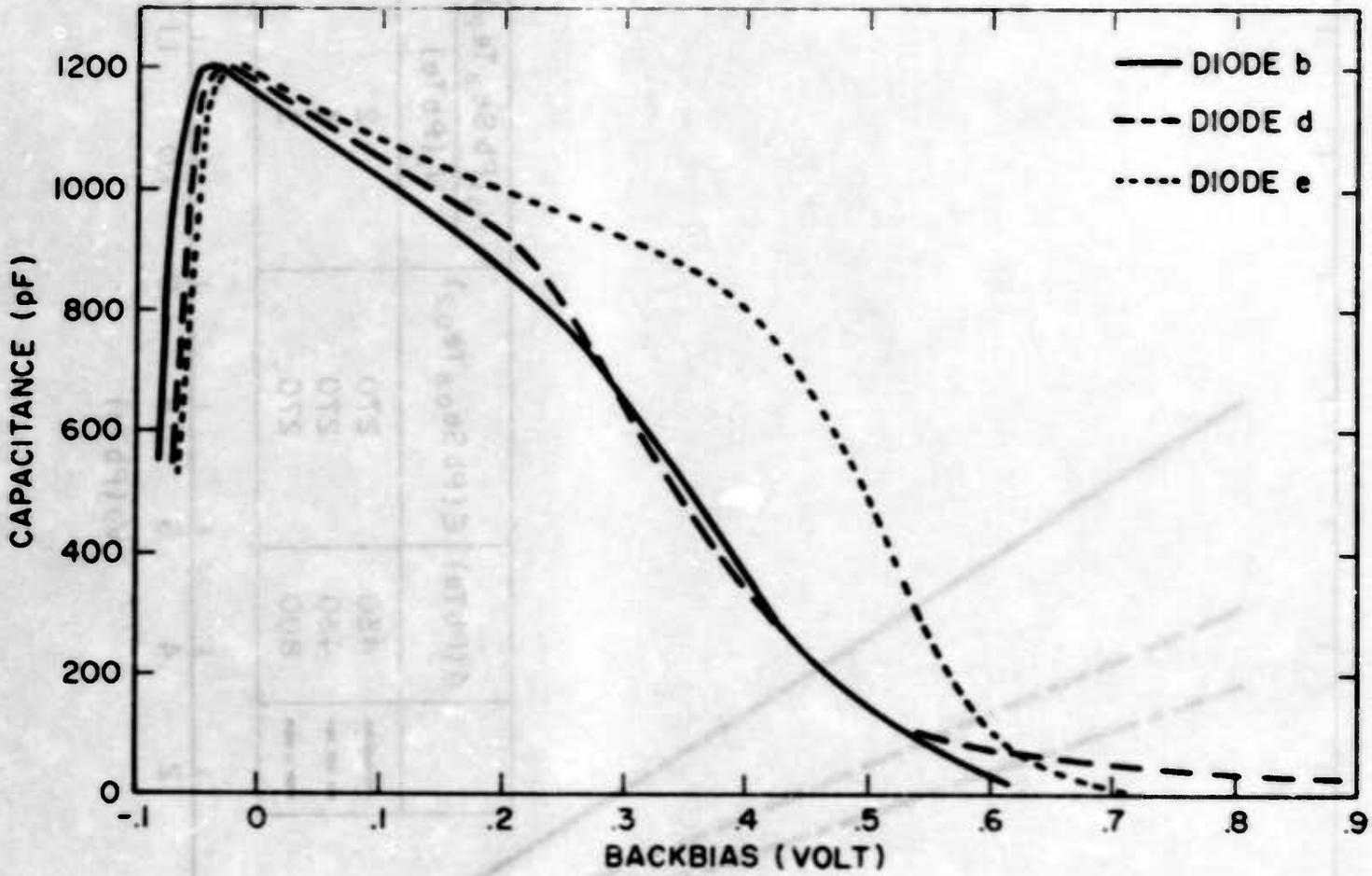

Fig. 51 C-V characteristics of λ/4 $PbSe_{0.8}Te_{0.2}$ diodes (HK207-2) at 80K.

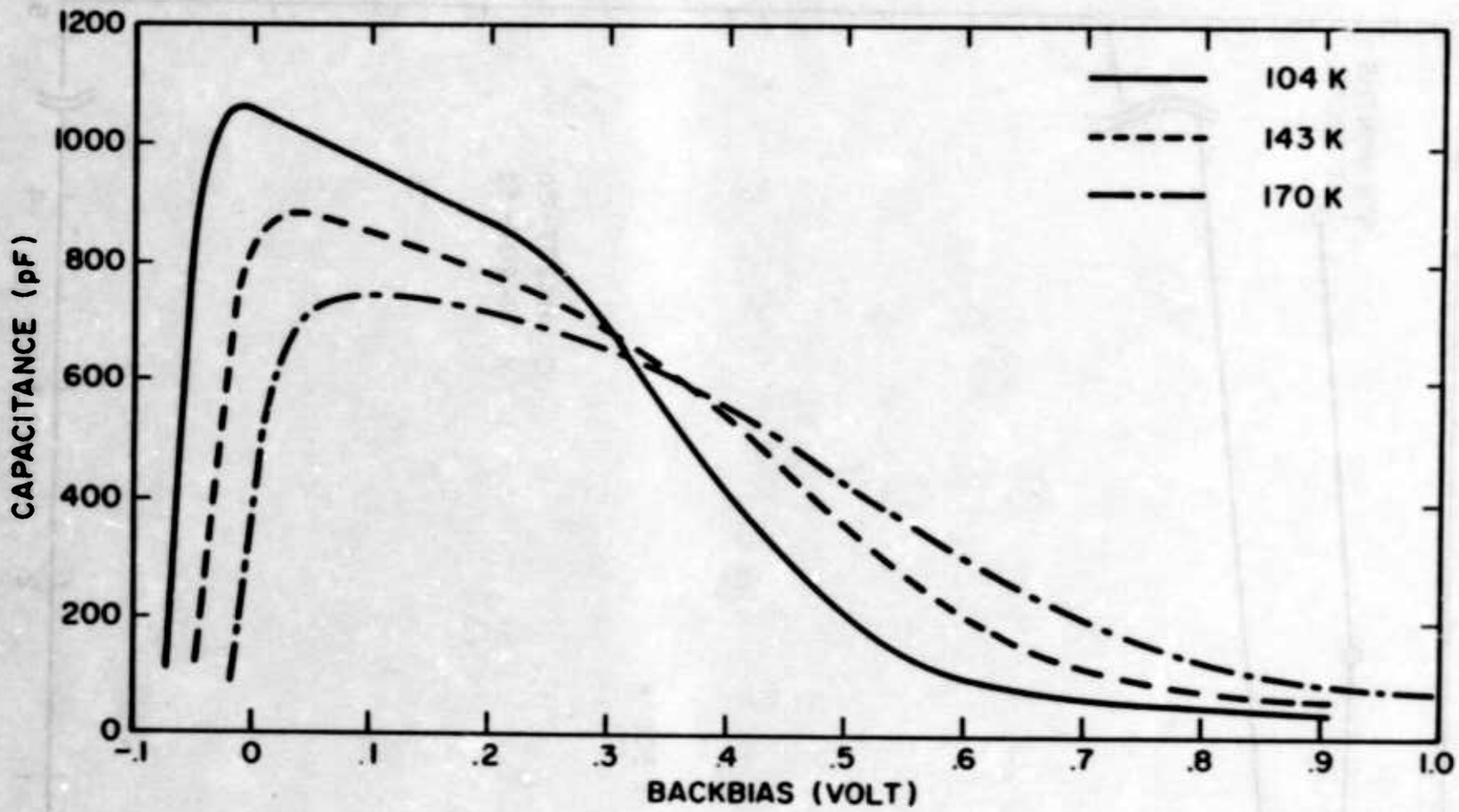

Fig. 52 Temperature dependence of C-V of a λ/4 $PbSe_{0.8}Te_{0.2}$ device (HK207-2d).

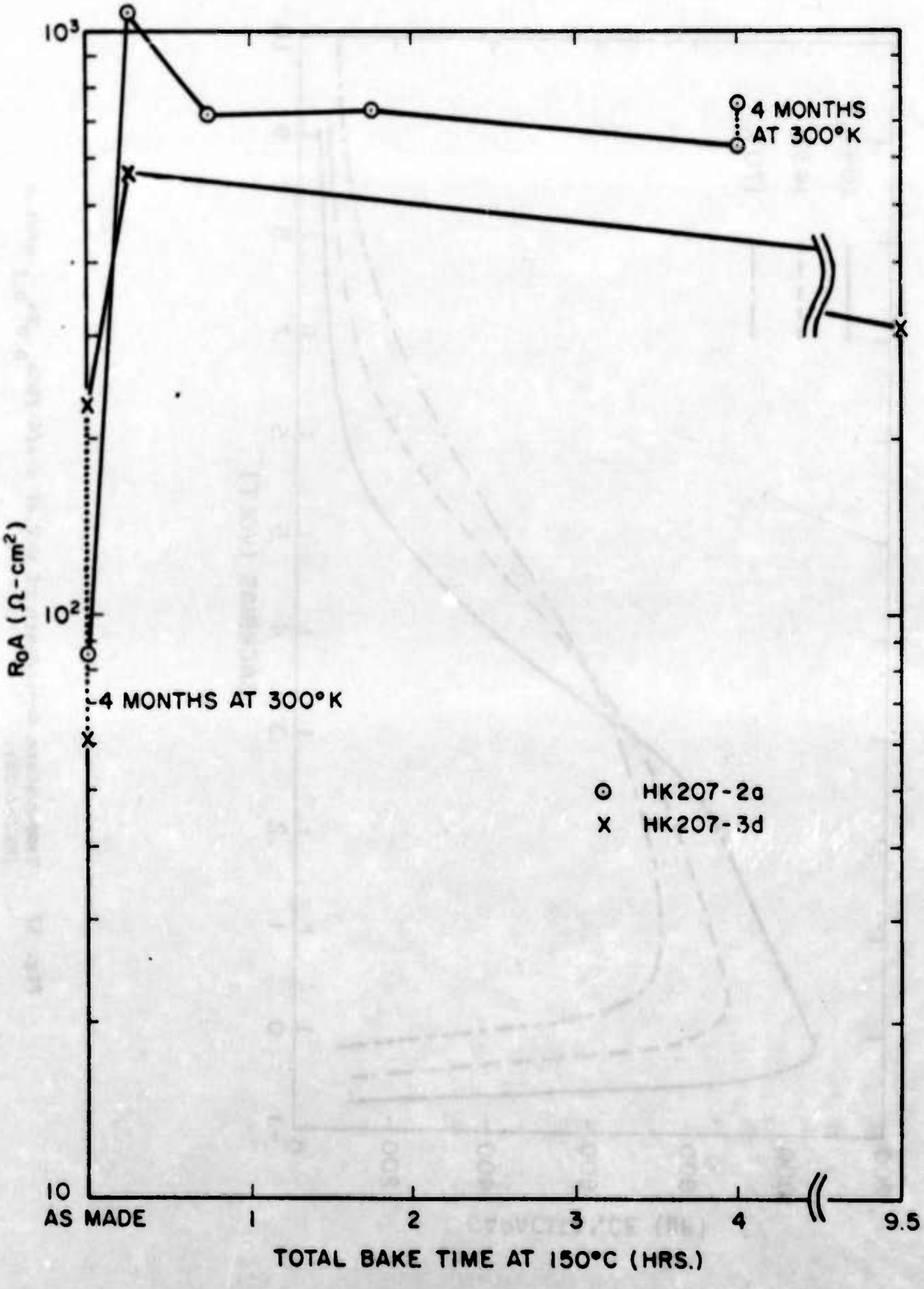

Fig. 53 R_oA of $\lambda/4$ $PbSe_{0.8}Te_{0.2}$ devices after baking at 150°C.

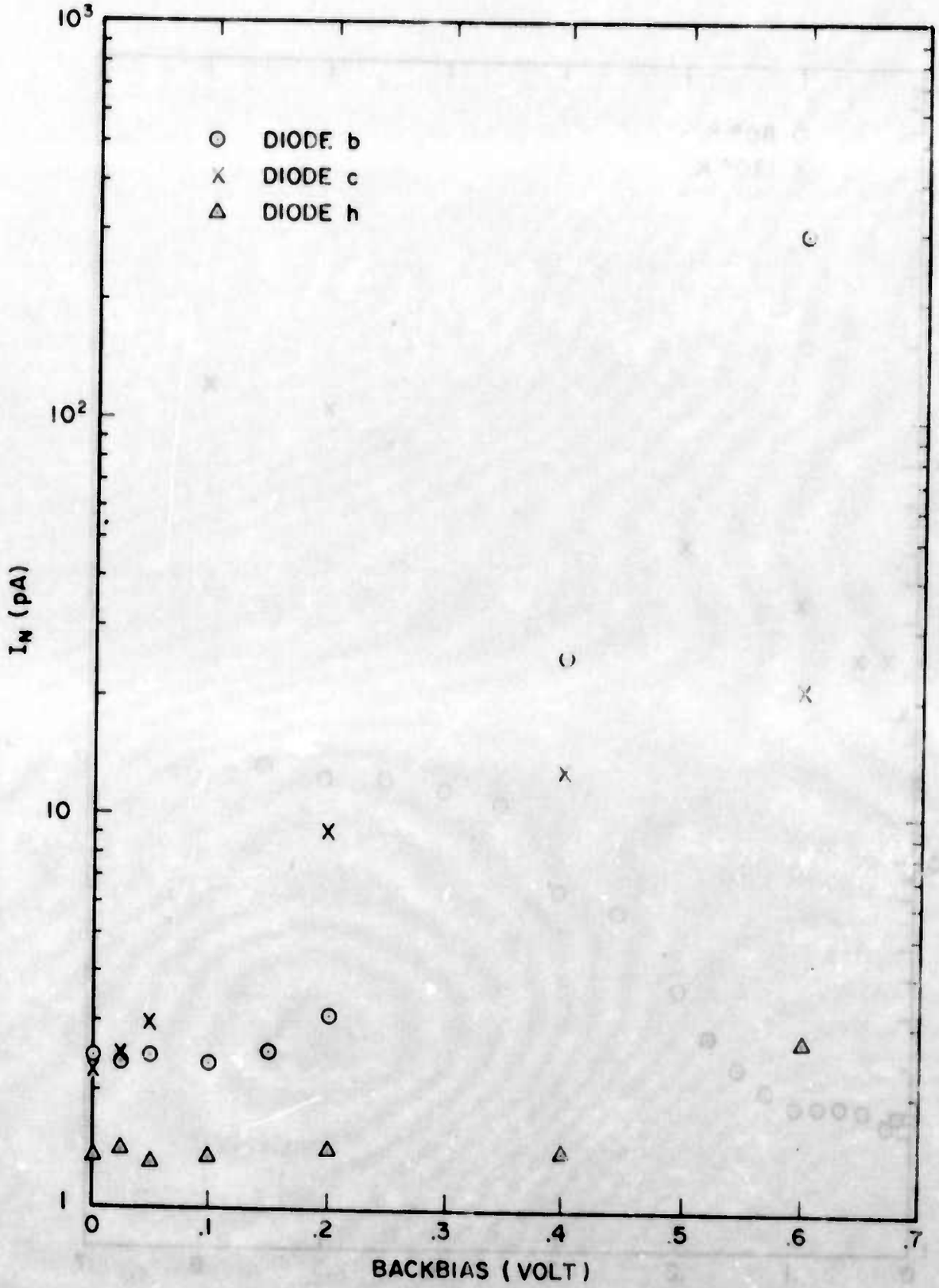

Fig. 54 Bias dependent noise (Δf = 7 Hz) of a 0.6 μm-thick $PbSe_{0.8}Te_{0.2}$ device (HK206-5) at 80K.

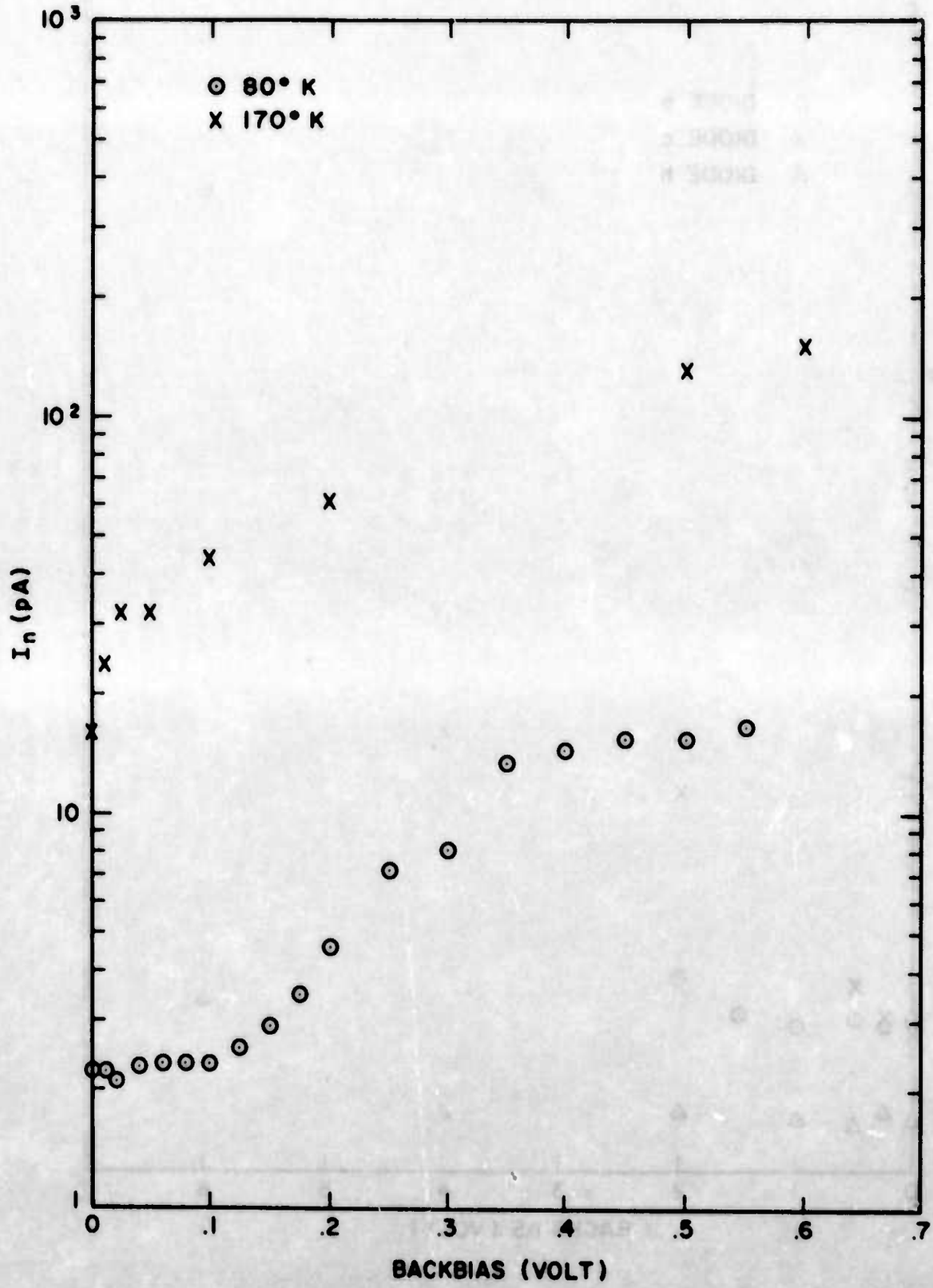

Fig. 55 Bias dependence noise (Δf = 7 Hz) of a $PbSe_{0.8}Te_{0.2}$ device (HK207-2d) at 80K and 170K.

are given in Table 11 and Figs. 56,57. In principle, low-noise pinched-off operation at 80K should be obtainable with a reduction in the acceptor concentration in the $PbSe_{0.8}Te_{0.2}$. A useful reduction in the capacitance has been obtained at 0.5V backbias and low-noise operation has been obtained at 0.4V backbias, although not in the same specimen. This led to a series of experiments in which subsidiary sources of Pb and Se were used in an attempt to define conditions for growth of $PbSe_{0.8}Te_{0.2}$ with $p < 10^{17} cm^{-3}$ rather than our usual $p \gtrsim 2 \times 10^{17} cm^{-3}$. This approach was unsuccessful; details are given in Appendix II.

Table 11 - Properties of a Quarter-Wave $PbSe_{0.8}Te_{0.2}$ Device (HK207-2d)

This specimen had area = $5.76 \times 10^{-4} cm^2$ and thickness = 0.18 ± 0.03 μm.
The measurements were made at 80K after baking for four hours at 150°C.

zero bias resistance = 4.17×10^5 ohm
background current = 1.71 μA
calc. background noise = 1.96 pA
bandwidth = 7 Hz

Backbias [mV]	Noise [pA] 990 Hz	5kHz	10 kHz	$\mathcal{R}_I$(500K) [AW^{-1}]	D*(4.9 μm) at 990 Hz [$cmHz^{\frac{1}{2}}W^{-1} \times 10^{10}$]	Capacitance [pF]
0	2.25	2.25		0.57	7.9	1220
50	2.3	2.2	2.5		7.7	1150
100	2.35	2.3	2.5		7.5	1100
150	2.9	2.3	2.6		6.1	1030
200	4.6	2.7	2.6	0.56	3.8	980
250	7.2	4.1	3.2		2.5	860
300	8.1	4.4	3.9		2.2	660
350	13	5.2	3.8		1.4	480
400	14.5	6.0	4.5		1.2	330
450	15.5	6.6	4.9		1.1	210
500	15.5	6.5	5.1	0.55	1.1	107
550	16.5	7.5	5.1		1.1	60
600						40
650						27
700						19

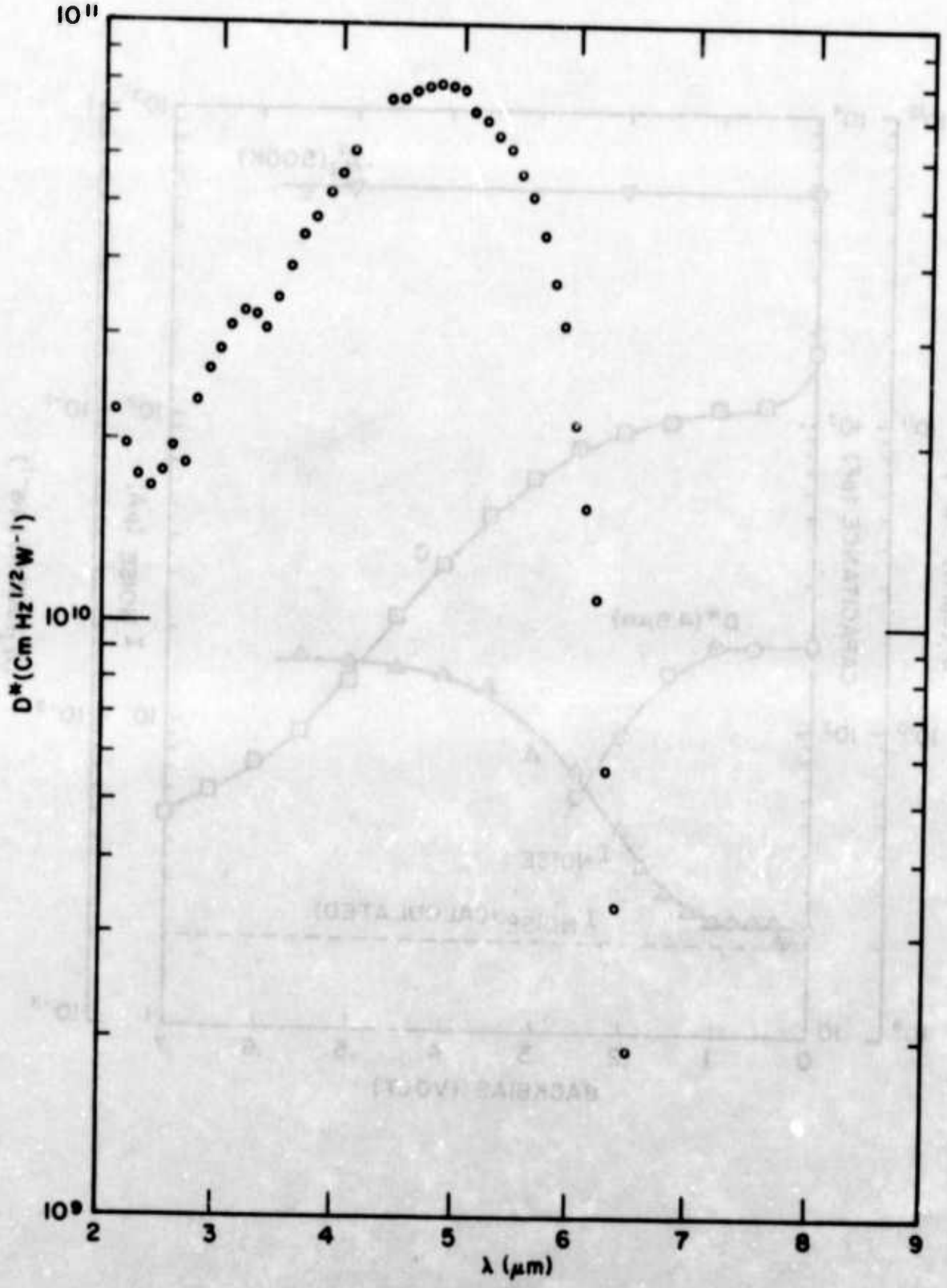

Fig. 56 HK207-2d. Spectral D* at 80K.

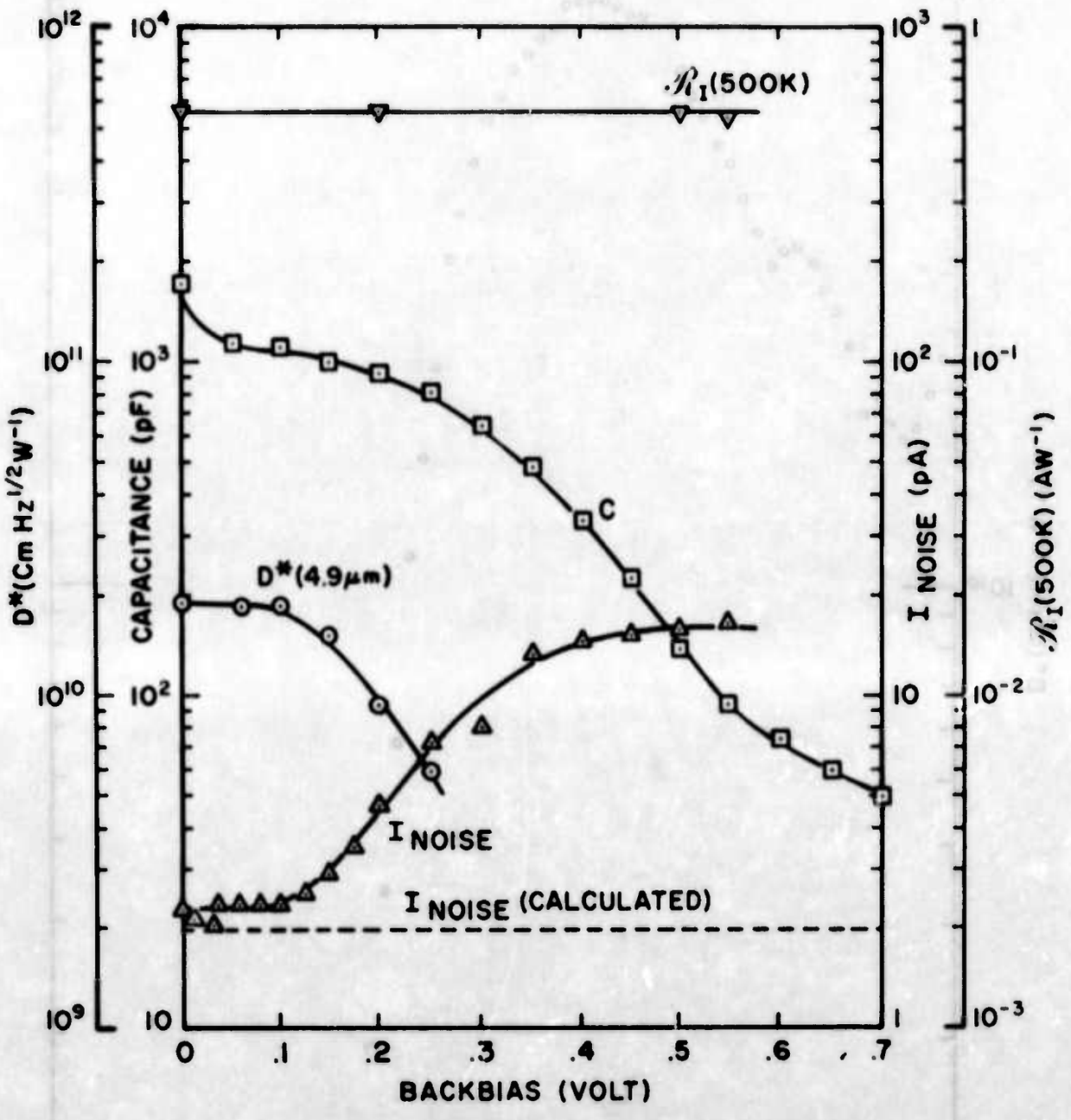

Fig. 57 HK207-2d. Bias dependent properties at 80K and 990 Hz.

4.5 Summary of Results for Pinched-off Photodiodes

For PbTe detectors that operate at 80K, the three-quarter-wave pinched-off photodiode provides one to two orders of magnitude reduction of the capacitance from that of conventional photodiodes. This capacitance reduction is obtained without any sacrifice in the other detector parameters, such as detectivity, quantum efficiency, and cutoff wavelength. The transit-time limitations upon the inherent speed of the pinched-off devices have yet to be determined, as has the physics of their collection mechanism. However, the result appears to make possible a useful increase of the rolloff frequency for the detectivity of detector/preamplifier combinations for the 3-5 μm spectral region. The pinched-off capacitance is expected to scale with the diode's periphery, rather than with its area, so the magnitude of the attainable capacitance reduction will depend upon the diode size. For typical diode dimensions of 2 mil x 2 mil we project that the junction capacitance may be reduced to 1 pF, which is more than one order of magnitude less than that of a conventional PbTe device.

The situation with operation of pinched-off 3-5 μm devices at 170K is less attractive. The three-quarter-wave devices require backbias for pinchoff and the backbias regime remains very noisy at 170K, despite our improvement of the backbias noise at 80K. The quarter-wave PbTe devices do offer reduced capacitance at 170K, but their thermal instability makes them unattractive for practical applications. For optimum 170K devices, one would prefer band-tailoring to extend the response to $\lambda = 5$ μm. Pinchoff has been demonstrated in quarter-wave $PbSe_{0.8}Te_{0.2}$ devices, but only at rather large backbiases. Pinched-off operation at smaller backbias appears to be

possible via development of techniques for growth of $PbSe_{0.8}Te_{0.2}$ layers with smaller carrier concentrations. This development, together with the demonstrated reduction of excess noise in backbias would permit low-capacitance, low-noise operation of quarter-wave $PbSe_{0.8}Te_{0.2}$ photodiodes at 80K. However, at present the excess noise in backbias at 170K would appear to make such devices unattractive for thermoelectrically-cooled operation.

An unexpected spin-off from the studies of pinched-off photodiodes is the development for both PbTe and $PbSe_{0.8}Te_{0.2}$ of improved processing techniques that permit bakeout at 150°C. The new processing also permitted the use of significant backbias at 80K without the intrusion of 1/f noise.

5. LATERAL COLLECTION PHOTODIODES

5.1 General Considerations

The lateral collection concept may be understood by referring to Fig. 58. In 58a we show a section of a conventional photodiode. Typically, the junction depth is smaller than the minority carrier diffusion length and larger than the optical absorption length. Under these conditions most of the photons are generated on the surface side of the junction, which acts as a nearly perfect sink so that the quantum efficiency approaches the reflection loss limit. Figure 58b shows a first attempt to reduce the capacitance by making the junction area smaller than the collection area. The trouble with this configuration is that the quantum efficiency is reduced because photogenerated minority carriers may diffuse into the bulk of the semiconductor and recombine there, rather than diffuse to the junction where they can be collected. This problem leads to the final configuration that is shown in Fig. 58c. Here a barrier is introduced to confine the photogenerated minority carriers to a skin near the surface. If this skin has a thickness much less than the minority carrier diffusion length the minority carrier concentration will be uniform across the skin and diffusion will only occur laterally toward the collector junctions.

In principle, the barrier may be made in a variety of ways. Thus, a potential barrier with height greater than 2kT may be achieved by increasing the doping level of the underlying material or by increasing its energy gap. A simpler scheme, adopted here, is to use an epitaxial layer of the semiconductor on an insulating substrate.

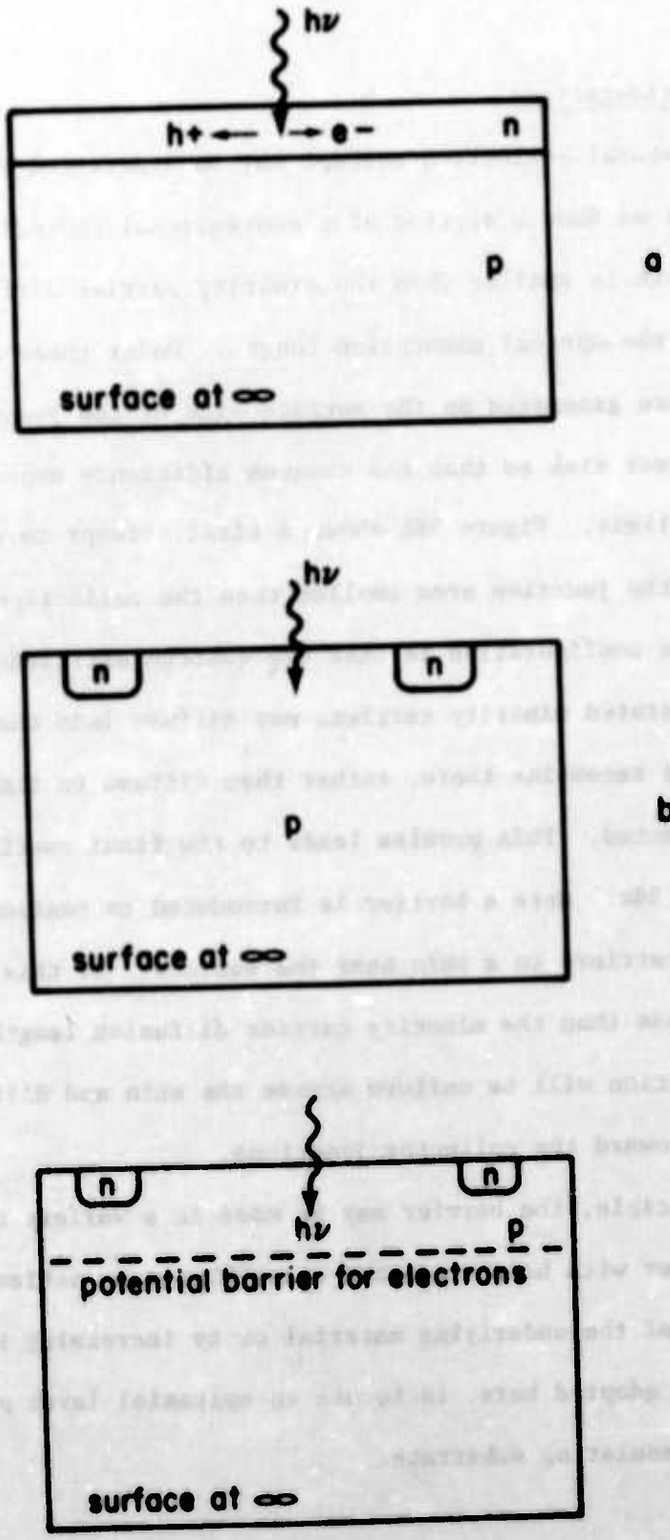

Fig. 58 The lateral collection concepts.

The scheme in Fig. 58c gives a photodiode in which the area for photon collection is larger than the junction area. In the following discussion we analyze the conditions under which this arrangement can give reduced capacitance without too much loss of quantum efficiency. As a bonus we find that the lateral collection arrangement offers the possibility of increases in the junction resistance which would increase the Johnson-noise-limited detectivity and hence the operating temperature.

5.1.1 Collection Efficiency of an Array of Stripes

Our previous work with thin-film photodiodes has shown that the quantum efficiency is limited only by reflection losses, i.e. every absorbed photon generates a minority carrier that is collected. In analyzing the behavior of lateral collection devices, with potentially less efficient collection, we define a collection efficiency, η_C, in terms of the overall quantum efficiency, η, and the reflection-loss-limited quantum efficiency, η_R, as follows

$$\eta = \eta_R \eta_C \ .$$

Consider the uniform array of stripes shown in Fig. 59a with exposure to light to give a uniform rate of photogeneration of minority carriers (G). The diffusion equation may be simplified to one dimension by approximating the real cross-section of Fig. 59b by that of Fig. 59c where the region under the n region is assumed to have perfect collection (as with a conventional thin-film diode) while the region from which lateral collection occurs is fitted to the boundary condition of a perfect sink (zero excess minority carrier concentration) at the projection of the n region (rather than at the boundary of the depletion region).

For the lateral collection region the diffusion equation

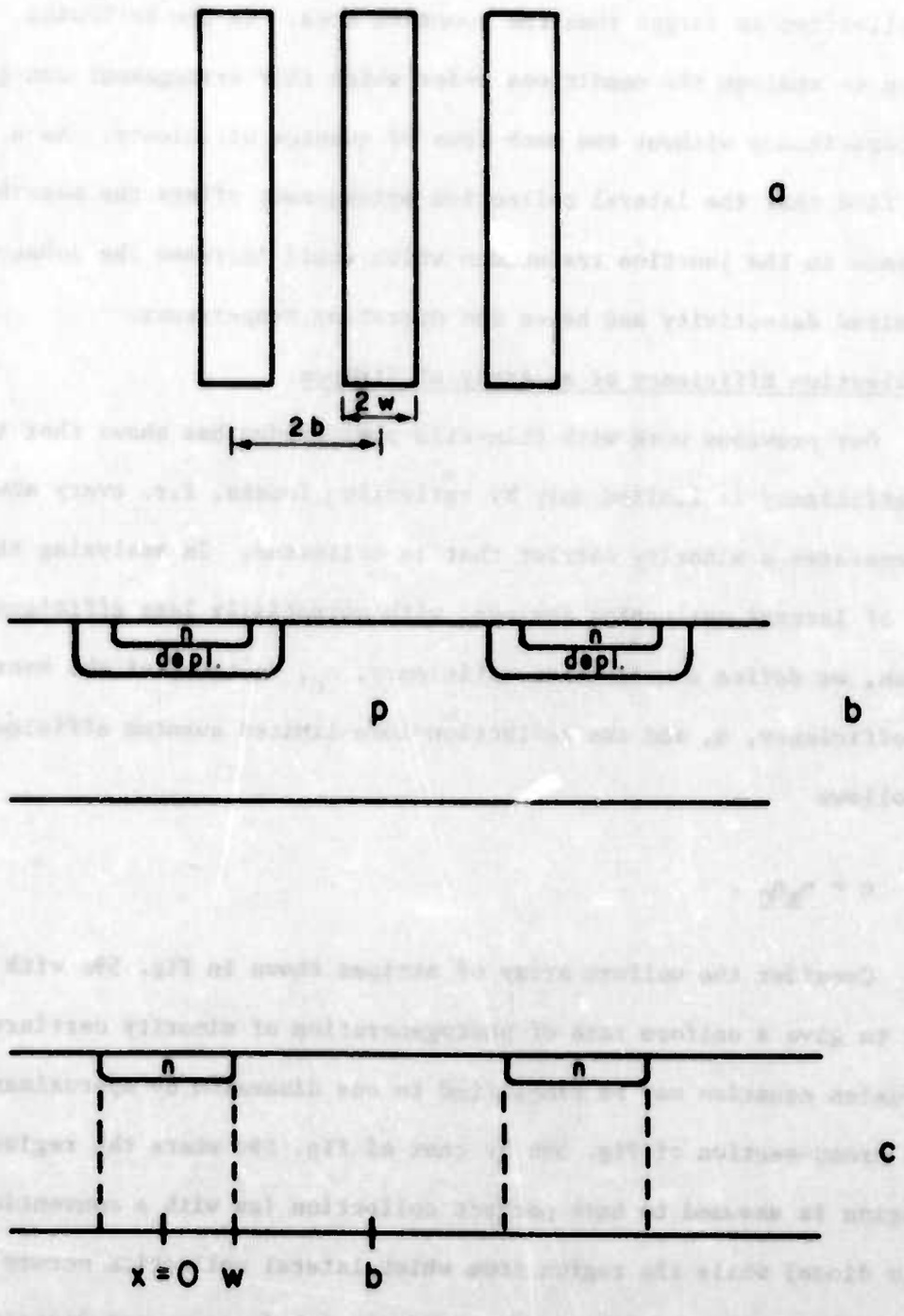

Fig. 59 Geometry for an array of stripe collectors.

$$\nabla^2 n - \frac{n}{L^2} + \frac{G}{D} = 0$$

reduces to one dimension with the solution

$$n = \alpha \exp\left[\frac{x}{L}\right] + \beta \exp\left[\frac{-x}{L}\right] + \frac{GL^2}{D}$$

where n is the excess minority carrier concentration,

$$L = \sqrt{D\tau}$$

is the minority carrier diffusion length, and

$$D = \frac{kT}{q}\mu$$

is the diffusion coefficient.

Imposing the boundary conditions

$$n\big|_{x = w} = 0 \ ,$$

$$\frac{dn}{dx}\bigg|_{x = b} = 0 \ ,$$

where the coordinates are those of Fig. 59c, we obtain

$$n = \frac{GL^2}{D}\left[1 - \frac{\cosh(B - X)}{\cosh(B - W)}\right] \ .$$

where

$$X = x/L \ ,$$

$$B = b/L \ ,$$

$$W = w/L \ .$$

The laterally-collected carrier flux into unit length of the collector is

$$J_{lat} = -D\frac{dn}{dx}\bigg|_{x = w} = GL\tanh(B - W)$$

whence, adding the directly collected flux and dividing by the total generation rate, we obtain the collection efficiency

$$\eta_C = \frac{W}{B} + \frac{\tanh(B - W)}{B} \quad .$$

A plot of this function is given in Fig. 60.

5.1.2 Collection Efficiency of an Array of Dots

For the array of dots shown in Fig. 61a we may approximate to radial symmetry with the coordinates of Fig. 61b and approximate the true configuration of Fig. 61c by that of Fig. 61d, with the same simplification of boundary conditions as in the stripe collector case.

The diffusion equation is now

$$\frac{d^2n}{dr^2} + \frac{1}{r}\frac{dn}{dr} - \frac{n}{L^2} + \frac{G}{D} = 0 \ ,$$

with the boundary conditions

$$n\big|_{r = w} = 0 \ ,$$

$$\frac{dn}{dr}\bigg|_{r = b} = 0$$

and the solution

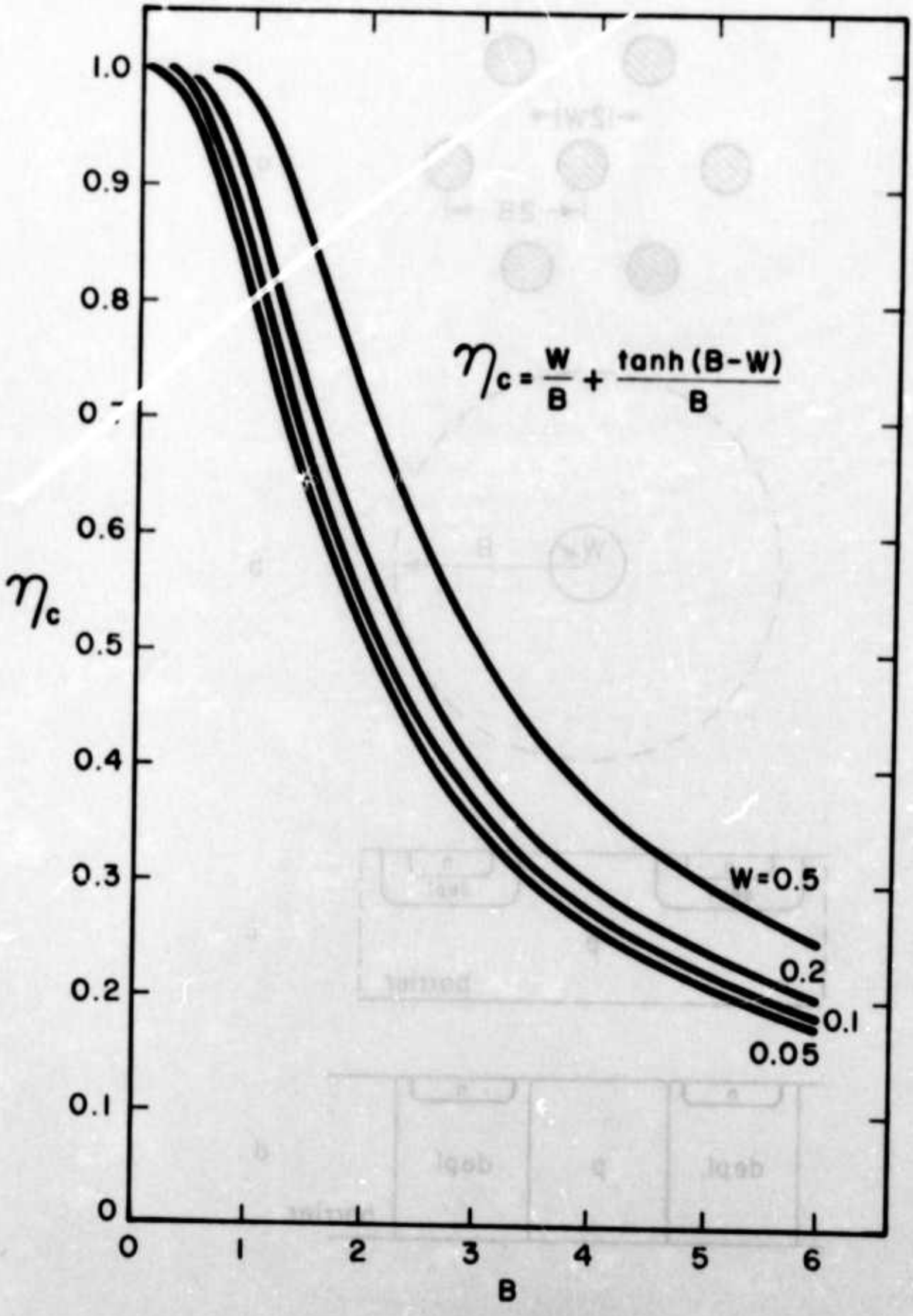

Fig. 60 Collection efficiency of an array of stripe collectors.

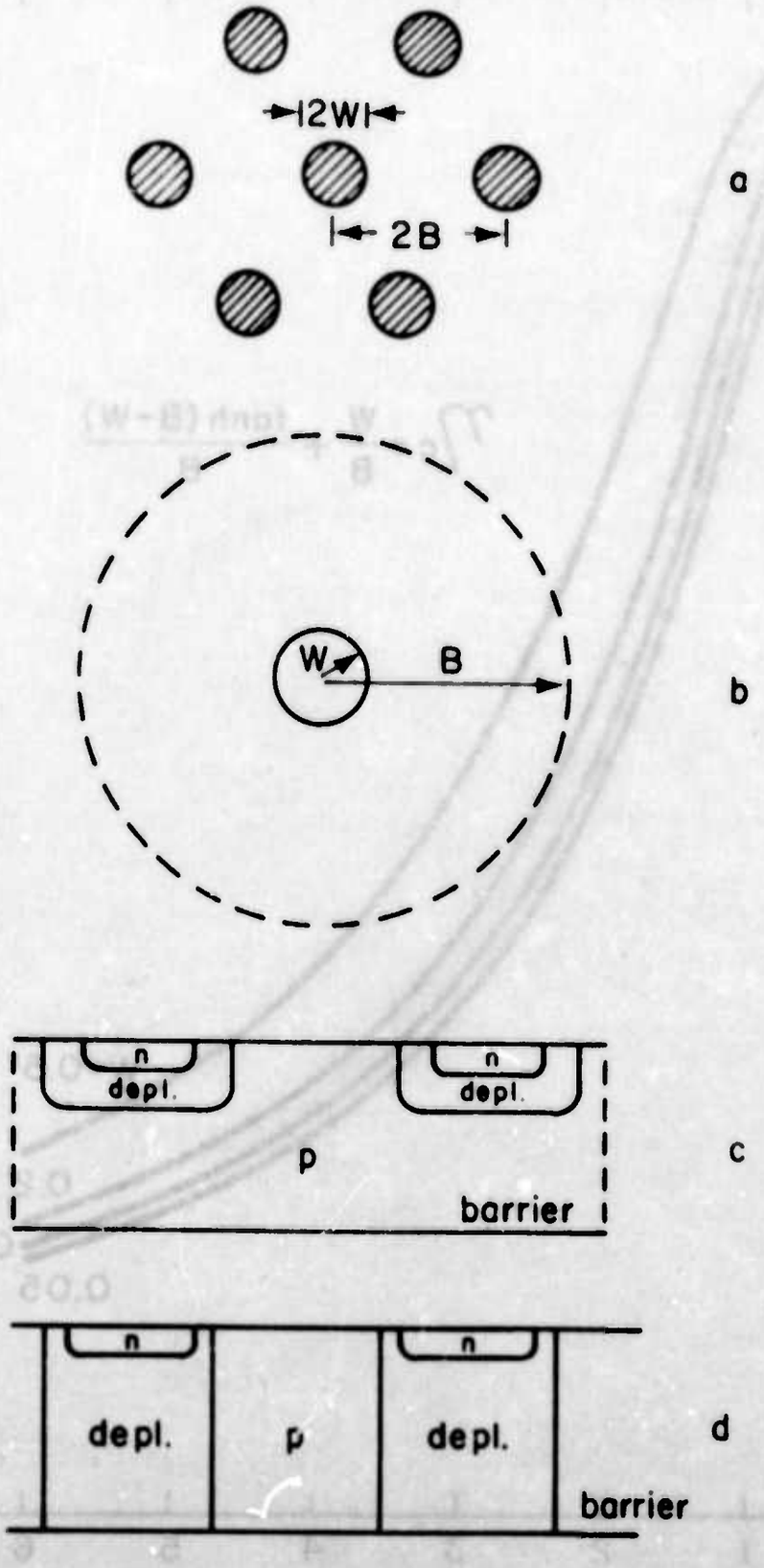

Fig. 61 Configuration of an array of dot collectors.

$$n = \frac{GL}{D}^2 \left[1 - \frac{G_1(B)I_0(R) + I_1(B)G_0(R)}{G_1(B)I_0(W) - I_1(B)G_0(W)} \right] .$$

where

$$B = b/L ,$$

$$W = w/L ,$$

$$R = r/L ,$$

and $I_n(x)$ and $G_n(x)$ are modified Bessel and Hankel functions defined by

$$I_n(x) = i^{-n} J_n(ix) ,$$

$$G_n(x) = i^{n+1} H_n^{(1)}(ix).$$

The total photocurrent into the junction is

$$I = G\pi w^2 + 2\pi wD \left.\frac{dn}{dr}\right|_w$$

where the first term is the contribution from the area under the n region. For complete collection $I \to G\pi b^2$, so

$$\eta_C = \frac{W^2}{B^2} + \frac{2W}{B} \left[\frac{I_1(B)G_1(W) - G_1(B)I_1(W)}{I_1(B)G_0(W) + G_1(B)I_0(W)} \right] .$$

A plot of this function is given in Fig. 62.

5.1.3 The Trade-off Between Quantum Efficiency and Capacitance Reduction

The analysis in Sections 5.1.1-.2 may be used to estimate the capacitance reduction that is attainable without too large a sacrifice in quantum efficiency. For the stripe collectors the junction capacitance, relative to that of a conventional photodiode, is W/B and plotting the

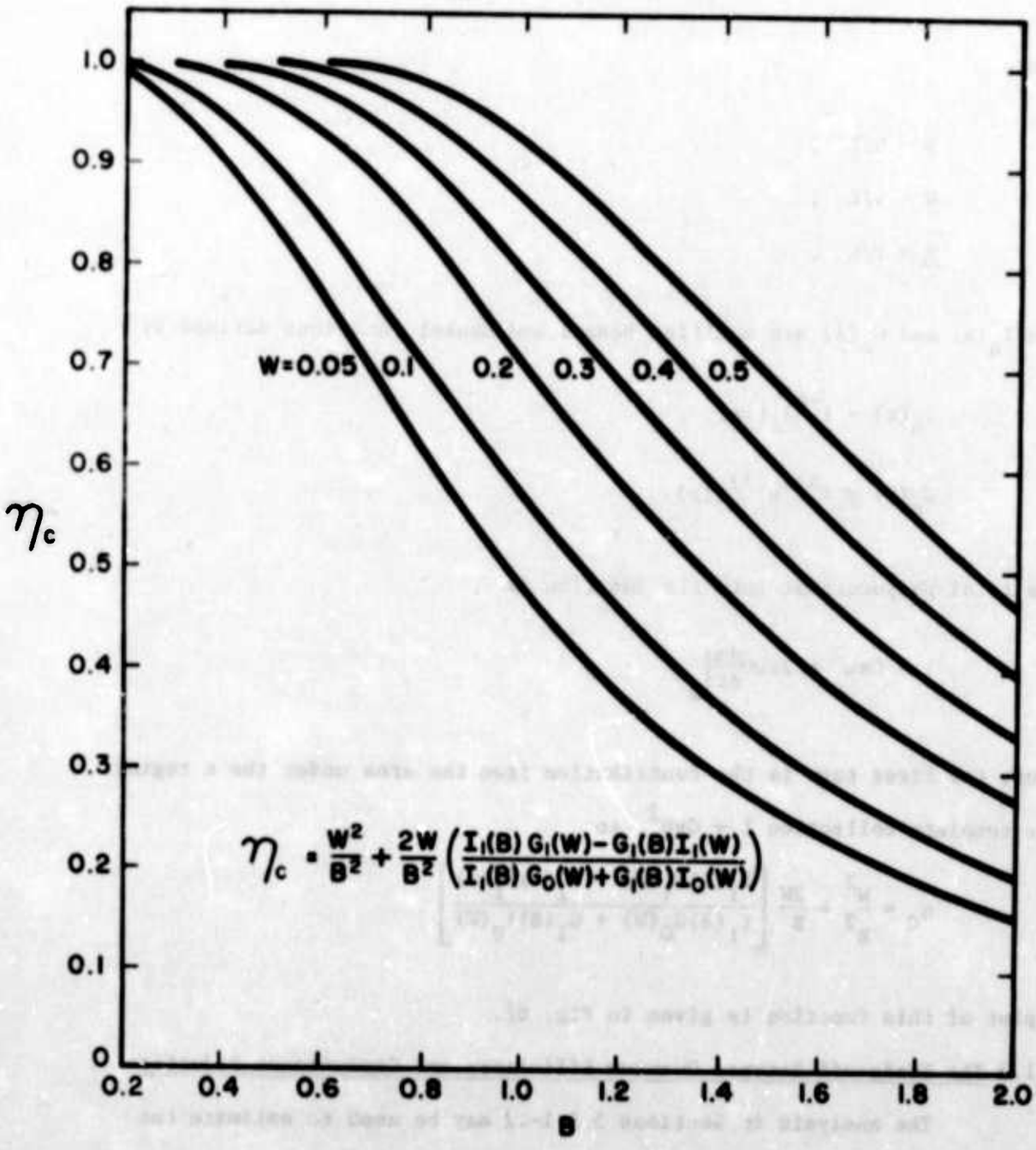

Fig. 62 Collection efficiency of an array of dot collectors.

relative capacitance against the relative quantum efficiency we obtain Fig. 63. Here the reduced half-width of the stripe (W) is taken as a parameter. Similarly, for the dot collectors, the relative capacitance is $(W/B)^2$ (where W is the reduced dot radius), which varies with the relative quantum efficiency as shown in Fig. 64. Arbitrarily assuming that one can accept a 10% decrease in quantum efficiency, the relative capacitance then varies with W as shown in Fig. 65.

For the purpose of this estimate we assume that the diffusion length (L) is 10 μm and that dots and stripes with widths of 5 μm (W = 0.25) are practicable. Now Fig. 65 shows that the relative capacitance is about 0.3 for stripe collectors and about 0.1 for dot collectors, when one accepts a 10% loss in quantum efficiency. Delineation of smaller collectors would yield smaller capacitances for the same quantum efficiencies.

5.1.4 Increased Detectivity a Simplified Model

At first sight there would appear to be little scope for major improvement of the Johnson-noise-limited detectivity of IV-VI photodiodes because, in this case

$$D^* \propto \eta(RA)^{\frac{1}{2}} ,$$

where both the quantum efficiency (η) and the diode RA product appear to be approaching fundamental limits. The quantum efficiency is currently limited by reflection losses (which may be made small) and the RA product is limited by the lifetime.

The fallacy in this argument is that the lifetime limitation is upon $R_{jn}A_{jn}$ while the D* expression requires $R_{jn}A_{det}$, where A_{jn} and A_{det} are

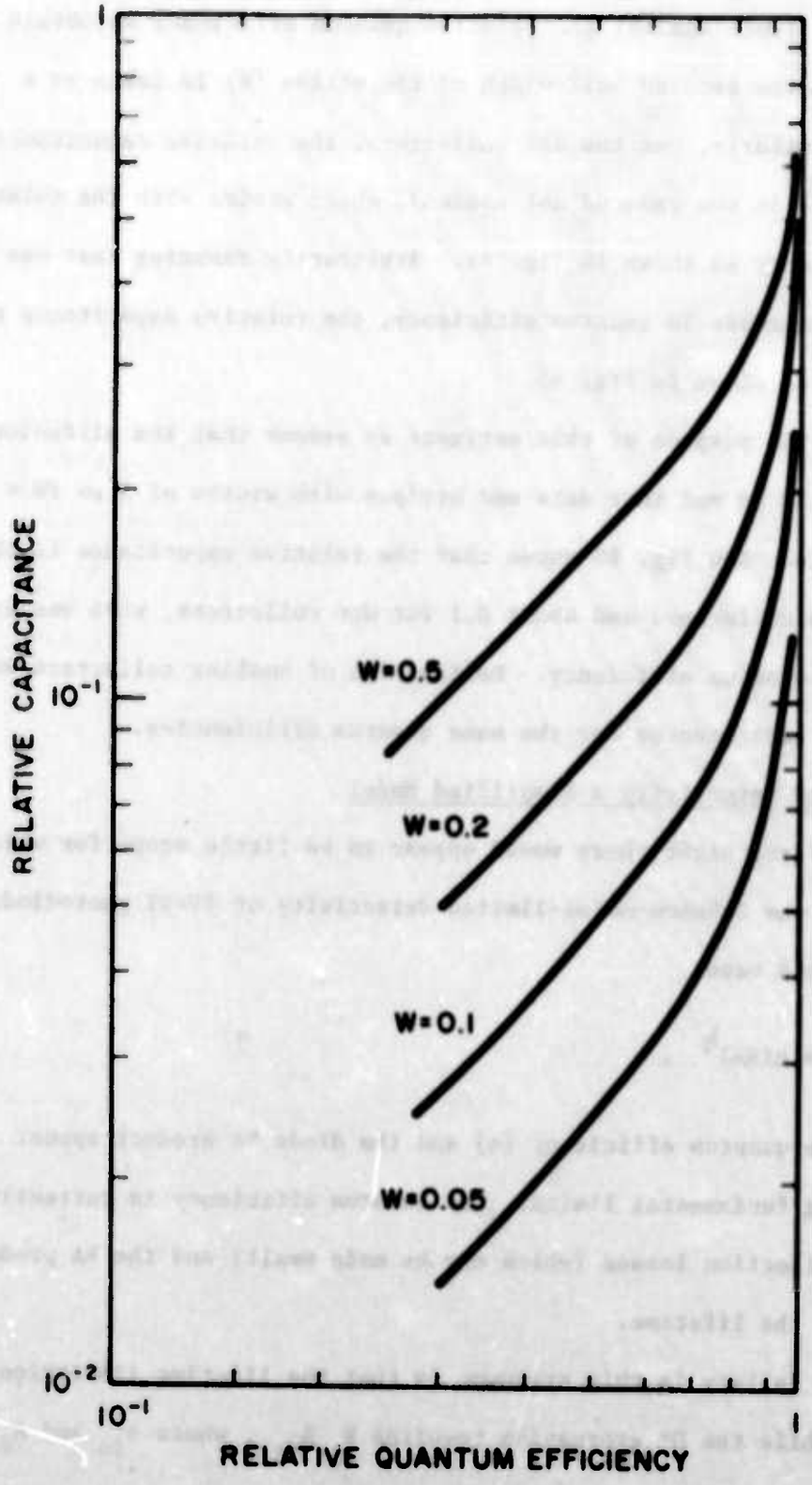

Fig. 63 The capacitance/relative quantum efficiency relationship for an array of stripe collectors.

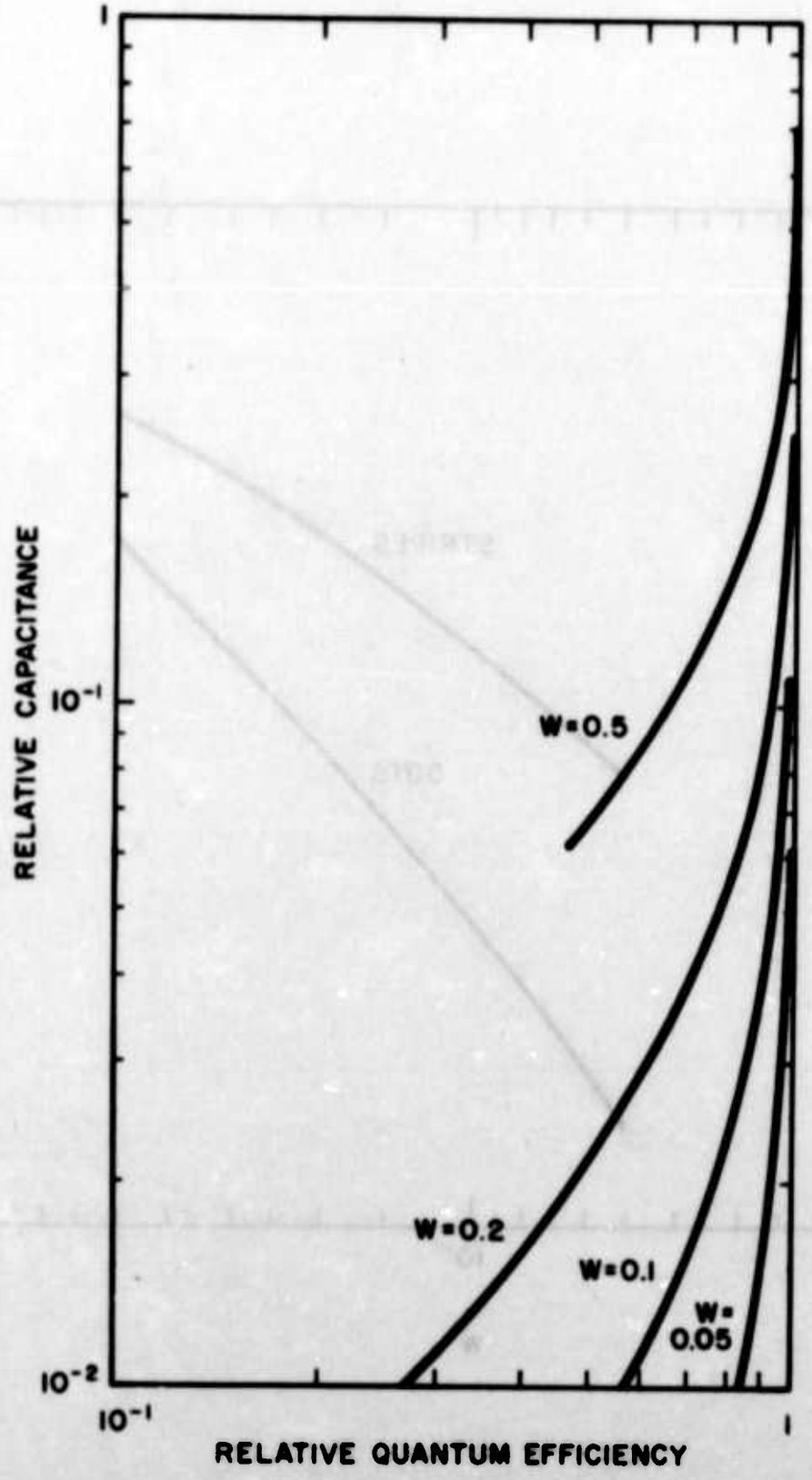

Fig. 64 The capacitance/relative quantum efficiency relationship for an array of dot collectors.

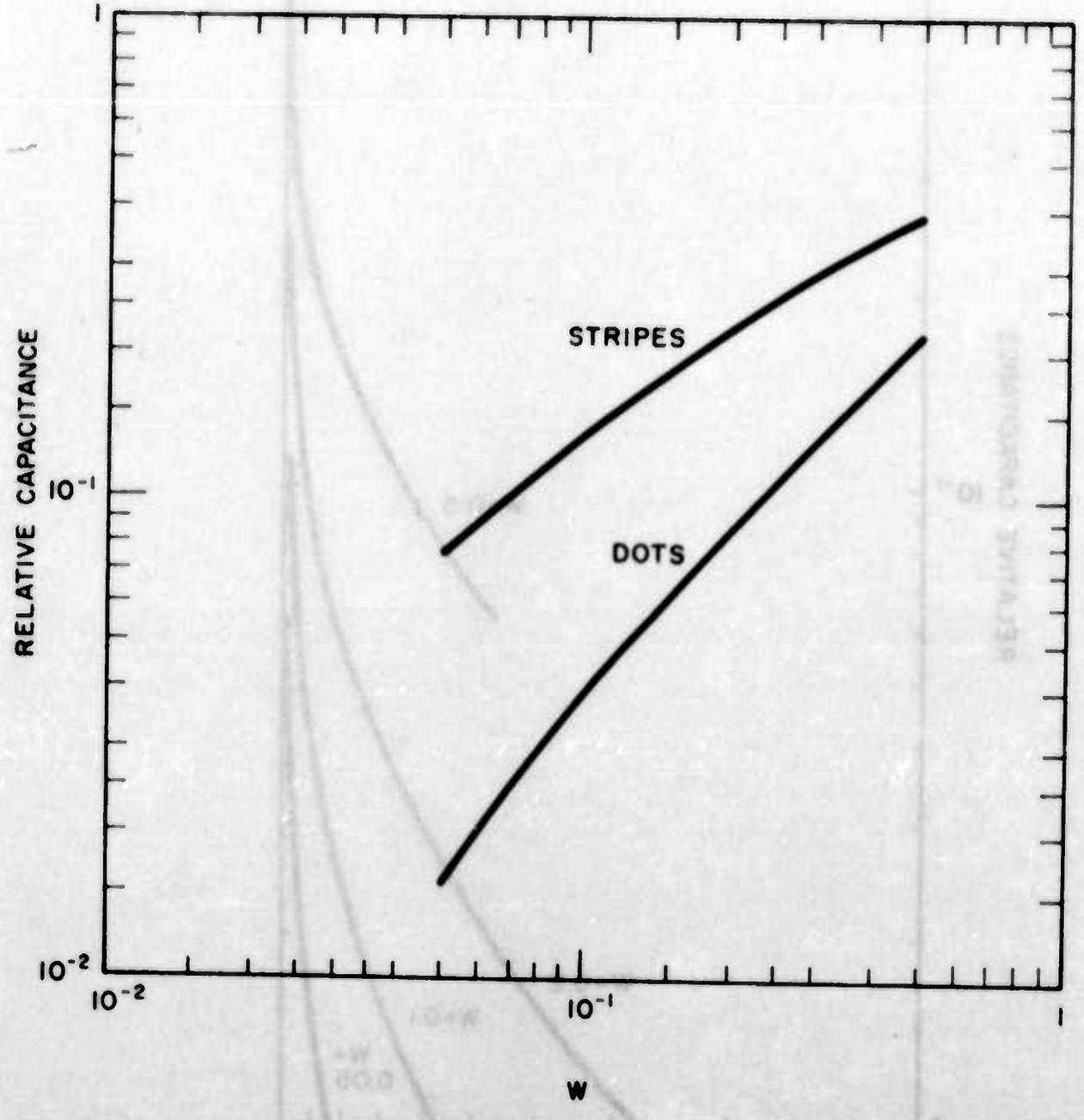

Fig. 65 Relative capacitance as a function of the reduced collector dimension W for a 10% sacrifice of quantum efficiency.

the areas of the junction and the detector, respectively. For conventional devices the distinction is trivial because the two areas are approximately equal. However, for lateral collection devices the two areas may differ by one or more orders of magnitude. $R_{jn}A_{det}$ should be capable of a significant increase, which must be considered in the light of a simultaneous decrease in η.

The preceding analyses show that the collection efficiencies of arrays of stripes and dots tend to decrease rather slowly as the collectors are separated. Since the separation also leads to an increase of $R_{jn}A_{det}$ it is intuitively obvious that the tradeoff between these changes will lead to an optimum collector separation for a maximum value for the Johnson-noise-limited detectivity. As a first approximation we consider the case where $R_{jn}A_{jn}$ is independent of the junction area. This gives a simple picture that will be subsequently modified to take account of the more complicated scaling of resistance that is to be expected with real photodiodes. The dimensions chosen are based upon the assumption that $L \approx 10$ μm for the IV-VI semiconductors in the temperature range that is of interest. Photolithographic processes are suitable for delineation of structures with dimensions of the order of 1 μm, so we consider values for the characteristic collector dimension.

$$W = w/L \sim 0.1$$

Figures 66 and 67 show the calculated relative values of the Johnson-noise-limited detectivity as a function of collector spacing for the stripe and dot collector arrangements, respectively. In this approximation, collectors

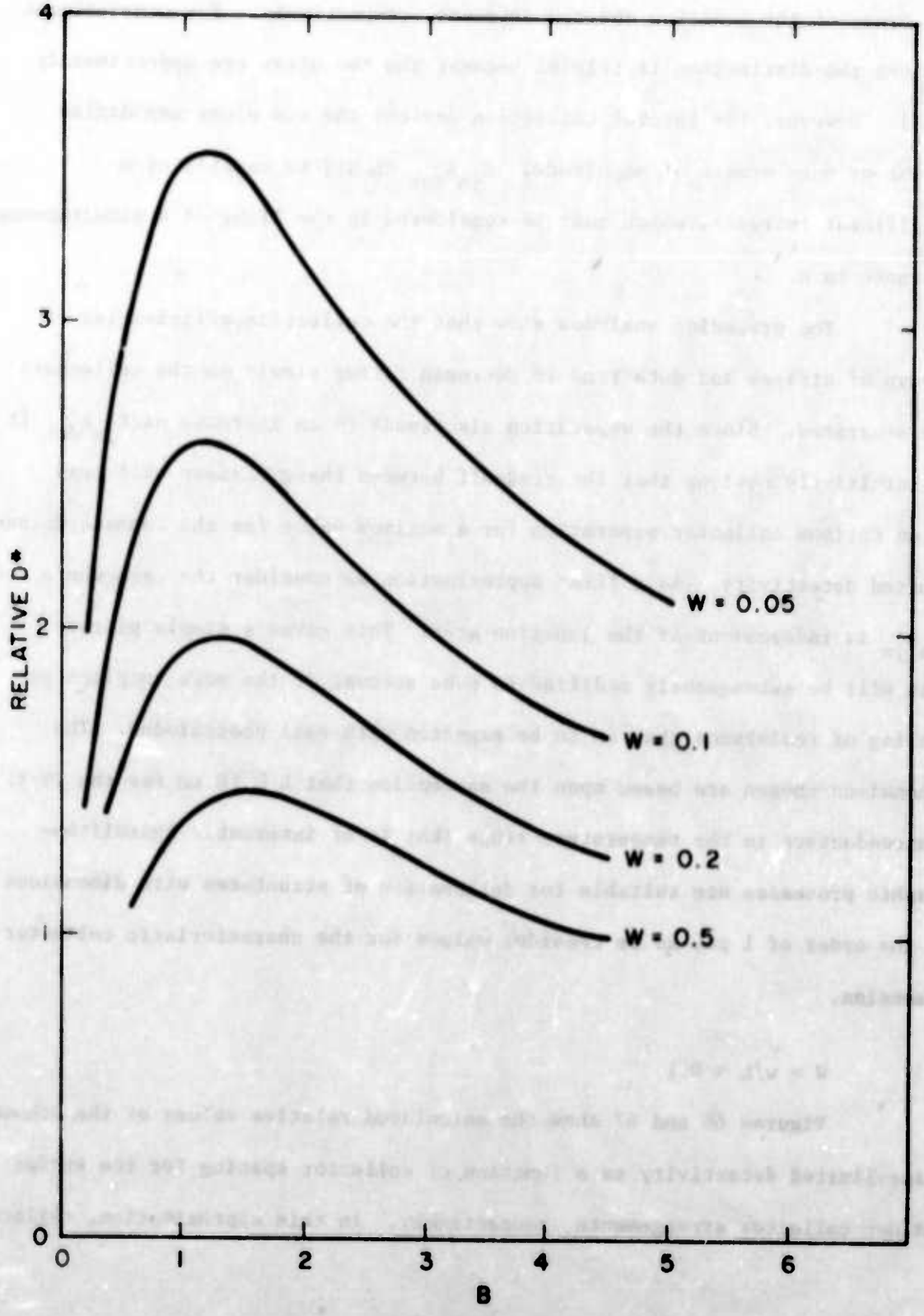

Fig. 66 Relative Johnson-noise-limited D* of an array of stripes.

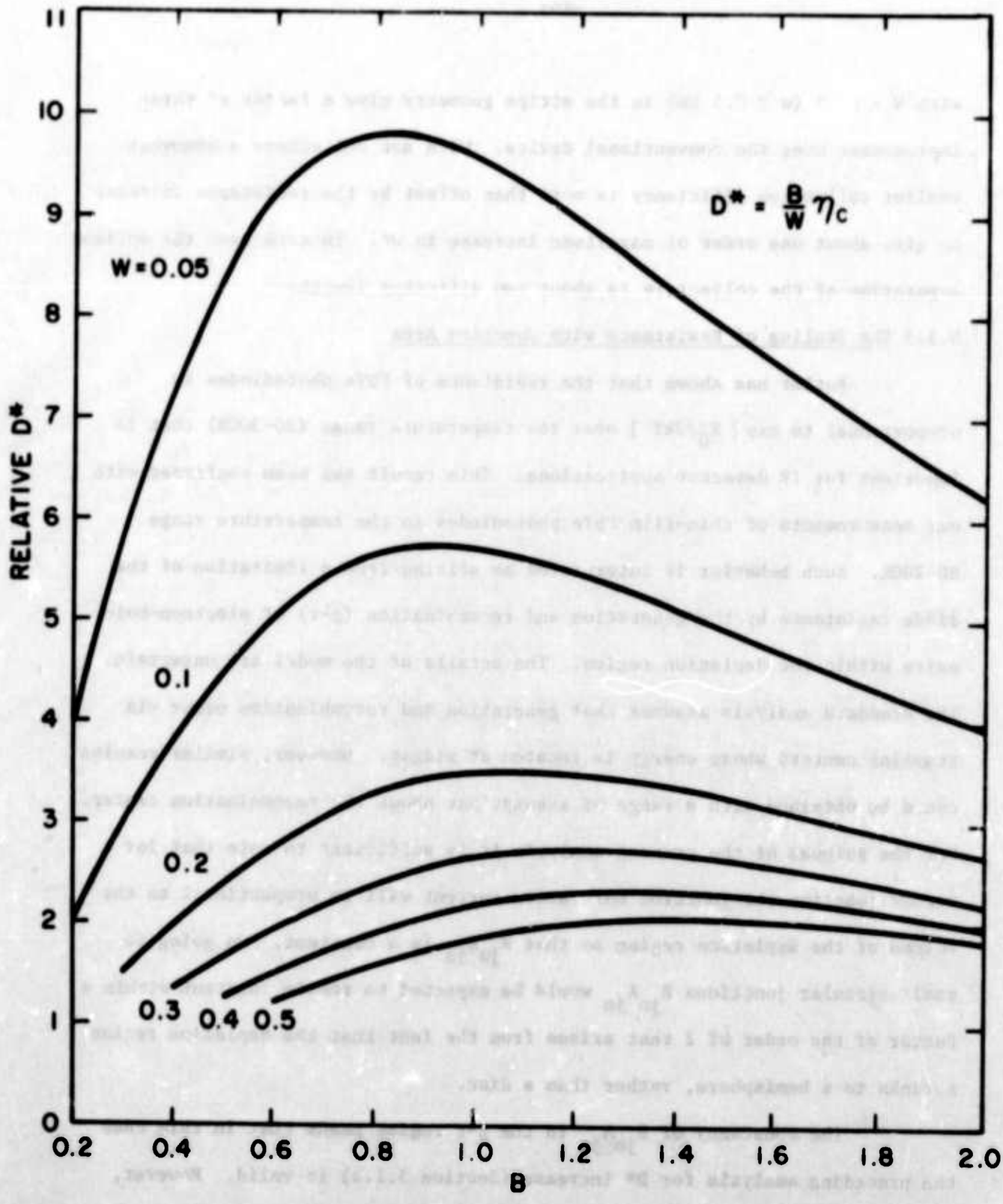

Fig. 67 Relative Johnson-noise-limited D* of an array of dots.

with W = 0.05 (w $\approx$ 0.5 μm) in the stripe geometry give a factor of three improvement over the conventional device. With dot collectors a somewhat smaller collection efficiency is more than offset by the resistance increase to give about one order of magnitude increase in D*. In each case the optimum separation of the collectors is about two diffusion lengths.

5.1.5 The Scaling of Resistance with Junction Area

Butler has shown that the resistance of PbTe photodiodes is proportional to exp [$E_G/2kT$] over the temperature range (80-300K) that is important for IR detector applications. This result has been confirmed with our measurements of thin-film PbTe photodiodes in the temperature range 80-200K. Such behavior is interpreted as arising from a limitation of the diode resistance by the generation and recombination (g-r) of electron-hole pairs within the depletion region. The details of the model are uncertain. The standard analysis assumes that generation and recombination occur via trapping centers whose energy is located at midgap. However, similar results could be obtained with a range of assumptions about the recombination center. For the purpose of the present analysis it is sufficient to note that for a planar junction the junction saturation current will be proportional to the volume of the depletion region so that $R_{jn}A_{jn}$ is a constant. On going to small circular junctions $R_{jn}A_{jn}$ would be expected to remain constant within a factor of the order of 2 that arises from the fact that the depletion region shrinks to a hemisphere, rather than a disc.

The constancy of $R_{jn}A_{jn}$ in the g-r regime means that in this case the preceding analysis for D* increase (Section 5.1.4) is valid. However, deviations from this ideal behavior are to be expected at higher temperatures,

where the diode resistance becomes diffusion limited, and at lower temperatures, where the resistance may become limited by surface leakage.

With progressive increase of the temperature one will eventually reach a point where the diode resistance becomes limited by thermal generation and diffusion of minority carriers from outside the junction. However, the use of a thin film leads to a larger diffusion-limited resistance than wuould be calculated from the Shockley model.

Consider first a large-area diode in a film with thickness b, as shown in Fig. 68. The diffusion equation for minority carriers in the p-region is

$$\frac{d^2n}{dx^2} - \frac{n}{L^2} + \frac{G}{D} = 0 ,$$

where, now, G is the rate of thermal generation

$$G = \frac{n_o}{\tau} = \frac{n_i^2}{p\tau} .$$

If we assume that the semiconductor/insulator interface does not affect the lifetime,

$$\left.\frac{dn}{dx}\right|_{x = b} = 0 .$$

Under reverse bias the depletion layer acts as a perfect sink and

$$n|_{x = 0} = 0 .$$

Whence,

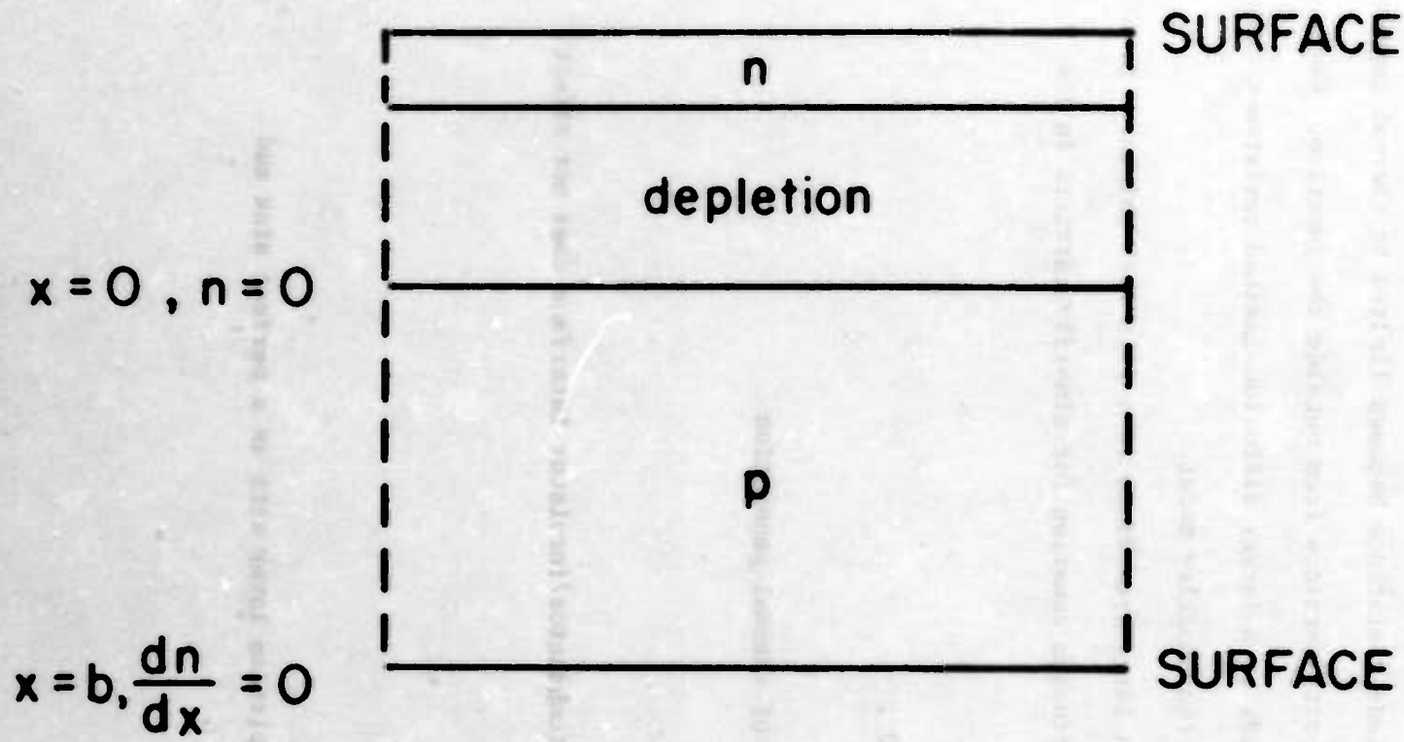

Fig. 68 Model for the diffusion current in a thin-film photodiode.

$$n = n_o \left[1 - \frac{\cosh\left(\frac{x - b}{L}\right)}{\cosh\left(\frac{b}{L}\right)} \right]$$

The saturation current density is now

$$J_{sat} = -qD\frac{dn}{dx}\Big|_{x = 0} = qn_o\left(\frac{D}{\tau}\right)^{\frac{1}{2}}\tanh\left(\frac{b}{L}\right) .$$

When b/L is large, tanh(b/L) → b/L and the junction resistance is L/b times that calculated from the Shockley model.

For the case when the large-area diode is replaced by an array of small-area diodes the saturation current is further reduced by the collection efficiency, η_C, discussed in Sections 5.1.1-2. Thus, the diode resistance becomes

$$R = \frac{L}{\eta_C b} R_{Shockley} .$$

Typically, $b \gtrsim 0.5$ μm and $\eta_C \gtrsim 0.5$ so that we will get $R \gtrsim 40\ R_{Shockley}$.

At sufficiently low temperatures, RA for most IV-VI photodiodes (both thin-film and bulk crystal) tends to saturate at values that are almost temperature-independent. In this regime the resistance-limiting mechanism has not been unequivocably determined. However, the extreme variability of the limiting values of RA, when compared with the values at higher temperatures, strongly suggests that the limitation is by surface leakage across the depletion region. At 77K, the RA of PbTe may attain g-r limited values ($\sim 10^4$ ohmcm^2), but is frequently much smaller. Similarly, with $Pb_{0.8}Sn_{0.2}Te$, most specimens give RA $\leq$ 1 ohmcm^2, although exceptionally RA $\sim$ 10 ohmcm^2 is observed.

The existence of a temperature-independent shunt resistance can impose an upper limit upon the increase of RA that is attainable with lateral collection devices. The magnitude of the effect may be estimated by comparing the limiting values of RA for conventional and LC devices that have the same active area. For a conventional square photodiode with side D the resistance will be given by

$$\frac{1}{R_{conv.}} = \alpha D^2 + 4\beta D ,$$

where α,β are constants and the second term represents the conductance due to leakage around the periphery. In the limit of domination by surface leakage this gives

$$(RA)_{conv.surf.} = \frac{D}{4\beta}$$

For comparison, consider a lateral collection device that consists of a square array of circular collectors with diameter d, specing b, and overall dimensions D X D. In this case

$$(RA)_{LC,surf.} = \frac{b^2}{\beta\pi d}$$

Note that, while the leakage of a conventional photodiode becomes more significant as its dimension D is reduced, the leakage of the LC device is independent of the active area and depends only upon the dimensions and spacing of the collectors.

Relative values of RA (in arbitrary units) for the two kinds of device with typical dimensions are shown in Fig. 69. It will be noted that,

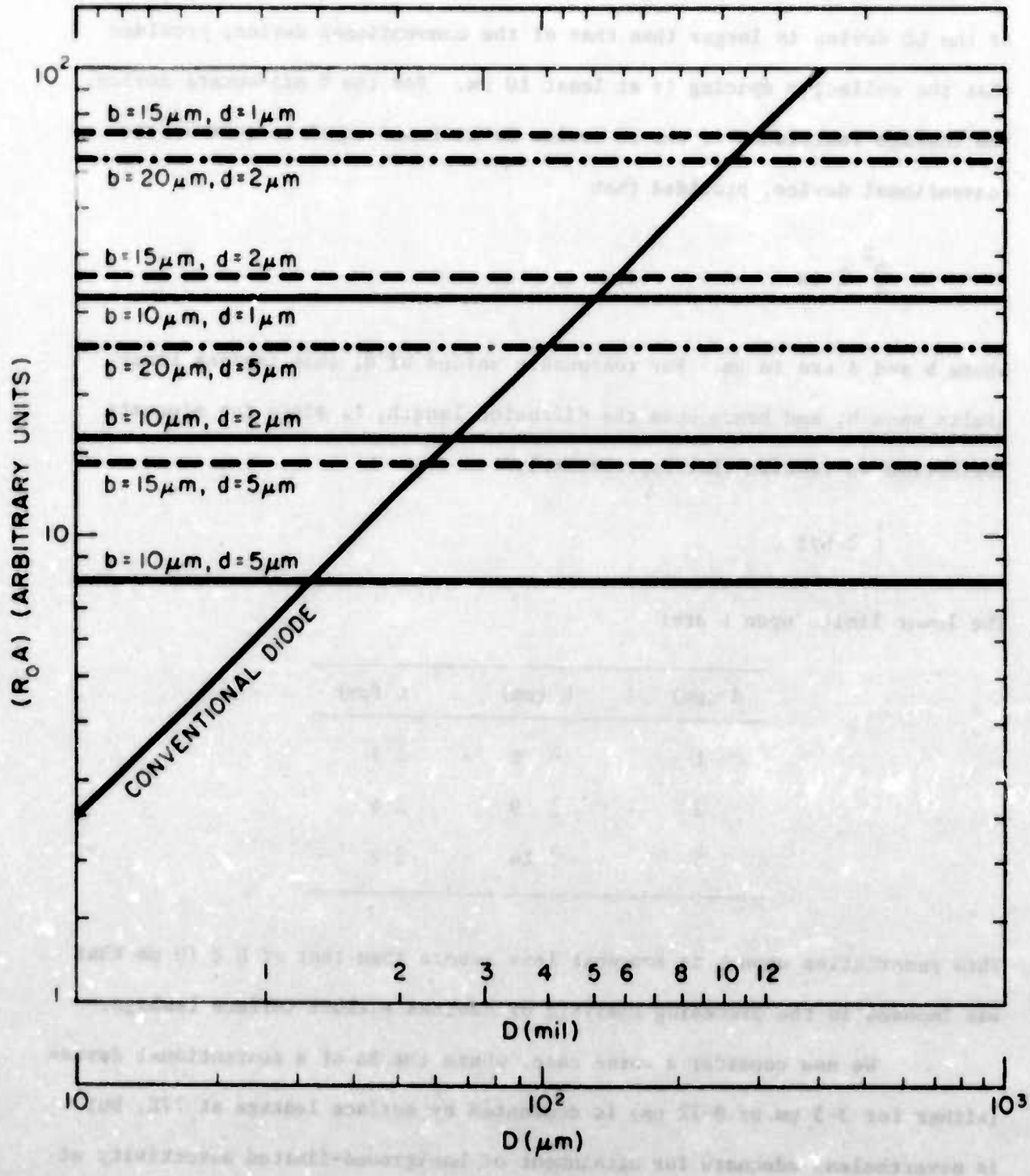

Fig. 69 Surface-leakage-limited R_oA products for conventional and lateral-collection devices.

for 2 mil-square detectors and 2 μm-diameter collectors, the leakage resistance of the LC device is larger than that of the conventional device, provided that the collector spacing is at least 10 μm. For the 2 mil-square device, the leakage resistance of the LC device is at least equal to that of the conventional device, provided that

$$\frac{b^2}{d} \geq 40$$

where b and d are in μm. For reasonable values of d, this imposes lower limits upon b, and hence upon the diffusion length, L, since for adequate collection we require that approximately

$$L \geq b/2 .$$

The lower limits upon L are:

d (μm)	b (μm)	L (μm)
1	$\geq$ 6	$\geq$ 3
2	$\geq$ 9	$\geq$ 4
5	$\geq$ 14	$\geq$ 7

This restriction upon L is somewhat less severe than that of L $\gtrsim$ 10 μm that was imposed in the preceding analysis of devices without surface leakage.

We now consider a worse case, where the RA of a conventional device (either for 3-5 μm or 8-12 μm) is dominated by surface leakage at 77K, but is nevertheless adequate for attainment of background-limited detectivity at that temperature. On warming to some intermediate operating temperature

(e.g. 170K) RA for the conventional device decreases, while its quantum efficiency remains almost constant. Thus, the conventional device eventually becomes Johnson-noise-limited. The corresonding LC device will also be background limited at 77K with a detectivity that is reduced from that of the conventional device by the factor $\eta_C^{\frac{1}{2}}$. In this case, reduction of the background photon flux will give similar increases in the detectivities of the conventional and LC devices. At the intermediate operating temperature the RA of the LC device may still be limited by surface leakage. However, in this case, if the criteria above are met, this condition will still give a background-limited detectivity.

We conclude that limitation of the LC diode resistance by surface leakage should not degrade the RA of such a device significantly below the maximum value that is attained by a conventional device with typical detector dimensions. Thus, while surface leakage might limit the improvement in the reduced-background performance at 77K that is attainable with lateral collection, it would not be expected to prevent the attainment of background-limited performance at intermediate operating temperatures.

5.1.6 Projected Detectivity of Lateral Collection Devices at 3-5 μm

Butler[15] has shown that diffused junctions in PbTe have

$$RA \propto \exp[E_G/2kT]$$

and has interpreted his results in terms of generation and recombination of electron-hole pairs within the depletion region. Similar results have been obtained with Schottky diodes made with thin films of PbTe[16] and PbSe[17]. Butler used a model[18] with generation-recombination (g-r) centers at midgap, for which the zero-bias resistance-area product is

$$R_oA = \frac{2kT}{q^2 w n_i} \cdot \tau_{depl.} ,$$

where w is the width of the depletion region and τ_{depl} is an effective lifetime that was found to be about 30 nsec.

The significance of τ_{depl}, as defined above, depends somewhat upon the details of the model used. Here we treat τ_{depl} as a phenomenological parameter and fit to the largest value of R_oA (= 2 X 10^4 ohmcm^2) reported for PbTe (with p = 1 X 10^{18} cm^{-3}) at 77K.[19] This gives $\tau_{depl} \approx$ 50 nsec, in fair agreement with Butler's estimate of 30 ns. This approach has previously given good agreement with the observed temperature dependence of both R_oA and D* for thin-film PbTe photodiodes.[2] Here we slightly modify the calculation to estimate the g-r-limited R_oA and D* for conventional IV-VI photodiodes that have been band-tailored for 5.0 μm cutoff (E_G = 0.248 eV) at their operating temperature.

Values of n_i have been calculated from the band-edge effective masses given by Dimmock's model for $Pb_{1-x}Sn_xTe$[20]* and the depletion layer width has been obtained from the approximation for a one-sided abrupt junction

$$w = \left(\frac{2\epsilon_s V_{bi}}{qp}\right)^{1/2} ,$$

with a static dielectric constant ϵ_s = 400 ϵ_o.

For comparison we have calculated the diffusion-limited R_oA for the abrupt one-sided junction using the Shockley model[18] for which

* At high enough temperatures, n_i of PbTe is increased by a contribution to the density of states from a lower-lying heavy hole band.[21] This may be neglected for T ≤ 250K and p ≤ 10^{18} cm^{-3}.

$$R_o A = \frac{pkT}{q^2 n_i^2} \left(\frac{\tau}{D}\right)^{\frac{1}{2}} ,$$

where

$$D = \frac{kT}{q} \mu ,$$

and

$$\mu = 5.2 \times 10^6 T^{-5/2} \text{ cm}^2\text{V}^{-1}\text{sec}^{-1} ,$$

in the temperature range of interest. The choice of τ is somewhat arbitrary. Direct measurements with $Pb_{0.8}Sn_{0.2}Te$ have given lifetimes of the order of 10 nsec in the temperature range 77-300K and we follow this for the diffusion-limited R_oA. This assumption is not likely to lead to a large overestimate of the diffusion-limited R_oA of 3.5 μm devices because our observation of reflection-loss-limited quantum efficiency in a 4.1 μm-thick PbTe diode[2] implies that $\tau \geq 5$ nsec in the range 80-170K.

The results of these calculations are shown in Fig. 70. The resistance-area product is dominated by the g-r mechanism at temperatures up to about 200K except for carrier concentrations less than about 3×10^{17} cm^{-3} where the diffusion mechanism may be significant for temperatures above about 170K. The corresponding detectivities at $\lambda = 5.0$ μm are shown in Fig. 71. Here the quantum efficiency has been assumed to be 0.5, corresponding approximately to a typical reflection loss limit for a IV-VI photodiode. For 180° field of view the background limited detectivity is 1.3×10^{11} $cmHz^{\frac{1}{2}}W^{-1}$ and the calculated Johnson-noise-limit is equal to this value in the temperature

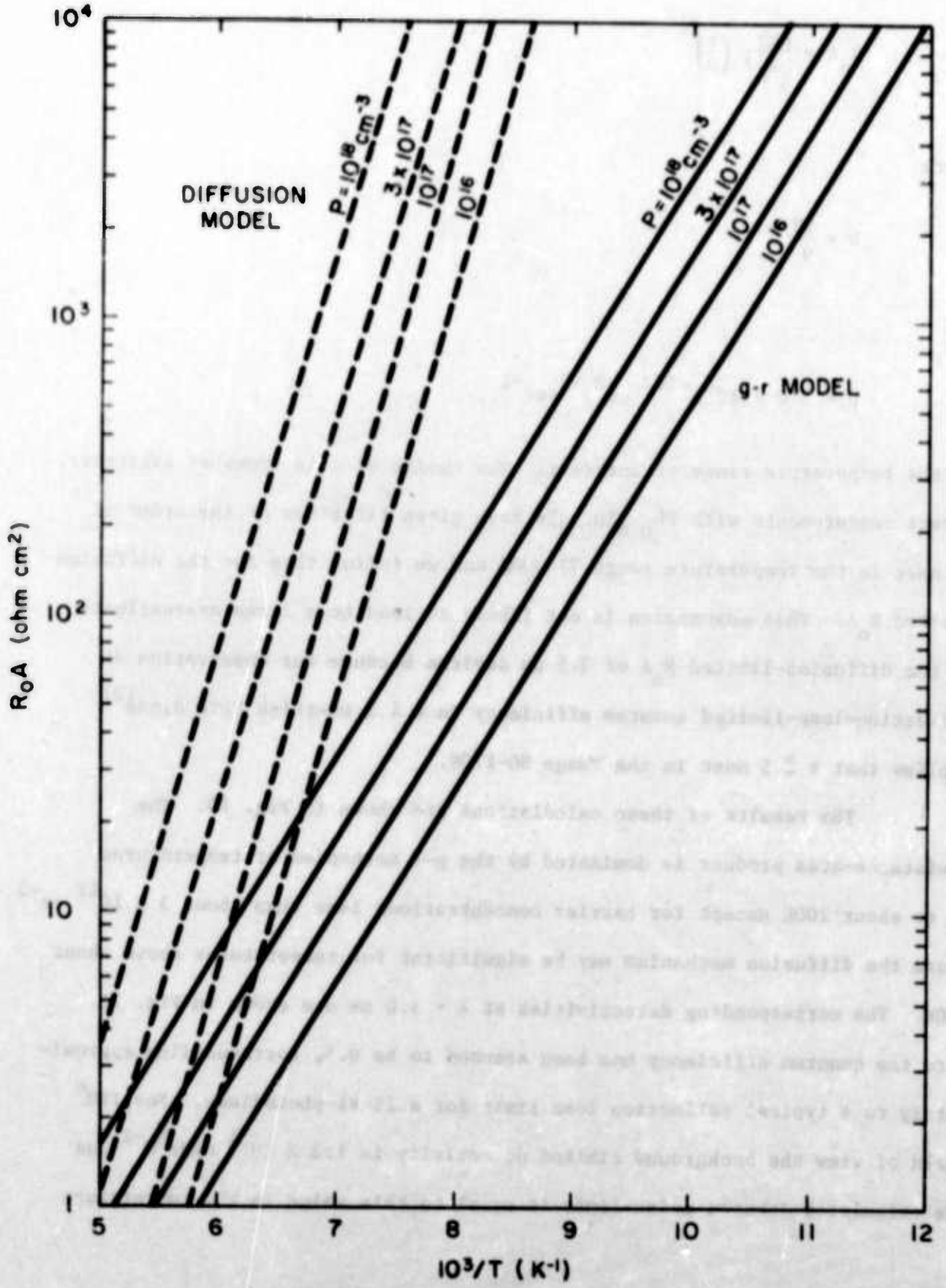

Fig. 70 Calculated R_oA for 5 μm cutoff conventional photodiodes.

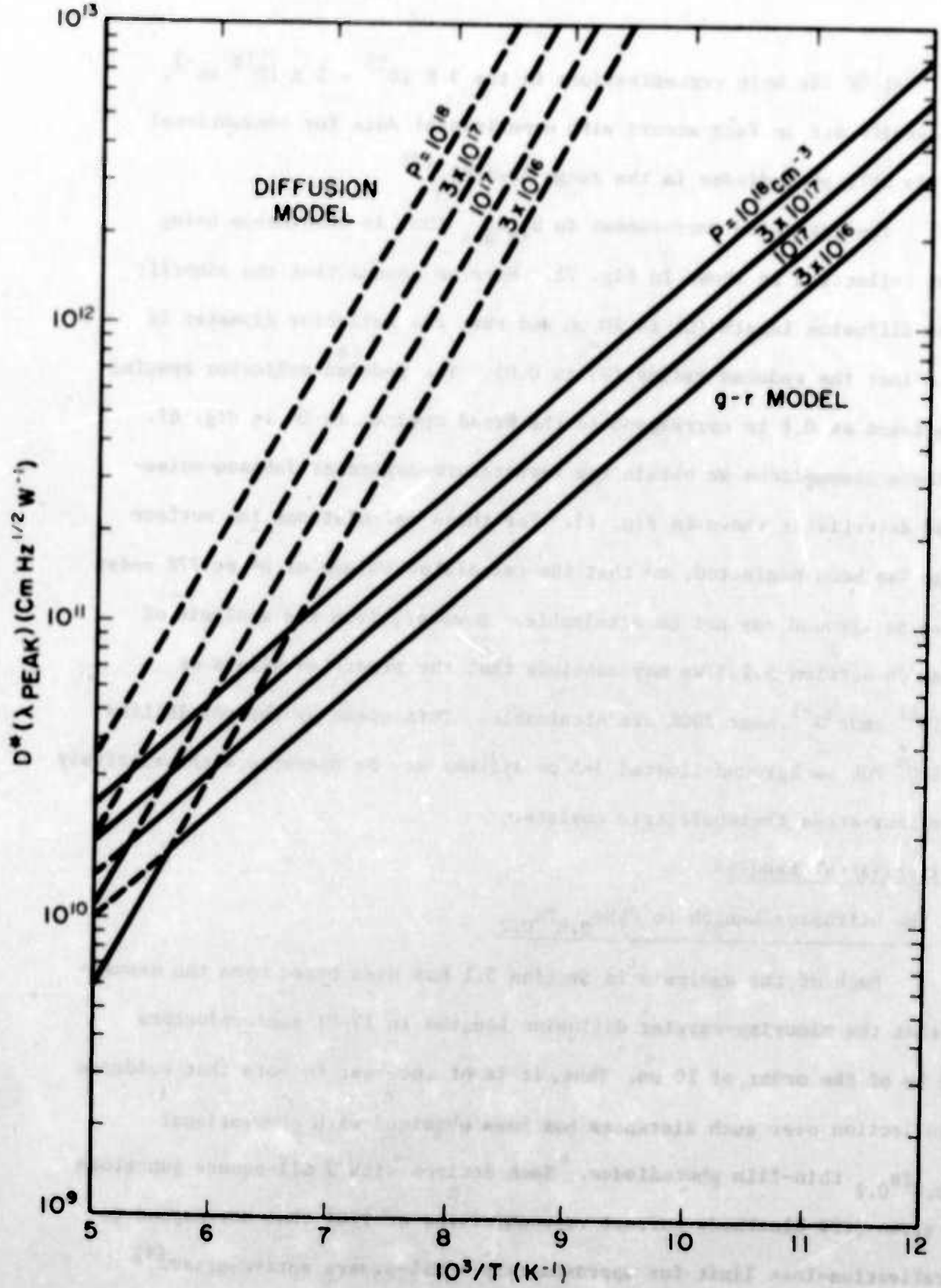

Fig. 71 Calculated peak D* for 5 μm cutoff conventional photodiodes.

range 120-140K for hole concentrations in the $3 \times 10^{16} - 1 \times 10^{18}$ cm^{-3}. These results are in fair accord with experimental data for conventional thin-film PbTe photodiodes in the range 80-170K.[2]

The estimated improvement in $R_{jn}A_{det}$ that is obtainable using lateral collection is shown in Fig. 72. Here we assume that the minority carrier diffusion length (L) is 10 μm and that the collector diameter is 1 μm so that the reduced radius (W) is 0.05. The reduced collector spacing (B) is taken as 0.8 to correspond to the broad optimum in D* in Fig. 67. With these assumptions we obtain the temperature-dependent Johnson-noise-limited detectivity shown in Fig. 73. For these calculations the surface leakage has been neglected, so that the calculated values of D* at 77K under reduced background may not be attainable. However, from the analysis of leakage in Section 5.1.5 we may conclude that the predicted values of $D^* \approx 10^{11}$ $cmHz^{\frac{1}{2}}W^{-1}$ near 200K are attainable. This opens up the possibility that 180° FOV background-limited 3-5 μm systems may be operable with relatively simple four-stage thermoelectric coolers.

5.2 Experimental Results

5.2.1 The Diffusion Length in $PbSe_{0.8}Te_{0.2}$

Much of the analysis in Section 5.1 has been based upon the assumption that the minority-carrier diffusion lengths in IV-VI semiconductors would be of the order of 10 μm. Thus, it is of interest to note that evidence for collection over such distances has been obtained with conventional $PbSe_{0.8}Te_{0.2}$ thin-film photodiodes. Such devices with 3 mil-square junctions have given 500K blackbody current responsivities at 170K that correspond to the reflection-loss limit for approximately 4 mil-square active areas.[4] This implies that the diffusion length is approximately 0.5 mil (≈ 10 μm).

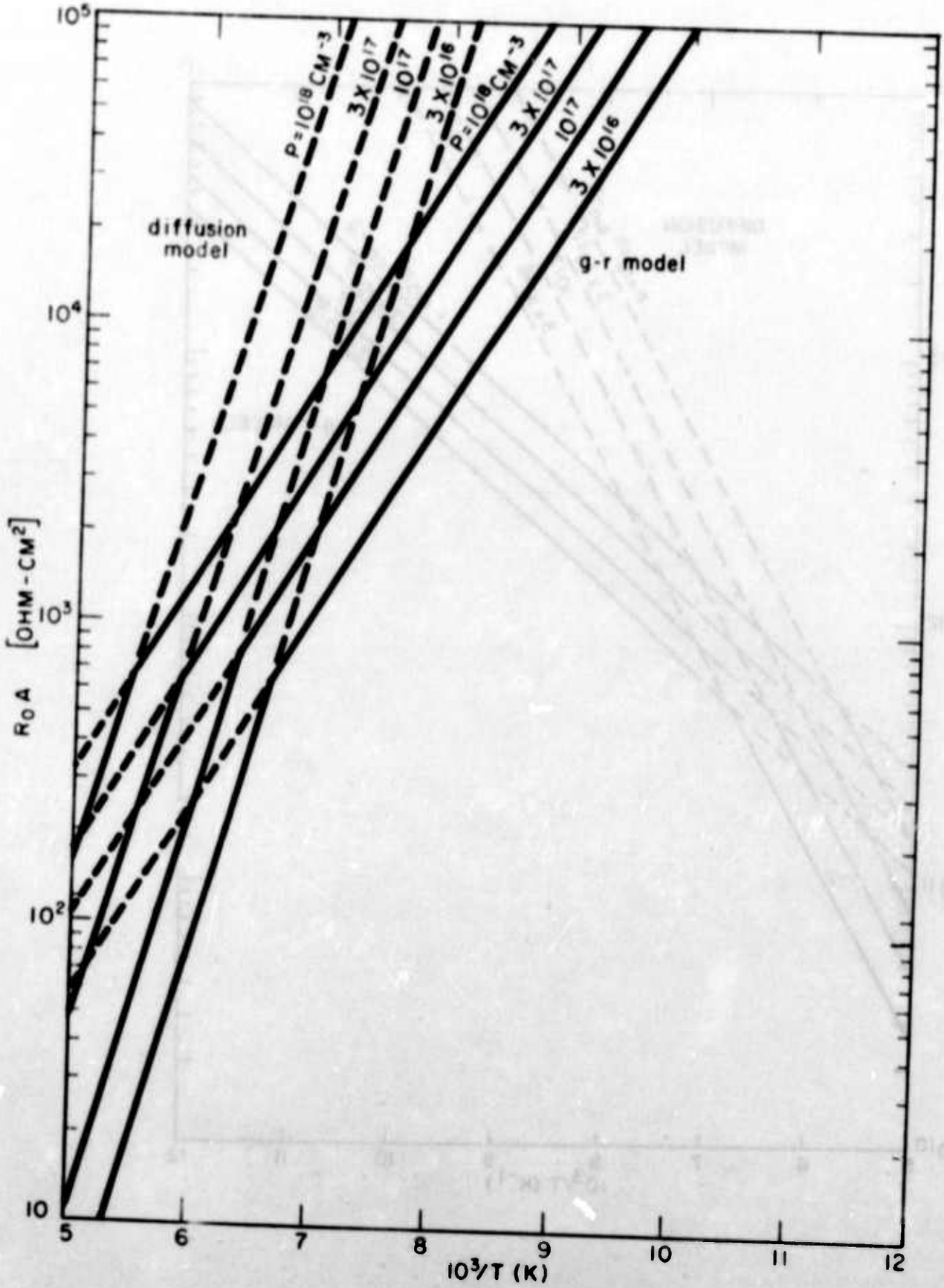

Fig. 72 Calculated R_0A for 5 μm cutoff lateral-collection photodiodes.

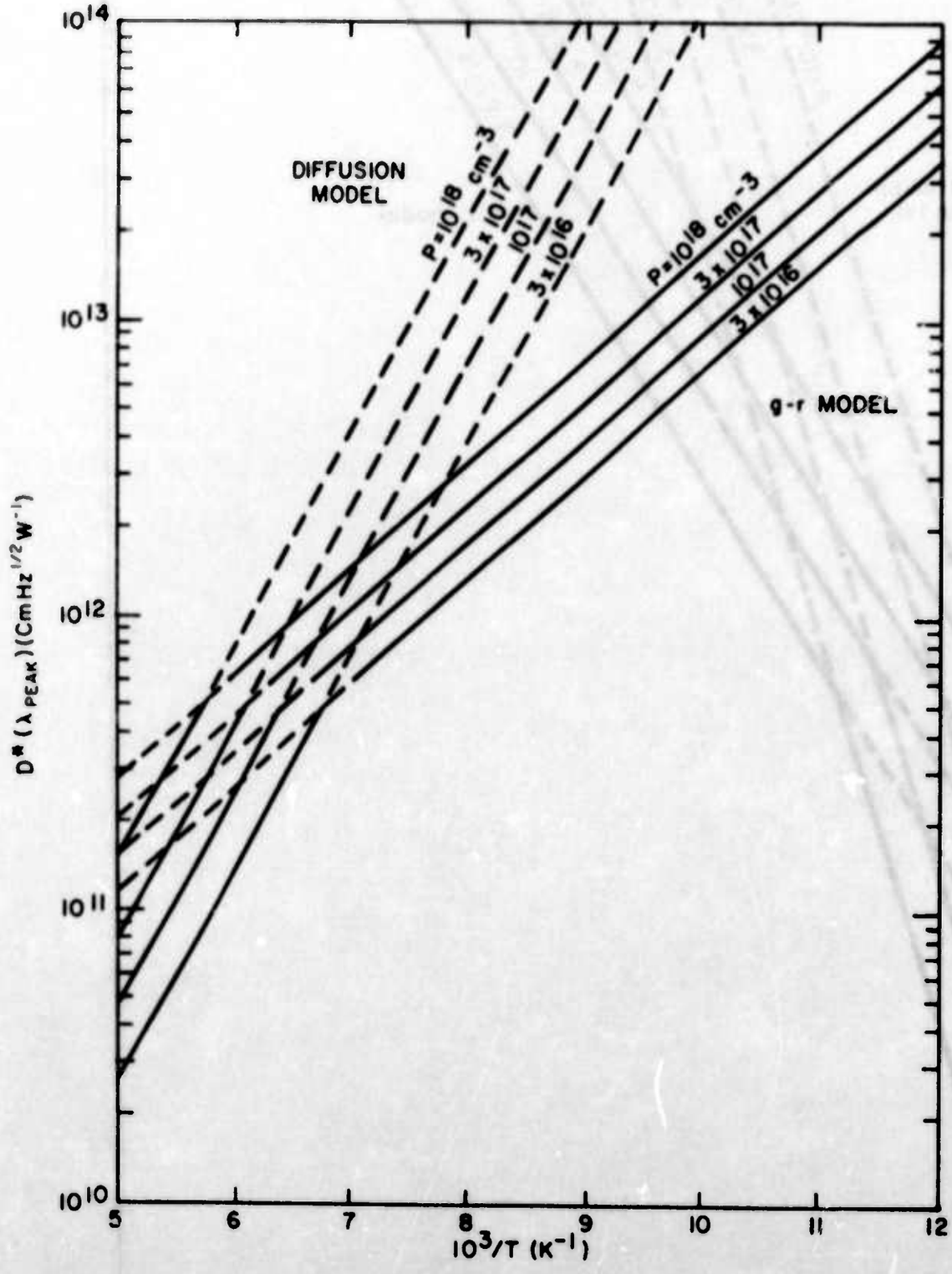

Fig. 73 Calculated peak D* for 5 μm cutoff lateral-collection photodiodes.

The lateral collection interpretation is confirmed by Fig. 74, which shows flying-spot scans for a pair of such diodes with a 3 mil space between them. It is evident that there is substantial collection from the region between the diodes and that the extent of the lateral collection increases as the temperature is decreased from 210K to 77K.

5.2.2 Fabrication of Lateral Collection Devices

In general, the methods that were used to make lateral collection devices were based on the delineation techniques that are described in Sections 4.2.1 and 4.3.1. Small collectors were made by evaporating Pb through a matrix of holes in a vacuum-deposited BaF_2 insulator. A common connection to the collectors was then provided by the remainder of the Pb layer. A schematic diagram of this arrangment is given in Fig. 75.

Nominally 12 mil-square active areas were obtained with arrays of approximately 5 μm-wide stripe collectors on 15 μm centers. For dot collectors the 12 mil-square active area was occupied by a hexagonal array of approximately 5 μm-diameter dots on 15 μm centers. For comparison, conventional 12 mil-square diodes were made on the same chip. This arrangment is shown in Fig. 76. For the nominal 5 μm line widths and dot diameters the capacitances of the lateral collection devices are 0.33 and 0.10 of the 12 mil control diodes. In practice, these values vary somewhat with changes in the width due to variations in photoresist processing. Thus, an increase of the line width from 5 μm to 7 μm changes the relative capacitance of the stripe diodes from 0.33 to 0.47.

Use of 1.7 μm-thick layers of Shippley AZ1350J resist permitted delineation of holes with diameters less than 5 μm in 0.3-0.6 μm-thick layers

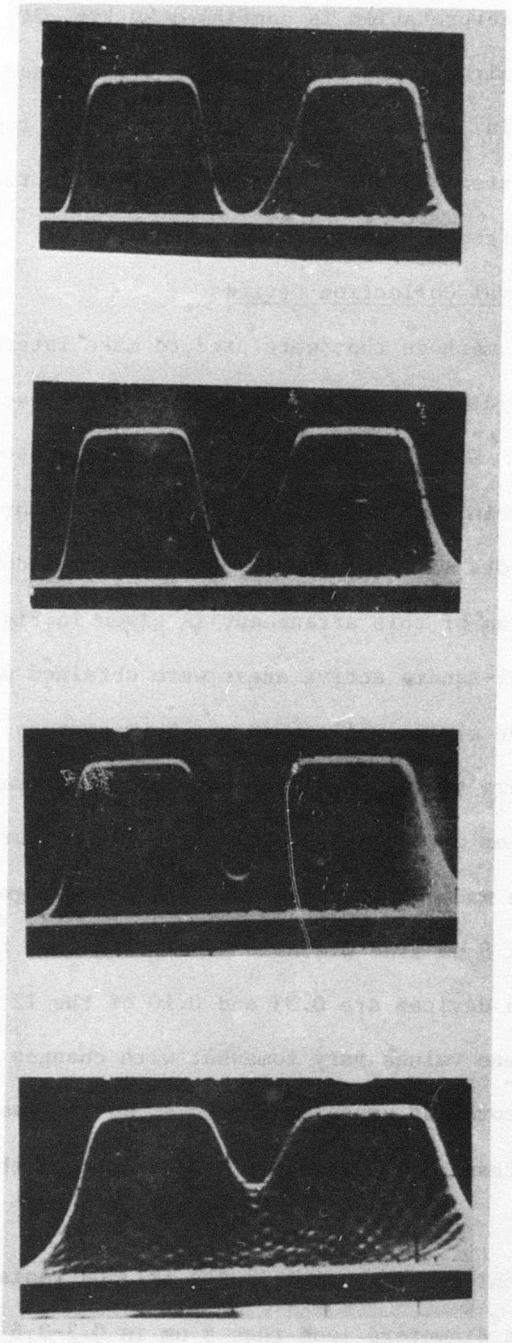

Fig. 74 Flying spot scans of a pair of 3 mil $PbSe_{0.8}Te_{0.2}$ diodes on 6 mil centers (This scan was supplied by NVL.)

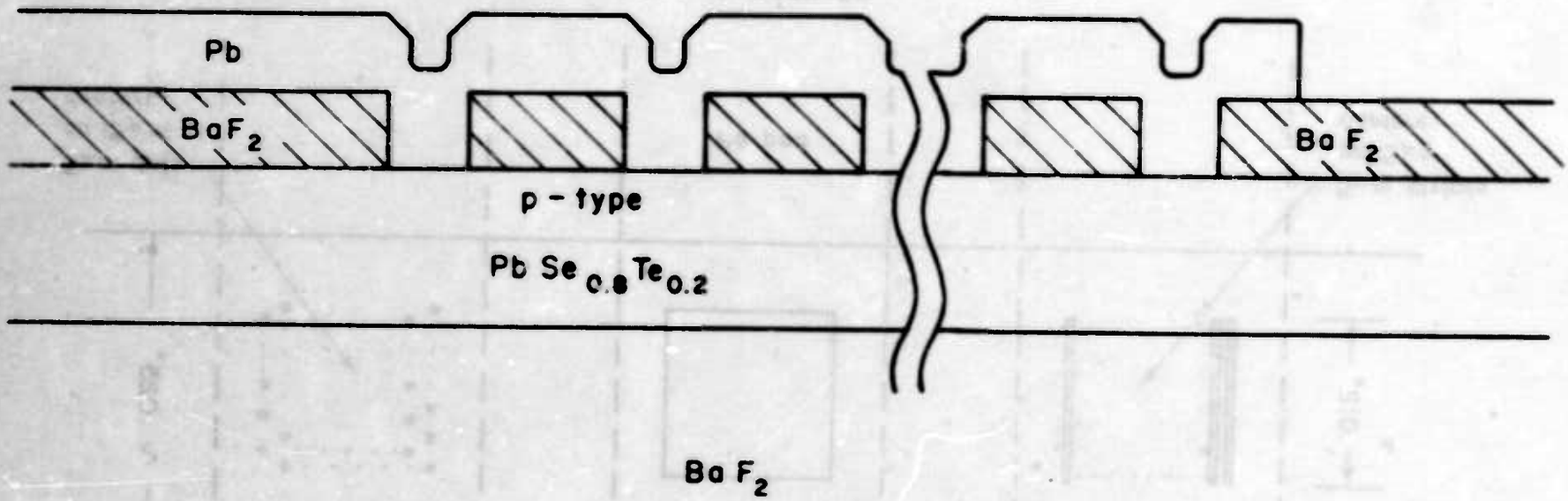

Fig. 75 Schematic cross-section of a lateral-collection device.

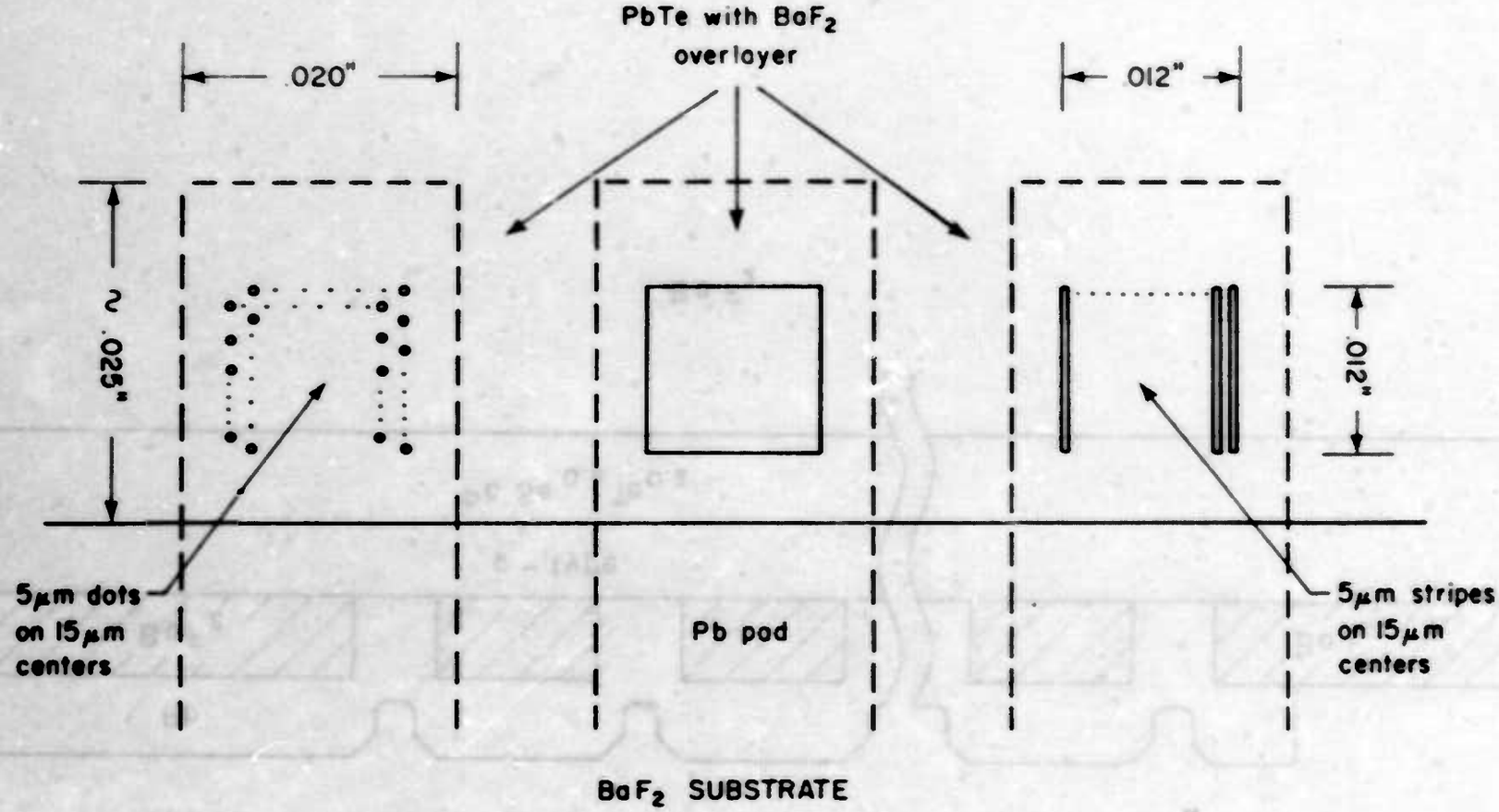

Fig. 76 Dimensions of lateral-collection devices.

of BaF_2. Figure 77 shows an example of this delineation. However, lateral collection diodes made in this way usually showed much smaller current response than the 12 mil control diodes. This reduced response was particularly marked with the arrays of dot collectors.

Flying spot-scans of such lateral collection devices (initially provided by NVL and later confirmed with the Ford scanner) showed that the responses of the small collectors were very nonuniform. Typically, only a fraction of the collectors within a device showed current response. An example of this behavior is shown in Fig. 78. The nonuniform response appears to occur because the Pb layer at the bottom of the hole in the BaF_2 is frequently not connected to the Pb pad. Scanning electron microscopy of the photoresist patterns revealed rounded edges as shown in Fig. 79. Subsequent vacuum deposition of BaF_2 and removal of the resist would then give holes with overhanging edges which would tend to make the Pb layer discontinuous.

At this stage we do not have a satisfactory process for making the Pb layer continuous. However, the nature of the problem was confirmed and lateral collection was demonstrated by overcoating the Pb layer with silver paint (#SC12, Microcircuits Company, New Buffalo, Michigan). Figure 80 shows spot scans of stripe and dot lateral collection devices together with that of a 12 mil control diode. Before silver painting neither of the lateral collection devices had given significant current response. After painting, the response of the stripe device was approximately equal to that of the control diode. Overall, the dot device attained about half of the response of the control. From Fig. 80 it is evident that this device has regions where the dots give full response and others when there is little or no response.

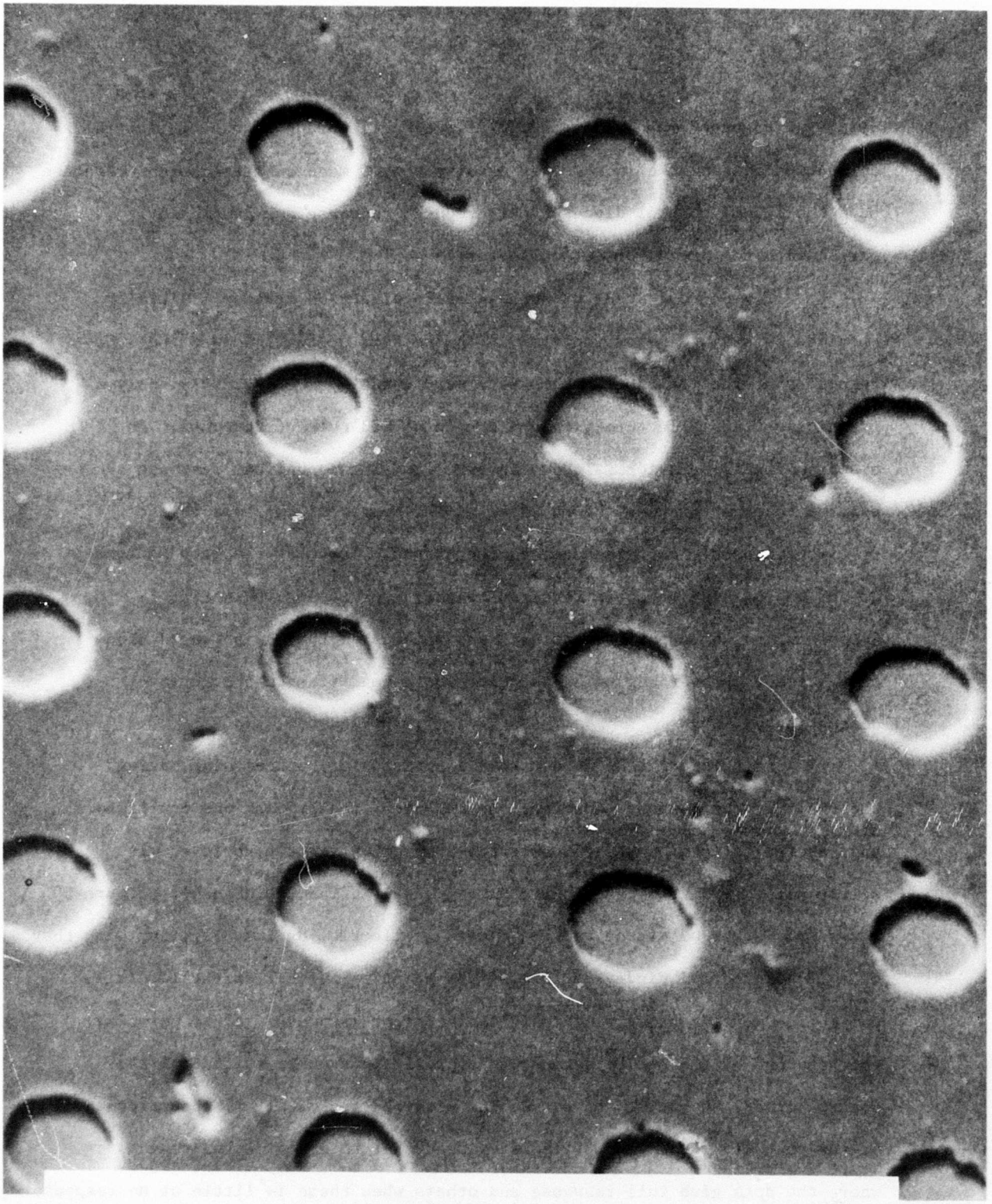

Fig. 77 Scanning electron micrograph of the delineated BaF_2 insulator prior to deposition of Pb to form a lateral-collection device. The holes are approximately 3.5 μm in diameter on 12 μm centers.

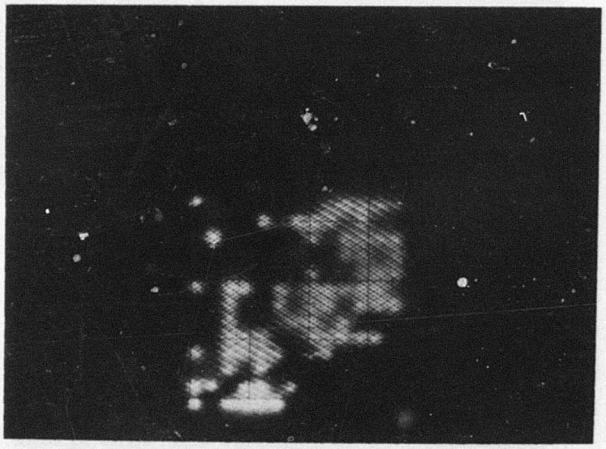

Fig. 78 Flying spot scan of an array of dot collectors showing nonuniform response. The geometry differs slightly from that discussed in the text. (This scan was supplied by NVL.)

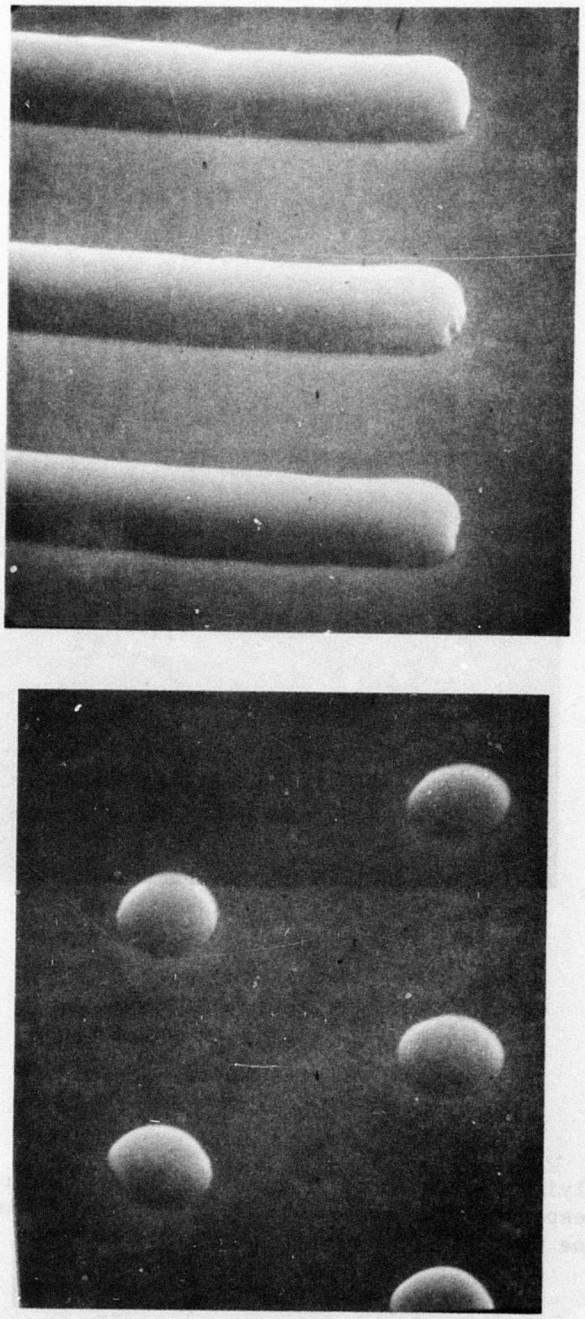

Fig. 79 Scanning electron micrographs of photoresist patterns prior to deposition of the BaF_2 insulator, showing rounded edges. The stripes and dots are approximately 5 μm wide.

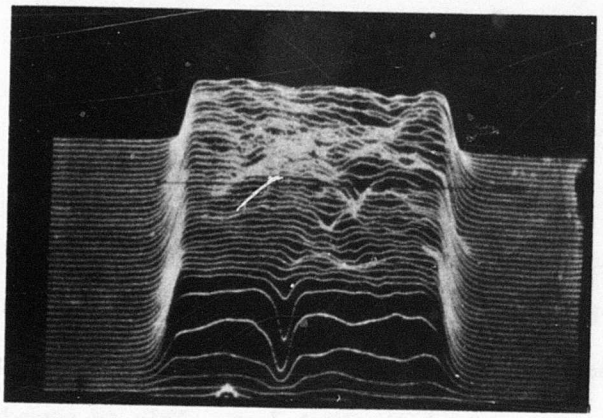

a.

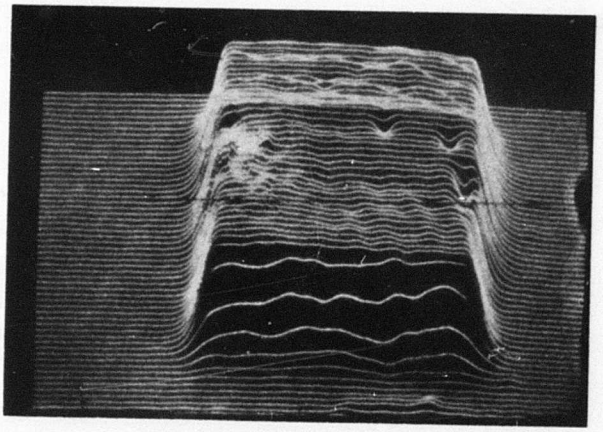

b.

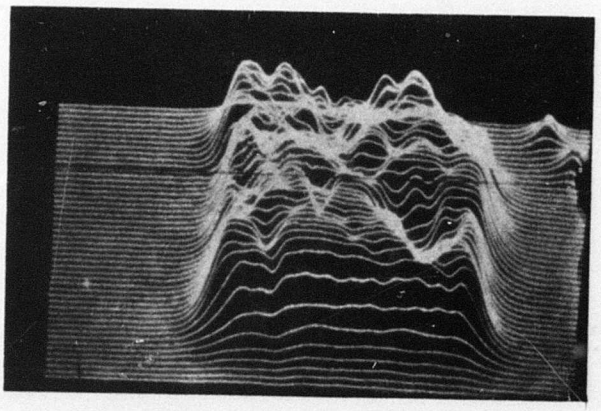

c.

Fig. 80 Flying spot scans of $PbSe_{0.8}Te_{0.2}$ lateral-collection devices at 80K.

a) 5 μm-wide stripes on 15 μm centers
b) 12 mil-square conventional control diode
c) 5 μm-diameter dots on 15 μm centers

5.2.3 Measurements of Devices with Stripe Collectors

In the following tables we present the results of detailed measurements of two $PbSe_{0.8}Te_{0.2}$ lateral collection specimens. In each case the stripe collectors were connected using silver paint. The semiconductor layer thicknesses were both about 3 μm. This is somewhat larger than for the optimum cases that are discussed in Sections 5.1.1-2, but satisfactory collection was obtained.

Table 12 - HK 241-4 at 80K

This specimen was made from $PbSe_{0.8}Te_{0.2}$ with thickness 3.0 μm and hole concentration $1.5 \times 10^{17} cm^{-3}$. The control diode had dimensions 306 μm x 306 μm = $9.36 \times 10^{-4} cm^2$ and the stripe diode had 21 nominally 5 μm-wide stripes on 15 μm centers. The ratio of the pad capacitances leads to an estimate of 8 μm for the actual stripe width. Measurements were made at 80K and 1 kHz or 5 kHz with 10 Hz bandwidth. Figs. 81-87 show the spectral detectivity, the C-V characteristics, the diode delineations and flying spot scans, together with extended data on the temperature dependence of the current responsivity and the RA product.

	diode h (control)	diode j (stripes)
Zero-bias resistance [ohm]	3.0×10^4	2.6×10^4
Background current [μA]	5.54	5.24
Calc. noise [pA]	4.2	4.1
$\mathcal{R}_I$(500K) [AW^{-1}]	0.84	0.79
η(4.9 μm)	0.81	0.76
Noise [pA]		
at 1 kHz	6.8	5.6
at 5 kHz	5.0	4.1
D*(500K) [$cmHz^{\frac{1}{2}}W^{-1}$]		
at 1 kHz	1.2×10^{10}	1.4×10^{10}
at 5 kHz	1.6×10^{10}	1.9×10^{10}
D*(4.9 μm) [$cmHz^{\frac{1}{2}}W^{-1}$]		
at 1 kHz	4.6×10^{10}	5.3×10^{10}
at 5 kHz	6.1×10^{10}	7.2×10^{10}
D*(6.0 μm) [$cmHz^{\frac{1}{2}}W^{-1}$]		
at 1 kHz	6.4×10^{10}	7.4×10^{10}
at 5 kHz	8.5×10^{10}	1.01×10^{11}
Zero-bias capacitance [pF]	750	420
Capacitance ratio*		0.53

* Allowing for 50 pF pad capacitance

Table 13 - HK241-4 at 170K

The details for this specimen are given in Table 12. Measurements were made at 170K with a frequency of 1 kHz and with 10 Hz bandwidth.

	diode h (control)	diode j (stripes)
Zero-bias resistance [ohm]	2.9×10^3	3.5×10^3
Background current [μA]	1.66	1.58
Calc. noise [nV]	16.1	17.4
$\mathcal{R}_I$(500K) [AW^{-1}]	0.55	0.55
η(5.0 μm)	0.92	0.92
Noise [nV]	17.5	21
D*(500K) [$cmHz^{\frac{1}{2}}W^{-1}$]	8.8×10^9	9.3×10^9
D*(5.0 μm) [$cmHz^{\frac{1}{2}}W^{-1}$]	5.9×10^{10}	6.3×10^{10}
Zero-bias capacitance [pF]	550	315
Capacitance ratio*		0.53

* Allowing for 50 pF pad capacitance

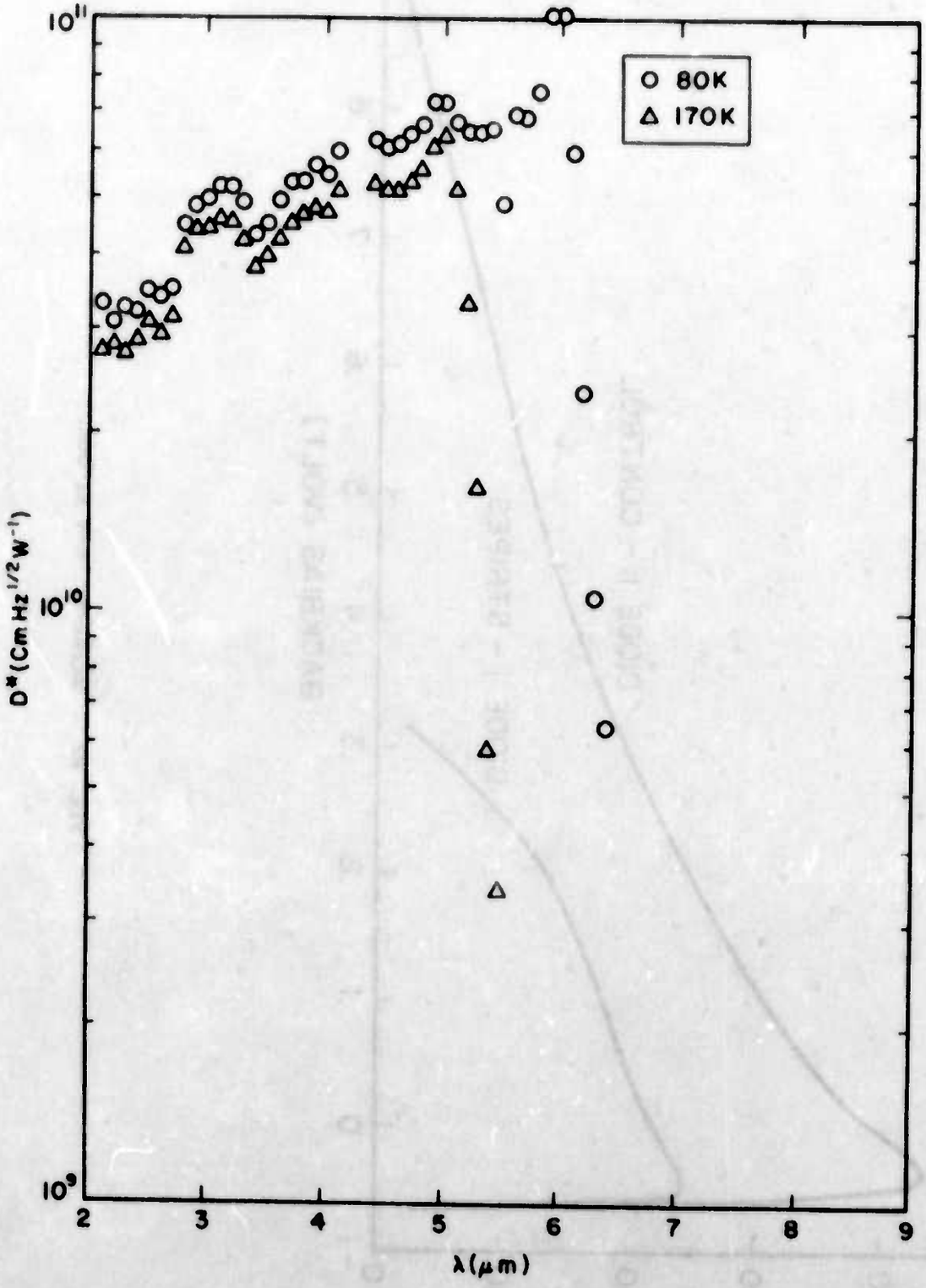

Fig. 81 HK241-4j spectral D* at 80K (5 kHz) at 170K (1 kHz).

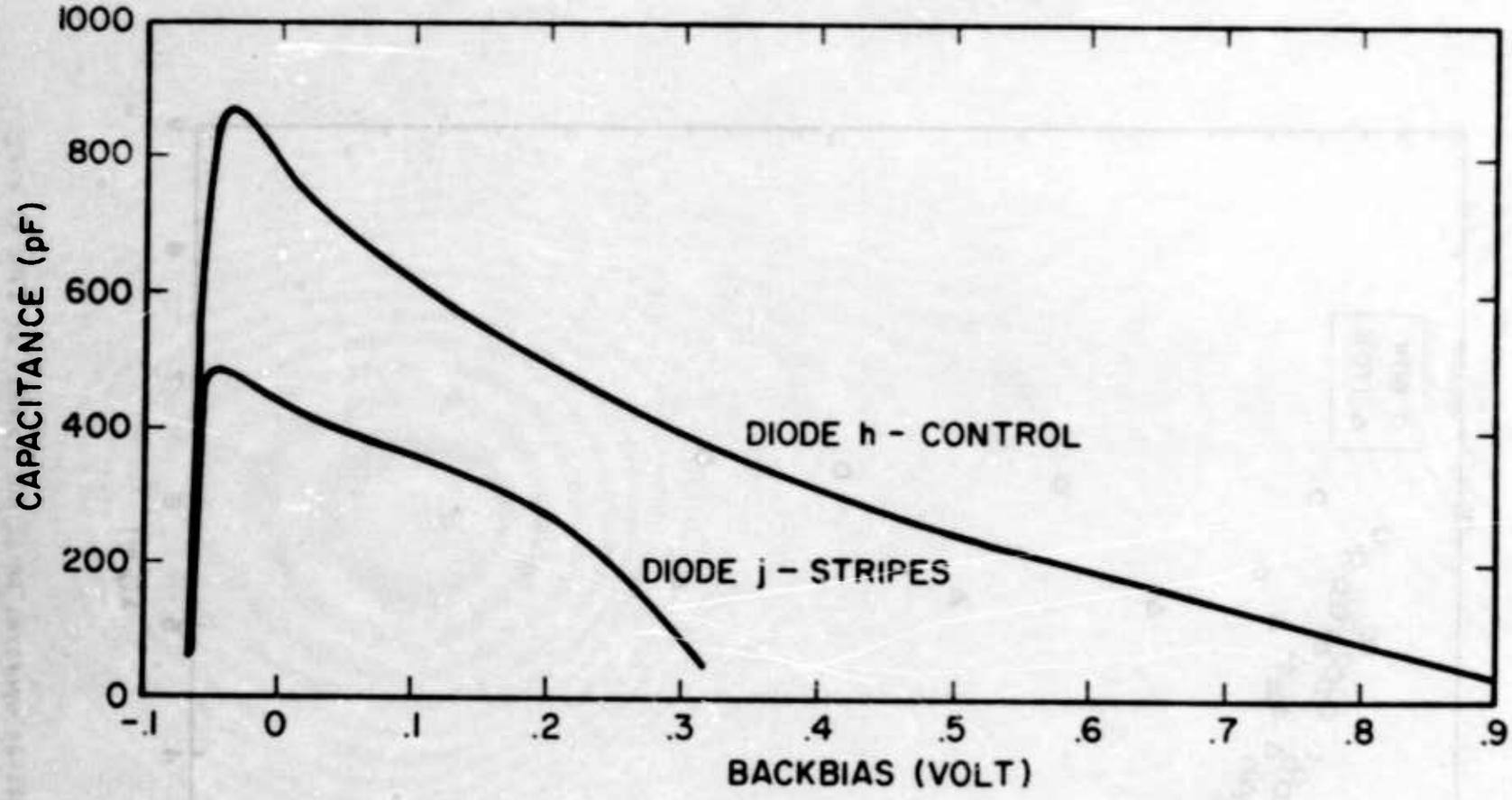

Fig. 82 HK241-4. C-V at 80K.

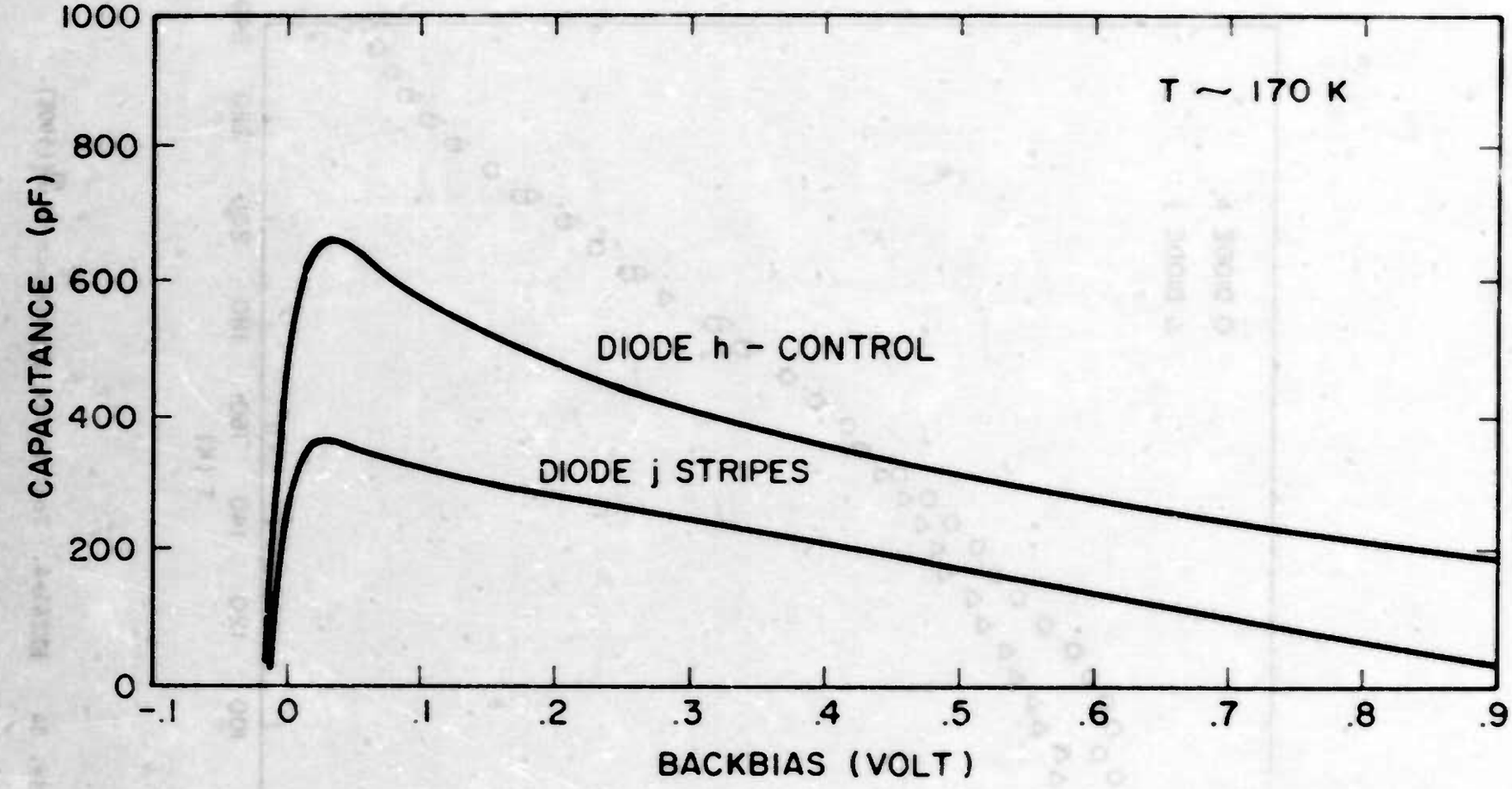

Fig. 83 HK241-4. C-V at 170K.

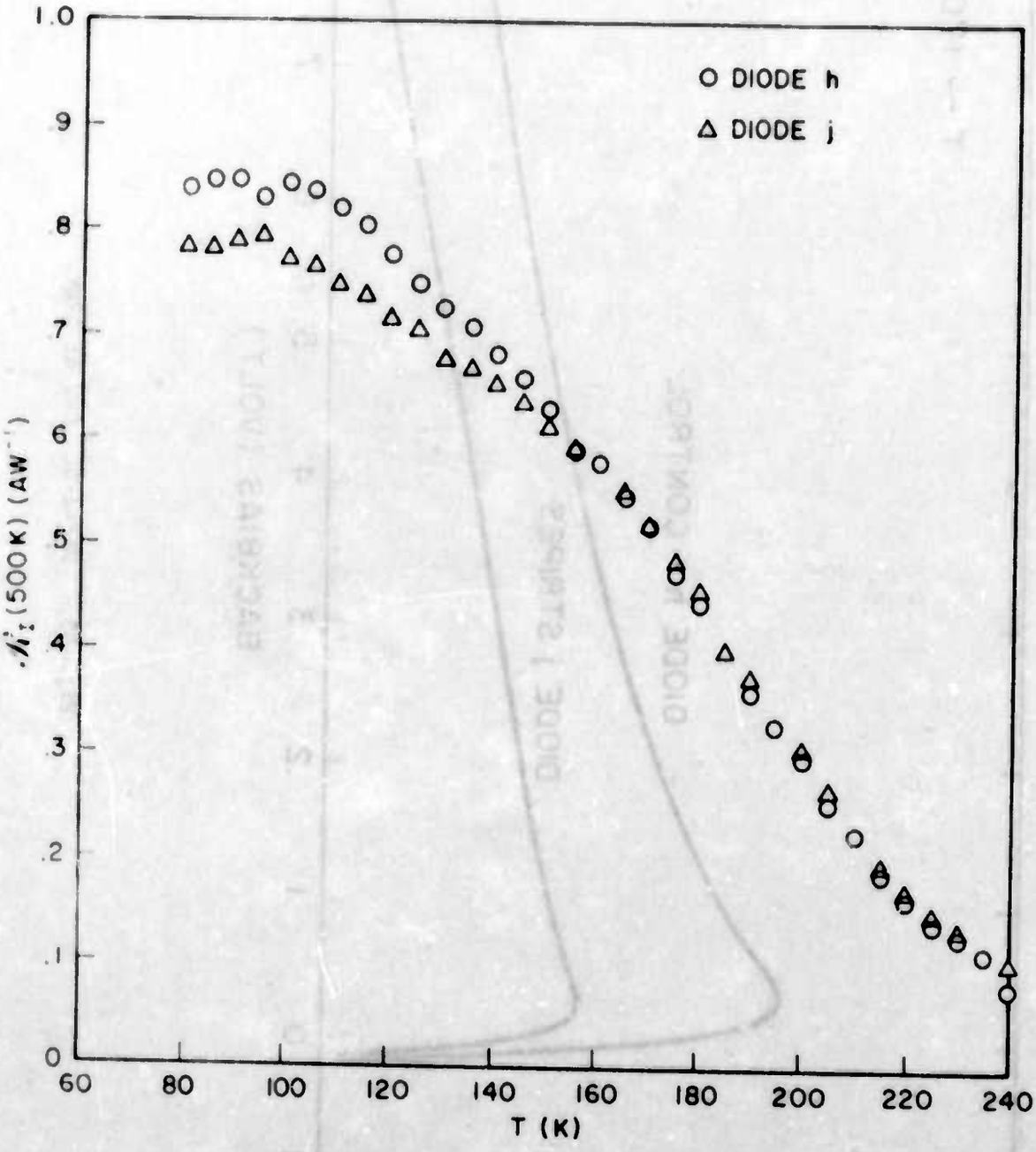

Fig. 84 HK241-4. Temperature dependence of $\mathcal{R}_i$(500K).

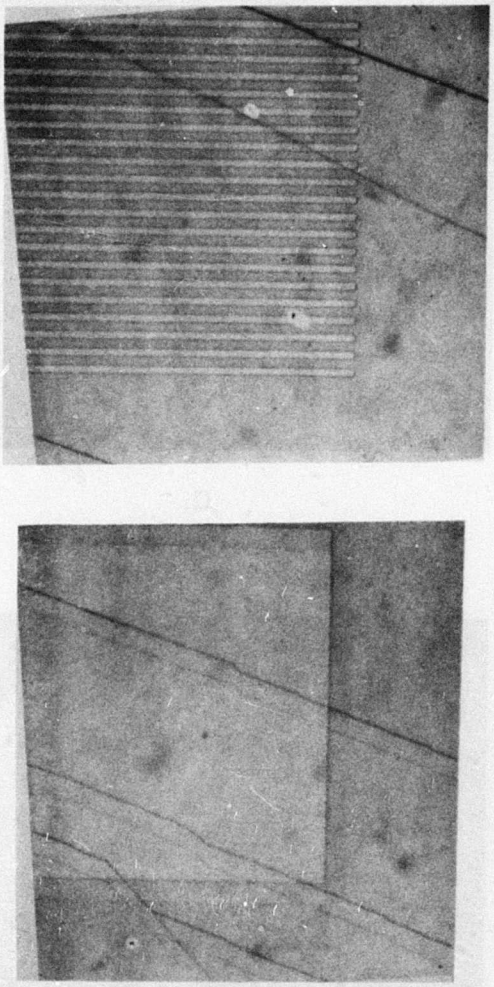

Fig. 85 HK241-4. Micrographs showing delineation of the lateral-collection and control diodes.

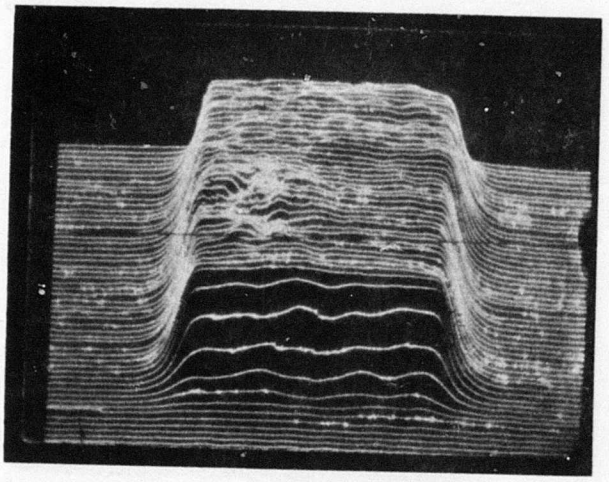

a.

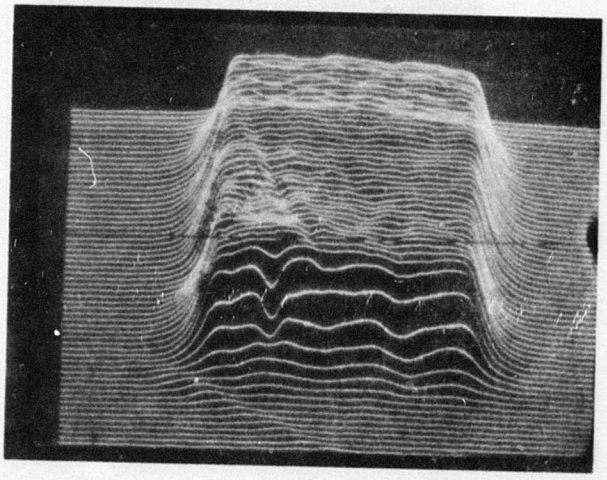

b.

Fig. 86 HK241-4. Flying spot scans at 80K.

a) diode h - 12 mil conventional control diode
b) diode j - stripe collectors

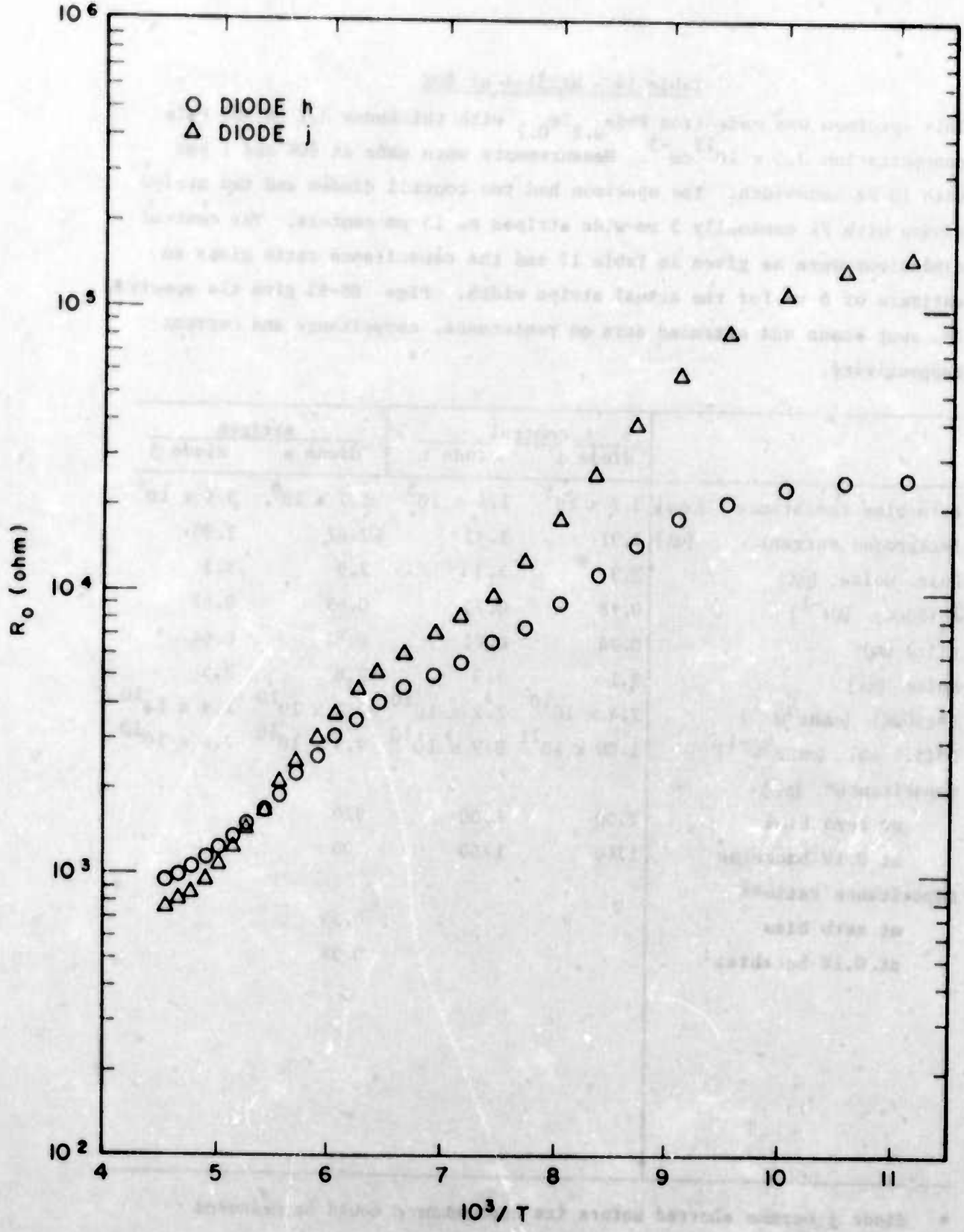

Fig. 87 HK241-4. Temperature dependence of R_o.

Table 14 - HK251-4 at 80K

This specimen was made from $PbSe_{0.8}Te_{0.2}$ with thickness 3.2 μm and hole concentration $3.5 \times 10^{17} cm^{-3}$. Measurements were made at 80K and 1 kHz with 10 Hz bandwidth. The specimen had two control diodes and two stripe diodes with 21 nominally 5 μm-wide stripes on 15 μm centers. The control dimensions were as given in Table 12 and the capacitance ratio gives an estimate of 6 μm for the actual stripe width. Figs. 88-93 give the spectral D*, spot scans and extended data on resistance, capacitance and current responsivity.

	control		stripes	
	diode d	diode h	diode e	diode j
Zero-bias resistance [ohm]	3.2×10^5	1.4×10^5	1.7×10^6	3.9×10^4
Background current [μA]	3.31	3.32	2.67	2.90
Calc. noise [pA]	3.3	3.3	2.9	3.3
$\mathcal{R}_I$(500K) [AW^{-1}]	0.78	0.74	0.65	0.67
η(5.3 μm)	0.74	0.71	0.62	0.64
Noise [pA]	3.1	3.3	2.8	3.5
D*(500K) [$cmHz^{\frac{1}{2}}J^{-1}$]	2.4×10^{10}	2.2×10^{10}	2.2×10^{10}	1.9×10^{10}
D*(5.4 μm) [$cmHz^{\frac{1}{2}}W^{-1}$]	1.00×10^{11}	8.9×10^{10}	9.3×10^{10}	7.6×10^{10}
Capacitance* [pF]				
at zero bias	2300	2300	920	
at 0.1V backbias	1740	1760	700	
Capacitance ratio**				
at zero bias			0.39	
at 0.1V backbias			0.38	

* diode j became shorted before its capacitance could be measured

** allowing for 50 pF pad capacitance

Table 15 - HK251-4 at 170K

The details for this specimen are given in Table 14. Measurements were made at 170K and 990 Hz with 10 Hz bandwidth.

	control		stripes	
	diode d	diode h	diode e	diode j
Zero-bias resistance [ohm]	2.6×10^3	3.4×10^3	6.0×10^3	1.6×10^3
Background current [μA]	1.09	1.09	0.91	0.93
Calc. noise [nV]	16.5	18.9	25.9	12.6
$\mathcal{R}_I$ (500K) [AW^{-1}]				
η(4.6 μm)	0.78	0.63	0.60	0.55
Noise [nV]	14.5	17.5	22.5	11.5
D*(500K) [$cmHz^{\frac{1}{2}}W^{-1}$]	7.0×10^9	6.9×10^9	7.3×10^9	5.2×10^9
D*(4.6 μm) [$cmHz^{\frac{1}{2}}W^{-1}$]	4.4×10^{10}	4.4×10^{10}	4.7×10^{10}	3.3×10^{10}
Capacitance* [pF]				
zero bias	1410	1550	700	220
0.1V backbias	1460	1460	630	590
Capacitance ratio**				
zero bias			0.45	0.12
0.1V backbias			0.41	0.38

* At 170K the C-V characteristic is anomalous near zero bias. This is particularly so for diode j (Fig. 90).

** Allowing for 50 pF pad capacitance

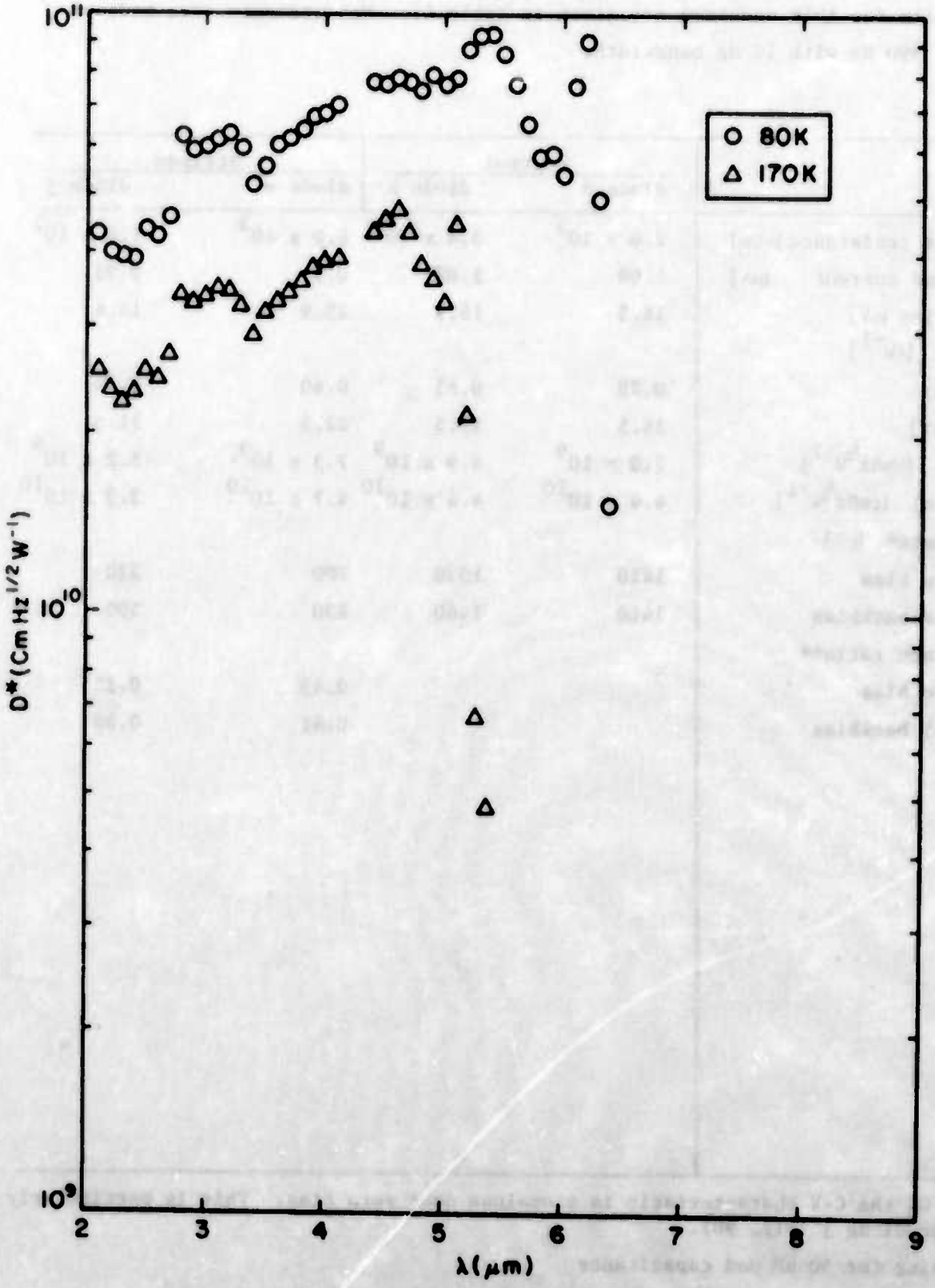

Fig. 88 HK251-4e. Spectral D* at 80K and 170K.

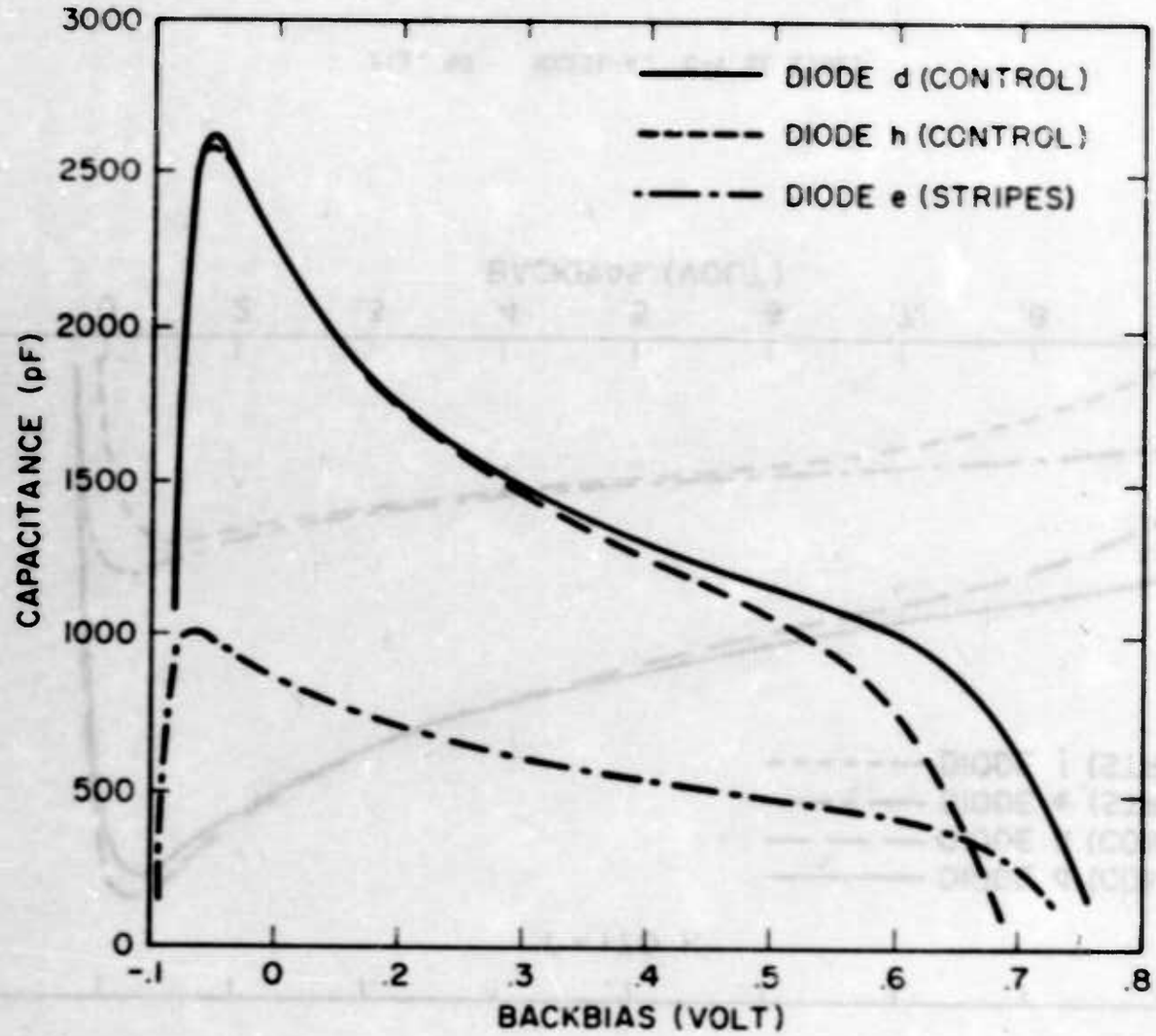

Fig. 89 HK251-4. C-V at 80K.

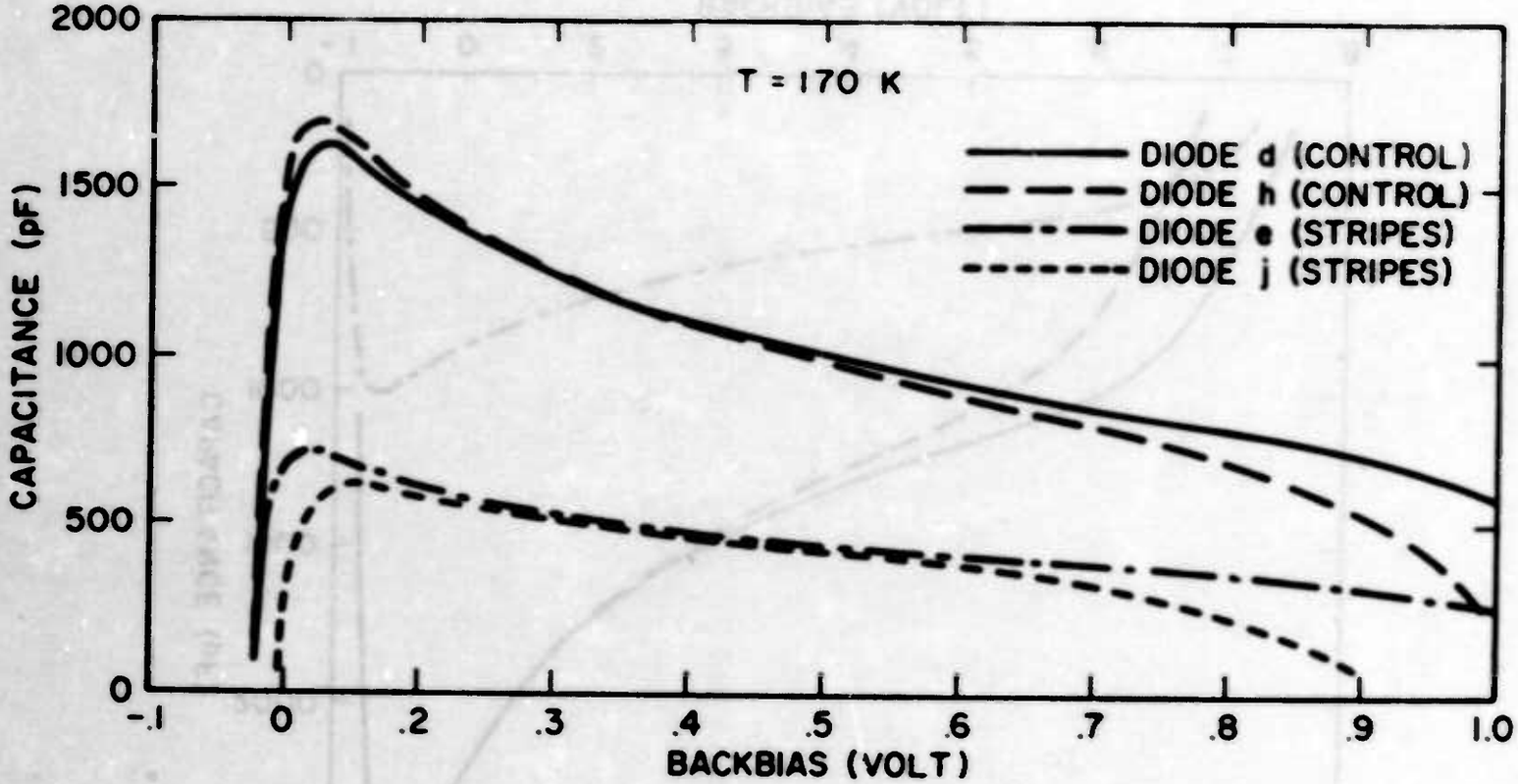

Fig. 90 HK251-4. C-V at 170K.

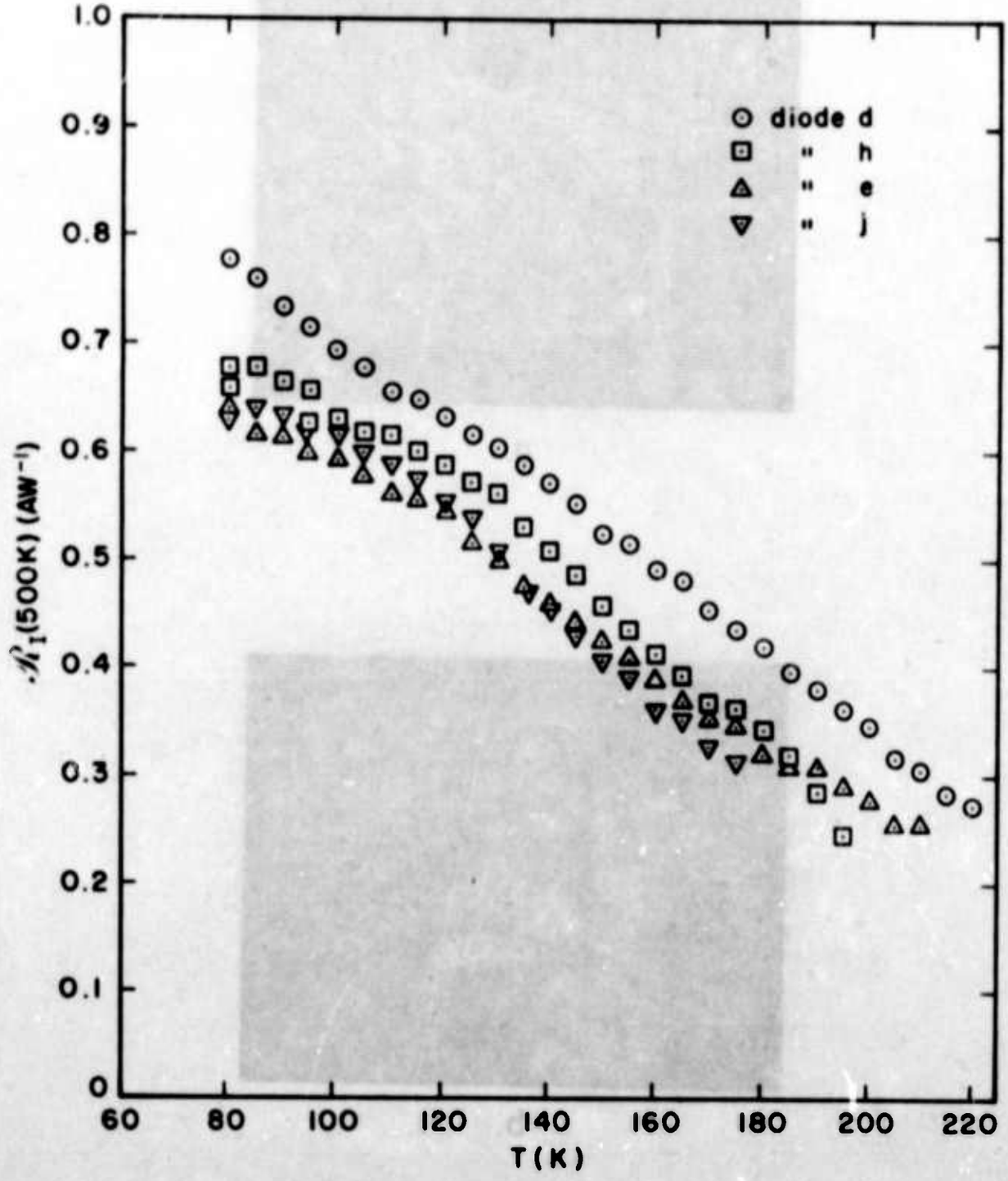

Fig. 91 HK251-4. Temperature dependence of $\mathcal{R}_I$(500K).

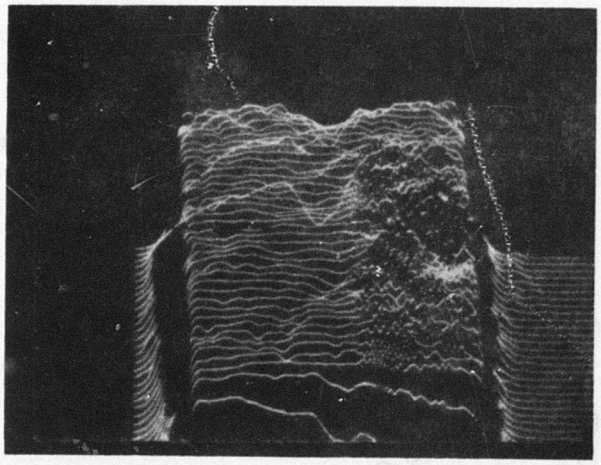

a.

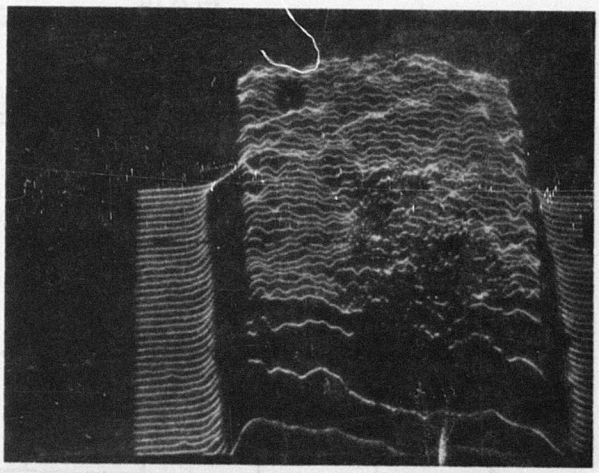

b.

Fig. 92 HK251-4. Flying spot scans at 80K.

a) diode h - conventional 12 mil-square control
b) diode j - stripe collectors

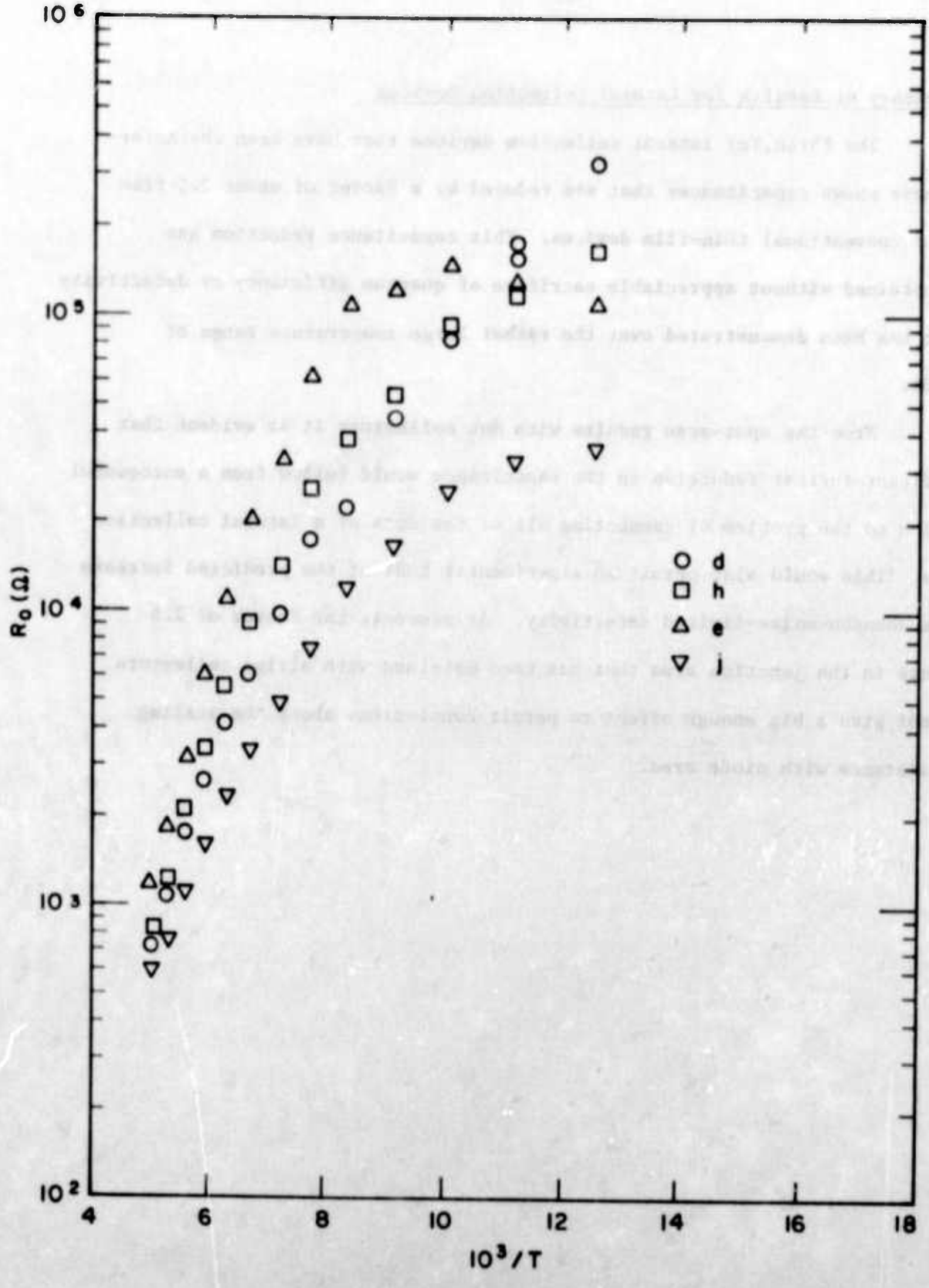

Fig. 93 HK251-4. Temperature dependence of R_o.

5.3 Summary of Results for Lateral Collection Devices

The Pb(Se,Te) lateral collection devices that have been characterized have shown capacitances that are reduced by a factor of about 2.5 from that of conventional thin-film devices. This capacitance reduction has been obtained without appreciable sacrifice of quantum efficiency or detectivity and it has been demonstrated over the rather large temperature range of 80-240K.

From the spot-scan results with dot collectors it is evident that significant further reduction in the capacitance would follow from a successful solution to the problem of connecting all of the dots of a lateral collection device. This would also permit an experimental test of the predicted increase in the Johnson-noise-limited detectivity. At present, the factor of 2.5 decrease in the junction area that has been obtained with stripe collectors does not give a big enough effect to permit conclusions about the scaling of resistance with diode area.

6. CONCLUSIONS

The two approaches that were taken in this work have both led to IV-VI photodiodes with substantially reduced capacitances. The pinched-off photodiode is particularly effective for PbTe near 80K, where a capacitance reduction of up to two orders of magnitude has been demonstrated. Further work is required on four aspects of this device:

(i) Development of theoretical models and their experimental verification. These are needed to understand both the collection mechanism and the transit time limitations upon operating frequency.

(ii) Measurements of speed of response.

(iii) Further reduction of the backbias noise to permit operation in the intermediate temperature range (170-200K) that is accessible with thermoelectric cooling.

(iv) Extension of the results to other IV-VI semiconductors (such as Pb(Se,Te) and (Pb,Sn)Se) for intermediate-temperature operation at 3-5 μm and for 80K operation at 8-12 μm.

The lateral-collection photodiode has been demonstrated to be effective with $PbSe_{0.8}Te_{0.2}$ over the temperature range 80-240K. Here, the demonstrated capacitance reduction, by about half an order of magnitude, is more modest than that for the pinched-off photodiode. However, with fabrication of optimum structures further improvements are to be expected to give at least one order of magnitude less capacitance than a conventional IV-VI photodiode. The optimum lateral-collection device has the further advantage

that it is predicted to permit an increase in the operating temperature from that of a conventional device. Further work is needed in the following areas:

(i) Development of fabrication techniques for small diameter ($\sim$ 1 μm) collectors.

(ii) Experimental studies of the relationship between junction area and diode resistance for very small ($\sim$ 1 μm) diodes.

(iii) Extension of the results from $PbSe_{0.8}Te_{0.2}$ for the 3-5 μm region to $Pb_{0.93}Sn_{0.07}Se$ for the 8-12 μm region.

APPENDIX I - Calculation of the RLL Quantum Efficiency for PbTe Devices

If one assumes complete collection of photogenerated minority carriers in a thin-film PbTe photodiode, the quantum efficiency is limited only by reflection and transmission losses to*

$$\eta = (1 - |R_{01}|^2)(1 - |R_{12}|^2 - \frac{n_3}{n_1}|T_{23}|^2) \quad ,$$

where the subscripts 0, 1, 2, and 3 refer to vacuum, BaF_2, PbTe, and Pb, respectively, and N_j is the complex refractive index of medium j,

$$N_j = n_j - ik_j \quad ,$$

and

$$R_{01} = \frac{1 - N_1}{1 + N_2} \quad ,$$

$$R_{12} = \frac{(N_1 - N_2)(N_2 + N_3)e^{\phi} + (N_1 + N_2)(N_2 - N_3)e^{-\phi}}{(N_1 + N_2)(N_2 + N_3)e^{\phi} + (N_1 - N_2)(N_2 - N_3)e^{-\phi}} \quad ,$$

$$T_{23} = \frac{4N_1N_2}{(N_1 + N_2)(N_2 + N_3)e^{\phi} + (N_1 - N_2)(N_2 - N_3)e^{-\phi}} \quad ,$$

$$\phi = 2\pi i \frac{N_2 d}{\lambda_o} \quad ,$$

where d is the PbTe film thickness and λ_o is the vacuum wavelength.

For BaF_2, refractive indices have been taken from Malitson[22], neglecting the small absorption. Experimental values for the real part

* These calculations are for normal incidence. However, the large refractive index of PbTe ($\sim$ 6) precludes large deviations from normal rays within it and the approach taken is a reasonable approximation.

of the PbTe index at 80K are from Piccioli.[23] The imaginary part of the PbTe index is from an optical absorption coefficient of the form given by Washwell and Cuff[24]

$$\alpha(\lambda) = \frac{C(1 + E_G/E_\lambda)(E_\lambda - E_G)^{\frac{1}{2}}}{1 + \exp[(RE_F + E_G - E_\lambda)/RkT]} ,$$

where

$$R = 1 + m^*_{D,V}/m^*_{D,C} = 2.02 ,$$

and $m^*_{D,V}$, $m^*_{D,C}$ are the density-of-states masses for the valence and conduction bands; E_F, E_G, and E_λ are the Fermi, gap, and photon energies, respectively. The constant C has been chosen to give agreement with Piccioli's experimental values at large photon energies ($\alpha = 1.5 \times 10^4$ cm^{-1} at $E_\lambda = 0.3$ eV). The optical constants of Pb are from Golovashkin.[25]

Comparison with calculations made assuming perfect reflection from PbTe/Pb shows that the main effect of the imperfectly reflecting interface is a shift of the predicted maxima to slightly longer wavelengths. The shift is too small for experimental verification with the present uncertainty in our film thickness measurement (± 0.03 μm).

The calculation has been extended to PbTe Schottky barrier diodes at 170K. Here we have retained 80K values of the real part of the PbTe index* and interpolated the Pb constants from Golovashkin's

---

* Experimentally we find that the absorption maxima do not shift significantly in the range 80-200K, so n_{PbTe} is essentially temperature-independent over most of the wavelength range of interest. The assumption may introduce a small error near the absorption edge where the index tends to increase.

80K and 300K values. The calculation shows that the only noticeable effect of temperature upon the reflection-loss limited spectral quantum efficiency arises from the shift of the absorption edge due to the change of the bandgap. Our previous work[2] has shown that the calculated RRL quantum efficiency is in respectable agreement with measurements on conventional thin-film PbTe photodiode at both 80K and 170K.

APPENDIX II - Attempt to Grow $PbSe_{0.8}Te_{0.2}$ with Reduced Acceptor Concentration

An attempt was made to grow $PbSe_{0.8}Te_{0.2}$ layers with reduced carrier concentrations by adjustment of the flux from a subsidiary selenium source. Layers with thickness 3 μm were grown at 2 μm/hr. onto cleaved BaF_2 substrates (from Harshaw) that were held at 350°C. The evaporation rate from the subsidiary selenium source (at 20 cm distance) was varied over almost two orders of magnitude. The resulting carrier concentrations (from 77K Hall measurements) are shown in Fig. 94. As expected, the carrier type changed from n to p with increase of the Se flux. However, the change with Se flux was too abrupt to permit controlled growth of layers with $p < 10^{17} cm^{-3}$. Similar results (though with more scatter) were obtained with a lead subsidiary source using different batches of PbTe and PbSe deposited at 450°C (Fig. 95).

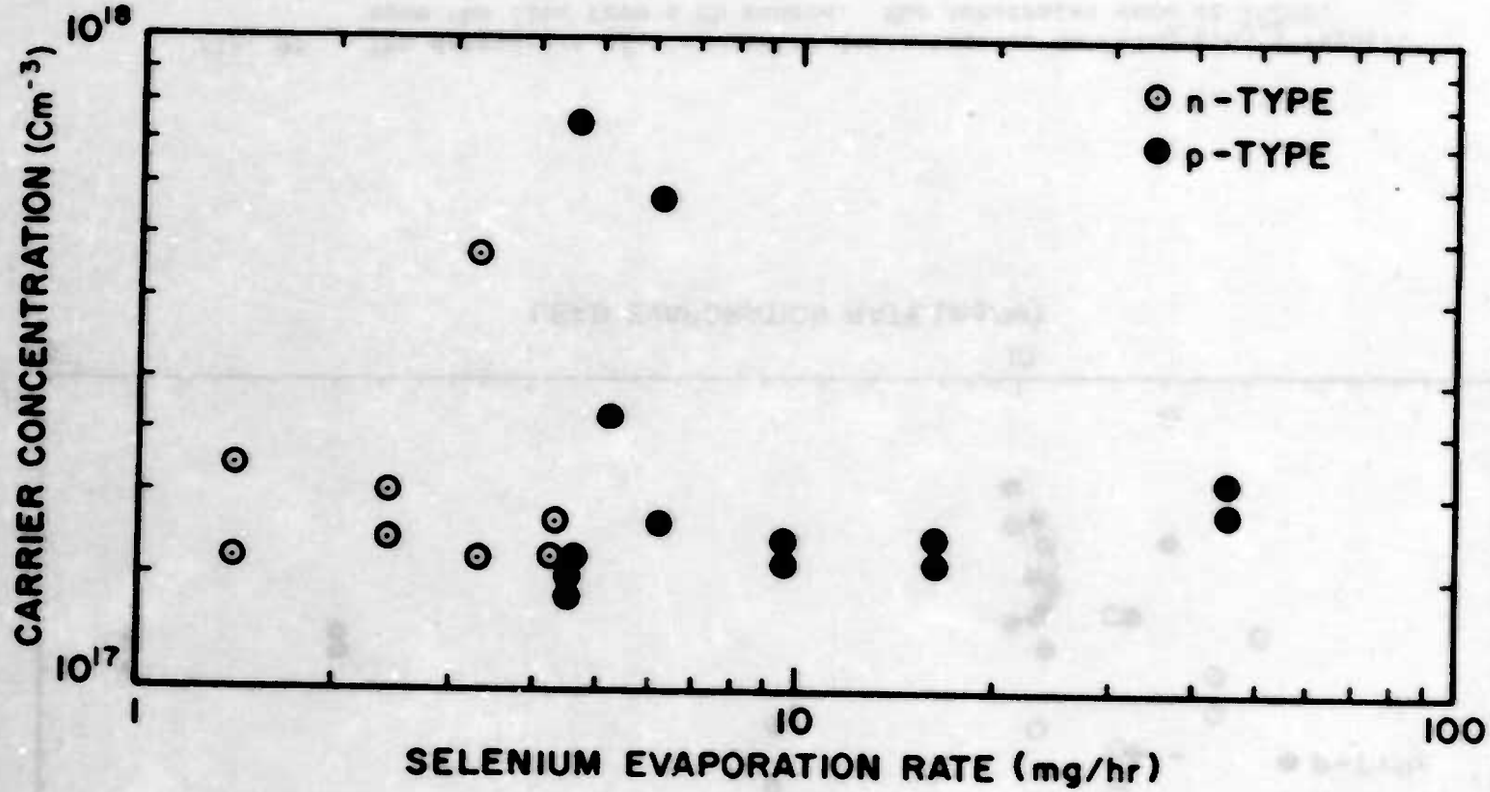

Fig. 94 The dependence of the carrier concentration in $PbSe_{0.8}Te_{0.2}$ layers upon the flux from a Se source. The substrates were at 350°C.

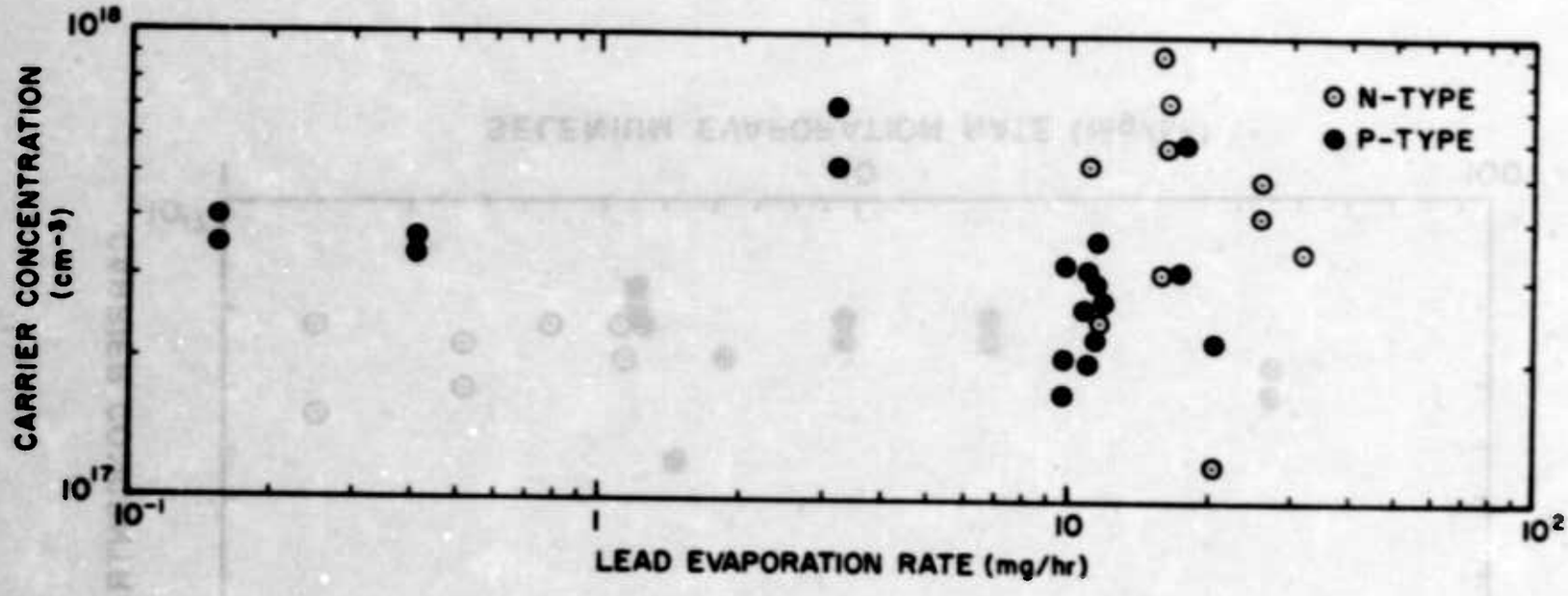

Fig. 95 The dependence of the carrier concentration in $PbSe_{0.8}Te_{0.2}$ layers upon the flux from a Pb source. The substrates were at 450°C.

References

1. Contract DAAK02-72-C-0391, Final Report (1973).

2. Contract DAAK02-73-C-0225, Final Report (1974).

3. Contract DAAK02-74-C-0124, Final Report (1975).

4. Contract DAAK02-74-C-0181, Final Report (1975).

5. H. Holloway, D. K. Hohnke, R. L. Crawley, and E. Wilkes, J. Vac. Sci. Technol. 7, 586 (1970).

6. A. M. Andrews, J. A. Higgins, J. T. Longo, E. R. Gertner, and J. G. Pasko Appl. Phys. Letters, 21, 285 (1972).

7. A. M. Andrews, J. T. Longo, J. E. Clarke, and E. R. Gertner, Appl. Phys. Letters, 26, 438 (1975).

8. R. T. Bate, D. L. Carter, and J. S. Wrobel, Phys. Rev. Letters, 25, 159 (1970).

9. H. Burkhard, G. Bauer, and A. Lopez-Otero, Solid State Comm., 18,773 (1976).

10. W. H. Rolls and D. V. Eddolls, Infrared Phys. 13, 143 (1973).

11. J. M. Tracy, A. M. Andrews, J. E. Clarke and J. T. Longo, Paper presented at IRIS Detector Specialty Group Meeting, Fort Monmouth, 1975

12. K. W. Nill, A. R. Calawa, T. C. Harman, and J. N. Walpole, Appl. Phys. Letters, 16, 375 (1970).

13. For example, R. F. Egerton and C. Juhasz, Brit. J. Appl. Phys., 18, 1009 (1967).

14. R. Dalren, Infrared Phys. 9, 141 (1969).

15. J. Butler, Paper presented at IRIS Detector Specialty Group Meeting, Orlando, 1972.

16. E. M. Logothetis, H. Holloway, A. J. Varga, and E. Wilkes, Appl. Phys. Letters, 19, 318 (1971).

17. D. K. Hohnke and H. Holloway, Appl. Phys. Letters, 24, 633 (1974).

18. S. M. Sze, Physics of Semiconductor Devices, Wiley, New York (1969). Chapter 4.

19. J. P. Donnelly, T. C. Harman, A. G. Foyt and W. T. Lindley, Appl. Phys. Letters, 20, 279 (1972).

20. J. O. Dimmock, Proc. Conf. Semimetals and Narrow-Gap Semiconductors, D. L. Carter and R. T. Bate, editors, Academic Press, New York (1970).

21. L. M. Rogers, Brit. J. Appl. Phys., 18, 1227 (1967), (This paper contains references to earlier work.)

22. I. H. Malitson, J. Opt. Soc. Am., 42, 684 (1964).

23. N. Piccioli, Thesis, University of Paris (1971).

24. E. R. Washwell and K. F. Cuff, Radiative Recombination Symposium, Paris, Academic Press, New York, (1964) page 11.

25. A. I. Golovashkin, Soviet Phys. JETP, 21, 548 (1965).